Biomimetic Models for Redox Enzyme Systems

Andrew A. Kennedy

Submitted in the Fulfilment of the Requirements for the Degree of Doctor of Philosophy

UNIVERSITY
of
GLASGOW

Department of Chemistry

August 2009

Abstract

Supramolecular chemistry involves the study of noncovalent interactions that take place between molecules. A supramolecule or host-guest complex is formed when a noncovalent binding or complexation event occurs between two such molecules. Hydrogen bonds, electrostatics, π-stacking, hydrophobic effects, solvatophobic effects and van der Waals forces are all types of noncovalent interactions. Biological systems have provided much of the inspiration for the development of supramolecular chemistry, and many synthetic supramolecular systems have been designed to mimic biological and enzymatic processes. Biomimetic modelling involves the synthesis of compounds containing similar functional groups to that of the specific enzyme's protein and cofactor. Subsequent analysis using chemical, physical or computational techniques can be used to gain a better understanding of the interactions taking place.

This study involves the investigation of various biomimetic redox enzyme systems. Firstly, model systems containing the 1- and 5-deazaflavin cofactor have been synthesised and studied to probe how their redox behaviour compares to that of riboflavin in a supramolecular environment using physical, electrochemical and computational techniques. Secondly, this study has focussed on the flavin cofactor but has expanded upon what factors influence its redox behaviour, and ability to noncovalently interact with other molecules, by examining how the presence of different dendritic architectures can affect its redox properties and noncovalent behaviour. A series of dendrons have been synthesised and studied that have a water-soluble dendron architecture attached to the flavin moiety, as well as a series of dendrons with branching designed to encapsulate the flavin unit. Finally, a biomimetic model of the pyrroloquinoline quinone cofactor has also been synthesised and studies carried out to investigate its redox behaviour in a supramolecular environment, and ability to noncovalently interact with other molecules.

The results of this study will hopefully contribute significantly to the body of chemical research in the area of supramolecular chemistry and biomimetics. Of particular interest will be the results from the flavin-based dendron research, as the prospect of purpose-built synthetic enzymes, designed and synthesised for whatever role is required, would surely be of great significance.

Acknowledgement

I would like to take this opportunity to give special thanks to my supervisor Dr. Graeme Cooke for his support and guidance during these past few years. My thanks also to post-docs past and present, Shanika Gutanilaka, Gouher Rabani, Stuart Caldwell and Mary-Margaret Westwater for their advice and enthusiasm, and to fellow PhD research students Niall McDonald, Claire Parkinson, Suhil Mabruk, Nadya Kryvohyzha, Catherine MacLean and Brian Fitzpatrick who have all made my time spent in the lab most enjoyable and entertaining (the official rules for lab cricket are in production!).

My thanks and appreciation also goes to Prof. Stuart Macgregor (Heriot-Watt University) for his help and advice on the computational studies, Dr. Dave Adam (NMR), Dr. Deliang Long (X-ray crystallography), Jim Tweedy (mass spectrometry), Kim Wilson (microanalysis) and also members of the Rotello group at the University of Massachusetts, along with Amitav Sanyal at Bogazici University in Turkey.

Thanks to all my friends in Glasgow who have made the past few years so enjoyable; Leighann, Donnie, Evan, Andy and everyone who contributed towards so many unforgettable nights out!

Finally I would like to thank my family for all their support (financial and otherwise!) throughout these past few years, in particular my Mum and Dad, as I would never have been able to finally accomplish this thesis without their support and encouragement.

Andrew Kennedy August 2009

Table of Contents

List of Figures

List of Schemes

List of Tables

Abbreviations

Ac	acetyl
AcOH	acetic acid
ADP	adenosine diphosphate
ATP	adenosine triphosphate
aq.	aqueous
BQQ	benzoquinoline quinone
Bn	benzyl
BNAH	benzyl nicotinamide (reduced)
br s	broad singlet
Bu	butyl
°C	degrees Celsius
$CDCl_3$	deuterated chloroform
CI	chemical ionisation
conc.	concentrated
CV	cyclic voltammetry
d	doublet
dd	doublet of doublets
DAP	diaminopyridine
DFT	density functional theory
DMAP	*N*, *N*-dimethyl-4-aminopyridine
DMF	*N*,*N*-dimethylformamide
DMSO	dimethylsulfoxide
DNA	deoxyribonucleic acid
ECE	electrochemical-chemical-electrochemical mechanism
ee	enantiomeric excess
EI	electron impact ionisation
Et	ethyl
EtOH	ethanol
eq.	equivalent(s)
ESI	electrospray ionisation
FAB	fast atom bombardment
Fl	flavin
FMN	flavin mononucleotide
FAD	flavin adenine dinucleotide
g	gram
h / hrs	hours
HCl	hydrochloric acid
Hz	Hertz
IR	infra-red
J	NMR spectra coupling constant
kg	kilogram
L	litre
lit.	literature
LSV	linear sweep voltammetry
m	multiplet
M	molar
λ_{max}	maximum UV absorbance
Me	methyl
MeOH	methanol
MeCN	acetonitrile
mg	milligram

MHz	megaHertz
mmol	millimole
mM	millimolar
mL	millilitre
mp	melting point
NADH	Nicotinamide Adenine Dinucleotide
NMR	nuclear magnetic resonance
NOESY	nuclear overhauser effect spectroscopy
PQQ	pyrroloquinoline quinone
Ph	phenyl
Pr	propyl
q	quartet
rt	room temperature
s	seconds or singlet
t	triplet
SWV	square wave voltammetry
T	temperature
THF	tetrahydrofuran
TLC	thin layer chromatography
Ts	tosyl or *para*-toluenesulfonyl
UV	ultraviolet

Author's Declaration

This thesis is submitted in part fulfilment of the requirement for the degree of Doctor of Philosophy at the University of Glasgow. This thesis represents the original work of Andrew A. Kennedy unless explicitly stated otherwise in the text. The research was carried out under the supervision of Dr. Graeme Cooke at Heriot-Watt University (October 2004 – August 2005) and the University of Glasgow (September 2005 – September 2007). Portions of the work described herein have been published elsewhere as listed below.

Dendron-based model systems for flavoenzyme activity: towards a new class of synthetic flavoenzyme – S. S. Agasti, S. T. Caldwell, G. Cooke, B. J. Jordan, A. Kennedy, G. Rabani, S. Rana, A. Sanyal, V. M. Rotello, *Chem. Commun.*, 2008, **35**, 4123-4125.

Andrew A. Kennedy August 2009

Chapter One

1 Chapter One – Introduction

1.1 Supramolecular Chemistry

Supramolecular chemistry has been described by one of its leading proponents, Nobel Prize winner Jean-Marie Lehn, as the "chemistry of molecular assemblies and of the intermolecular bond".[1] Expressed in simpler terms, supramolecular chemistry is the study of chemistry *beyond* the molecule, investigating new molecular systems in which the most important feature is that the components are held together reversibly by intermolecular forces and not covalent bonds. This area of chemistry is of course complementary to more traditional aspects of chemistry that mainly describe the covalent bonds that form molecules. Supramolecular chemistry, as it is now defined, is a young discipline dating back no more than fifty years, however its concepts and roots can be traced back to the beginnings of modern chemistry. Indeed supramolecular chemists can be thought of as architects synthesising and combining individual covalently bonded molecular building blocks, designed to be held together by intermolecular forces, ultimately creating functional architectures.[2]

In its simplest sense, supramolecular chemistry involves some kind of non-covalent binding or complexation event, generally considered as one molecule (a 'host') binding with another molecule (a 'guest') to produce a 'host-guest' system or supramolecule. Commonly the host is a large molecule or aggregate such as an enzyme or synthetic cyclic compound possessing a sizeable central hole or cavity, although hosts are certainly not limited to these structures.

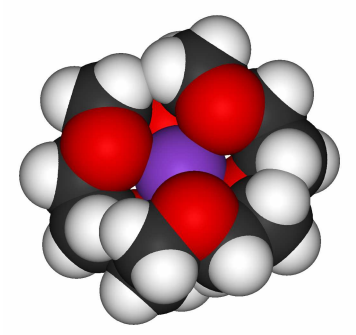

Figure 1.1 18-Crown-6 coordinating a potassium ion

The guest may be a monatomic cation (Figure 1.1), simple inorganic anion or a more sophisticated molecule such as a hormone, pheromone or neurotransmitter. More formally,

the host is defined as the molecular entity possessing *convergent* binding sites (e.g. Lewis base donor atoms, hydrogen bond donors etc.). The guest possesses *divergent* binding sites (e.g. a spherical, Lewis acid metal cation or hydrogen bond acceptor halide anion.). In 1986, Donald Cram[3] defined the relationship with the resulting host-guest complex as follows:

> "Complexes are composed of two or more molecules or ions held together in unique structural relationships by electrostatic forces other than those of full covalent bonds…molecular complexes are usually held together by hydrogen bonding, by ion-pairing, by π-acid to π-base interactions, by metal to ligand binding, by van der Waals attractive forces, by solvent reorganising…High structural organisation is usually produced only through multiple binding sites…A host-guest relationship involves a complementary stereoelectronic arrangement of binding sites in host and guest."[4]

Cram described how a range of attractive and repulsive forces were involved in non-covalent complexation. When studying a supramolecular system it, is vital to consider the interplay of all interactions and effects relating both to the host and guest as well as their surroundings (e.g. solvation, crystal lattice, gas phase etc.).

1.2 Complementarity and the Lock and Key Analogy

Biological systems have provided much of the inspiration for the development of supramolecular chemistry.[5] Many synthetic supramolecular systems have been designed to mimic the structure and function of more complex biological processes.[6] Such artificial, non-biological molecules or reaction mimics are termed *models*; meaning that on a smaller scale, the artificial systems resemble and help chemists to understand some or all of the properties of real-life biological chemistry.

The biological concept of *Complementarity* is central to the understanding of biological systems and their models. An enzyme may catalyse a single reaction with high or total specificity; the active site of the enzyme (host) being complementary to the substrate (guest), or more specifically to the transition state of the catalysed reaction. Host-guest (or receptor-substrate) chemistry is based upon three historical concepts:[7]

1. Paul Ehrlich's realisation in 1906 that molecules do not act if they do not bind, thereby introducing the concept of a biological receptor.

2. The recognition by Emil Fischer in 1894 that binding must be selective, as part of the study of receptor-substrate binding by enzymes. He described this by a 'lock and key' image of steric fit in which the guest has a geometric size or shape complementary to that of the host. This concept laid the basis for *molecular recognition*, the discrimination by a host between a number of different guests.

3. Werner's 1893 theory of coordination chemistry, in which metal ions are coordinated by a sphere of ligands, described by the fact that selective binding must involve an attraction or mutual affinity between host and guest.

These three concepts arose independently of one another, and it was many years before the various disciplines from which they originated merged to form the highly interdisciplinary field of supramolecular chemistry. Fischer's lock and key principle (Figure 1.2) is still central to the concept of molecular recognition and complementary binding. The arrangement of the binding sites in the host (lock) is complementary to the guest (key) both sterically and electronically.

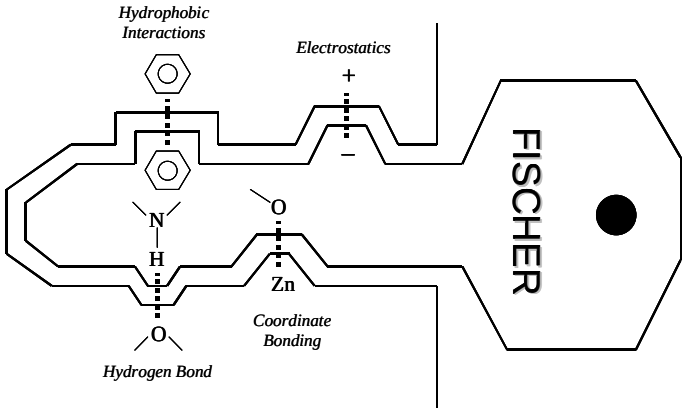

Figure 1.2 A stylised representation of the lock and key principle.

1.3 Preorganisation and Selectivity

In order to bind, a host must have binding sites that are of the correct electronic character to complement those of the guest (hydrogen bond donors must match acceptors, Lewis acids must match Lewis bases etc.). Furthermore those binding sites must be spaced out on the host in such a way as to make it possible for them to interact with the guest in the binding conformation of the host molecule, thus fulfilling the concept of complementarity. If the conformation of the host molecule does not change significantly upon guest binding,

the host is said to be *preorganised*. Host preorganisation is pivotal as it represents a major, if not in some cases decisive, enhancement to the overall free energy change of guest complexation. Neglecting the effects of solvation, the binding process can be loosely divided into two stages. There is firstly an activation stage in which the host undergoes conformational readjustment in order to arrange its binding sites in a more complementary manner to the guest, whilst minimising the unfavourable interactions between binding sites on the host. This process is energetically unfavourable and this loss in energy is never recovered throughout the lifetime of the complex, as the conformation must be held during this time. However, following rearrangement, binding occurs which is energetically favourable due to the enthalpically stabilising attraction between mutually complementary binding sites of the host and guest. The overall free energy of complexation represents the difference the unfavourable reorganisation energy, and the favourable binding energy. If the reorganisation energy is large, then the overall free energy is reduced, destabilising the complex. If the host is preorganised, this rearrangement energy is small.

Central to this idea of preorganisation is guest binding kinetics. Rigidly preorganised hosts may have significant difficulty in passing through a complexation transition state, and so tend to exhibit slow guest binding kinetics. Conformationally mobile hosts are able to adjust rapidly to changing conditions, and both complexation and decomplexation are rapid. Solvation enhances the effects of preorganisation since the solvation stabilisation of the unbound host is often greater than the case when it is wrapped around the guest, effectively presenting less surface area to the surrounding medium.

1.4 Thermodynamic and Kinetic Selectivity

The ultimate aim of supramolecular host design in both nature and artificial systems is the achievement of selectivity i.e. the discrimination by the host between one guest and another. Nature has succeeded in this goal in a variety of examples including selective O_2 uptake by haemoglobin when in the presence of similarly sized molecules such as N_2, water and carbon dioxide. The affinity of a host for a particular guest can be assessed by its binding constant, *K*, which represents the thermodynamic equilibrium constant for the binding process, Host + Guest ⇆ (Host.Guest):

$$K = \frac{[Host \cdot Guest]}{[Host] \times [Guest]}$$

In thermodynamic terms, selectivity is simply the ratio of the binding constant for one guest over another:

$$Selectivity = \frac{K_{Guest1}}{K_{Guest2}}$$

This kind of selectivity tends to be the easiest to achieve, as it is highly susceptible to manipulation by intelligent application of concepts such as the lock and key analogy, preorganisation and complementarity, coupled with a detailed knowledge of the host guest interactions. Another type of selectivity relates to the rate of transformation of competing substrates along a reaction path, and is termed kinetic selectivity. This type of selectivity is the basis for directing the flow of directional processes such as enzymatic catalysis and guest sensing and signalling. Put simply, it is the guest that is transformed the *fastest*, rather than the one that is bound the strongest, that the system is said to be selective for. In such time-resolved processes, large binding constants are inhibitory to the system since kinetics are slowed down. Many biochemical enzymes are kinetically selective and examination of their structures reveals that while they are perfectly complementary for the desired, sometimes transitory, state of the guest at any given instant, they are not generally preorganised in a rigid way since this would preclude rapid catalysis. In artificial systems, the engineering of time-resolved selectivity, as in the design of mimics, is a much more difficult process since it requires the adaptation of the host to the changing needs of the guest as the system proceeds along its reactive pathway.

1.4.1 Binding Constants

The thermodynamic stability of a metal-macrocycle complex in a given solvent (often water or methanol) is gauged by measurement of the binding constant, *K* (the terms formation, association or stability constant are also often used). Ignoring activity effects, this is merely the equilibrium constant for the reaction of the metal, M, and the host ligand, L, in water.

$$M(H_2O)_n^{m+} + L \leftrightarrow ML^{m+} + nH_2O$$

$$K = \frac{[ML^{m+}]}{[M(H_2O)_n^{m+}][L]}$$

Thus a large binding constant corresponds to a high equilibrium concentration of bound metal, and hence a more stable metal-macrocycle complex. Typical binding constants for crown ethers and alkali metal cations in water are in the range $10^1 – 10^2$. In methanol this increases up to 10^6 for the association of K^+ with [18]-crown-6, and 10^{10} for K^+ with [2.2.2]-cryptand.

Because binding constants are thermodynamic parameters, they are related to the free energy of the association process according to the Gibbs equation: $\Delta G° = -RT\ lnK$. Thus the general affinity of a host for a guest under specific conditions (solvent, temperature etc.) may be given either in terms of K or $-\Delta G°$ values. In energy terms, complexation free energies may range from magnitudes of 20 to 100 $kJ.mol^{-1}$ for alkali metal cation complexes. A large K value of about 10^{10} corresponds to a $-\Delta G°$ of about $52kJ.mol^{-1}$. Binding constants may also be defined in terms of the rate constants (k) of the complexation and decomplexation reactions:

$$M^+ + L \rightarrow [M^+ \cdot L] \qquad k_1$$

$$[M^+ \cdot L] \rightarrow M^+ + L \qquad k_{-1}$$

$$K = \frac{k_1}{k_{-1}}$$

In principle, binding constants may be assessed by any experimental technique that can yield information about the concentration of a complex, $[M^+ \cdot L]$, as a function of changing concentration of M^+. There are many methods that can achieve this including potentiometric titration, fluorescence titration, calorimetric titration and extraction experiments. However one of the most commonly used methods is that of nuclear magnetic resonance (NMR) titration.[8]

1.4.2 Measurement of Binding Constants by NMR Titration

If the exchange of complexed and uncomplexed guest is slow on the NMR timescale, then the binding constant may be evaluated under the prevailing conditions of concentration, temperature, solvent etc. by the simple integration of the NMR signals for the bound and unbound host or guest. Most host-guest equilibriums are fast in the NMR timescale, and the chemical shift observed for a particular resonance (which is sensitive to the

complexation) is a weighted average between the chemical shift of the free and bound species. In a typical NMR titration experiment, the small aliquots of guest may be added to a solution of host with a known concentration in a deuterated solvent and the NMR spectrum of the sample is monitored as a function of guest concentration or host:guest ratio. Commonly, changes in chemical shift ($\Delta\delta$) are noted for various atomic nuclei present (e.g. ^{1}H in ^{1}H NMR) as a function of the influence the guest binding has on their magnetic environment. As a result, two kinds of information are gained. Firstly, the location of the nuclei most affected may give qualitative information about the regioselectivity of guest binding. More importantly however, the shape of the titration curve (a plot of $\Delta\delta$ vs. guest concentration) gives quantitative information about the binding constant. Such titration curves are often analysed by computer least-squares curve fitting, using the following equation to determine optimum values of δ_{mn} (chemical shift of each species present, where mn is the ratio of host, H, and guest, G), and β_{mn} (stepwise binding constant).[9]

$$\delta_{calc} = \sum_{m=1}^{m=i} \sum_{n=0}^{n=j} \frac{\delta_{mn} \beta_{mn} m [G]^m [H]^n}{[G]_{total}}$$

A key aspect of such calculations is the use of the correct stoichiometry model (i.e. the ratio of host to guest, which must be assumed). There is a strong bias in the supramolecular chemistry literature towards the fitting of data to 1:1 stoichiometries, and it is a common mistake to neglect higher aggregates. Binding stoichiometry may be confirmed in most kinds of titration experiments that allow the concentration of complex to be determined by preparing a series of solutions with varying host:guest ratios such that the total concentration of host and guest is constant. Monitoring the changing concentration of the host-guest complex in these samples allows a plot of [Complex] vs. ([Host]/([Host] + [Guest])) to be constructed. For a 1:1 complex, this kind of representation, referred to as a Job plot) should give a peak at 0.5.

1.5 Noncovalent Interactions

While natural biological systems provide some of the most elegant examples of complementary molecular interactions (e.g. DNA double-helix, enzyme catalysis etc.), supramolecular chemists are more concerned with the design, synthesis, coordination and assembly properties of molecules. Noncovalent interactions are essentially the ‘glue’ used

by chemists to hold these molecular aggregates together, and there are a number of such interactions that can be utilised.[10] They include:

(a) Electrostatics (ion-ion, ion-dipole and dipole-dipole);
(b) Hydrogen bonding;
(c) π-π Stacking interactions;
(d) Dispersion and induction forces (van der Waals forces);
(e) Hydrophobic or solvatophobic effects.

The bond energy of a typical single covalent bond is around 350 kJmol^{-1} rising up to 942 kJmol^{-1} for the very stable triple bond in diatomic nitrogen. The strengths of many of the noncovalent interaction used by supramolecular chemists are generally much weaker, ranging from 2 kJmol^{-1} for dispersion forces, through to 20 kJmol^{-1} for a hydrogen bond, to 250 kJmol^{-1} for an ion-ion interaction. The power of supramolecular chemistry lies in the combination of a number of weak interactions, allowing strong and selective recognition of specific guest to be achieved.

1.5.1 Electrostatic interactions

Ionic bonding is comparable in strength to covalent bonding (bond energy = 100-350 kJmol^{-1}). Ions are produced when atoms can obtain a stable number of electrons by either losing or gaining electrons. A typical ionic solid is sodium chloride, which has a cubic lattice structure where each sodium cation is surrounded by six chlorine anions (Figure 1.3).

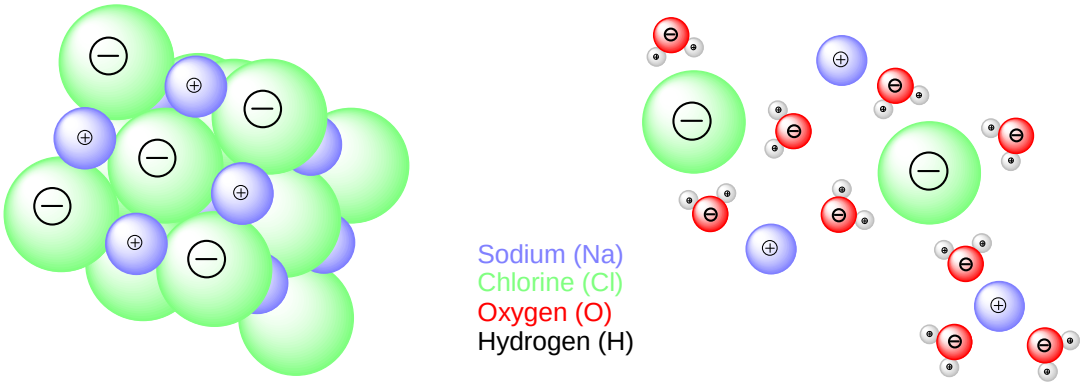

Figure 1.3 The NaCl ionic lattice and the effect of solvation in water.

Although sodium chloride would not typically be regarded as a supramolecular compound, this simple lattice structure does illustrate the way in which a sodium cation can organise six complementary donor atoms about itself in order to maximise noncovalent ion-ion interactions. This kind of lattice does however break down in solution due to solvation effects to give species such as the labile $Na(H_2O)_6^+$. An example of supramolecular ion-ion would be that of the organic *tris*(diazabicyclooctane) host, which carries a 3+ charge, with anions such as $Fe(CN)_6^{3-}$ (Figure 1.4).

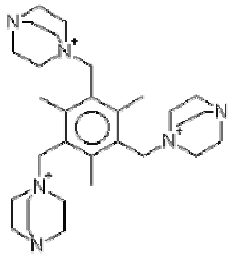

Figure 1.4 Structure of the *tris(diazabicyclooctane*) organic host.

Ion-ion interactions are non-directional whilst for ion-dipole interactions the dipole must be suitably aligned for optimal binding efficiency (bond energy = 50-200 kJ.mol^{-1}). The bonding of an ion such as Na^+, with a polar molecule such as water, is an example of an ion-dipole interaction. This kind of bonding is seen in the solid state and in solution. Supramolecular analogues are readily apparent in the structures of complexes of alkali metal cations with macrocyclic crown ethers.[11] In those complexes, as with aqueous sodium ions, the lone pairs of electrons on the oxygen atoms are attracted to the cationic positive charge (Figure 1.5).

ion-ion interaction ion-dipole interaction

Figure 1.5 Electrostatic interactions.

Ion-dipole interactions also include coordinative bonds, which are mostly electrostatic in nature in the case of interactions of non-polarisable metal cations and hard bases. Coordinate (dative) bonds with a significant covalent component, as in $[Ru(2,2'\text{-bipyridinyl})_3]^{2+}$, are often used in supramolecular assembly.

Alignment of one dipole with another (dipole-dipole interactions, bond energy = 5-50 kJmol^{-1}) can result in significant attractive interactions from matching of either a single

pair of poles on adjacent molecules (type I) or opposing alignment of one dipole with the other (type II, Figure 1.6). Organic carbonyl compounds show this behaviour well in the solid state, with bond energies comparable with moderately strong hydrogen bonds (≈20 $kJmol^{-1}$).

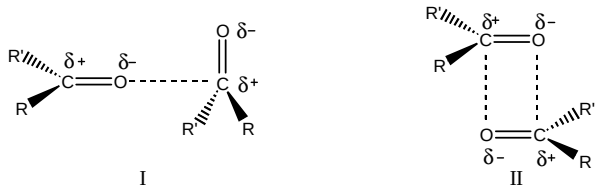

Figure 1.6 Dipole-dipole interactions in carbonyls.

1.5.2 Hydrogen bonding

A hydrogen bond may be regarded as a particular type of dipole-dipole interaction in which a hydrogen atom attached to an electronegative atom (or an electron withdrawing group) is attracted to a neighbouring dipole on an adjacent molecule or functional group.[12] The protonated electronegative element, often termed a hydrogen bond donor (D), comes into close contact with a second electronegative element. This second species must either bear a formal negative charge or a free lone pair that can be donated to the proton, and is termed the hydrogen bond acceptor (A) – Figure 1.7.[13] Because of its relatively strong (bond energy = 4-120 $kJmol^{-1}$) and highly directional nature, hydrogen bonding has been described as the 'master-key interaction' in supramolecular chemistry. In particular, hydrogen bonds are responsible for the overall shape of many proteins, recognition of substrates by numerous enzymes, and for the double helix structure of DNA.[14]

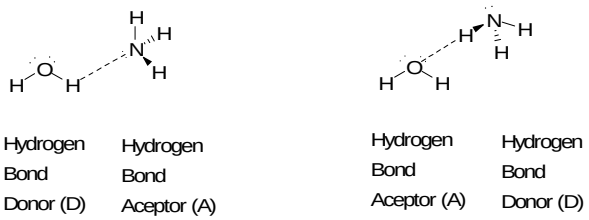

Figure 1.7 Hydrogen bonding between water and ammonia molecules.

The classic example of hydrogen bonding is observed between water molecules. The electronegative oxygen atom draws the electrons in the bonds it shares with hydrogen towards itself, resulting in a net positive charge on the hydrogen atoms, and a net negative

charge on the oxygen. Together with the short distance between the oxygen and hydrogen atoms, this results in water possessing a large *dipole moment*. Two water molecules can then form a strong electrostatic interaction. This interaction is known as a hydrogen bond, and in water it is normally around 2.80 Å in length measured from oxygen to oxygen. This distance results from the interplay between the electrostatic stabilising factor, and the repulsion effect between the oxygen atoms as they come closer.

Hydrogen bonds come in a wide range of lengths, strengths and geometries. A single, strong hydrogen bond per molecule may be sufficient to determine solid state structure and exert a marked influence on the solution and gas phases. Typical values of bond lengths are between 2.50-2.80 Å from donor to acceptor, although interactions in excess of 3.00 Å may also be sufficient. Even though the general definition of hydrogen bonding can be regarded as fairly simple, it seems more difficult to understand its electronic nature than that for covalent or ionic bonds and van der Waals forces. This is mainly due to the term 'hydrogen bond' applying to a wide range of interactions. Very strong hydrogen bonds are similar in their nature to covalent bonds, while very weak hydrogen bonds are closer to van der Waals forces. Most hydrogen bonds vary between these two extremes.

1.5.3 π-π Stacking interactions

π-π Stacking interactions are weak electrostatic interactions that occur between aromatic rings, often in situations where one ring is relatively electron rich and one is electron poor (bond energy = 0-50 $kJmol^{-1}$).[15] There are two general types of π-stacking: face-to-face (perfect and offset arrangements) and edge-to-face, although a wide variety of intermediate geometries are known (Figure 1.8).

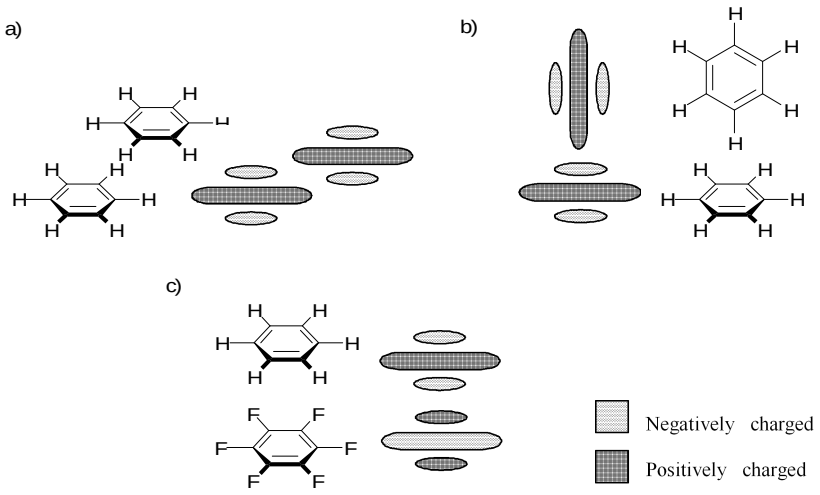

Figure 1.8 **Structure and common representation of π-stacking arrangements: (a) Face-to-face (offset) stacking. (b) Edge-to-face stacking. (c) Face-to-face (perfect) stacking.**

Face-to-face π-stacking interactions are responsible for the slippery feel of graphite and its useful lubricant properties. Similar π-stacking interactions between the aryl rings of nucleobase pairs also help stabilise the DNA double helix. Edge-to-face interactions may also be regarded as weak forms of hydrogen bonds between the slightly electron deficient hydrogen atoms of one aromatic ring, and the electron rich π-electron cloud of another. Edge-to-face interactions are responsible for the characteristic 'herringbone' packing in the crystal structure of a range of small aromatic hydrocarbons, including benzene.

Sanders and Hunter[15] have proposed a simple model based on competing electrostatic and van der Waals influences to explain the variety of geometries observed for π-π stacking interactions, and to predict quantitatively the interaction energies. Their model is based upon the overall attractive van der Waals interaction between the negatively charged π-electron cloud of one molecule, and the positively charged σ-framework of an adjacent molecule. The relative orientation of the two interacting molecules is determined by the electrostatic repulsions between the negatively charged π-systems. Sanders and Hunter stress the importance of the interactions between individual atoms rather than the molecules as a whole and, while their approach has been relatively successful, there is still a great deal of current debate over the nature of π-π stacking interactions. In particular, work involving substituent effects by Wilcox[16] suggests that London dispersion forces might play a more important role than electrostatic interactions.

1.5.4 Van der Waals forces

Van der Waals interactions arise from the polarisation of an electron cloud by the proximity of an adjacent nucleus, resulting in a weak electrostatic attraction with a typical energetic value of less than 5 $kJmol^{-1}$. They are non-directional, and therefore possess only limited scope in the design of specific hosts for selective complexation of particular guests. This is the force involved in interactions between most polarisable species such as the noble gases. In supramolecular chemistry they are most important in the formation of *inclusion* compounds in which small, typically organic molecules are loosely incorporated within crystalline lattices or molecular cavities.

1.5.5 Dispersion and Induction Forces

Dispersion forces (or induced dipole-induced dipole interactions) are attractive forces between molecules that occur when instantaneous dipoles in the electron clouds around each molecule interact favourably. These van der Waals forces are believed to provide additional enthalpic stabilisation to the coordination of a hydrophobic guest into a hydrophobic cavity. They are however, of a very general nature and consequently the design of receptors specifically to take full advantage of them is difficult.

However one such system that has taken advantage of such effects has been synthesised by Rebek[17] and co-workers, colloquially described as the self-assembling ‘tennis ball’. This self-complementary unit, comprised of two hydrogen bonded molecules, is curved due to steric hindrance and forms a ‘tennis ball’ like molecular capsule with a hollow centre allowing the encapsulation of small molecules (e.g. methane, xenon) by use of the van der Waals interactions (Figure 1.9)

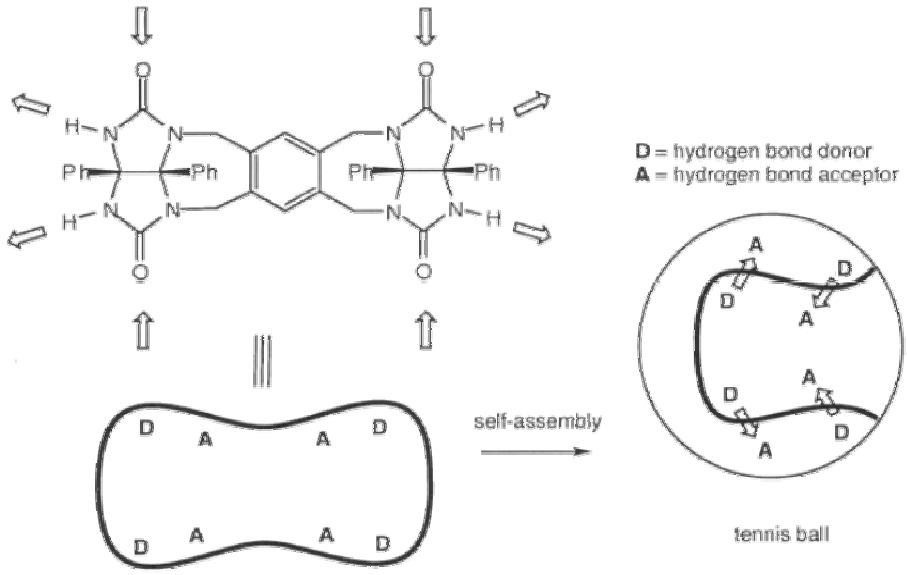

Figure 1.9 The formation of a molecular 'tennis ball'.[2]

1.5.6 Hydrophobic Effects

Although occasionally mistaken for a force, hydrophobic or solvatophobic effects generally relate to the exclusion from polar solvents, particularly water, of large particles or those that are weakly solvated (e.g. via hydrogen bonds or dipolar interactions).[18] The effect is obvious in the immiscibility of mineral oil and water. The water molecules are attracted strongly to one another resulting in a natural agglomeration of other species (such as non-polar organic molecules) as they are 'squeezed' out of the way of strong inter-solvent interactions. This can produce effects resembling attraction between one organic molecule and another, although there are in addition van der Waals and π-π stacking attractions between organic molecules themselves.

The hydrophobic effect is the specific driving force for the association of apolar binding partners in aqueous solution. Water molecules around the apolar surfaces of a hydrophobic cavity arrange themselves to form a structured array. Upon guest complexation, the water molecules are released and become disordered. This results in a favourable increase in entropy. In addition, there is also an enthalpic component to the hydrophobic effect. This involves the stabilisation of water molecules that are driven from a host cavity upon guest binding. Since intracavity water does not interact strongly with the hydrophobic host walls, it is of high energy and upon release into the bulk solvent, is stabilised by interactions (such as hydrogen bonding) with other water molecules. Both entropic and enthalpic effects promote apolar guest coordination and complex formation. Receptors containing

hydrophobic interior cavities designed to encapsulate organic guest molecules in aqueous solution include the cyclophanes and cyclodextrins.[19]

1.6 Proteins and Enzymes

1.6.1 Enzyme Characteristics

Enzymes are dynamic macromolecules with a molecular weight generally in excess of 10,000 Da. They are made up of polypeptide chains, which in turn are polymers of the protein amino acids.[1, 20] These chains are folded into a unique conformation giving a globular structure incorporating surface clefts and crevices. Substrate binding in enzymatic catalysis occurs within one of these clefts, termed the *active site*. The initial binding is a thermodynamically controlled equilibrium process and is highly selective, usually proceeding on an induced fit basis. Binding occurs by three-dimensional contact between the enzyme and substrate, and involves various noncovalent interactions including hydrogen bonding, salt bridges, and hydrophobic effects to name a few. However proteins consisting only of amino acids cannot catalyse oxidation-reduction reactions, and are therefore only active in the presence of a suitable cofactor. This cofactor is usually a redox-active molecule that binds within a cleft of the protein backbone (apoprotein). The apoprotein cleft microenvironment tunes the redox properties of the cofactor to meet the function of the enzyme, and both act in concert to catalyse a reaction.

Enzyme structure is essentially derived from the shape of the protein backbone. Proteins have a complex three-dimensional structure that can be divided into primary, secondary, tertiary and quaternary features.

1.6.1.1 Primary Protein Structure

The most basic level of organisation of a protein is its primary structure. This is simply the order of the sequence of amino acid residues on the polypeptide chain and is determined by the way in which the enzyme is synthesised.[21] The primary structure may be thought of as a complete description of covalent bonding in a polypeptide chain or protein. Primary structure is, by convention, always described from amino end to carboxyl end with each amino acid written as its standard three-letter abbreviation (this can also be shortened to a standard single letter depending on the context in which it is used). An example is shown below of the primary structure of insulin comprising of two polypeptide chains, with each

three-letter abbreviation representing one of twenty basic amino acids found in living organisms.

Chain1: Gly-Ile-Val-Glu-Gln-Cys-Cys-Thr-Ser-Ile-Cys-Ser-Leu-Tyr-Gln-Leu-Glu-Asn-Tyr-Cys-Asn

Chain 2: Phe-Val-Asn-Gln-His-Leu-Cys-Gly-Asp-His-Leu-Val-Glu-Ala-Leu-Tyr-Leu-Val-Cys-Gly-Glu-Arg-Gly-Phe-Phe-Tyr-Thr-Pro-Lys-Thr

1.6.1.2 Secondary Protein Structure

The secondary structure of a protein refers to certain common repeating structures found in localised regions of a polypeptide chain or protein molecule. There are various forms of secondary structures, however the most stable are the α-helix and β-pleated sheet (others include the random coil and the β-turn). Secondary structure arises from the geometry of the bond angle between the amino acids as well as hydrogen bonds to nearby amino acids. A single poly peptide chain or protein molecule may contain multiple secondary structures (Figure 1.10).[22]

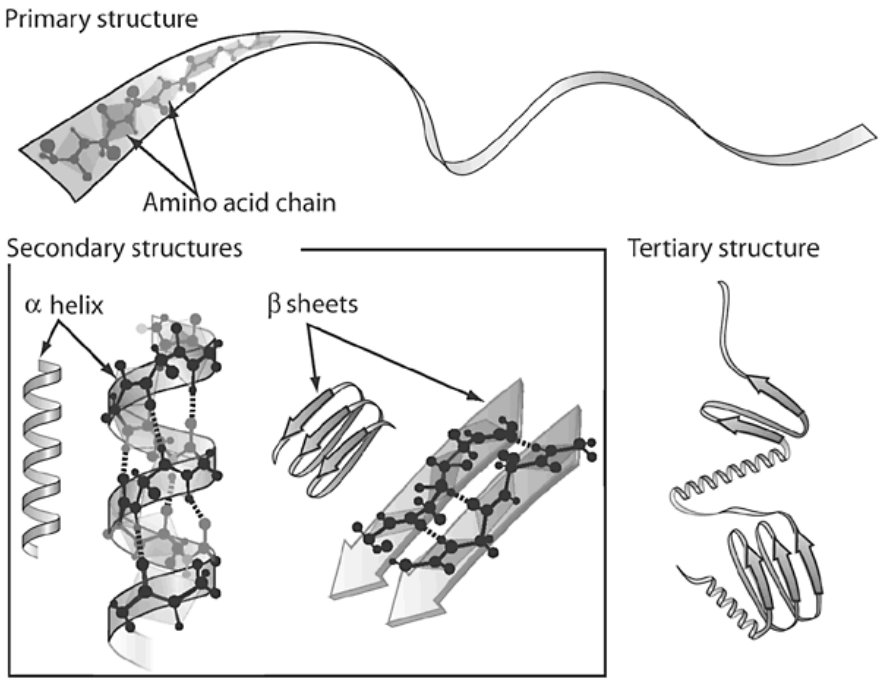

Figure 1.10 Common features in protein structure

In the α-helix, the polypeptide chain is coiled tightly in the fashion of a spring. The chain backbone forms the inner part of the coil with side chains extending outwards. The helix is

stabilised by intramolecular and intermolecular hydrogen bonds between the secondary amine group of one amino acid and the carboxyl group of the fourth amino acid away from it. α-Helices can be either right or left handed, however all naturally occurring α-helices are right handed.

β-Pleated sheets consist of two or more amino acid sequences within the same protein that are arranged adjacently and in parallel, but with alternating orientation such that hydrogen bonds can form between the two strands. The amino acid chain is almost fully extended throughout a β-strand, with the secondary amine groups in the backbone of one strand establishing hydrogen bonds with the carboxyl groups in the backbone of the adjacent parallel strand(s). The cumulative effect of multiple hydrogen bonds arranged in this way contributes to the sheet's stability, structural rigidity and integrity. The side chains from the amino acid residues found in a β-sheet structure may also be arranged in such that many of the adjacent side chains on one side of the β-sheet are hydrophobic, while many of those adjacent to each other on the alternate side of the sheet are polar or charged (hydrophilic).

1.6.1.3 Tertiary Protein Structure

The tertiary structure of a protein is the final specific geometric shape that a protein assumes. The final shape is determined by a variety of bonding interactions between the side chains on the amino acids. These bonding interactions may be stronger than the hydrogen bonds within a helix or sheet and as a result, may cause a number of folds, bends and loops in a protein chain. There are four main types of bonding interactions between side chains including hydrogen bonding, disulfide linkages, salt bridges, and non-polar hydrophobic interactions. Different regions of the protein chain may form hydrogen bonds or disulfide linkages with each other causing a change in shape. Salt bridges result from the neutralisation of an acid and an amine on side chains, with the final ionic interaction between the positive ammonium group and the negative acid group. Finally, different regions of the protein chain are hydrophilic or hydrophobic and arrange themselves accordingly in aqueous solution. The hydrophobic interactions of non-polar side chains are believed to contribute significantly to the stabilisation of tertiary structures in proteins.

1.6.1.4 Quaternary Protein Structure

Quaternary structure only exists when more than one polypeptide chain is present. It involves the clustering of several individual peptide or protein chains into a final specific shape. A variety of bonding interactions including hydrogen bonding, salt bridges and disulfide bonds hold the various chains in a particular geometry. There are two major categories of proteins with quaternary structure – fibrous and globular.

Fibrous proteins, such as keratins in hair and mysin in muscle tissue, have quaternary structures mostly consisting of one type of secondary structure (α-helices, β-sheets etc.), that ultimately result in a fibre-like shape, usually possessing strong and more rigid properties. Globular proteins, such as insulin and haemoglobin, may have a combination of secondary structures massed into the shape of a ball. Although simplified, these two types of quaternary structures can have quite complex arrangements. The main stabilising forces of subunits in the quaternary structure are hydrophobic interactions. When a single polypeptide chain folds into a three-dimensional shape to expose its polar side chains to an aqueous environment (shielding its non-polar side chains), there are still some hydrophobic sections on the exposed surface. When two or more chains are present, they will assemble so that their exposed hydrophobic sections are in contact.[1]

1.6.2 Cofactors and Coenzymes

In order to catalyse a chemical reaction, some enzymes do not need any additional components to exhibit full activity. However, others require non-protein molecules to be bound for activity and these molecules are termed cofactors. Cofactors can be either inorganic (e.g. metal ions and iron-sulphur clusters) or organic (e.g. flavin adenine dinucleotide and haem) in nature. Organic cofactors can be either prosthetic groups, which are tightly bound to an enzyme, or coenzymes which are released from the enzyme's active site as a normal part of the catalytic cycle. Examples of coenzymes include nicotinamide adenine dinucleotide (NADH), its phosphate derivative (NADPH) and adenosine triphosphate. These molecules all act to transfer chemical groups between enzymes.

1.6.2.1 Flavin Adenine Dinucleotide (FAD) Cofactor

In biochemistry, FAD is a redox cofactor involved in several important reactions in metabolism.[23] This cofactor can exist in two different redox states: the fully oxidised FAD, and its reduced form $FADH_2$ (Figure 1.11).

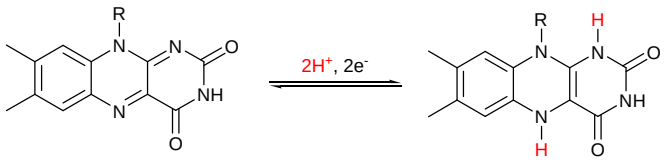

Figure 1.11 Two accessible redox states of FAD

The structure of FAD is derived from the parent compound riboflavin, and many oxidoreductases, known as flavoenzymes or flavoproteins, require FAD as a prosthetic group which functions in electron transfers. $FADH_2$ is an energy-carrying molecule, and the reduced cofactor can be used as a substrate for oxidative phosphorylation in the mitochondria. $FADH_2$ is re-oxidised to FAD, which makes it possible to produce two moles of the universal energy carrier ATP. Without this cofactor, the apoprotein belonging to a particular flavoenzyme is non-functioning and cannot carry out its required catalytic function.

1.6.2.2 Nicotinamide Adenine Dinucleotide (NADH) Coenzyme

NADH is utilised as a coenzyme in around 700 enzymes, and for this reason it is hugely important to consider its involvement when attempting to mimic some enzyme systems. The coenzyme is found in two oxidation forms in living cells: As NAD^+, as an oxidising agent, and NADH, a reducing agent (Figure 1.12).

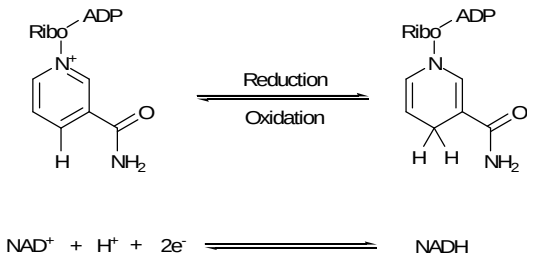

Figure 1.12 The redox reactions of nicotinamide adenine dinucleotide

NADH has several essential roles in metabolism, acting as a coenzyme in redox reactions, as a donor of ADP-ribose groups in ADP-ribosylation reactions, as well as acting as a

substrate for bacterial DNA ligases and a group of enzymes called sirtuins that use NAD^+ (the oxidised derivative of NADH) to remove acetyl groups from proteins.

However its main role in metabolism is the transfer of electrons from one redox reaction to another. This coenzyme accepts or donates electrons in redox reactions. Such reactions involve the removal of two hydrogen atoms from the reactant (R) in the form of a hydride ion, and a proton. The proton is released into solution, while the reductant (RH_2) is oxidised and NAD^+ reduced to form NADH by transfer of the hydride to the nicotinamide ring.

$$RH_2 + NAD^+ \rightarrow R + NADH + H^+$$

This type of reaction is catalysed by a large group of enzymes called the oxidoreductases, but are also often referred to as dehydrogenases or reductases. When bound to a protein, NAD^+ and NADH are usually held within a structural motif known as the Rossmann fold. The energy that is transferred to NAD^+ by reduction of NADH is done so as part of glycolysis and the citric acid cycle. The NADH is then oxidised in turn by the electron transport chain, which pumps protons across a membrane and generates ATP through oxidative phosphorylation. Since both the oxidised and reduced forms of nicotinamide adenine dinucleotide are used in linked reactions of glycolysis, they remain in approximately equal concentrations in cells, allowing this coenzyme to act as both an oxidising and reducing agent (Figure 1.13).

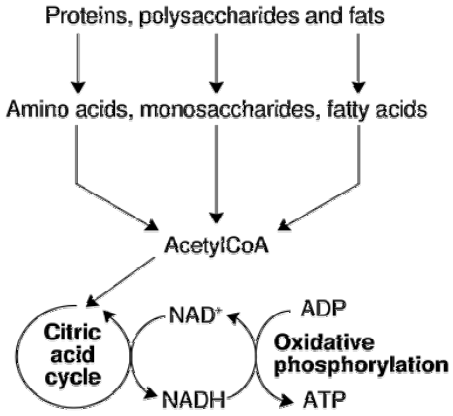

Figure 1.13 A simplified outline of redox metabolism

This type of redox reaction and regeneration of coenzyme is not uncommon in catalytic cycles, and is present so that respective concentrations of coenzyme and product are maintained at a steady level within the cell.

Enzymes that require a cofactor but do not have one bound are called apoenzymes or apoproteins. In fact most cofactors are not covalently attached to the enzyme, but are very tightly bound by noncovalent interactions. An apoenzyme coupled with its cofactor is known as a haloenzyme (the active form). This noncovalent nature between the protein backbone and prosthetic group, gives rise to the assumption that a prosthetic group may be able to be removed or even substituted to form a derivative of the parent enzyme.

1.7 Biomimetic Modelling

1.7.1 Enzyme Modification

Following research into naturally occurring enzyme systems, the next stage for scientists is the modification of these enzymes in order to change their properties and activity to suit a desired purpose. Two general, but very different, branches of this research can be identified. The first uses biological mutations and practical modification, by comparing the activity and properties of a given enzyme while the native cofactor is substituted by synthetic derivatives. The second uses models designed to mimic one specific type of interaction, between the cofactor and apoprotein, in order to quantify each effect in the absence of others when possible. Both of these types of research are prevalent particularly in the study of flavoenzymes.

1.7.1.1 Protein Engineering

Although findings in enzyme mutation is an established discipline, a recent piece of work by Massey[23, 24] and co-workers, specifically on flavoenzymes, described the modification of flavoenzyme activity by substituting the native cofactor bound within a protein cleft by a synthetic derivative (Figure 1.14). Provided it is possible to remove the original cofactor under conditions that avoid denaturing the protein, most apoproteins will accept a synthetic cofactor into their active sites. A completely different function can now be achieved by the newly formed protein, in some cases the exact opposite of that held by the native enzyme.

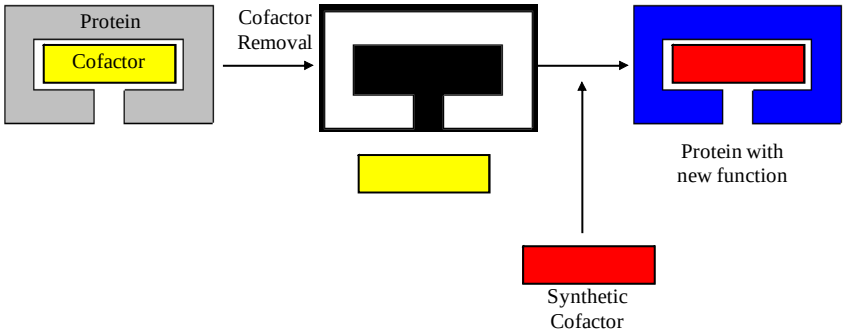

Figure 1.14 Natural enzyme cofactor replacement accompanied by a change in enzymatic function

1.7.1.2 The 'Single-Event' Approach

A variety of novel techniques and results were achieved in the last decade utilising the previous approach. It can definitely be said that the complexity of the interaction between the cofactor and apoenzyme is tremendous. In order to achieve a better insight into the intricate mix of events and ultimately the enzyme activity as a whole is to analyse each event or interaction separately and quantify their involvement. Of course, some interactions may be diminished when they are removed from their environment, and great care must be taken to compile the overall results. Apoenzyme and cofactor molecular structures, combined with crystallographic data, provide a great deal of information regarding the type of noncovalent interactions that are encountered between the two species. The 'single-event' approach involves a virtual breakdown of the active site area in order to individually identify and study the molecular groups that could give rise to a supramolecular interaction. Each function is isolated, and correlation between the apoenzyme and cofactor can be studied. Using the data obtained, synthetic models can be designed to mimic the single identified noncovalent interaction (Figure 1.15).

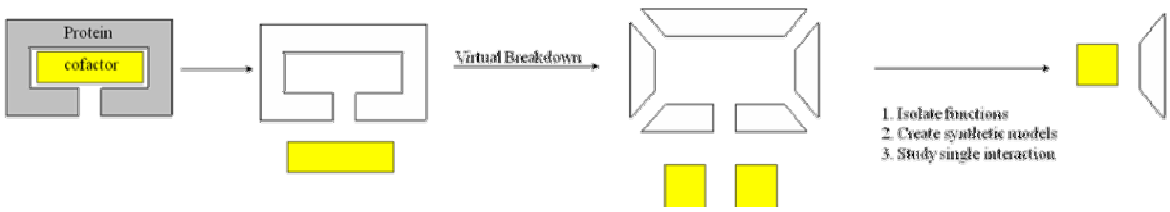

Figure 1.15 The 'single-event' approach

Interactions between the cofactor an apoenzyme at the active site are known to be, in most cases, purely non-covalent. Hydrogen bonding, π-stacking and dipole interactions have been identified as the dominant supramolecular forces involved in these systems. Simple

biomimetic models can be synthesised to investigate these interactions on an individual level.

1.7.2 Macro Design

More recently, steps have been taken to design mimics of biological systems using completely synthetic components.[25] Instead of isolating individual interactions that occur in a given system, chemists have been striving to create molecules that mimic the synthetic backbone of the protein that can also interact with a species mimicking the behaviour of a suitable cofactor. There are two classes of compounds that have been able to at least begin to recreate the type of environment found in naturally occurring biological systems; polymers and dendrimers.

1.7.2.1 Polymers

A polymer is defined as a substance of large molecular mass composed of repeating structural units or monomers connected by covalent bonds.[26] By definition a protein can certainly be considered to be a type of natural polymer, consisting of a number of repeating amino acid residues as monomer units. A supramolecular polymer is a species whereby its monomer units are reversibly held together by non-covalent interactions and not covalent bonds. However in the area of biomimetics, chemists are ideally looking for a polymer that will mimic the protein backbone, and where the non-covalent interactions exist between the host and guest i.e. between a large aggregate molecule and a suitable cofactor. Of course as in protein systems, non-covalent interactions such as hydrogen bonding can exist between various monomer units allowing the formation of tertiary structure, ultimately creating characteristics similar to those found in natural systems, such as internal cavities and hydrophobic pockets.

Recent research by Cooke and co-workers[25] has found that by using a water soluble polymer to mimic the protein backbone, a local hydrophobic environment can be created which not only isolates and shields the cofactor of interest from the external environment, but whose structure can provide specific interactions to modulate the properties of the cofactor involved. In their example, an oligoethylene glycol backbone is used as the backbone to interact with a flavin cofactor, which results in the creation of a local hydrophobic environment (investigated by UV spectroscopic analysis), and also the means to tune the redox potential of the flavin cofactor in an aqueous environment, whereby it is

reminiscent of that of the apoenzyme of naturally occurring flavoenzymes. Further studies also proved that the catalytic activity of the flavin cofactor was affected by the hydrophobic pocket on the polymer. This research provides grounding for the development of other biomimetic derivatives to investigate further the effect of isolation, redox tuning and reactivity by the backbone mimic, polymeric or otherwise, on the flavin cofactor and indeed on cofactors of many other similar systems.

1.7.2.2 Dendrimers

One of the most remarkable classes of compounds to be discovered in recent years, from synthetic, structural and functional point of view is that of the dendrimers.[27] Derived from physiological terminology, a dendrite or dendron is a tree-like branched extension of a nerve or cell. Dendrimers are ideally monodisperse macromolecules with a highly branched, three-dimensional architecture. A dendrimer may be regarded as a multi-component compound that has grown from a central core in a tree-like fashion. The synthesis of a dendrimer molecule therefore usually begins with a multifunctional root or core, and from each core springs another multifunctional repeat unit to give an oligomer with a central core and a number of functionalised pendant arms. This level of branching can be extended through a number of generations, ultimately achieving a well defined three-dimensional polymer (Figure 1.16).

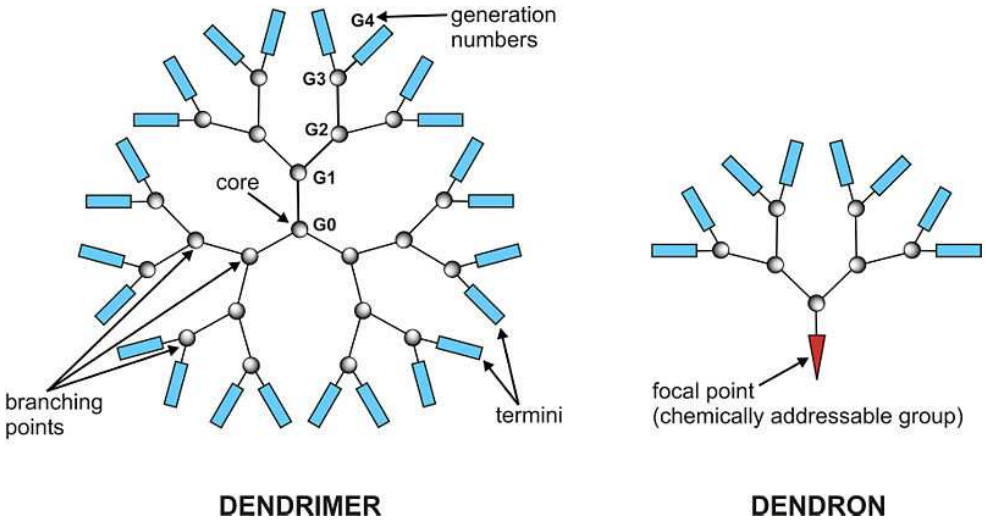

Figure 1.16 Dendrimer and dendron

Dendrimers are of interest in a variety of contexts such as host-guest chemistry and catalysis, in which the dendritic core region, which is often highly porous, can exhibit interesting host behaviour, whilst the densely packed outer layer acts to shield the interior

region from the surrounding medium. This suggests applications in mimicking the hydrophobic pocket region in enzymes. In addition, the well defined structural relationship of one layer to another and the narrow molecular weight range (monodispersity), of well designed dendrimers make their behaviour easier to characterise than polymeric bulk materials, even though they may reach very high molecular weights and display bulk properties.

In terms of their host-guest chemistry, the dense outer sheath of a dendrimer of any type can result in two interesting kinds of behaviour: site isolation and guest inclusion. Site isolation involves the construction of the dendrimer from a functional core, which becomes to a large extent, shielded from external medium as the dendrimer grows. This results in the ability to study the behaviour of the core in isolation from the effects of solvation and self-association reactions. An example of this can be seen from research by Dandliker and co-workers[28] who were able to construct a dendrimer comprising of polyethylene glycol arms extending from an iron(III) porphyrin core, which resulted in an isolated, water-soluble haem analogue. Comparison of the first- and second- generation dendrimers revealed a 420mV shift to positive potential in the reduction of the iron(III) centre. Guest encapsulation (often termed topological trapping) occurs when the low density experienced in the core of many dendrimers results in the inclusion of a molecule and consequent isolation from the external medium. This phenomenon is irreversible if bulky groups are used at the outer layer of the dendrimer. The effect of this encapsulation can be as apparent as a fluorescent molecule, which would normally have its fluorescence quenched at a certain wavelength, becoming active as the dendritic architecture effectively shields the active molecule from outside influences.

When considering using a dendrimer to model biological systems, their affinity for forming hydrophobic pocket-like environments is certainly appealing. Couple this with their ability to bind to, or encapsulate, an optically or redox-active molecule, and the building blocks of an enzyme mimic becomes clear.

1.8 Supramolecular Electrochemistry

1.8.1 Electrochemical Theory

Electrochemistry is a branch of science with a long and prestigious history.[29] Its foundations were first laid out by prominent scientists such as Faraday, Volta, Galvani

amongst many others, and now these scientists names are routinely used to designate constants, units and types of cells used in electrochemical theory and practice. Electrochemistry can be defined in a very general way as the study of chemical reactions to produce electric power or use electricity to affect chemical processes or systems. The first perspective concerns galvanic cells, while the second relates to electrolytic processes. Electron transfer processes can be viewed as the simplest type of chemical reactions, and are at the core of electrochemistry. The fundamental science behind this area of chemistry is the fact that oxidation-reduction reactions can be performed in such ways that allow the direct harvesting of the free energy released in these processes. For example, when considering the spontaneous reaction between Zn metal in a solution of Cu^{2+} ions, the oxidation (dissolution) of zinc is observed while the simultaneous reduction of copper ions takes place in the form of metallic copper deposits.

$$Zn(s) + Cu^{2+}(aq) \rightarrow Zn^{2+}(aq) + Cu(s)$$

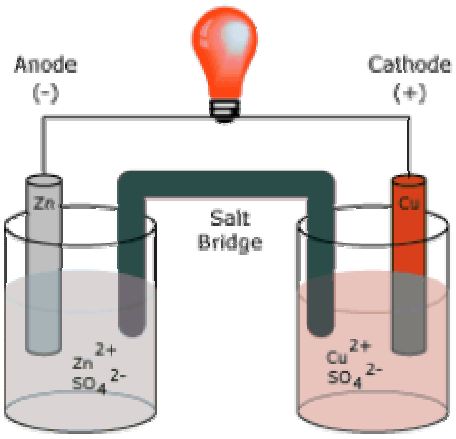

Figure 1.17 Components of a Galvanic Cell.

The same overall reaction can be carried out by immersing a Zn strip in a solution of Zn^{2+} ions and a Cu strip in a solution of Cu^{2+} ions (Figure 1.17). In this example, the reaction only starts when a clear pathway for the charges (electrons and ions) to circulate between the sites at which the Zn oxidation and Cu^{2+} reduction reactions that take place can be established. This is achieved by using a salt bridge, which allows the circulation of ions between the two solutions whilst preventing their mixing with one another. Under these conditions, a potential difference between the Zn and Cu strips develops. If the circuit is closed externally, the existing potential difference will give rise to a current, a flow of electrons moving from the Zn electrode (negative pole) to the Cu electrode (positive pole).

The free energy (ΔG°) of the overall chemical reaction taking place in the cell can be readily calculated as follows:

$$\Delta G^\circ = -nFE^\circ_{cell}$$

Where n is the total number of electrons transferred in the reaction, F is Faraday's constant and E°_{cell} is the standard cell potential of the cell. Electrochemical reactions are heterogeneous in nature as they take place at interfaces, usually metal-solution boundaries. By definition, an electrode where a reduction (uptake of electrons by a solution species) takes place is called a *cathode*. Conversely, an *anode* is an electrode where an oxidation (loss of electrons by a solution species) occurs. By applying these definitions to the cell in Figure 1.17 we can conclude that the Zn electrode is the anode and the Cu electrode serves as the cathode.

A net electrochemical reaction implies the transfer of charge across the corresponding metal-solution boundary and the flow of current across the electrode. The current, i, a basic electrical quantity, affords an instantaneous measurement of the rate of the electrochemical reaction according to the following equation:

$$i = nFAr$$

Where n is the number of electrons transferred in the interfacial reduction or oxidation process, F is Faraday's constant, A is the surface area of the metal-solution boundary, and r is the instantaneous reaction rate. Since current measurements are easily done with modern instrumentation, a peculiar feature of electrochemical techniques is that they provide a continuous monitoring of the reaction rate. Integration of the current over a period of time affords the electrical charge, Q, which can be transformed in to the amount of material in moles, N, converted in the electrochemical reaction using Faraday's law:

$$Q = nFN$$

Another quantity of fundamental importance in electrochemistry is the electrode potential, which can be considered as an adjustable driving force for the electrochemical reactions. In general terms, as the potential of an electrode is made more negative, the average energy of the electrons in the metal, which is approximately equal to its Fermi level, becomes higher, giving the electrode more reducing power. Similarly, the oxidising power of an electrode can be increased by making its potential more positive. While these qualitative arguments

are perfectly straightforward, the definition of electrode potentials is complicated by the fact that the potential of a single electrode is not an experimentally measurable quantity. In simple terms, electrode potentials are always measured against a second, reference electrode, whose value is arbitrarily taken as zero. The potential of the standard hydrogen electrode (SHE) is generally assigned as a standard value of zero and serves as the primary reference for any other electrodes. For a generalised process involving the transfer of *n* electrons:

$$Ox + ne \rightarrow Red$$

Where *Ox* or *Red* represent the oxidised and reduced partners of the redox couple, the thermodynamic potential, *E*, of the corresponding electrode is given by the well known Nernst equation, which is unquestionably one of the most important equations in electrochemistry:

$$E = E^{\circ} - \frac{RT}{nF} \ln \frac{a_{ox}}{a_{red}}$$

Where E° is the potential under standard conditions, a_{ox} and a_{red} are the activities of the respective oxidised and reduced species, *R* is the universal gas constant and *T* is the temperature in degrees Kelvin. To avoid the complications associated with the use of thermodynamic activities and activity coefficients, very often activities are replace with concentrations. In this case, the standard potential is replaced by the formal potential, $E^{\circ\prime}$, which is usually dependant upon medium conditions since it includes the activity coefficients. Therefore, a more practical version of the Nernst equation is as follows (the factor 2.303 reflects the replacement of natural by decimal logarithms):

$$E = E^{\circ\prime} - \frac{2.303RT}{nF} \log \frac{[Ox]}{[\mathrm{Re}\,d]}$$

The Nernst equation is a thermodynamic equation and thus can only be rigorously applied to equilibrium situations ($i = 0$). However, regardless of this apparent limitation, the above equation is successfully applied when current flows across the electrode in question, as long as the heterogeneous electron transfer process is fast, or in electrochemical terms, reversible. Under these conditions, the equation is useful to calculate the concentrations at the electrode surface of *Ox* and *Red* that are generated when specific potential values are imposed on the electrode. Fast electron transfer kinetics allows the electrochemical

reaction to adapt quickly to the changing potential values on the electrode surface, maintaining a pseudo-equilibrium situation as well as the validity of the Nernst equation. Finally, in order to complete the picture of the galvanic cell, the potential of a cell can be calculated using the following equation:

$$E_{cell} = E_{cathode} - E_{anode}$$

In this equation, the cathode and anode potentials are obtained individually using the above Nernst equation.

1.8.2 Potential Sweep Methods: Voltammetry

In potential sweep methods the potential of the working electrode (measured against the reference electrode of choice) is varied continuously according to a predetermined potential waveform (excitation function), while the current is measured as a function of the potential. Potential sweep methods or voltammetric techniques are in widespread use today as they provide a quick and straightforward assessment of the redox behaviour of molecular systems, and constitute the group of electrochemical techniques most commonly used by supramolecular chemists.[30]

1.8.2.1 Linear Sweep Voltammetry

The simplest potential sweep method is linear sweep voltammetry (LSV). In this technique the potential of the working electrode is varied linearly with time between two values, the initial and final potentials (E_i and E_f , Fig. 1.18). Since the electrode potential is always changing throughout the experiment, a level of capacitive or charging current flows continuously. Faradaic current will also flow when the potential reaches values at which the species in solution can undergo electrochemical conversions. For example, in an experiment where a solution contains a reducible compound *Ox* as the only electroactive species, a voltammetric scan can begin at a potential at which no electrochemical reactions take place, $E>E_{½}$, Usually the potential will be linearly scanned in the negative direction and faradaic currents will be detected near, around, and beyond the half-wave value, where the conversion $Ox \rightarrow Red$ is favoured. If the solution is kept quiescent (so that diffusion is the only mass transport mechanism possible) and the *Ox*/*Red* couple is chemically reversible, the electrochemical conversion gives rise to a characteristic cathodic wave (Fig. 1.19), with a maximum current value given by the Randles-Sevčik equation:

$$i_p = (2.69x10^5)n^{2/3}AC_{Ox}(D_{Ox}v)^{1/2}$$

Where the peak current i_p is given in μA, A is the projected electrode area (in cm^2), D_{Ox} is the diffusion coefficient of the electroactive species expressed in cm^2/s, C_{Ox} is its concentration (mM), and ν is the scan rate in V/s. It is important to use the specified units as the equation contains a numeric factor that results from the evaluation of several constants. The Randles-Sevčik equation is one of the most important equations in voltammetry, however it only applies when the current is diffusion controlled and hemispherical diffusion is unimportant (assuming that a planar electrode of conventional size is used).

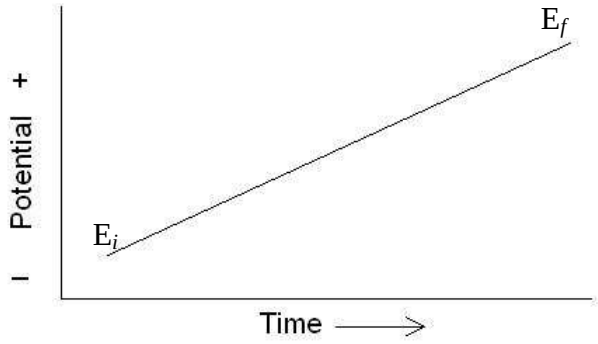

Figure 1.18 Excitation waveform used in linear sweep voltammetry (cathodic scan).

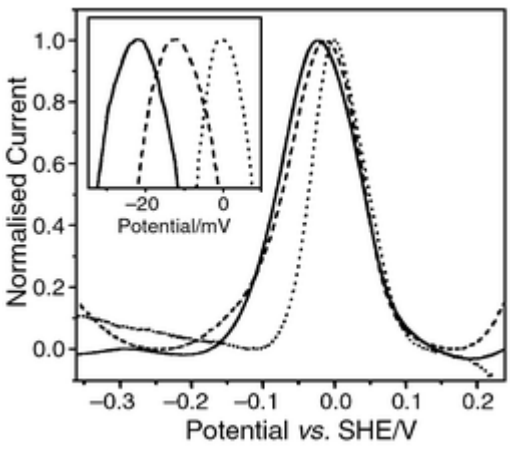

Figure 1.19 An example of a linear sweep voltammogram.

An important point to note is that the potential of the voltammetric peak does not equal the half-wave potential of the corresponding redox couple. For reversible electrochemical couples, the cathodic peak occurs at 20-30 mV more negative than the $E_{½}$ value and its position is independent of the scan rate. The position of the peak represents the onset of

diffusion control on the current, whereby beyond the peak potential the current is no longer dependant upon the potential, and is fully controlled by the rate of diffusion, which decreases gradually as the thickness of the diffusion layer increases, therefore it is necessary to go past the half-wave potential to reach so-called Cottrell-like conditions. For slower (irreversible) electrochemical couples, a peak may or may not be reached. If the voltammogram exhibits a peak, the corresponding peak potential will shift cathodically as the scan rate increases.

1.8.2.2 Cyclic Voltammetry

Cyclic voltammetry (CV) is based upon the same principles as linear sweep voltammetry, however in CV the potential of the working electrode is scanned back after reaching a certain value E_s, the switching potential. Figure 1.20 shows a typical excitation waveform for CV, whereby the reverse scan is set to end at the initial potential and the experiment is run for two cycles, but this does not have to be the case in every CV experiment. It is possible to utilise excitation waveforms with any number of linear segments. It is not unusual to extend the reverse scan past the initial potential and have a third linear segment to take it back to the initial value. Scan rates can also be varied for each linear segment of the waveform.

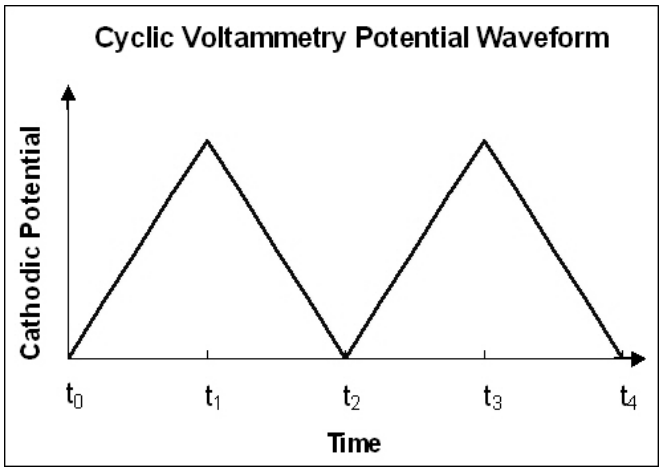

Figure 1.20 A typical potential excitation waveform used in CV

The key advantage of CV over simple LSV results from the reverse scan. Reversing the scan after the electrochemical generation of a species is a direct and straightforward way to probe its stability. A stable electrochemically generated species will remain in the vicinity of the electrode surface and yield a current wave of opposite polarity to that observed in the forward scan. An unstable species will react as it is formed and no current wave will be

detected on the reverse scan. A typical cyclic voltammogram for the reversible reaction of *Ox* to *Red* is shown in Figure 1.21.

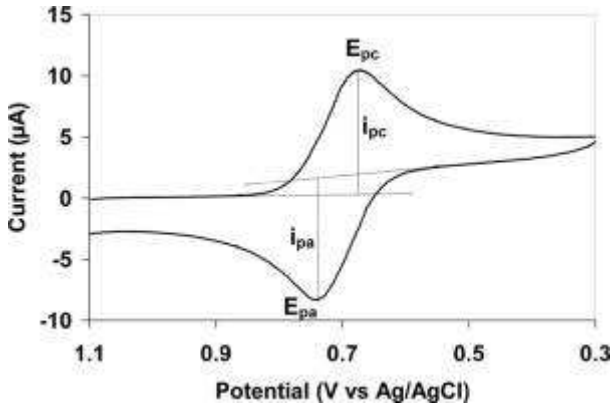

Figure 1.21 Cyclic voltammetric response for a reversible redox couple.

The electrochemical process is fast in the time scale of the experiment and the electrochemically generated species *Red* is perfectly stable in the electrolytic solution. Under those conditions, and assuming the solution is kept unstirred during the experiment, the ratio of the cathodic and anodic peak currents, measured in the forward and reverse scans respectively, should be equal to one. Deviations from unity reveal the presence of chemical reactions involving either redox partner (*Ox* or *Red*) or both partners. The average of the two peak potentials affords the half-wave potential for the corresponding couple:

$$E_{1/2} = \frac{(E_{pc} + E_{pa})}{2}$$

In the forward scan of an experiment, the peak current is given by the Randles-Sevčik equation as it is in LSV experiments. This equation is often used to analyse the behaviour of a redox couple by plotting peak currents as a function of the square root of the scan rate. A linear plot is often taken as evidence for the reversible character of the couple and demonstrates that the currents are controlled by planar diffusion to the electrode surface. The slope of such a plot can also be used to determine the diffusion coefficient of the electroactive species if both A and C_{ox} are known. However this is not a recommended method to determine diffusion coefficient values, as the peak currents are usually obtained with sizeable error margins and the slope of the plot depends only on the square root of the diffusion coefficient. Voltammetric experiments with ultra-microelectrodes are much preferred for the determination of coefficient values.

Another method to assess the reversibility of a redox couple is the evaluation of the potential difference between the peak potentials (ΔE_p) of the anodic and cathodic peaks associated with the couple. Based on numerical solutions of the current-potential response in CV experiments,[30] a value of 57/n mV (at 25°C, first cycle voltammogram) is expected for a reversible redox couple. It is important to realise that this value will only be obtained if the switching potential is at least 200 mV beyond the peak potential observed in the forward scan. The proximity of the switching potential to the voltammetric peaks leads to increased ΔE_p values. Furthermore, the presence of uncompensated cell resistance also leads to increased ΔE_p values. If care is taken to ensure levels of uncompensated resistance are small and that the switching potential is at least 200 mV beyond the forward scan peak potential, the observed deviations from the theoretical ΔE_p value can be used to estimate the standard rate constant ($k°$) for the heterogeneous electron transfer process.

As previously mentioned, the half-wave potential ($E_{½}$) can be readily obtained from the midpoint between the two peak potentials for a reversible or quasi-reversible redox couple. This value is characteristic of a redox couple and is typically within a few mV of the formal potential for the couple ($E°´$) according to the following equation:

$$E_{1/2} = E°' - \frac{RT}{2nF} \ln \frac{D_{ox}}{D_{red}}$$

In this equation, the ratio of the diffusion coefficients D_{ox} and D_{red} is usually very close to unity. The easy determination of half-wave potentials and estimation of formal potentials is an extremely attractive feature of CV.

1.8.2.3 Square Wave Voltammetry

This technique relies on excitation functions that combine the features of a large-amplitude square wave modulation with a simple staircase waveform (Figure 1.22). The current is sampled at the end of each potential plateau. In each potential cycle, the current function is the differential value between the forward and reverse currents $\delta i = i_{for} - i_{rev}$ which, when plotted against the average potential of each waveform cycle, affords peak-shaped voltammograms with excellent sensitivity and charging current rejection (Figure 1.23). The peak height is directly proportional to concentration of the electroactive species and direct detection limits as low as 10^{-8} M are possible.

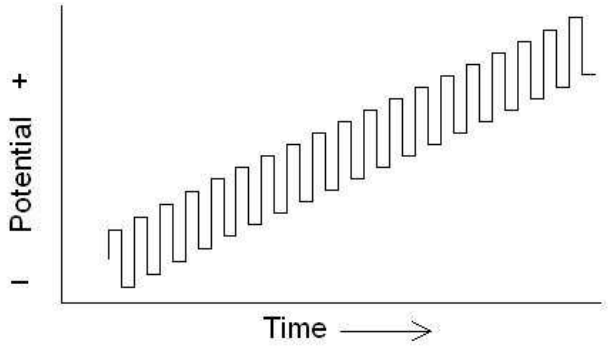

Figure 1.22 A typical excitation function for square wave voltammetry

Square wave voltammetry has several advantages. Among these are its sensitivity and rejection of current backgrounds, but others include its speed and ability to be computer controlled. By combining the two latter properties, experiments can be carried out repetitively with an increase in the signal to noise ratio. Applications for this technique include the study of electrode kinetics with regards to preceding, following or catalytic homogenous chemical reactions and the determination of some species at trace levels.

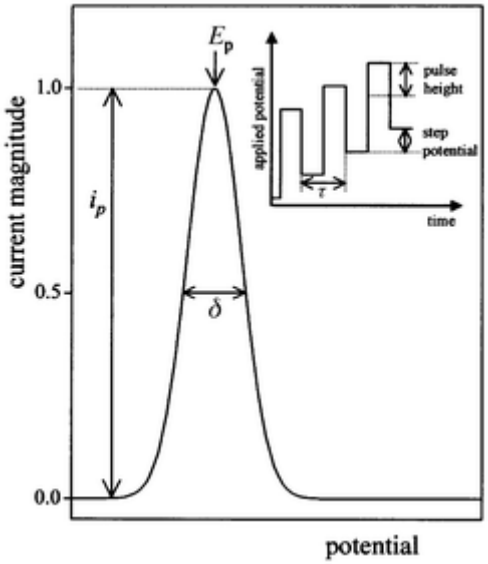

Figure 1.23 An example of a square wave voltammetric response.

Chapter Two

2 Chapter Two – Deazaflavin Model Systems

2.1 Introduction

2.1.1 Outline

Non-covalent supramolecular interactions involving flavin molecules are present in a wide range of biological systems, predominantly those involving electron transfer processes.[31, 32] The deazaflavins are a subclass of the parent flavin species, whereby one or more of the nitrogen atoms of the parent isoalloxazine ring are replaced by a CH group.

Although extensive research has been carried out on riboflavin and its derivatives, little interest has been paid to the deazaflavin family of compounds, and to what effect its structural changes have on its ability to non-covalently bind to another species, or undergo electron transfer processes.

2.1.2 The Flavin Cofactor

2.1.2.1 Background

Since their discovery and chemical characterisation in the late 1930s, flavins have been recognised as being capable of both one- and two-electron transfer processes, and as playing a pivotal role in the coupling of the two-electron oxidation of most organic substrates to the one-electron transfers of the respiratory chain.[33, 34] In addition, they are now known as versatile compounds that can function as electrophiles and nucleophiles, with covalent intermediates of the flavin and substrate frequently being involved in catalysis.[35, 36] Flavins and flavoproteins are involved in a wide variety of biological processes including the production of superoxide, the reduction of hydroperoxide, hydroxylation of aromatic compounds, and the production of light in bioluminescent bacteria to mention a few.[37, 38] The chemical versatility of flavoproteins is controlled by specific interactions with the protein with which they are bound.[39, 40] A large section of current research surrounding flavins and flavoproteins is to try and define the nature of these interactions, and to understand in chemical terms the various steps involved in catalysis by flavoprotein enzymes.

2.1.2.2 Structure and Function

Flavoenzymes consist of two essential components, a flavin-based redox cofactor and the apoprotein. In naturally occurring systems, the flavin cofactor is usually present as either flavin mononucleotide (FMN) or flavin adenine dinucleotide (FAD). Both of these species are derived from riboflavin (vitamin B_2). Figure 2.1 shows the structures of these three main flavin derivatives.

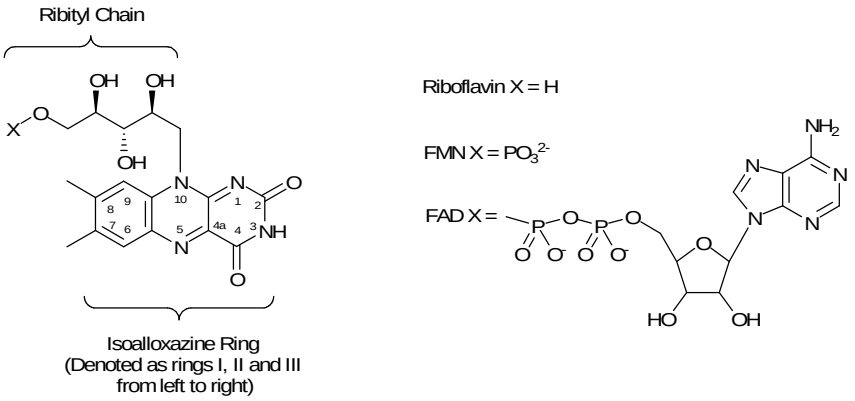

Figure 2.1 Structure of riboflavin, FMN and FAD

The apoprotein in flavoenzymes serves both to form a binding pocket for the cofactor and to regulate cofactor redox properties. The distinctive differences between flavin microenvironments in different flavoenzymes effectively tune the redox properties of the cofactor to meet the desired function of the given flavoenzyme. X-ray crystallography has provided a great deal of information on the identities and relative positions of the components of the flavoprotein microenvironment, but does not yield direct insight into the mechanism or redox/recognition properties of the enzymes. [23]

The heterocyclic flavin cofactor is composed of a hydrophobic xylene moiety and a relatively hydrophilic pyrimidine unit capable of forming hydrogen bonds to the apoenzyme. The pyrimidine is fused to the central heterocyclic ring forming a pteridine-like structure (a closely related family of compounds also possessing important biological activity). The fusing of all three aromatic rings form the isoalloxazine core of the flavin compound. Flavins possess three accessible oxidation states: oxidised, semiquinone radical (or semiquinoid) and fully reduced. At each of these levels, the chemical properties of the flavin are very different, particularly those associated with the pyrimidine moiety. Protonation can occur at various positions of the isoalloxazine core, N(1), N(3) and N(5).

With electrochemical behaviour closely related to that of the quinones, the oxidised flavin (**Fl_{ox}**) can be reduced in a two-electron process to form the flavohydroquinone anion (**$Fl_{red}H^-$**). Reduction can also occur sequentially via a two-electron process involving the flavosemiquinone radical, in either the anionic (**Fl_{rad}^-**) or neutral (**$Fl_{rad}H$**) form, illustrated in Figure 2.2.[24, 35]

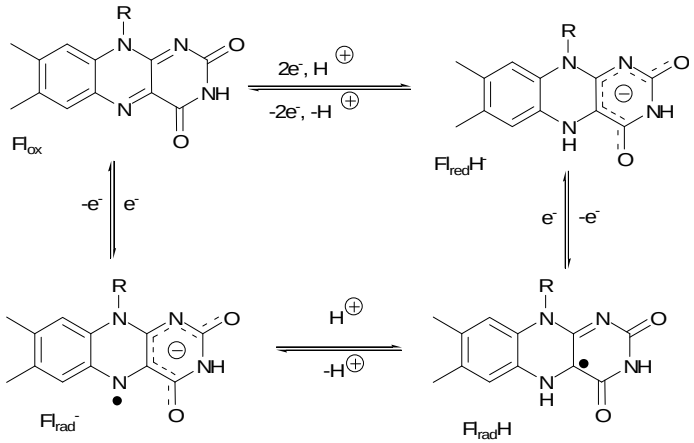

Figure 2.2 Common redox and protonation states of the flavin cofactor

When compared with other types of biologically active enzymes, flavoenzymes can be considered as unique catalysts owing to their ability to carry out a wide range of biological processes. They can catalyse a variety of redox transformations including the oxidation of amines to imines, thiols to disulfides and the hydroxylation of aromatic species. Also included in their researched activity is the ability to mediate between single electron redox processes involving iron-heme and iron-sulphur clusters and the essential two-electron redox processes of NADH. There are five classes of flavoenzyme-catalysed reactions: dehydrogenation, disulfide reductions, one- or two-electron transfer, and oxygen activation leading to the formation of hydroperoxide or oxygen insertion (Figure 2.3). Since the flavin cofactor cannot easily dissociate from the apoprotein, each catalytic cycle contains an oxidative and reductive half reaction.

Dehydrogenases:

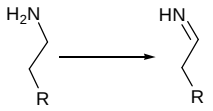

Disulphide Reductases:

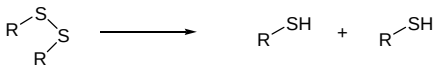

Electron Transferases:

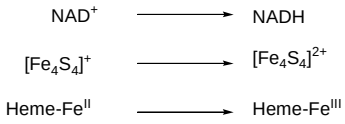

Oxidases:

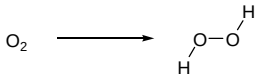

Mono-oxygenases:

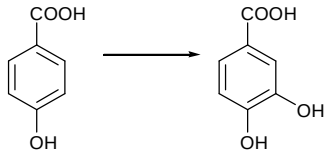

Figure 2.3 Classes of flavoenzymes and their types of catalysed reactions.

Most flavoenzymes will carry out two of the above mentioned categories of reactions. Dehydrogenation often constitutes the reductive half-reaction. Cofactor modification is the key to the catalytic activity and diversity of flavoenzymes. Free flavin will only catalyse the above mentioned reactions in rare circumstances[41] and only under extreme conditions.[42, 43] Since with only a few exceptions, the flavin cofactor is non-covalently bound to the apoprotein, this cofactor modification is achieved through molecular recognition interactions such as hydrogen bonding, π-stacking, dipolar and hydrophobic interactions.[34, 44]

2.1.2.3 Flavin Electrochemistry

Redox events and molecular recognition are intrinsically linked in most biological enzyme systems, and more obviously in the case of the flavoenzymes, where proteins and cofactors interact to regulate the reactivity of the cofactor. Enzymes containing redox-active organic molecules such as quinones, flavins, nicotinamides and pterins selectively stabilise specific oxidation and protonation states of the cofactor through certain non-covalent interactions.

The effects of such non-covalent interactions are difficult to isolate and quantify in biological systems. However using synthetic model systems, the effects of various molecular recognition elements on the redox behaviour and physical properties of the redox-active molecules can be probed.

Flavoenzymes are able to control the redox pathways that the cofactor follows, allowing catalysis of both one- and two- electron redox processes. The processes occurring during the reduction of flavins in aprotic organic solvents have been the subject of much speculation and controversy over the past 30 years. A combination of techniques, including cyclic voltammetry (CV), simultaneous electrochemical electron paramagnetic resonance (SEEPR) and UV-vis spectro-electrochemistry have been used to establish that intermolecular proton transfer of the acidic imide proton of the oxidised flavin (**Fl_{ox}**) causes the coupled electrochemical an chemical reactions shown in Figure 2.4.

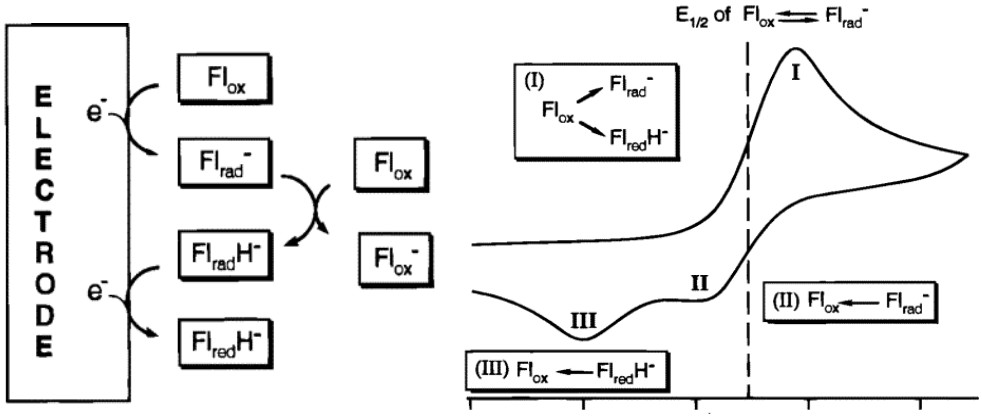

Figure 2.4 **(a) Schematic representation of the *ece* pathway for two-electron reduction of isobutyl flavin in aprotic media and (b) Cyclic Voltammogram of isobutyl flavin consisting of the reduction wave I and oxidation waves II and III caused by reoxidation of Fl_{rad}^- and $Fl_{red}H^-$ respectively.**

In this process, **Fl_{ox}** is reduced to the radical anion **Fl_{rad}^-** at the electrode.[45] A portion of this anionic species is then protonated by the imide of **Fl_{ox}** in the bulk solution, yielding the neutral radical **$Fl_{rad}H$**. Since **$Fl_{rad}H$** has more positive reduction potential than **Fl_{ox}**, it is instantly reduced to the **$Fl_{red}H^-$**. This *ece* (electrochemical-chemical-electrochemical) process gives rise to only one reduction wave in the cyclic voltammogram. During the re-oxidation process, **Fl_{rad}^-** is oxidised at more negative potentials than **$Fl_{red}H^-$**, resulting in the two oxidation waves observed. Because the **Fl_{ox}** $\rightarrow$ **Fl_{rad}^-** couple is essentially reversible, the ΔG value for this process can be obtained directly from the half-wave potential $E_{½}$.

The electrostatic potential map fully oxidised flavin and radical anion flavin were generated using B3LYP wave function calculations (Figure 2.5).[35] It shows the highly electron deficient flavin nucleus with distinct areas of positive potential potential (blue) adjacent to the C(4a)-C(10a) ring juncture of the flavin. These areas would be expected to interact favourably with donor atoms. Reduction of the flavin to the radical anion converts this region of the surface to negative potentials diminishing interactions with donor atoms. This loss of the favourable donor atom-selective binding of the oxidised flavin should make the reduction of the flavin more difficult, resulting in the modulation of the flavin redox potential to more negative values.

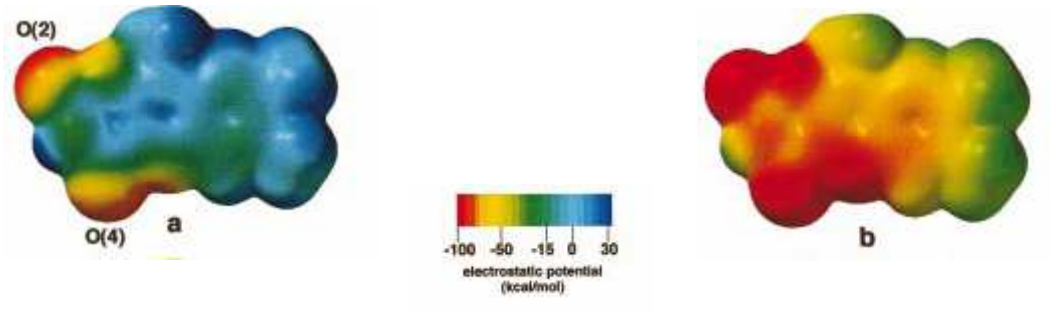

Figure 2.5 Electrostatic potential maps of (a) oxidised flavin (Fl_{ox}) and (b) flavin radical anion (Fl_{rad}^{-}).[35]

2.1.2.4 Redox Modulation through Non-Covalent Interactions

The bonding of the flavin cofactor to the protein backbone provides two main functions. Firstly to enable retention and overall orientation of the cofactor, but also to enable control the redox behaviour of the cofactor through selective stabilisation of different oxidation and protonation states. Hydrogen bonding, π-stacking and dipolar interactions are essentially electrostatic in nature, therefore molecular recognition events are expected to be sensitive to electron density distribution within the host-guest complex, and this electron density is affected by the oxidation state of the molecule concerned. In the case of the flavin unit, in the oxidised state, the central ring of the flavin has a more positive character, allowing generally more favourable π-stacking interactions with electron rich aromatic systems and favourable interactions with electron-rich functional groups. However, in the radical anion state, the central ring of the flavin has a more negative character, making interactions with adjacent electron-rich systems highly unfavourable. It is also observed that upon a one-electron reduction of the flavin, the potential of the carbonyl O(2) and O(4) atoms becomes more negative, and therefore act as stronger hydrogen bond donors.

These carbonyl oxygens, O(2) and O(4), along with the imide proton N(3)H have been identified as a key motif in enzyme-cofactor interactions.[46] The study of this particular functional group is of huge importance when attempting to understand the processes that take place at the active site of the enzyme. Biomimetics allows the synthesis of small molecules that replicate complementary hydrogen donor/acceptor groups that would be present at the active site of the enzyme. Figure 2.6 shows a suitable host-guest system, developed by Rotello and co-workers, between a flavin unit and a diaminopyridine (DAP) molecule. The interaction between the two can be followed by a number of techniques, however NMR titration and cyclic voltammetry can provide accurate results quickly and easily.[45]

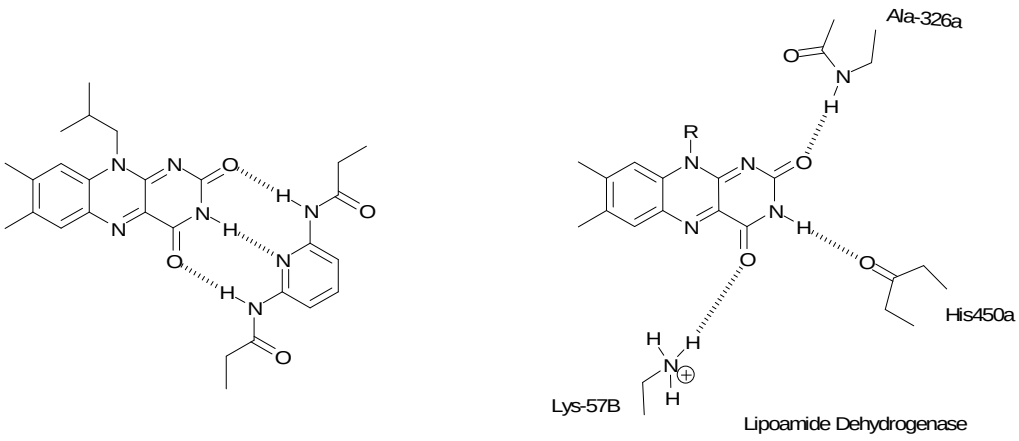

Figure 2.6 Flavin-DAP supramolecular system and the active site of Lipoamide Dehydrogenase.

This complementary three-point binding between the two molecules was studied by plotting the chemical shift of N(3)H of the flavin unit in deuterated chloroform while increasing equivalents of diaminopyridine were added. Furthermore, investigation using cyclic voltammetry showed that not only did the reduction potential of the flavin become more positive when bonded to the DAP unit (110-120 mV increase), but the first oxidation wave of the flavin (corresponding to the re-oxidation of $\mathbf{Fl_{rad}^-}$) becomes more defined, indicating a suppression of *ece* within the complex. The observed shift in redox potential illustrates just how the flavin radical anion is stabilised by the existence of the three-point hydrogen bond system.

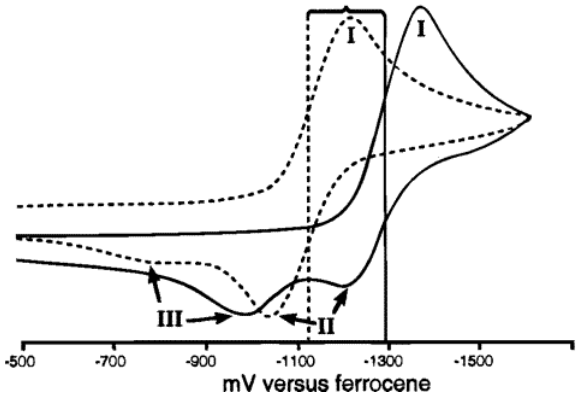

Figure 2.7 **Cyclic voltammograms for isobutyl flavin and the isobutyl flavin-DAP complex showing the single reduction wave (I) and the two oxidation waves (II) and (III).[45]**

As predicted computationally, the reduction of $\mathbf{Fl_{ox}^{-}}$ to $\mathbf{Fl_{rad}^{-}}$ leads to an increase in charge density on the carbony oxygens O(2) and O(4) of the flavin, making them stronger hydrogen bond donors. This redox-based enhancement in recognition can be quantified through the use of a thermodynamic cycle, where experimentally accessible K_a and $E_{½}$ values are used to determine the ΔG and K_a for binding of $\mathbf{Fl_{rad}^{-}}$ to the receptor.[35] Using this method, a 500-fold increase in binding constant to the DAP unit was observed upon reduction of $\mathbf{Fl_{ox}^{-}}$ to $\mathbf{Fl_{rad}^{-}}$. This relationship was calculated using the following equation:

$$K_a(red) / K_a(ox) = \mathbf{e}^{(nF/RT)(E½(bound) - E½(unbound))}$$

Where $K_a(ox)$ *and* $K_a(red)$ are the association constants in the oxidised and reduced form of isobutyl flavin, and the $E_{½}(unbound)$ *and* $E_{½}$ *(bound)* are the standard potentials in the unbound and bound form. According to this equation, enhanced binding ($K_a(red)/K_a(ox) > 1$) inherently accompanied a positive shift in the $E_{½}$ value ($E_{½}(bound) - E_{½}(unbound)$) and vice versa. The substituent on the pyridine side chain alters the hydrogen bonds between the flavin and receptor, by either making them stronger or weaker.

2.1.3 The Deazaflavin Cofactor

Riboflavin and nicotinamide are by far the most common carbon-based redox cofactors used by enzymes, but there are several other heterocyclic redox cofactors used by particular enzymes.[47]

The deazaflavins are a subclass of the parent flavin species whereby one or more of the nitrogen atoms of the parent isoalloxazine ring is replaced by a CH group. Factor F_{420} was

isolated in 1978 by methanogenic bacteria (strictly anaerobic bacteria which ferment acetate to methane and carbon dioxide) in yields of up to 100 $mg.kg^{-1}$ cells. It was found to have a structure similar to that of riboflavin, except that the N(5) atom is replaced by a CH group. The discovery of this deazaflavin prompted an investigation into the properties of other deaza-analogues of riboflavin, shown in Figure 2.8, with the most common analogues being the 1- and 5-deazaflavins.[48]

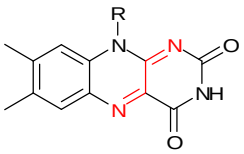

Flavin
One and two electron transfer
E_o= -210mV

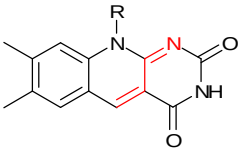

5-Deazaflavin
Two electron transfer ONLY
(unstable semiquinone radical)
E_o= -310mV

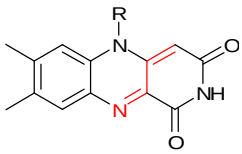

1-Deazaflavin
One and two electron transfer
E_o= -280mV

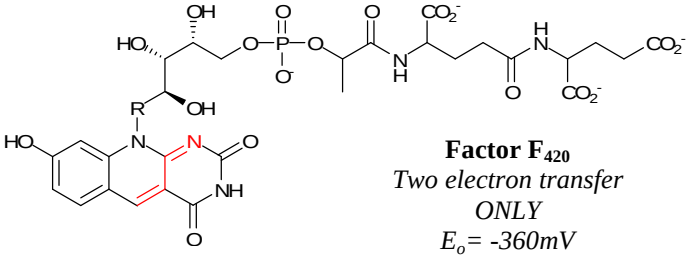

Factor F_{420}
Two electron transfer ONLY
E_o= -360mV

Figure 2.8 Structure and potentials of natural and synthetic deazaflavins.

Subtle alterations in the structure of the isoalloxazine ring results in major changes in flavin electrochemistry. Of the species shown in Figure 2.8, both the parent flavin and its 1-deazaflavin analogue are capable of participating in one and two electron transfer reactions, with the 1-deazaflavin possessing a lower redox potential than its parent. Factor F_{420} and the 5-deazaflavin analogue on the other hand are only capable of participating in one-electron transfer reactions (since neither has a stable semiquinone form), accompanied by a 100mV decrease in redox potential. In terms of redox potential and electron transfer reactivity, both 5-deazaflavin analogues are more closely associated with the nicotinamide cofactor than its parent compound, further illustrating the affect of changes in the isoalloxazine ring structure.

Factor F_{420} is used as a cofactor in, amongst other enzymes, a nickel (Ni^{2+})-dependent hydrogenase enzyme found in methanogenic bacteria which uses hydrogen gas to reduce carbon dioxide to methane. Its role appears to be as one component of a complex chain of

electron carriers in this multi-enzyme complex. The redox potential of F_{420} is ideally suited for its role in this enzyme, since at -0.36 V its potential is higher than the redox potential for hydrogen (-0.42 V), but lower than the redox potentials of other redox cofactors such as NADH and flavin. Therefore, F_{420} is able to accept electrons from hydrogen and transfer them to NAD^+ of FAD. Recent research into the crystal structure of various F_{420} containing enzymes has resulted in successful resolution of the active site of one of these enzymes, showing how F_{420} binds within the active site.[49]

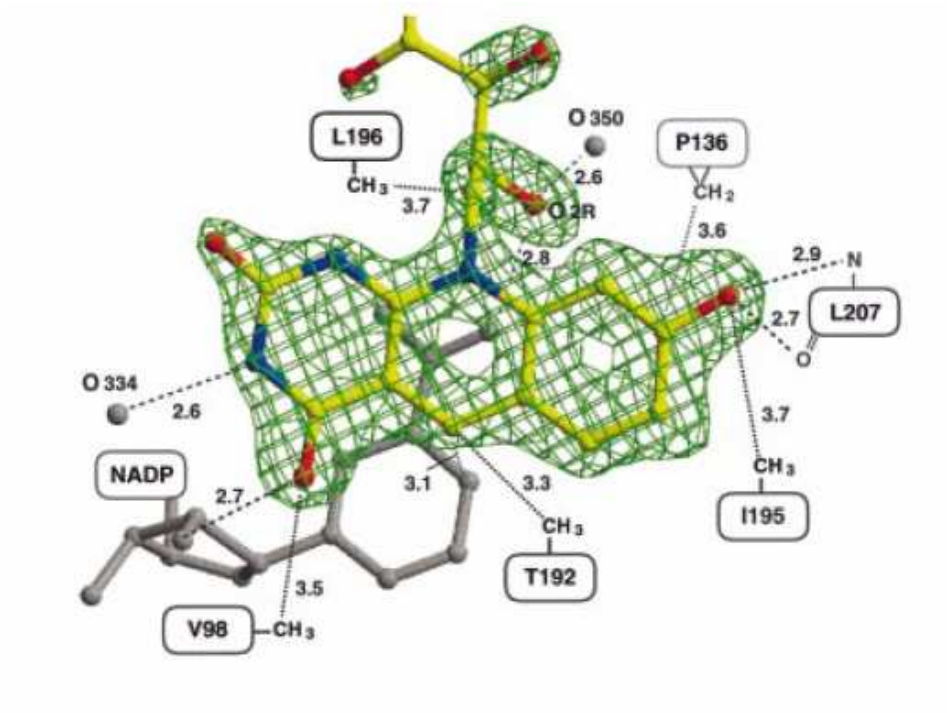

Figure 2.9 **Crystal structure of the active site of $F_{420}H_2$:$NADP^+$ oxidoreductase showing F420 and NADP including important noncovalent interactions.[49]**

2.1.4 Aim

Although extensive research has been carried out on riboflavin and its flavin derivatives as to their electrochemical, chemical and biological activity, little interest has been paid to similar reactivity of the deazaflavins and their reactivity when bound non-covalently to a guest species, most likely due to difficulties in their synthesis.[48] This study has probed the behaviour of the 1- and 5-deazaflavin derivatives when bound non-covalently to a guest species such as a diaminopyridine derivative as shown in Figure 2.10. In addition to the

synthesis and experimental study, computational calculations have also been carried out on the adduct analogues to gain a better insight into their geometric and electronic structure.

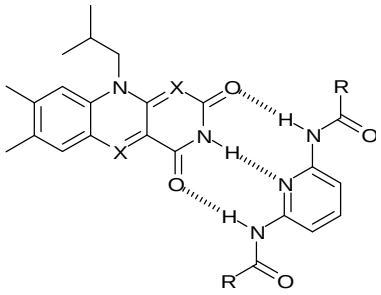

Figure 2.10 A target supramolecular deazaflavin-diaminopyridine complex (where X = NH or CH).

2.2 Results and Discussion

2.2.1 Synthesis

2.2.1.1 1-Deazaflavin Synthesis

The synthesis of the 1-deazaflavin derivative (**6**) has been successfully carried out based on the synthetic route developed by Kiessling and co-workers.[48] This route is outlined in Scheme 2.1.

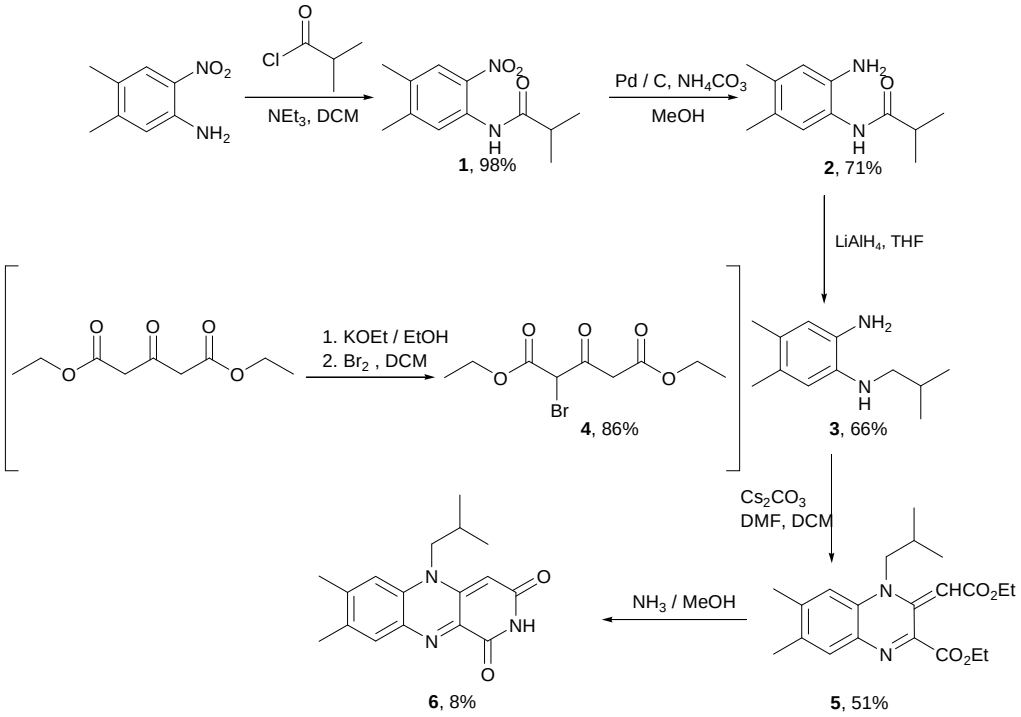

Scheme 2.1 Synthesis of the 1-deazaflavin derivative.

Acylation of 4,5-dimethyl-2-nitroaniline with isobutyryl chloride, followed by two subsequent reduction steps, afforded the alkylated amine compound (**3**). This was then coupled to the mono-α-brominated derivative (**4**), developed as shown from 1,3-acetonedicarboxylate, to afford the bicyclic compound (**5**) in 52% crude yield. Purification at this stage only served to decompose this unstable intermediate, and so the crude product was taken directly through to the next step. The crude residue was treated with methanolic ammonia to afford the 1-deazaflavin product (**6**) as a purple/black solid. The very low final yield is expected to be a result of its precursor's tendency to decompose rapidly.

2.2.1.2 5-Deazaflavin Synthesis

The synthesis of the 5-deazaflavin derivative (**9**) has been carried out based on the synthetic route reported by Yoneda and co-workers,[50] but incorporating some improvements developed by Kiessling and co-workers. This route is outline in Scheme 2.2.

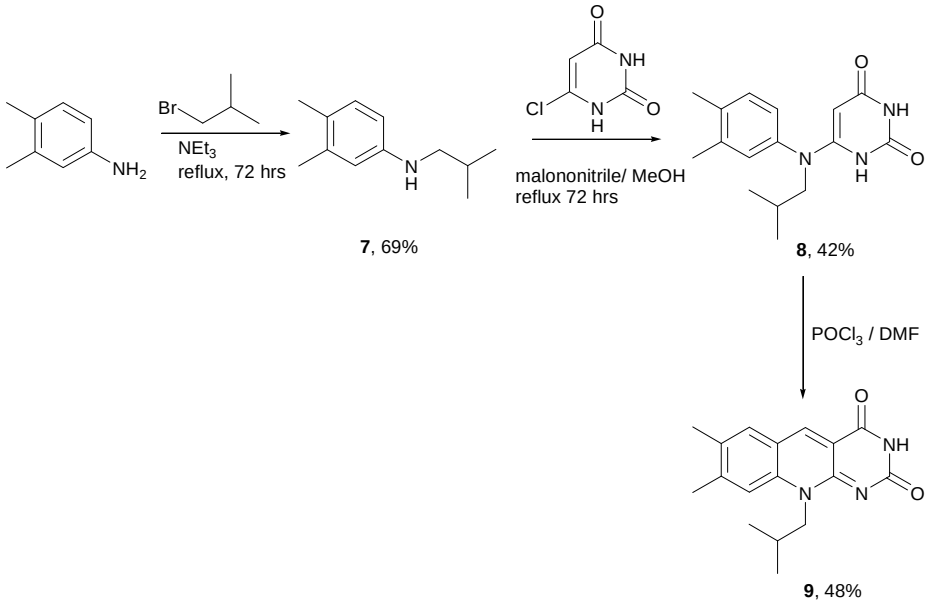

Scheme 2.2 Synthesis of the 5-deazaflavin derivative.

Treatment of 3,4-dimethyl aniline with 1-bromo-2-methyl pentane successfully afforded the alkylated product (**7**), which was then reacted with 6-chlorouracil in the presence of malononitrile to give the bicyclic alkyl anilino species (**8**). The final product (**9**) was then successfully prepared via the Vilsmeier method by treatment of **8** with phosphorous oxychloride in DMF. In contrast to the method reported by Keissling for this step, it was found that precipitation of the final product occurred without the need to neutralise the solution with ammonium hydroxide.

2.2.1.3 Isobutyl Flavin Synthesis

Scheme 2.3 outlines the synthetic route taken to produce isobutyl flavin. Acyl substitution of nitroaninline was carried out using isobutyryl chloride, followed by sequential reduction of the nitro group and the acyl group to afford the fully reduced flavin precursor (**12**). Coupling of this derivative to alloxan monohydrate afforded isobutyl flavin (**13**) in 59% yield.

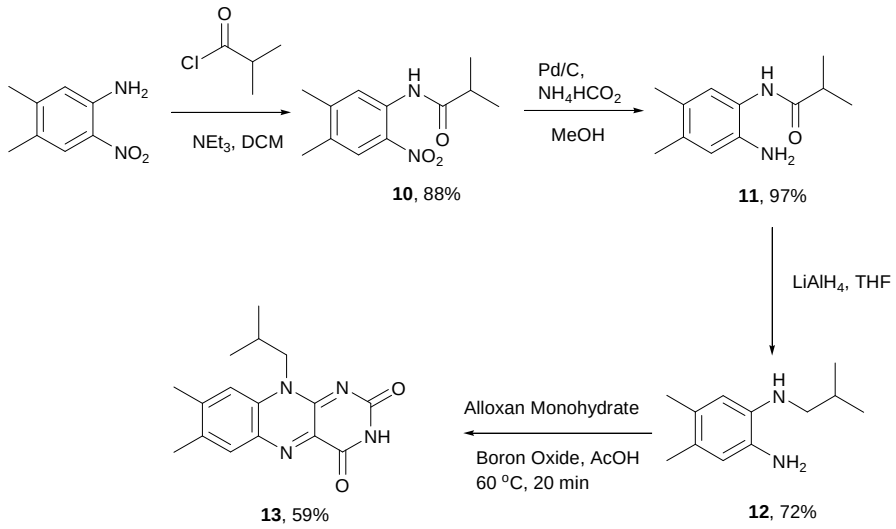

Scheme 2.3 Synthesis of *N*(10)-isobutyl flavin.

2.2.1.4 Diaminopyridine Synthesis

Synthesis of the proposed hydrogen bonded partner to the deazaflavins in this project, the diaminopyridine derivative (**14**), was carried out according to Scheme 2.4.

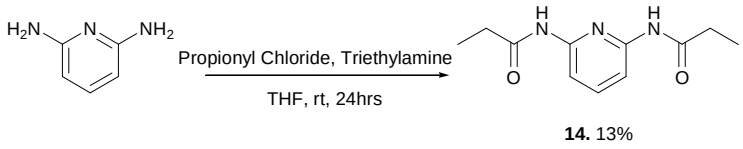

Scheme 2.4 Synthesis of the diaminopyridine derivative.

Treatment of 1,3-diaminopyridine with propionyl chloride in the presence of triethylamine in tetrahydrofuran afforded products of both the mono- and di-substituted isomers, with the di-isomer (**14**) in 13% yield.

2.2.2 Molecular Modelling

Density Functional Theory (DFT) calculations have been carried out on both the 1-deazaflavin and 5-deazaflavin models. This computational molecular modelling focuses on both the neutral and radical anion species in a supramolecular environment i.e. when non-covalently bound to the diaminopyridine derivative, and when no other compound is present. Calculations were carried out using the Gaussian 03 software at the B3LYP level. Firstly, the geometry of the deazaflavin alone was optimised using the 6-31G** basis set.

This geometry was then used to run a single point energy calculation at each redox state to determine the global minimum energy level. It is at this energy level that the electrostatic charges of the species were calculated. The same process was used to calculate the electrostatic charges of the deazaflavins when non-covalently bound to a receptor. This process results in the calculation of the electrostatic charges across the supramolecular complex in both redox states, and hence provides a picture of the electron density within the deazaflavin species.

2.2.2.1 1-Deazaflavin DFT Calculations

DFT calculations have been carried out on the 1-deazaflavin compound in both the neutral and radical anion electronic states (Figure 2.11a).

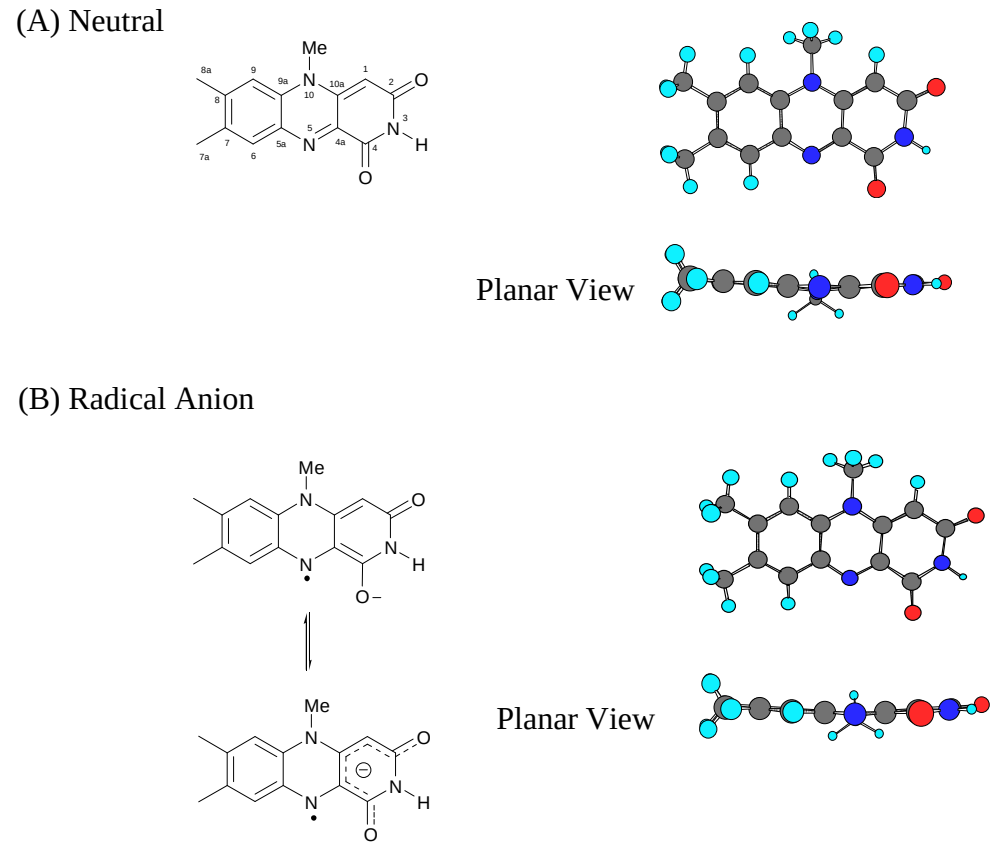

Figure 2.11a The 1-deazaflavin species in the (A) neutral and (B) radical-anion oxidation state.

Table 2.1 shows the charges and spin densities of relevant atoms within the 1-deazaflavin molecule.

Atom	Neutral	Radical Anion	
	Charge	Charge	Spin Density
C1	-0.254416	-0.292049	0.034831
C2	0.585217	0.565825	0.017787
(C2)O	-0.536440	-0.610975	0.055649
N3	-0.601736	-0.606521	-0.014520
(N3)H	0.281972	0.235118	-0.000279
C4	0.610350	0.534845	0.032303
(C4)O	-0.536748	-0.565504	0.086567
C4a	0.319236	0.106475	0.146870
N5	-0.584696	-0.606632	0.324666
N10	-0.576316	-0.631663	0.075811
C10a	0.234758	0.393460	0.016247

Table 2.1 Charges and spin densities of relevant atoms within the 1-deazaflavin molecule.

The results show the 1-deazaflavin has a planar structure across all three rings of the isoalloxazine system in both redox states. In the radical anion state, the radical electron is associated with the N(5) nitrogen, while the nearest carbonyl oxygen adopts the anionic charge. This can be rapidly delocalised across the π-electron system as shown in Figure 2.11a (B). The next set of calculations aimed to investigate the geometric and electronic structure of the 1-deazaflavin-DAP supramolecular adduct, in both the neutral and radical anion states. Figure 2.11b shows the neutral and radical anion 1-deazaflavin analogue when non-covalently bound to DAP.

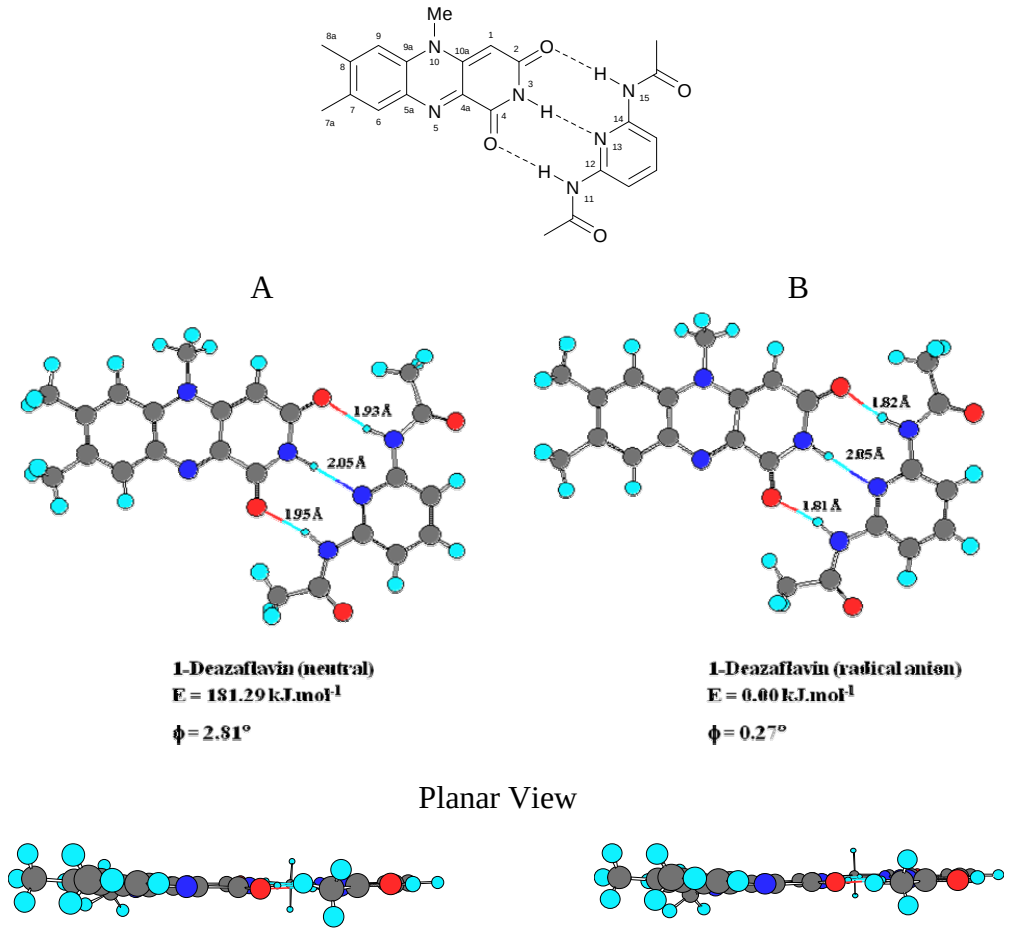

Figure 2.11b **Structure of the (A) neutral 1-deazaflavin and DAP complex and (B) the radical-anion 1-deazaflavin and DAP complex. Relative free energies are shown in kJ.mol^{-1}, and the torsion angle (Φ) between the two units given in degrees.**

Table 2.2 shows the charges and spin densities of relevant atoms within the complexes.

Atom	Neutral	Radical Anion	
	Charge	Charge	Spin Density
C1	-0.259810	-0.275807	0.000476
C2	0.616550	0.590352	0.033498
(C2)O	-0.538311	-0.626274	0.047846
N3	-0.648807	-0.644171	-0.016854
(N3)H	0.318697	0.302490	0.000049
C4	-0.177818	0.562429	0.061735
(C4)O	-0.500112	-0.587154	0.076561
C4a	0.162798	0.125855	0.094515
N5	-0.517294	-0.605041	0.368203
N10	-0.645342	-0.635167	0.086818
C10a	0.433904	0.399118	0.030864
N11	-0.628015	-0.624789	-0.000141
(N11)H	0.301285	0.321250	-0.000800
C12	0.502084	0.491556	0.000019
N13	-0.650479	-0.623075	0.000002
C14	0.501253	0.490411	-0.000026
N15	-0.629324	-0.623720	-0.000073
(N15)H	0.302116	0.319301	-0.000492

Table 2.2 Charges and spin densities of relevant atoms within the 1-deazaflavin-DAP complex.

Figure 2.11b shows Chem3D representations of the 1-deazaflavin-DAP complex in both redox states. The relative energies are given in $kJ.mol^{-1}$ and shows that the radical anion complex is 181.29 $kJ.mol^{-1}$ more stable than the corresponding neutral form. This is to be expected as the increased electron density across the carbonyl oxygens would allow stronger hydrogen bonds to form with the DAP partner. This stronger bonding is evident by the decrease in hydrogen bond length between the carbonyl oxygens from the deazaflavin species and the NH groups from the DAP unit of just over 0.1 Å. However the hydrogen bond distance of the central noncovalent interaction between the imido NH and DAP carbonyl does not change, indicating that the methyl “wings” of the DAP species bend toward the deazaflavin unit.

2.2.2.2 5-Deazaflavin DFT Calculations

DFT calculations have been carried out on the 5-deazaflavin compound in both the neutral and radical anion electronic states (Figure 2.12a).

(A) Neutral

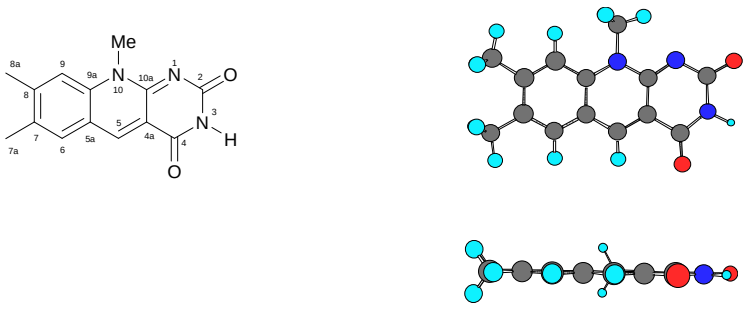

(B) Radical Anion

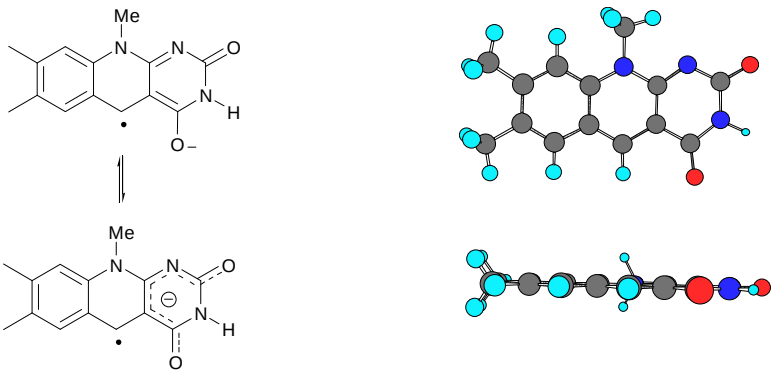

Figure 2.12a The 5-deazaflavin species in the (A) neutral and (B) radical-anion oxidation state.

Table 2.3 shows charges and spin densities of relevant atoms within the 5-deazaflavin molecule.

Atom	Neutral	Radical Anion	
	Charge	Charge	Spin Density
N1	0.095599	-0.638115	-0.001130
C2	0.687217	0.653681	0.011900
(C2)O	-0.490182	-0.580715	0.032601
N3	-0.599284	-0.590901	-0.005499
(N3)H	0.280518	0.238151	-0.000253
C4	0.595766	0.528283	0.037535
(C4)O	-0.509228	-0.589708	0.049721
C4a	-0.015898	-0.012020	0.039044
C5	-0.098815	-0.182038	0.440630
N10	-0.642771	-0.640553	0.071608
C10a	0.554569	0.500423	0.040340

Table 2.3 Charges and spin densities of relevant atoms within the 5-deazaflavin molecule.

The results show the 5-deazaflavin, like the 1-deazaflavin analogue, has a planar structure across all three rings of the isoalloxazine system in both redox states. In the radical anion state, the radical electron is associated with the C(5) carbon, while the nearest carbonyl oxygen adopts the anionic charge. This can be rapidly delocalised across the π-electron system as shown in Figure 2.11b (B). The next set of calculations aimed to investigate the geometric and electronic structure of the 5-deazaflavin-DAP supramolecular adduct, in both the neutral and radical anion states. Figure 2.12b shows the neutral and radical anion 5-deazaflavin analogue when non-covalently bound to DAP.

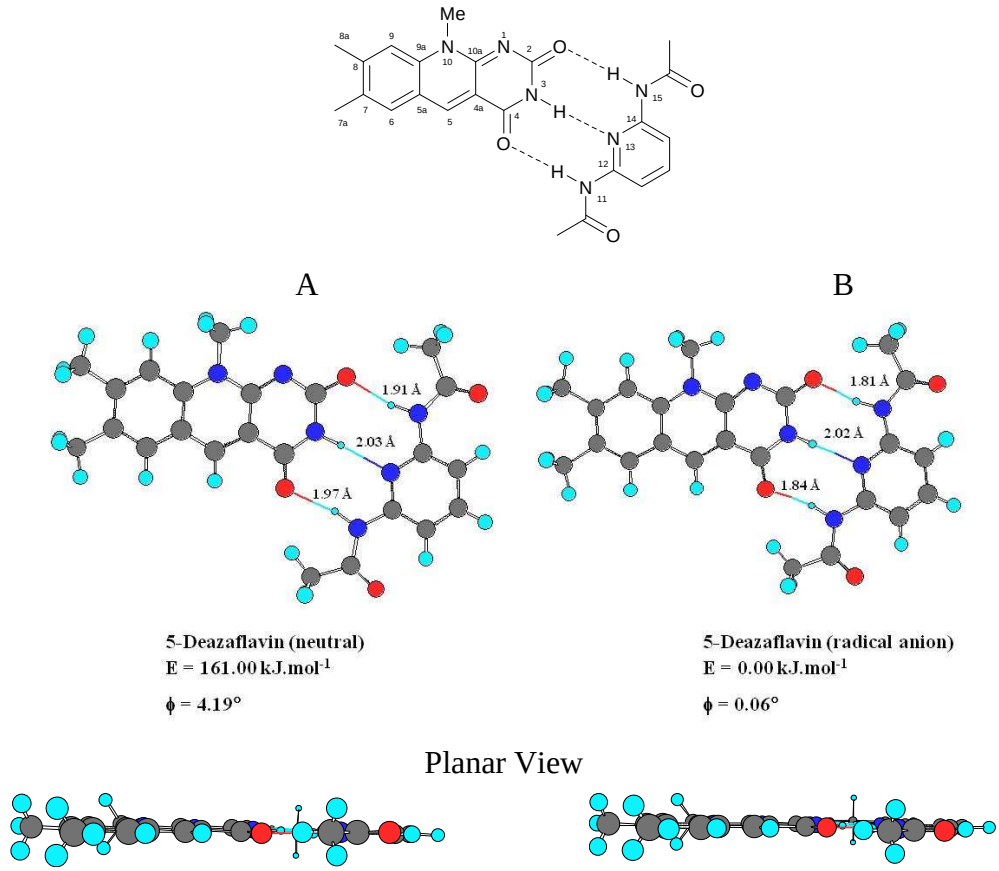

Figure 2.12b Structure of the (A) neutral 5-deazaflavin and DAP complex and (B) the radical-anion 5-deazaflavin and DAP complex. Relative free energies are shown in kJ.mol^{-1}, and the torsion angle (Φ) between the two units given in degrees.

Table 2.4 shows the charges and spin densities of relevant atoms within the complexes.

Atom	Neutral	Radical Anion	
	Charge	Charge	Spin Density
N1	-0.604561	-0.631140	-0.013118
C2	0.712915	0.690766	0.021672
(C2)O	-0.511497	-0.594103	0.029900
N3	-0.631867	0.305509	-0.007739
(N3)H	0.321368	0.305509	-0.000101
C4	0.616457	0.551556	0.061413
(C4)O	-0.537691	-0.611227	0.047038
C4a	-0.009128	0.003077	0.002692
C5	-0.091200	-0.173004	0.486367
N10	-0.643425	-0.643543	0.075846
C10a	0.561775	0.510418	0.041814
N11	-0.629533	-0.625010	-0.000089
(N11)H	0.300805	0.319130	-0.000477
C12	0.501291	0.492389	0.000037
N13	-0.650607	-0.625167	-0.000005
C14	0.502128	0.492476	-0.000015
N15	-0.630256	-0.624771	-0.000047
(N15)H	0.304742	0.320487	-0.000307

Table 2.4 Charges and spin densities of relevant atoms within the 5-deazaflavin-DAP complex.

Figure 2.12b shows the 5-deazaflavin-DAP complex in both redox states. The relative energies are given in $kJ.mol^{-1}$ and shows that the radical anion complex is 161.00 $kJ.mol^{-1}$ more stable than the corresponding neutral form. This is to be expected as the increased electron density across the carbonyl oxygens would allow stronger hydrogen bonds to form with the DAP partner. This stronger bonding is evident by the decrease in hydrogen bond length between the carbonyl oxygens from the deazaflavin species and the NH groups from the DAP unit of just over 0.1 Å. However the hydrogen bond distance of the central noncovalent interaction between the imido NH and DAP carbonyl does not change, indicating that the methyl "wings" of the DAP species bend toward the deazaflavin unit, as seen in the 1-deazaflavin calculations.

2.2.3 X-Ray Crystallography

Attempts to gain crystallography data for both the 1- and 5-deazaflavin analogues were made, however only data for the 1-deazaflavin could be successfully obtained. A single crystal of the 5-deazazaflavin species could not be successfully isolated. The crystal structure for the 1-deazaflavin species is given in Figure 2.13. Please refer to Appendix 9.2 for tabulated data, including respective single-crystal bond lengths and angles.

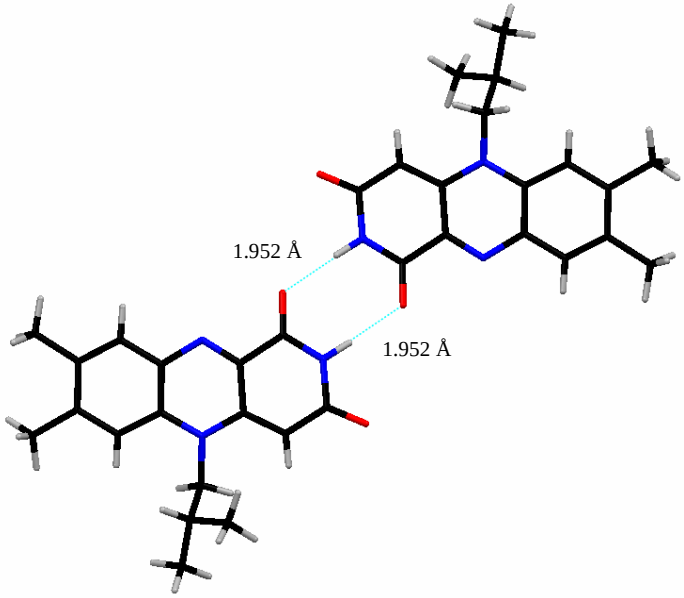

Figure 2.13 Crystal structure obtained for the 1-deazaflavin derivative

On examination of the X-ray crystal data, it appears the 1-deazaflavin analogue exists as a supramolecular dimer, with two point hydrogen bonding between the carbonyl and imido groups of one deazaflavin unit and the carbonyl and imido groups of another. Analysis also indicates planar packing of the molecules into "sheets" with aromatic π-stacking interactions between layers.

2.2.4 Binding Studies

This section investigates the intermolecular non-covalent interactions that exist between each of the deazaflavin derivatives and the DAP unit through hydrogen bond interactions. Experimental details can be found in Chapter Seven.

2.2.4.1 Isobutyl-flavin Binding Studies

Hydrogen bonding was confirmed between the isobutyl flavin compound **13** and the DAP unit **14** using ^{1}H-NMR spectroscopy. A solution of isobutyl flavin **13** in $CDCl_3$ was treated with additional aliquots of the DAP species from 0.00 equivalents to 3.00 equivalents in 0.25 equivalent increments. Monitoring of the N(3)H of the flavin unit by NMR resulted in a smooth downfield shift of its resonance value. Plotting this shift against relative concentration of DAP resulted in a curve that was fitted to a 1:1 binding isotherm and gave an association constant of 557 ± 56 M^{-1} for the complex (Figure 2.14).

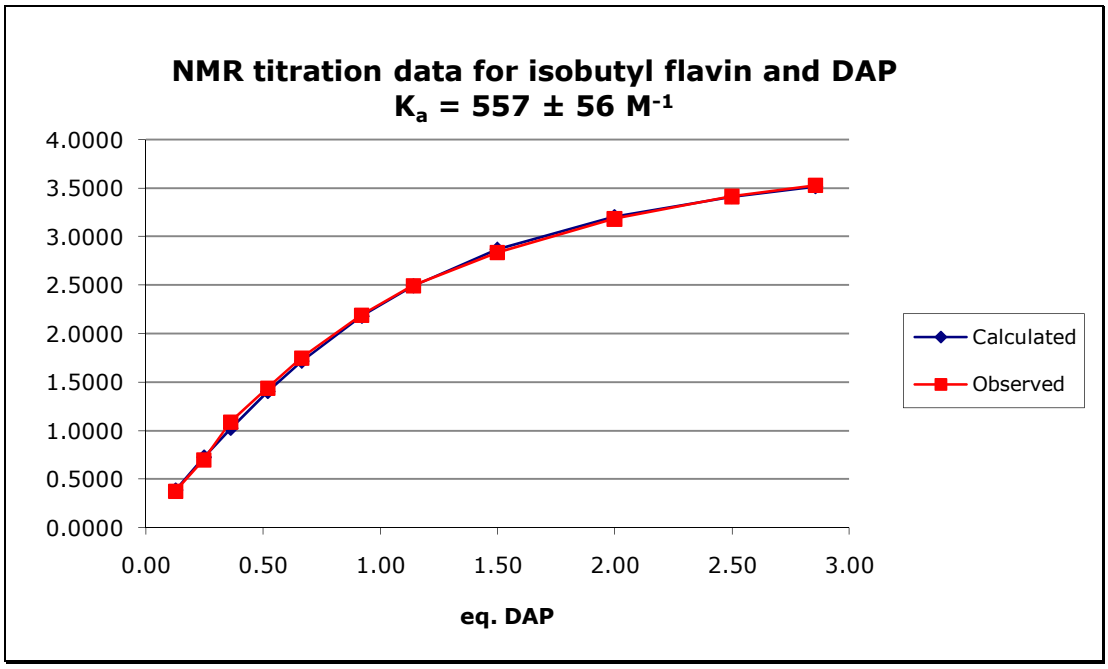

Figure 2.14 NMR titration data for the isobutyl flavin species in the presence of aliquots of DAP (K_a = 557 ± 56 M^{-1}) in $CDCl_3$ at 20 °C.

Comparison of the ^{1}H NMR spectrum of isobutyl flavin when dissolved in $CDCl_3$ in the presence of an excess of DAP, versus the spectrum of isobutyl flavin alone, clearly shows that hydrogen bonding is taking place by the relative downfield position of the imido NH of the flavin unit and the downfield positions of the two amido groups of the pyrimidine group on the DAP molecule.

2.2.4.2 1-Deazaflavin Binding Studies

Hydrogen bonding was confirmed between the 1-deazaflavin compound **6** and the DAP unit **14** using ^{1}H-NMR spectroscopy. A solution of 1-deazaflavin **6** in $CDCl_3$ was treated with additional aliquots of the DAP species from 0.00 equivalents to 3.00 equivalents in

0.25 equivalent increments. Monitoring of the N(3)H of the flavin unit by NMR resulted in a smooth downfield shift of its resonance value. Plotting this shift against relative concentration of DAP resulted in a curve that was fitted to a 1:1 binding isotherm and gave an association constant of 443 ± 44 M^{-1} for the complex (Figure 2.15).

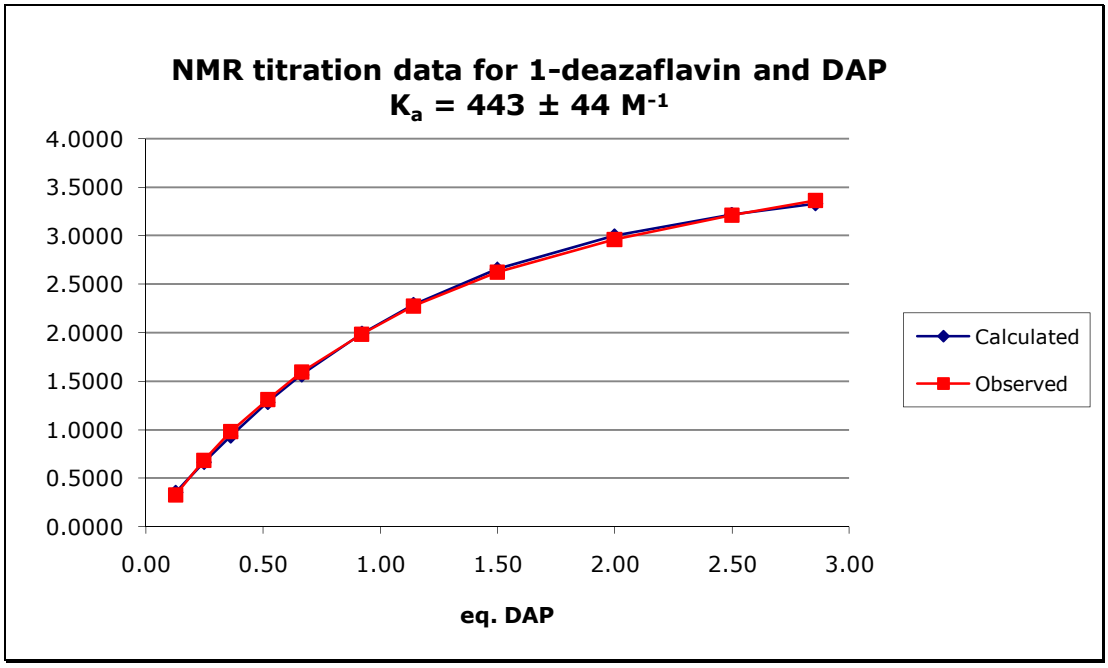

Figure 2.15 **NMR titration data for the 1-deazaflavin species in the presence of aliquots of DAP (K_a = 443 ± 44 M^{-1}) in $CDCl_3$ at 20 °C.**

Comparison of the ^1H NMR spectrum of the 1-deazaflavin analogue when dissolved in $CDCl_3$ in the presence of an excess of DAP, versus the spectrum of the deazaflavin compound alone, clearly shows that hydrogen bonding is taking place by the relative downfield position of the imido NH of the flavin unit and the downfield positions of the two amido groups of the pyrimidine group on the DAP molecule. This is analogous to the results found for isobutyl flavin, however the association constant between the two molecules in the case of the deazaflavin is of a value around 100 M^{-1} less. This indicates that the binding between the two species is not as strong, most likely a side-effect from the reduced electron density within ring III of the deazaflavin species when the NH group is replaced by a CH group.

2.2.4.3 5-Deazaflavin Binding Studies

Hydrogen bonding was confirmed between the 5-deazaflavin compound **9** and the DAP unit **14** using ^1H-NMR spectroscopy. A solution of 5-deazaflavin **9** in $CDCl_3$ was treated with additional aliquots of the DAP species from 0.00 equivalents to 3.00 equivalents in

0.25 equivalent increments. Monitoring of the N(3)H of the flavin unit by NMR resulted in a smooth downfield shift of its resonance value. Plotting this shift against relative concentration of DAP resulted in a curve that was fitted to a 1:1 binding isotherm and gave an association constant of 810 ± 81 M^{-1} for the complex (Figure 2.16).

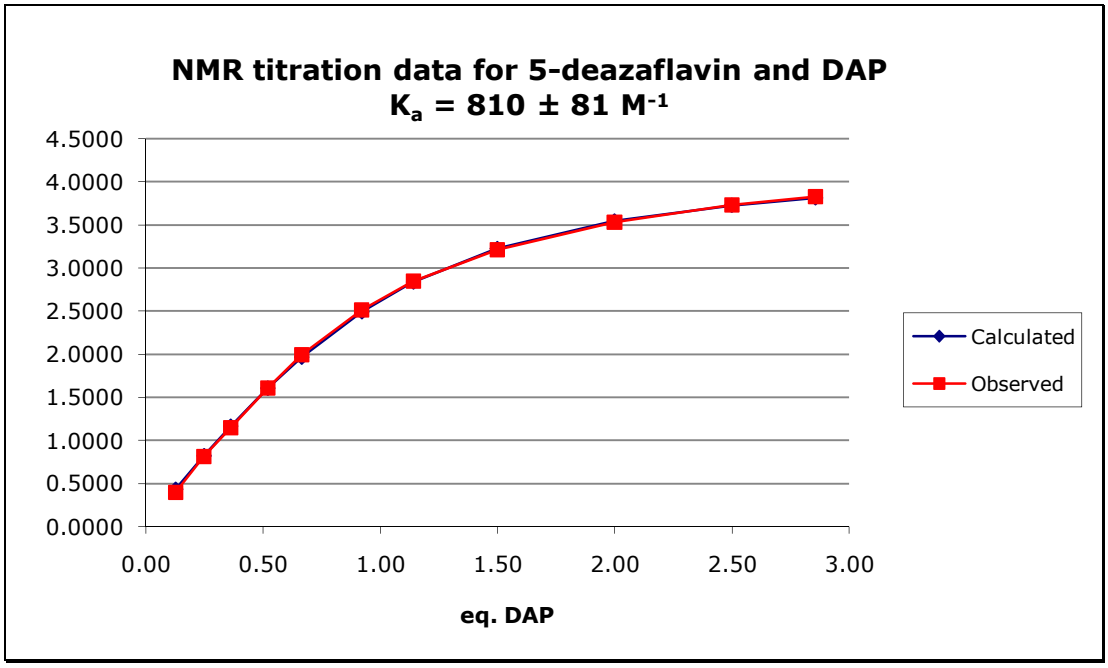

Figure 2.16 **NMR titration data for the 5-deazaflavin species in the presence of aliquots of DAP (K_a = 810 ± 81 M^{-1}) in $CDCl_3$ at 20 °C.**

Comparison of the ^1H NMR spectrum of the 5-deazaflavin analogue when dissolved in $CDCl_3$ in the presence of an excess of DAP, versus the spectrum of the deazaflavin compound alone, clearly shows that hydrogen bonding is taking place by the relative downfield position of the imido NH of the flavin unit and the downfield positions of the two amido groups of the pyrimidine group on the DAP molecule. This is analogous to the results found for isobutyl flavin, however the association constant between the two molecules in the case of this deazaflavin is of a value around 250 M^{-1} more. This indicates that the binding between the two species is stronger for the 5-deazaflavin system.

When taking into account this increase in association constant with the relative decrease in association constant found in the 1-deazaflavin system, it would be reasonable to suggest that replacing the nitrogen atoms with a CH group restricts the type of electron delocalisation and conjugation that usually takes place in the flavin system (as found with isobutyl flavin). In the case of the 5-dazaflavin, electrons from the N(1) atom are no longer delocalised to the same extent across rings II and III to the N(5) position, and therefore the

electron density on the N(1) atom is increased along with that of ring III as a whole, allowing greater association through hydrogen bonding to the DAP unit.

2.2.5 UV-vis Studies

The UV-vis spectra of all three flavin analogues were recorded in chloroform solution (1×10^{-5} mol.L^{-1}) and are shown in Figure 2.17. Isobutyl flavin shows λ_{max} values of 348 and 448 nm. The first λ_{max} peak at 348 nm reflects the S_0-S_2 transition of the flavin nucleus.

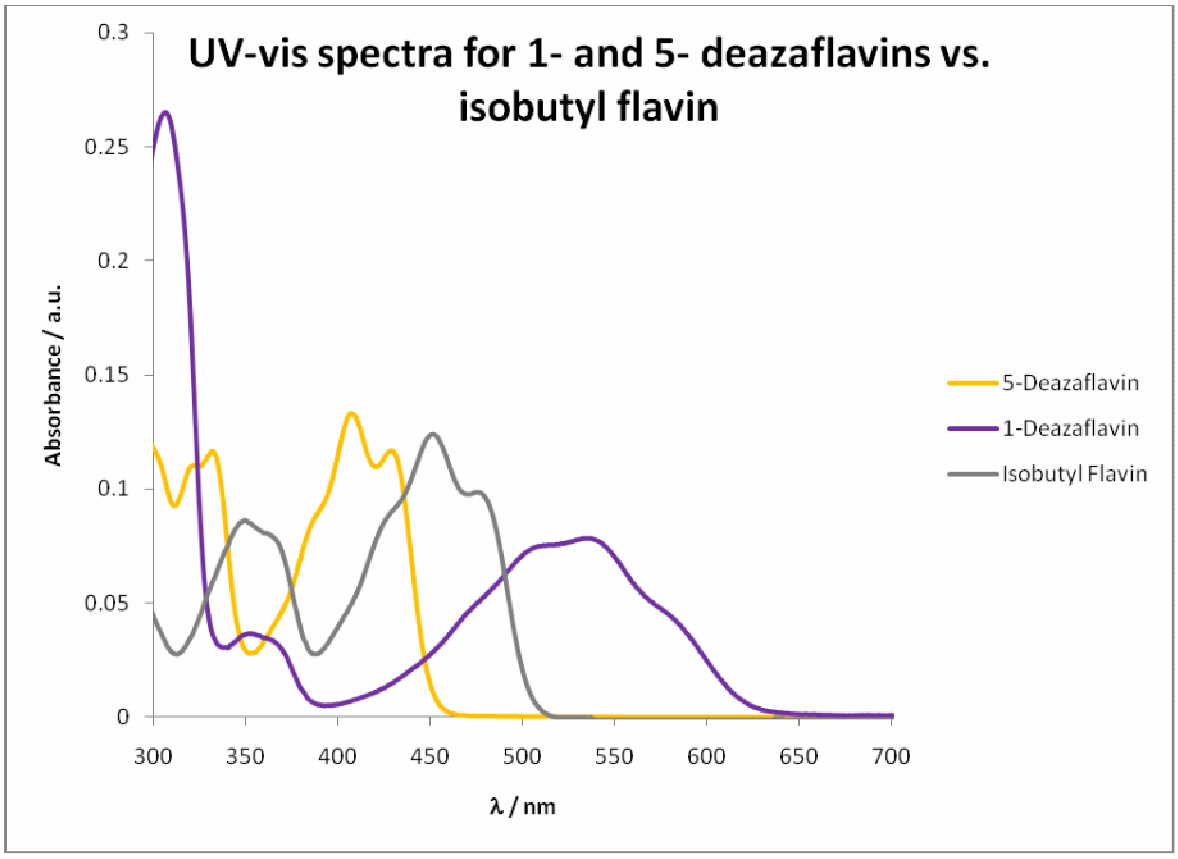

Figure 2.17 UV-vis spectra recorded for isobutyl flavin, 1-deazaflavin and 5-deazaflavin analogues (1 x 10^{-5} M solutions in $CHCl_3$).

Comparison of the spectra recorded of the 5-deazaflavin unit shows a blue-shift of around 20 - 40 nm for both λ_{max} values from 348 and 448 nm, to 329 and 405 nm respectively. However examination of the UV-vis spectra recorded for the 1-deazaflavin analogue shows that although there is little change in the value of the S_0-S_2 transition (329 to 365 nm), there is a large red-shift of the upper λ_{max} value from 448 nm to 534 nm, a shift of almost 100 nm.

2.2.6 Electrochemistry

2.2.6.1 1- and 5- Deazaflavin Electrochemistry

The solution electrochemistry of the 1- and 5-deazaflavin compounds has been studied using cyclic voltammetry (CV), and compared to that of isobutyl flavin (Figure 2.18).

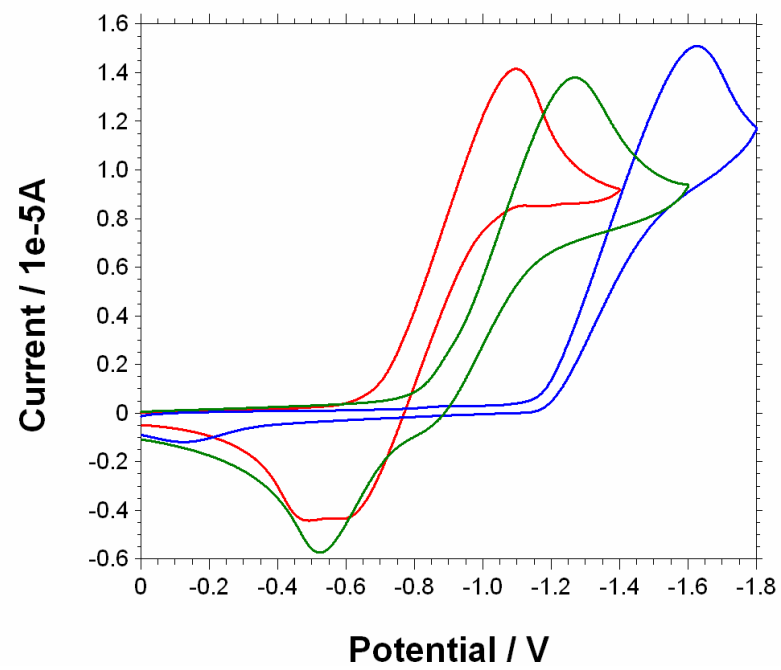

Figure 2.18 **CV data for compound isobutyl flavin (red line Δ $E_{½}$ = -0.83 V), 5-deazaflavin green line Δ $E_{½}$ = -1.03 V), 1-deazaflavin (blue line, $E_{½}$ = -1.37 V) (1x10^{-5} M in 0.1 M Bu_4NPF_6). Solvent is dichloromethane. Scan rate = 0.1 V.s^{-1}. Reference electrode was Ag/AgCl.**

Upon reduction of isobutyl flavin **13** (red line), a single reduction wave and two distinct oxidation waves were observed (Figure 2.18). The former process is due to the reversible formation of the flavin radical anion $\mathbf{13_{rad}^-}$ ($E_{½}$ = -0.83 V), whereas the second reoxidation wave ($E_{½}$ = -0.78 V) arises from an electrochemical-chemical-electrochemical (e-c-e) process whereby a portion of $\mathbf{13_{rad}^-}$ formed at the electrode surface rapidly deprotonates **13** in bulk medium. The protonated flavin ($\mathbf{13_{rad}H}$) radical produced in this process undergoes a further one-electron reduction at the working electrode surface to form the relatively stable fully reduced flavin anion ($\mathbf{13_{red}H^-}$), which is subsequently reoxidised at a less negative potential than $\mathbf{13_{rad}^-}$.

Similarly, upon reduction of the 5-deazaflavin **9** (green line), a single reduction wave and two oxidation waves are observed, again illustrating the presence of a pronounced *ece* peak ($E_{½}$ = -1.03 V). However, upon reduction of the 1-deazaflavin **6** (blue line), the

voltammogram shows an irreversible process with $E_{½}$ = -1.37 V. This data shows that the lack of the NH group within ring III of the isoalloxazine moiety, not only extinguishes any fluorescence emission, but is also responsible for the irreversible nature of the 1-deazaflavin compound. The increased $E_{½}$ value of the 1-deazaflavin also illustrates the increased difficulty in order to reduce the compound compared to that of the 5-deazflavin or the parent isobutyl flavin compound. In terms of substitution of analogous flavin units within flavoenzymes with the 1-deazaflavin compound, the increased redox potential would suggest a slowing of the flavin reduction step in catalysis.

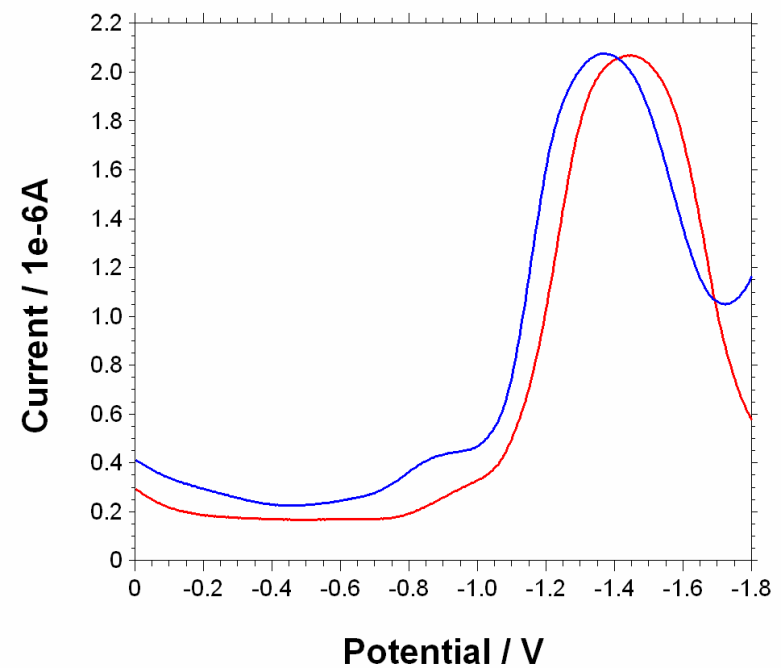

Figure 2.19 **Square wave voltammetry of 5-deazaflavin (red line E = -1.44 V) (1 x 10^{-5} M) and upon the addition of DAP (blue line E = -1.36 V) (1 x 10^{-4} M). Solvent is dichloromethane.**

Unfortunately, due to the irreversible nature of the 1-deazaflavin's electrochemistry, the change in reduction potential upon the addition of DAP could not be measured. However the electrochemical results for the 5-deazaflavin in the presence of DAP recorded by square-wave voltammetry are shown in Figure 2.19. Upon addition of DAP to the 5-deazaflavin species, a stabilising shift of +80 mV is observed, corresponding to a stabilisation of the flavin radical anion of 7.7 kJ.mol^{-1}.

2.3 Conclusions

The 1- and 5-deazaflavin analogues of *N*(10)-isobutyl flavin have been successfully synthesised and characterised via UV-vis spectroscopy, cyclic voltammetry and DFT

modelling. The λ_{max} values for the deazaflavin analogues compared to the parent isobutyl flavin show a blue-shift in the visible spectrum for the 5-deazaflavin species, and a red-shift for the 1-deazaflavin species, indicating that the position and presence of the NH group within the isoalloxazine nucleus has a substantial effect on the flavin's photochemistry. The electrochemistry observed via cyclic voltammetry showed a decrease in reduction potential to more negative values for both the 1- and 5-deazaflavin analogues, compared to that of the parent isobutyl flavin, with the most negative being the 1-deazaflavin species. This would indicate that replacing certain NH groups of the isoalloxazine ring with CH groups greatly effect the redox capability and reversibility of the flavin unit.

In the presence of a suitable hydrogen-bond partner such as DAP, the resulting complex formed with the 5-deazaflavin species exhibits a stabilising shift of +80 mV. Unfortunately due to the irreversible nature of the 1-deazaflavin analogue, the electrochemistry of this species could not be obtained. Examination of the 1- and 5-deazaflavin:DAP complex by NMR titration shows an increase in association constant for the 5-deazaflavin complex, but a decrease in association constant for the 1-deazaflavin species, when compared to the parent isobutyl flavin complex. This data shows that removal of the NH group from ring III of the isoalloxazine nucleus has a destabilising effect on the three-point hydrogen bonding between the flavin unit and a non-covalently bound partner.

2.4 Acknowledgements

The author gratefully acknowledges the contributions to this study from fellow members of the Cooke research group, in particular those of Stuart Caldwell and Shanika Gutanilaka.

Chapter Three

3 Chapter Three – Water-Soluble Flavin Dendrons: Towards Synthetic Flavoenzymes

3.1 Introduction

3.1.1 Outline

In recent years, there has been increasing interest in the development of dendritic architectures that model specific aspects of biological function.[27, 51] Their highly branched structure, monodispersed molecular weight, and the large number of functional groups at the periphery as well as internal cavities are important characteristics, particularly for evaluation in areas of biochemistry such as drug delivery.[52] Initially dendrimer chemistry was concerned with the development of suitable synthetic protocols to produce cascade molecules with a well-defined number of generations,[53, 54] however in more recent years the study of more functional dendrimers has increased, and of particular interest is the discovery of specific functions and properties that are a direct consequence of the dendritic architecture.

Dendrimers make unique biological models owing to their three-dimensional nano-scale structures, which can be synthesised in a controllable manner, and these species exhibit certain advantages over more conventional polymeric systems. Of particular interest in this study was the possibility of creating a synthetic biological mimic of a flavoenzyme, one that incorporated a synthetic dendritic backbone structure, with a flavin moiety at its core. Previous research has shown that polymer-based model systems of flavoenzymes have been created by attaching flavin analogues to biomolecules,[55, 56] synthetic polymers[57] and peptides.[58] However, the lack of active site structural homogeneity and lengthy synthetic protocol limit their potential applications. Therefore, a highly efficient synthetic flavoenzyme model system still remains a great challenge for the synthetic community.

The aim of this study is to successfully synthesise a series of dendron molecules that mimic the biological behaviour and function of a flavoenzyme. The design of these molecules consists of specific selection of both the dendritic backbone and of the central flavin unit at the core of the molecule. The combination of these components will allow the creation of a molecule that, like a flavoenzyme, has a hydrophilic exterior with a

hydrophobic cavity at its core, which houses the flavin functionality and provides a suitable environment in which flavin-catalysed reactions can occur.

3.1.2 Dendrimers and Dendrons: Structure and Function

Dendrimers are regular tree-like macromolecules accessible by chemical synthesis from a variety of building blocks. Their topology enforces a globular shape that offers a unique opportunity to design artificial enzymes. Catalytic groups such as metal complexes and cofactors can be placed at the dendrimer core to exploit the microenvironment and selectivity effects of the dendritic shell. Furthermore, attaching catalytic groups in multiple copies at the end of the dendritic branches may lead to co-operativity effects, while exploration of dendritic structural space by screening combinatorial libraries of peptide dendrimers for catalytic activity can lead to the discovery of functional dendrimers with enzyme-like properties, in a process mimicking natural selection.

The properties of a dendritic superstructure are particularly relevant to this biomimetic study, when compared to analogous polymeric systems, in view of their superior structural characteristics for creating effective biomimetic environments.[59] In particular, dendron architectures can confer a well-defined monodisperse structure as well as a large number of terminal functionalities that offer effective interactions with their surrounding media, whilst at the same time isolating reactive functionality at their foci.[60] Functionality placed at the exterior of a dendrimer is important for determining its solubility.[61] For biomimetic model systems, aqueous solubility is clearly an important target, while the overall structure would best model the relative rigid microenvironment found in the interior of protein structures. This study uses water-soluble, polyethylene glycol branches along with aryl branching points to confer the required solubility to the system, as well as maintaining a balance between the structure's rigidity and flexibility.

Since the initial synthesis of dendrimers by Vogtle,[62] Tomalia[63] and Newkome,[64] the dendrimer concept has proven exceptionally successful at delivering functional macromolecules in preparatively useful amounts from a variety of building blocks and coupling chemistries. Applications range from biology and medicine to industrial catalysis and polymers.[65] Dendrimer-based catalysis has been the object of numerous studies[27, 66, 67] since initial reports by Brunner and co-workers in 1994 to create a so-called 'dendrizyme',[68] and polycarbosilane dendrimers reported by van Koten and co-workers catalysing the Karasch reaction.[69] These systems focused on modulating the efficiency and

selectivity of catalytic groups by placing them either as a single copy at the core of a dendrimer or in multiple copies at the dendrimer surface.[70]

In 1993, a key finding by Frechet and co-workers showed that dendritic branching could modulate physical properties at the dendrimer core.[71] This was achieved by synthesising dendritic wedges of varying generational sizes, each containing a solvatochromic probe at the focal point, the UV/Vis absorption of which is dependant upon solvent polarity (see Figure 3.1).

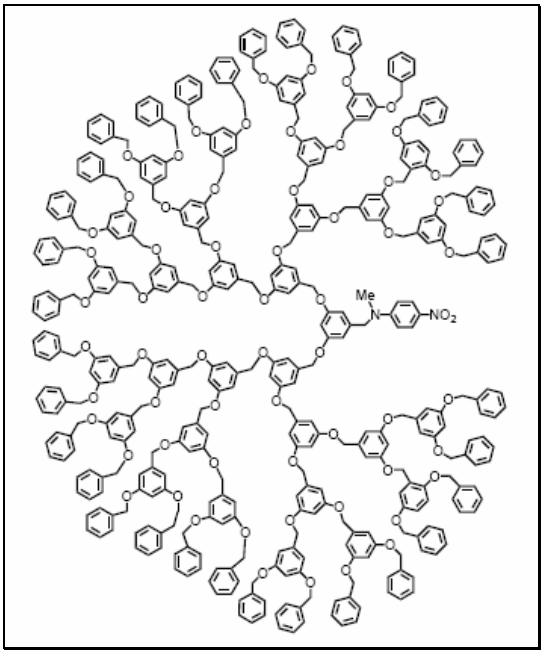

Figure 3.1 Fifth-generation ([G-5]) dendritic wedge with a solvatochromic probe at the focus.[27]

With increasing generation number and size of the dendritic wedge, the UV/vis absorption band of the central chromophore in CCl_4 shifted to longer wavelengths. As the dendritic wedge expands, the solvatochromic probe is increasingly shielded from the bulk apolar solvent and the effective polarity in its surroundings increases, causing the observed bathochromic absorption shift. Such an effect was not observed when the bulk solvent was more polar. The authors also noted a discontinuity in the absorption band shift between the third- and fourth-generation dendritic branching and argued that at this point the structure of their wedge became more globular, encapsulating the probe even more effectively. This result is of considerable importance as it indicates the existence of a distinct microenvironment inside a dendrimer, resembling those found in proteins. It is proposed that large changes in pK_a of functional groups located inside dendrimers will be analogous

to those of the altered pK_a values of amino acid chains depending on their exact location within proteins.[47]

Another remarkable example of the modulation of physical properties by an enzyme superstructure is provided by the electron-transfer proteins based on the heme Fe^{III}/Fe^{II} redox couple. The metal centre in cytochrome *c* has an oxidation potential 300 – 400 mV more positive than that of heme model systems with similar metal ion ligation.[72] It is proposed that the hydrophobic polypeptide shell plays a critical role in controlling the redox behaviour of the heme-bound metal ion. Diederich and co-workers have reported a water-soluble second generation dendritic Fe^{III} porphyrin as a cytochrome *c* model (Figure 3.2).[73]

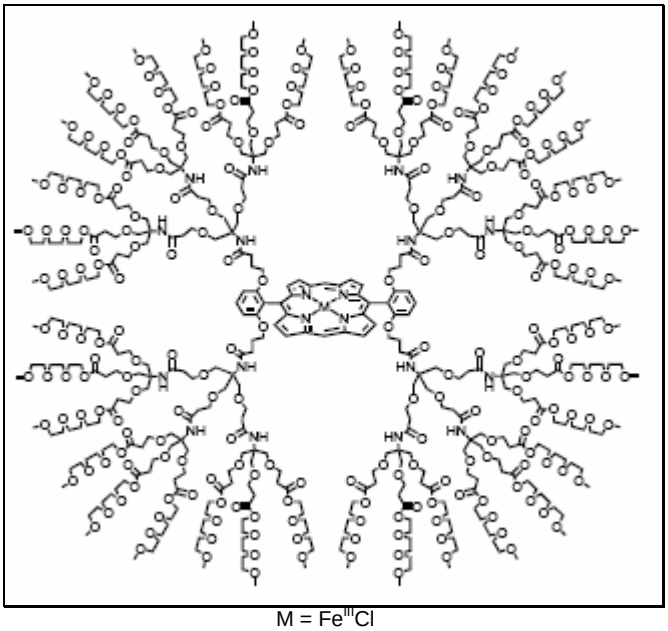

Figure 3.2 A second-generation Fe^{III} porphyrin-based dendrimer ([G-2]), which acts as a model system for cytochrome *c*.[27]

They investigated the electrochemical properties of the model compound and the corresponding smaller first-generation dendrimer in both dichloromethane and water. Progressing from the [G-1] to the [G-2] derivative in DCM, the redox potential of the biologically relevant Fe^{III}/Fe^{II} couple remained virtually unchanged, whereas in aqueous solution, the [G-2] derivative exhibited a potential 420 mV more positive than the lower generation compound. The large difference between these potentials in water was attributed to the differences in solvation of the core electrophore. The relatively open branches in the first-generation compound do not impede access of the bulk solvent to the central core, whereas the densely packed dendritic superstructure of the second generation compound significantly reduces contact between the heme and external solvent. As a

result, the more charged Fe^{III} state is destabilised relative to Fe^{II} and the redox potential is strongly shifted to a more positive value.

Enzymes consist of a catalytic pocket equipped with precisely positioned functional groups for catalysis, surrounded by a protein shell. Several studies of dendrimers as enzyme-like catalysts have focused on the combination of catalytic groups at the dendritic core with dendritic branches to modulate catalyst selectivity.[74] The so-called 'dendrizyme' prepared by Brunner was achieved by growing chiral dendritic branches around an achiral metal chelate in order to catalyse the cyclopropanation of styrene with ethyl diazoacetate to form the cyclopropane carboxylates (see Figure 3.3).[68]

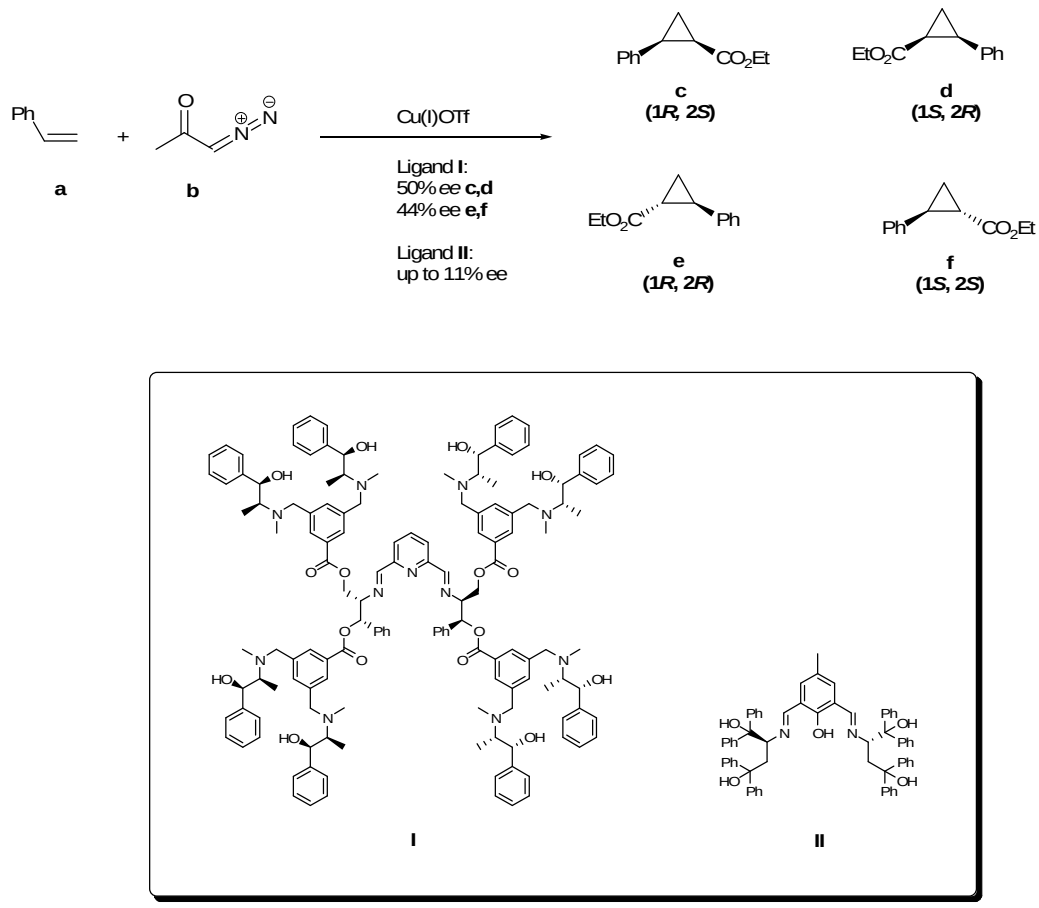

Figure 3.3 Brunner's dendrizyme ligands, active for the cyclopropanation of styrene.[59]

Ligand **I** with two chiral branches, gave products with 50 % enantiomeric excess (**c, d**) and 44% (**e**, **f**) without stereoselectivity, but the more dendritic complex **II** gave no more than 11 % enantiomeric excess. Studies by other groups involving different metal complexes and reactions gave similar results, with approximately 2-3 fold modulation of either reaction rate or selectivity upon attachment of dendritic branches to a catalytic core. Suslick and co-workers have reported dendrimer metalloporphyrins as oxidation

catalysts.[75] A manganese containing porphyrin was surrounded by four dendritic branches and used for the epoxidation of alkenes in dichloromethane solution using iodosylbenzene as oxidant. The turnover numbers of the dendritic catalyst were similar to the porphyrin alone (2-4 s^{-1}), however the dendrimer displayed a 2-3 fold increase in selectivity towards terminal alkenes over cyclic or disubstituted alkenes when compared to the porphyrin alone.

Catalysis by organic cofactors at the dendrimer core has also been studied. Seebach and co-workers investigated the reaction of phenyl methyl ketone with methanol to give methyl 2-methylphenylacetate, under catalysis by a chiral diamine (1 mol % in toluene) at the core of a chiral Frechet-type dendrimer. This resulted in higher enantioselectivity (50 % *ee*) compared with that of the non-dendritic amine catalyst (15 % *ee*).[76] Diederich and co-workers have prepared thiazolio-cyclophanes decorated by dendritic branches as mimics for pyruvate decarboxylase.[77] This construct promoted an aldehyde to ester oxidation by a flavin cofactor, but the reaction was two orders of magnitude slower than the system without dendritic branches. This appears to suggest that the type and structure of dendron architecture has a dramatic effect on the outcome of any potential catalysis of chemical reactions.

Recent efforts to create artificial enzymes using peptide dendrimers have been attempted which capitalise on the simplified synthesis and enforced globular shape of dendritic peptides.[78] This strategy circumvents the difficult problem of protein folding, and should render peptide dendrimers relatively more stable towards denaturing conditions (high temperature or non-aqueous conditions) and biodegradation relative to natural proteins. The enforced globular shape is also optimally suited to favour intramolecular interactions between amino acids that lead to macromolecular function, rather than intermolecular interactions leading to aggregation and precipitation, as is often observed with linear synthetic peptides. Peptide dendrimers have been used previously for the multivalent display of ligands, and have been used as diagnostic reagents, protein mimetics, anti-cancer and anti-viral agents, vaccines and drug and gene delivery vehicles.[79] Polylysine dendrimers decorated with various end-groups are also being evaluated as drugs, one example being that of multivalent aryl sulphonates that can be used for the prevention of HIV infections.[79]

Although still very far from rivalling natural or modified enzymes, dendritic catalysts are capable of rate accelerations and selectivities comparable with those observed with enzyme

models based on antibodies,[80] non-catalytic proteins[81] and small peptides.[82] However, by radically departing from their linear topology of natural proteins, dendrimers might avoid inherent limitations of protein-based designs, in particular thermal instability and solvent incompatibility due to unfolding and aggregation. By contrast to the current research on natural enzymes, there is currently a significant lack of structural characterisation[83] or molecular modelling studies with dendrimers.[84] This study hopes to add to the breadth of research in the area by synthesising a new family of biomimetic models of flavoenzymes, incorporating a flavin cofactor within the hydrophobic cavity of a water-soluble dendritic architecture.

3.1.3 Flavin Cofactor

Flavoenzymes are an important class of redox enzymes that are involves in a variety of biological processes including electron transfer, redox transformations and signal transduction.[31, 32] The redox active flavin groups, or cofactors (e.g. riboflavin, FMN or FAD – Figure 3.4), are usually bound to the active-site of the apoenzyme via a range of noncovalent interactions.[40] The delicate cooperation of these interactions are thought to be responsible for fine tuning the redox properties of the cofactor, and also for creating a hydrophobic binding pocket to isolate the cofactor from interactions within the aqueous environment.

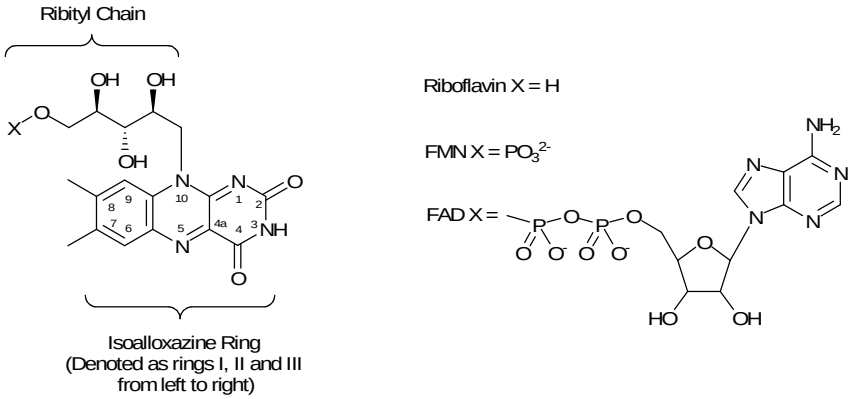

Figure 3.4 General structure of the flavin cofactor and various derivatives

To simulate flavoenzyme activity within an artificial enzyme that synthetically mimics the binding site and catalytic sites of the naturally occurring enzyme, a detailed understanding of the non-covalent interactions in the supramolecular architecture is necessary. A range of molecular model systems have been synthesised and studied to elucidate the role of various noncovalent interactions (e.g. hydrogen bonding, π-stacking and donor atom-π

interactions) have in modulating the redox properties[35, 85] and reactivity[86, 87] of the flavin moiety of flavoenzymes. Although these systems have provided some insight into how these interactions modulate the redox potential of the flavin, they have failed to recreate the biomimetic environment that surrounds the flavin cofactor. In this study, the flavin derivative in Figure 3.5 was attached to a series of increasing generations of dendritic architectures.

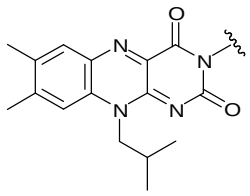

Figure 3.5 Structure of the model flavin cofactor

The ribityl-chain attached to the N(10) atom of the flavin structure has been replaced with an isobutyl group to simplify the model. This peripheral chain acts to anchor the flavin moiety within the hydrophobic pocket of the protein backbone in naturally occurring systems, and modifying this group has little effect on the redox properties of the cofactor. It has been shown that the noncovalent interactions between the side-chains attached to the protein within the binding pocket and the flavin moiety greatly affect the flavin's redox properties, causing up to a 600 mV shift in the redox potential of naturally occurring flavoenzymes.[32] The dendritic backbone is attached to the N(3) nitrogen atom, and subsequent study of the effect of the dendron attachment will provide important information on how the varying increasing generations of dendron backbone affects the redox properties and catalytic activity of the flavin cofactor.

A true measure of a model system is the ability to replicate the behaviour of its prototype.[25] In the case of flavoprotein enzymes, a popular reaction with which to measure the efficiency of various model systems is that of the aerobic oxidation of NADH, using suitable analogues.[88] Most biological oxidation reactions involve the activation of one or more C-H bonds, with concomitant transfer of two electrons to a suitable acceptor molecule. In the case of oxidation reactions catalysed by simple pyridine-nucleotide-linked enzymes, the acceptor is NAD^+ or $NADP^+$ and the resultant NAD(P)H needs to be reoxidised by coupling with a second pyridine-nucleotide-linked enzyme. In the case of flavoproteins, the flavin being tightly bound to the protein, a second substrate serves to reoxidise the reduced flavin to complete the catalytic cycle. Thus catalysis by flavoprotein enzymes always involves a reductive half-reaction, where the enzyme-bound flavin is

reduced, and an oxidative half reaction, where the reduced flavin is reoxidised. In most cases it is possible to study these two half-reactions separately, a feature which has permitted the detailed analysis of catalytic events not possible with most other enzymes (Figure 3.6).[23]

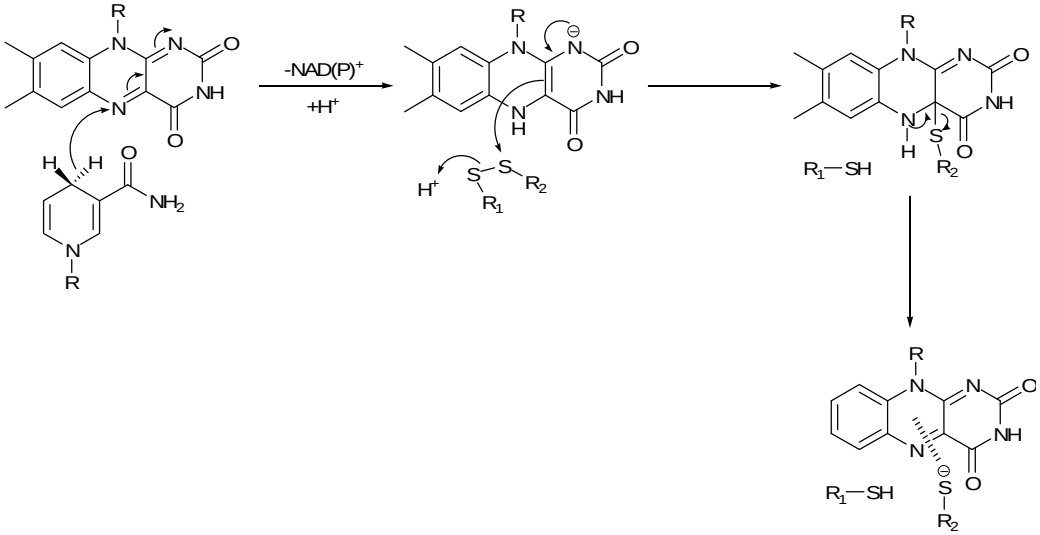

Figure 3.6 Reductive half-reaction of a typical flavoprotein disulphide reductase.

Glutathione reductase is an FAD containing enzyme in which the oxidation of NADPH by the flavin unit occurs by direct transfer of a hydride equivalent between the C(4) of the pyridine nucleotide and the N(5) position of the flavin unit. This concept is supported by the crystallographic data on glutathione reductases, which shows the nicotinamide ring stacked over the flavin pyrazine ring with the *S*-hydrogen at its C(4) position close to the flavin N(5) position.[89] Such an arrangement of these atoms is essential for hydride transfer, in distinction to a radical mechanism, where orbital overlap between the pyridine nucleotide and the flavin units would not have to be so restrictive.

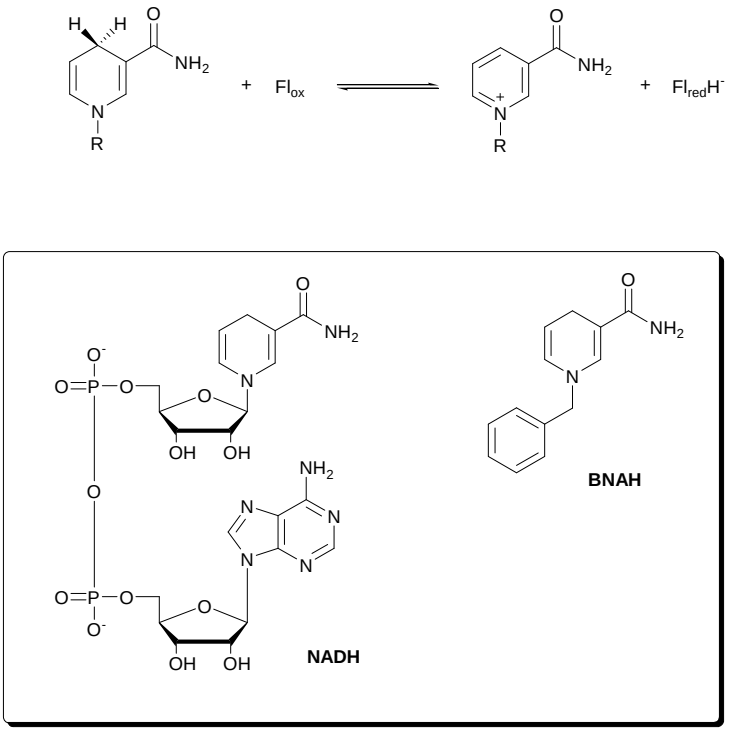

Figure 3.7 Flavin catalysed oxidation of a pyridine nucleotide and analogue structures.

In this study, the ability of the dendron-flavin model systems to oxidise the NADH analogue BNAH (Figure 3.7) will be measured and compared to that of riboflavin – a suitable FAD analogue. The results may shed light on whether the presence of a dendritic backbone, instead of a protein shell, allows the reaction to not only take place, but also to conclude whether the different architecture has any effect on the catalytic efficiency of the flavin species.

3.2 Results and Discussion

3.2.1 Synthesis

The syntheses of the three flavin dendrons were carried out using a convergent synthetic approach.[90] This convergent approach involves synthesising the dendron architecture beginning from the outer-most peripheral groups and continuing towards the core or focal-point. Ethylene glycol groups were used at the periphery to create a hydrophilic exterior, with the flavin group attached at the final step of the synthesis. The synthesis of the first generation water-soluble flavin dendron is outlined in Scheme 3.1.

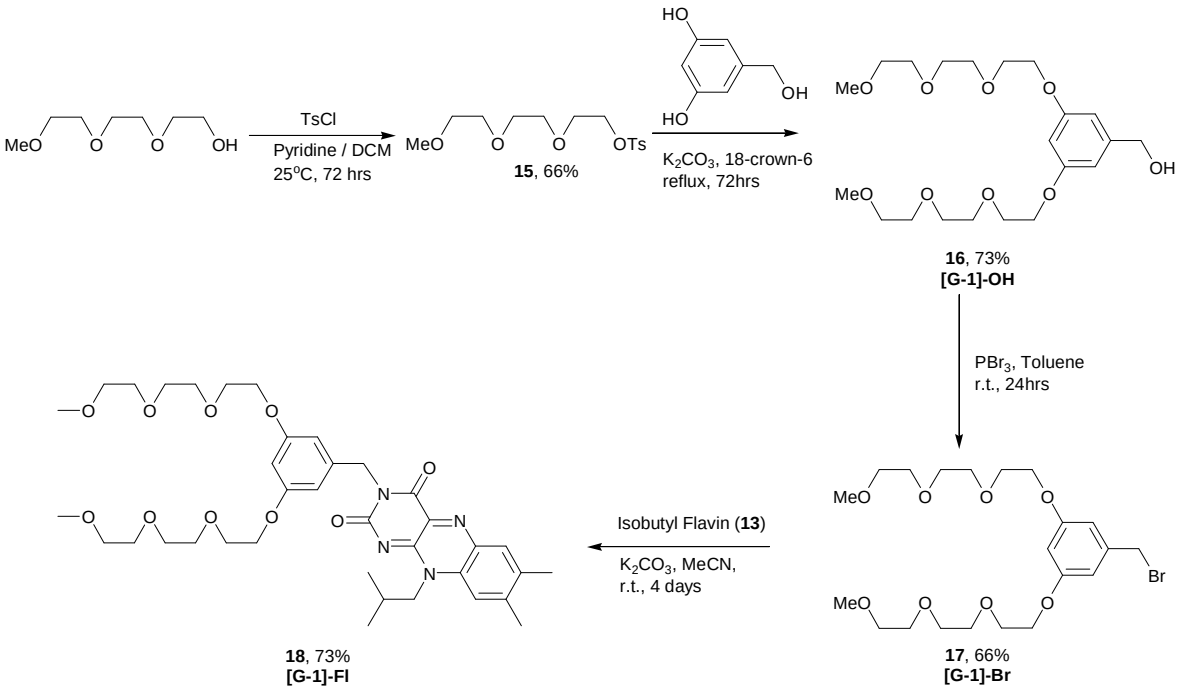

Scheme 3.1 Convergent synthesis of the 1st generation water-soluble flavin dendron.

Treatment of triethylene glycol monomethyl ether with *p*-toluene sulfonyl chloride gave the protected product **15** in good yield. This was then coupled to 3,5-dihydroxybenzyl alcohol in the presence of potassium carbonate as base and 18-crown-6 to afford the first generation hydroxy-terminated dendron ([G-1]-OH) **16** in 73% yield. This species was then brominated at the hydroxy function by using phosphorous tribromide to afford the first generation bromo-terminated dendron ([G-1]-Br) **17** in 66% yield. The final step involved coupling of isobutyl flavin (**13**) to compound **17** in the presence of base to afford the target first generation flavin-terminated dendron **18**. The isobutyl flavin moiety was synthesised according to the scheme outlined in Scheme 3.2.

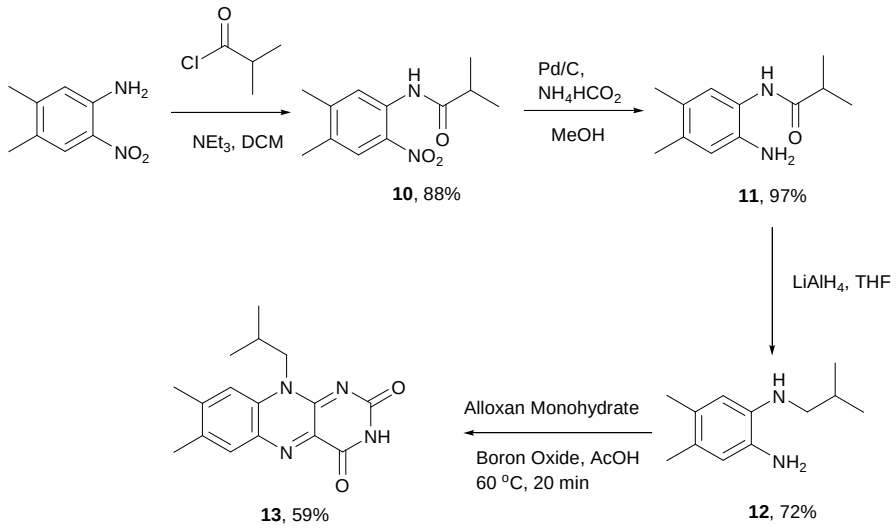

Scheme 3.2 Synthesis of N(10)-isobutyl flavin.

Acyl substitution of nitroaninline was carried out using isobutyryl chloride, followed by sequential reduction of the nitro group and the amide group to afford the fully reduced flavin precursor **12**. Coupling of this derivative to alloxan monohydrate afforded isobutyl flavin (**13**) in 59% yield.

The synthesis of the second- and third- generations of the flavin-terminated dendrons is achieved by using an iterative approach of coupling the bromo-functionalised dendron derivative of n^{th} generation to 3,5-dihydroxybenzyl alcohol, which affords the hydroxy-functionalised dendron of $n+1^{th}$ generation. The schemes outlining the synthesis of the second- and third-generation flavin-functionalised dendrons are outlined in Schemes 3.3 and 3.4 respectively.

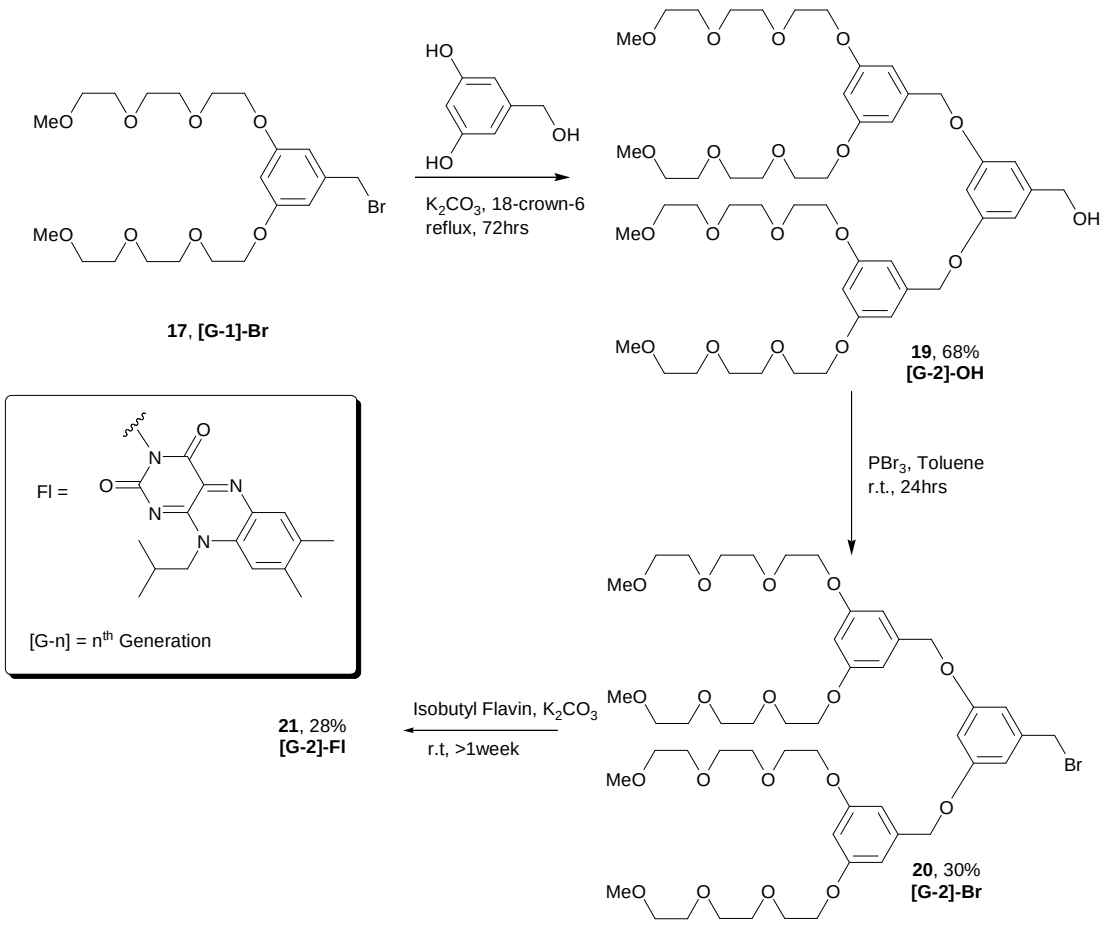

Scheme 3.3 Synthesis of the 2nd generation flavin-terminated dendron

Scheme 3.3 shows the synthetic route employed to create the 2nd generation dendron ([G-2]-Fl, with the structure of the flavin species shown on the left. All steps were carried out in a similar fashion to the synthesis of the first-generation dendron, however a drop in final product yield was observed. This was expected as increasing levels of dendritic branching tend to sterically hinder the likelihood of reaction at the focal point. This effect was observed also in the necessary increase in reaction time of the final coupling of the flavin compound to the dendron species from a few days to over a week at room temperature.

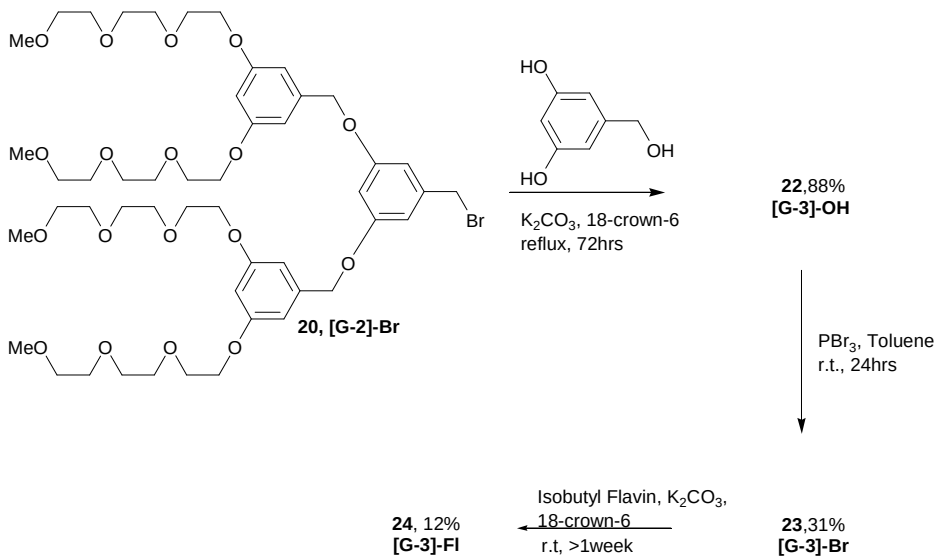

Scheme 3.4 Synthesis of the 3rd generation dendron

Scheme 3.4 shows the synthesis of the third-generation dendron, using the bromo-functionalised compound ([G-2]-Br) to couple to 3,5-dihydroxybenzyl alcohol, affording the hydroxy-terminated species with the necessary n+1 increment in dendritic branching. Again, this increase in branching proved troublesome to the synthesis, as final product yield dropped further, along with an increase in reaction time needed for the final coupling, ranging from nine days to fourteen days, dependent upon conditions.

3.2.2 Molecular Modelling

The hyperbranched structure of dendrimers is now an increasingly prevalent motif employed by researchers utilising this architecture in applications such as molecular recognition,[91] surface modification,[92] asymmetric synthesis[68] and small molecule encapsulation.[93] It is of great interest to elucidate the geometric features of dendrimers such as their shape, size and internal organisation. As current research stands, a number of experimental and computational approaches have been devised to provide a physical picture of dendrimers including their overall shape and their internal structure. However, to date, this picture of dendrimer conformation is far from complete. Most notably, the effect of the primary structure of the dendrimer on its overall three-dimensional structure has not been elucidated. Therefore, little information is available for the development of rational design strategies and establishment of molecular structure-property relationships. Such information will be essential to the successful rational implementation of dendrimers in the aforementioned applications.

Gorman and co-workers have done extensive research into how the conformational flexibility of dendrimer repeat units affect the overall geometry and organisation of a dendrimer using atomistic molecular dynamics simulations.[94] This relationship is explored over a size range of dendrimer models that are computationally feasible to equilibrate and constitute reasonable synthetic targets. Repeat units that are alternatively "flexible" and "stiff" were compared (Figure 3.8).

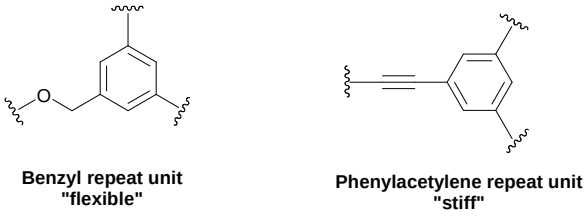

Figure 3.8 Examples of Gorman's dendrimer repeat units.[94]

Their results indicate that dendrimers employing "stiff" repeat units generally give rise to disk-shaped super-structures, whereas those employing "flexible" repeat units give rise to globular shaped super-structures. The globular shapes elucidated by these computations resulted from contraction of dendron arms around the topological core. In this study of water-soluble dendrons, similarly flexible dendron repeat units were employed consisting of benzyl branching units with ethylene glycol functionalities at the termini. Comparisons between the results of calculations carried out on these structures should be comparable to those carried out by Gorman and will possibly elucidate globular super-structures that encapsulate the flavin functionality at the core.

Molecular dynamics simulations were performed on all three first-, second-, and third-generation flavin dendrons using the MacroModel program in Maestro v8.0 from Schrodinger Inc. The specific calculation settings can be found in the experimental section in chapter seven. The results of these calculations showed that as the dendron generation increased from G-1 to G-3, the degree of encapsulation of the flavin residue by the dendron architecture increases accordingly. The dendron arms can be seen to contract around the flavin core when moving from G-1 to G-2, and this effect becomes more prominent on examination of G-3. The third-generation flavin-functionalised dendron is also found to be partially located in a hydrophobic environment that is near the surface. This feature is commonly observed in flavin-based electron-transfer proteins (Figure 3.9).

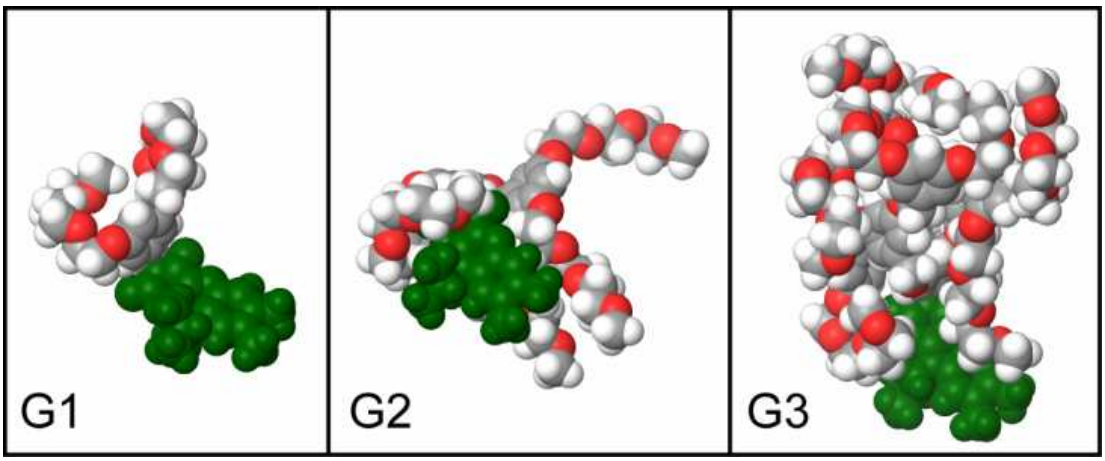

Figure 3.9 **Molecular dynamics simulations of dendron generations ([G-1] to [G-3]) demonstrating encapsulation of the flavin unit (green) within the dendron wedges. Water molecules have been omitted for clarity.**

These results confirm the predicted globular shape of the dendritic architecture, which is particularly prevalent in the third-generation system. Further studies on increased generation size would be of particular interest to evaluate whether this conformation is continued throughout the series and how well this compares to the globular structure of naturally occurring flavoproteins. In particular, how well formed and shielded the hydrophobic pocket can be from aqueous media as the generation size increases. Previous computational research by Cooke and co-workers on similar flavin-based systems incorporating a polymer backbone with a flavin cofactor has elucidated a similar globular super-structure with a hydrophobic pocket containing the flavin unit.[25] However this system lacks the monodispersed molecular weight and highly branched structure inherent to dendrimer-based systems.

3.2.3 Physical Analysis

3.2.3.1 UV-vis Studies

The isoalloxazine ring structure, which is inherent to the flavin species, has been identified as possessing highly solvochromic S_0-S_2 transitions.[95] Previous studies have observed the λ_{max} of FMN to occur at 374 nm in aqueous media and 358 nm in ethanolic solution.[96] It is this behaviour that identifies the flavin unit as a very effective system for probing the polarity of its surrounding microenvironment. The amphiphilicity of the heterocyclic flavin nucleus plays two key roles in microenvironment sensing. Firstly, it allows solubilisation without any aggregation in virtually any solvent using non-interfering side-chains at the N(10) position. Secondly, it provides a non-invasive procedure for the characterisation of

dynamic media. By examining the optical behaviour of the flavin unit attached to a dendritic architecture, it is possible to gain effective insight into the surrounding microenvironment of the flavin unit in all three generations of dendron species that have been synthesised, and to asses any changes of this environment as the degree of dendritic branching increases.

The UV-vis spectra of riboflavin and the flavin dendrons in pH = 8.0 phosphate buffer/isopropanol (95:5) was recorded.[95] The studies by Rotello and co-workers has shown that the S_0-S_2 transition of the flavin nucleus is solvatochromic and undergoes a bathochromic shift when transferred from non-polar to polar media.[97] Figure 3.10 shows the overlaid UV-vis spectra of riboflavin and the first-, second- and third-generations of the flavin dendrons.

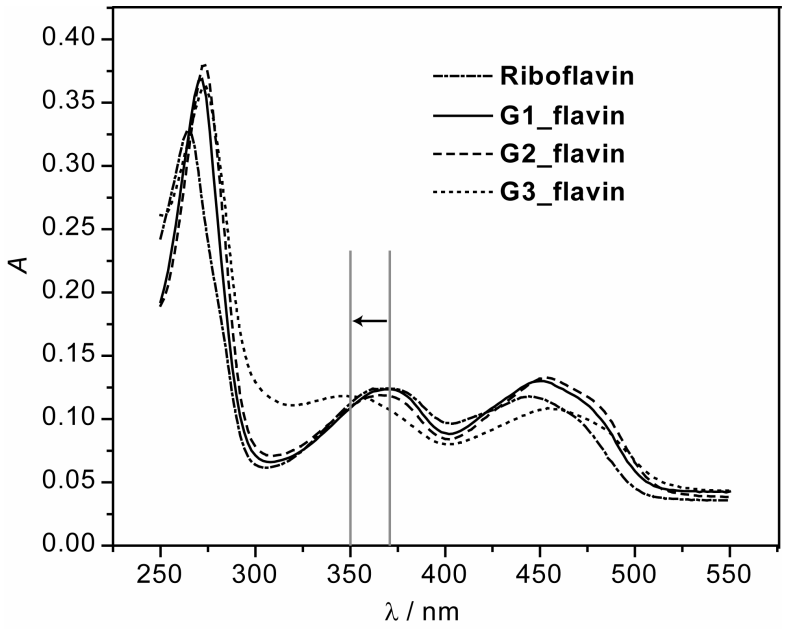

Figure 3.10 Overlaid UV-vis spectra of riboflavin and flavin dendrons (5 mM solutions in sodium phosphate buffer/isopropanol (95:5), pH = 8.0).

The S_0-S_2 transition for riboflavin and the first and second generation flavin dendrons were shown to be very similar and occurred at around 370 nm. However, for the third generation flavin dendron, the S_0-S_2 transition was shifted 20 nm to a shorter wavelength (λ_{max} = 370 nm for riboflavin versus λ_{max} = 350 nm for [G-3]-Fl). This blue shift is consistent with the ethylene glycol moieties of the third generation dendron creating a hydrophobic pocket for the flavin unit in aqueous media.[25]

Cooke and co-workers have also used a similar method to deduce the microenvironment surrounding the flavin sub-unit with their polymeric model system.[25] A blue-shift of the

flavin's λ_{max} value of -16 nm was observed for the S_0-S_2 transition when comparing FMN to the polymer-bound flavin system. This is consistent with the ethylene glycol moieties of the polymer creating a relative biomimetic hydrophobic pocket for the flavin chromophore in aqueous media. The same conclusion can be drawn for the third-generation dendron system examined in this study, whereby the poly-aryl branches, terminated with ethylene glycol units at the periphery, create a similar hydrophobic pocket in which the flavin is situated.

3.2.3.2 Fluorescence Studies

Examination of the fluorescence activity of the flavin species has been widely utilised as an additional tool with which to probe the microenvironment surrounding the molecule. This method is not strictly limited to flavins and flavoproteins, but is also used for a wide range of organic dyes. The effect of π-stacking interactions on the fluorescence activity of such molecules has been extensively documented, and results show that quenching of fluorescent activity by such interactions is a common phenomenon.[98] Studies by Sauer and co-workers observe the inter- and intra-molecular fluorescence quenching of organic dyes by tryptophan, commonly present in peptides and proteins, which can be attributed to the presence of a heterocyclic π-system in its side-chain.[99] Furthermore, Becker and co-workers document the specific role that π-interactions play in modulating the reduction potential of the flavin species in certain flavoproteins, and also how the presence of tryptophan, in close proximity to the flavin unit, quenches the fluorescence of the flavin.[100]

To further probe the microenvironment of the flavin unit, and consequent interactions with the dendron superstructure, the fluorescence spectra of the three flavin dendron generations and of riboflavin were recorded (Figure 3.11).

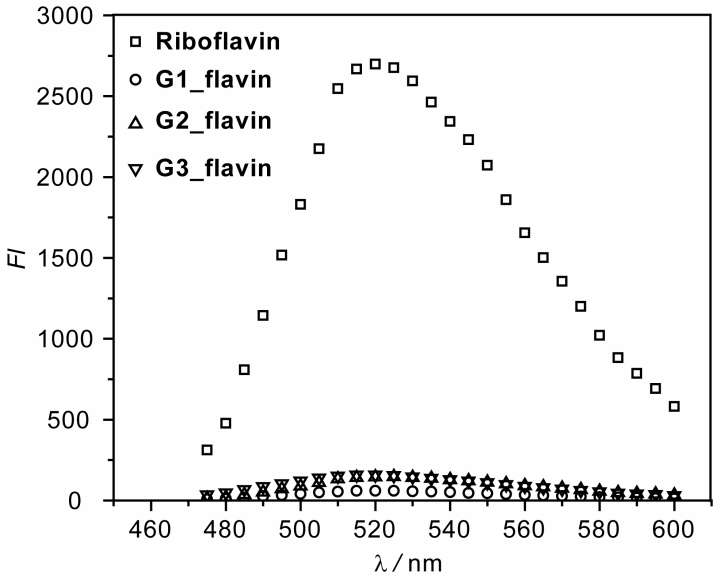

Figure 3.11 Fluorescence spectra of riboflavin and the flavin dendrons in pH = 8.0 sodium phosphate buffer/isopropanol (95:5) solution at 30 °C (λ_{ex} = 450 nm).

Examination of the results shows that the dendron moieties significantly quenched the fluorescence of the flavin units, compared to that of free riboflavin. This can be attributed to the aromatic π-interactions between the electron deficient flavin unit and the electron rich aromatic branches of the dendron moiety. The fluorescence of the dendron-bound flavin's is observed to be around 10% of that seen for free riboflavin, indicating that fluorescence quenching is indeed significant and almost total, when the flavin unit is surrounded by the poly-aryl branches of the dendron. This effect is observed in all three generations of dendron molecules.

3.2.3.3 Electrochemical Studies

Further examination by Cooke and co-workers on their polymeric flavin-based model system by square-wave voltammetry showed that the polymeric backbone had significant influence on the electrochemical properties of the flavin moiety.[25] The reduction potential of the flavin unit in the polymer system was seen to shift by -61 mV compared to that of free FMN. This shift, relating to a destabilisation of the reduced flavin, was attributed to donor atom-π interactions between the electron rich ethylene glycol side-chains of the binding pocket, and the flavin derivative. In addition, the decreased polarity of the flavin microenvironment, as seen in the optical studies, was also considered to be a factor. Therefore, similar experiments have been carried out in this study of the solution electrochemistry of the dendron systems.

The solution electrochemistry of riboflavin was compared to the three generations of flavin dendrons using square-wave voltammetry. The volatammetry experiments were carried out in pH = 8.0 phosphate buffer/isopropanol (95:5, Figures 3.12 and 3.13).

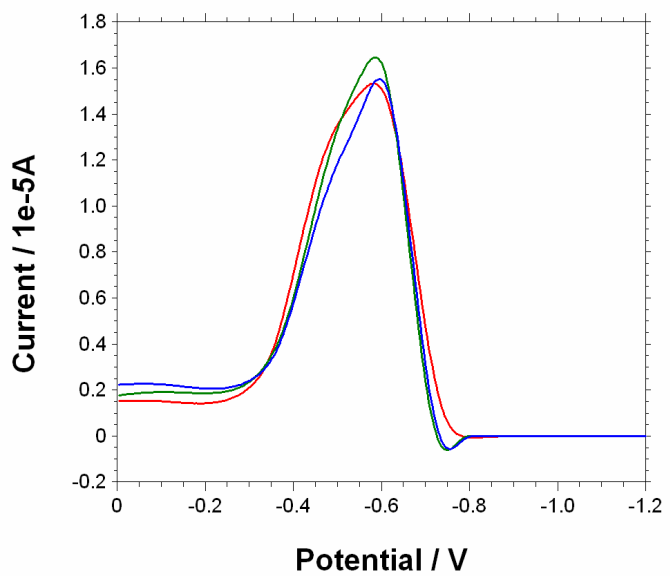

Figure 3.12 **Square wave voltammetry of [G-1]-flavin (red line), [G-2]-flavin (blue line) and [G-3]-flavin (green line) in pH = 8.0 sodium phosphate buffer/isopropanol 95:5 (4×10^{-5} M). E = -0.6 V versus Ag/AgCl.**

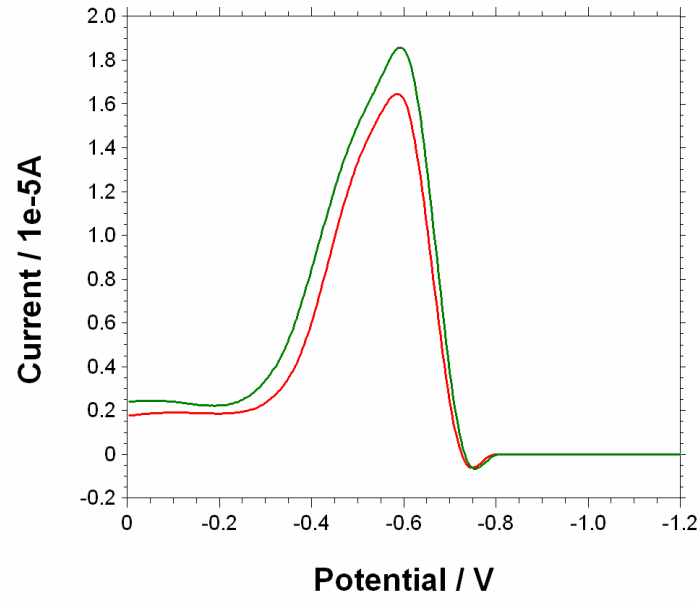

Figure 3.13 **Square wave voltammetry of [G-3]-flavin (red line) and riboflavin (green line) in pH = 8.0 sodium phosphate buffer/isopropanol 95:5 (4×10^{-5} M). E = -0.6 V versus Ag/AgCl.**

It is clear that from these electrochemical results, the dendritic architecture has little influence on the electrochemical properties of the flavin unit. There is no significant change in redox potential when moving from the n^{th} generation to the $n+1^{th}$ generation of flavin dendron, or between the highest (third) generation flavin dendron and riboflavin. These results do not concur with previous findings showing how electron-rich superstructures affect the reduction potential of the flavin sub-unit. It is unclear as to why this effect is not observed in these systems, however it may be that the position of the ethylene glycol side chains relative to the flavin unit is not of sufficient proximity to allow electron transfer, or that since the aromatic interactions of the aryl-branches, which have previously been seen to play an important role in creating the microenvironment of the flavin, may be restricting such an effect taking place.

3.2.4 Catalytic Activity Studies

Although results from the electrochemical studies fail to highlight any effect of the dendron backbone on the reduction potential of the flavin, the fluorescence and UV-vis studies certainly suggest a hydrophobic pocket microenvironment has formed around the flavin nucleus. This would suggest mimickery of a flavoprotein to a certain extent. However, a true measure of an enzymatic model system is its ability to replicate the behaviour of its prototype, therefore an examination into the flavin-based dendron's ability to catalyse a reaction specific to a flavoprotein would be a suitable benchmark.

Since flavoenzymes are an important class of redox enzymes involved in a variety of biological processes, the next stage of this study involves investigating the role that dendron generation plays with respect to the flavin unit, and the effect it has on tuning the catalytic activity of the redox active cofactor. In this study, the kinetics of the aerobic oxidation of the NADH analogue BNAH (Figure 3.7), by riboflavin and all three generations of water-soluble flavin dendrons have been investigated (please refer to acknowledgements section 3.4).

The catalytic oxidation activities of riboflavin and the flavin dendrons were studied by varying the concentrations of the substrate (BNAH) to quantify the kinetic parameters. Since BNAH is rapidly oxidised in the presence of flavins and disappears from the reaction medium, the catalysis was followed by monitoring the decrease in absorbance of BNAH at 358 nm. Figure 3.14 shows the Lineweaver-Burk plots of initial reaction velocity (v_0) vs. BNAH concentration for riboflavin and the flavin dendrons. The initial velocities were

recorded after addition of aliquots of first-, second-, or third-generation flavin dendrons to fresh solutions of BNAH. The observation of straight-line correlation in the kinetic plots indicates the existence of pseudo-first order kinetic behaviour for these reactions, and indicates they do not follow the Michealis-Menten saturation kinetics of typical enzymes. Instead, all three generations of flavin-dendrons exhibit pseudo-first order kinetics where only the initial portion of the saturation kinetics (which is linear) can be experimentally observed since the saturation of BNAH cannot be reached.[101] Non-linear least-squares curve fitting analysis was then used to evaluate the pseudo-first order (k_{pseudo}) and second order (k_2) rate constants for the reactions. The rate constants are compiled in Table 3.1.

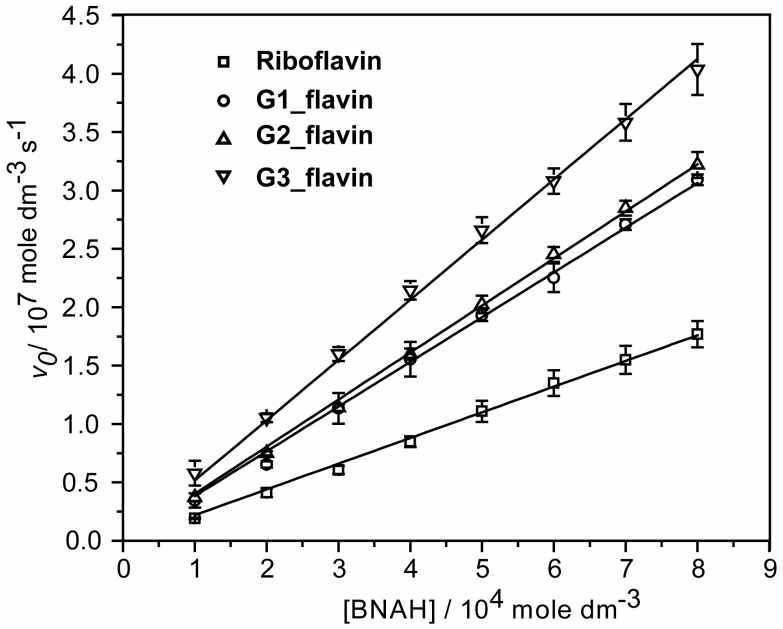

Figure 3.14 **Plots of initial velocities (v_0) vs. substrate concentration for the BNAH oxidation by riboflavin and flavin dendrons. The lines represent the best-fit of the data using pseudo first-order reaction kinetics.**

Substrate	Flavin Derivative	k_{pseudo} / 10^{-5} s^{-1}	k_2 / $mol.dm^{-3}.s^{-1}$
BNAH	Riboflavin	22	44
	[G-1]-Fl	38	76
	[G-2]-Fl	40	80
	[G-3]-Fl	52	104

Table 3.1 **Effect of dendron generation on kinetic parameters for the flavin catalysed oxidation of BNAH. The concentration of the flavin unit in all cases is maintained at 5 μmol.dm^{-3}.**

The comparison of the rate constants in Table 3.1 reveals a significant increase of the catalytic reaction rate for the flavin dendrons compared to riboflavin. In addition, an increased second-order rate constant of 1.7-2.4 fold was observed in the case of riboflavin relative to the flavin dendrons. This is consistent with previous research which shows that within the dendron family a significant rate acceleration can also be noticed upon an increase in dendron generation.[102] The increased reaction rates for the dendron systems compared to riboflavin can be attributed to an enhanced association between the substrate (BNAH) and the catalyst. This enhanced association for the dendron systems most likely originates from the π-stacking interactions between the aryl moieties of the dendrons and the reduced form of BNAH. As the dendron generation is increased, this feature becomes more prominent with the third-generation flavin dendron system, presumably aided by the presence of a hydrophobic pocket which helps localise the hydrophobic BNAH moiety near the flavin unit. Cooke and co-workers observed a similar result when studying the catalytic rate constants of their flavin-based polymer system against that of FMN. The presence of a hydrophobic pocket, in which the flavin unit was positioned, resulted in an increase of 2-4 fold for the catalytic rate constant, compared to that of free FMN.[25]

3.3 Conclusions

To summarise the work carried out in this study, a family of water-soluble flavin dendrons have been synthesised, using a convergent synthetic method, and subsequently analysed to examine their properties and behaviour. Optical analysis using UV-vis and fluorescence spectrometry confirms that encapsulation of the flavin sub-unit by the dendron super-structure is taking place in all three generations of compounds. However it is clear that in

the third-generation compound, a hydrophobic pocket is formed around the flavin unit. This is supported by a bathochromic shift in the UV-vis spectra, along with molecular dynamics simulations of the dendron species. Although results from cyclic voltammetry experiments showed that the presence of the dendron architecture has little effect on the redox properties of the flavin core, the results from UV-vis and fluorescence spectroscopy experiments showed encapsulation of the core redox unit certainly takes place. The precise explanation for the lack of electrochemical influence from the dendritic architecture still remains unclear.

It has also been shown that the ethylene glycol branches provide both a biomimetic hydrophobic binding pocket and a means of tuning the catalytic properties of the flavin unit in aqueous environments.[103] Catalytic activity studies show an increase in the rate of reaction for the aerobic oxidation of BNAH (a model NADH compound) for all three dendron generations, which increases to around double that of free riboflavin for the third-generation species. As the flavin dendrons behave similarly to the apoenzyme of natural flavoenzymes, this study paves the way for the synthesis of more elaborate derivatives, whereby functionality can be introduced to control the redox properties and reactivity of the flavin moiety. The development of systems displaying improved catalytic and electron transfer properties is the next development stage of this project.

3.4 Acknowledgements

The author gratefully acknowledges the contribution to this work, in particular performing the catalytic activity studies, made by Vincent M. Rotello, Sarit S. Agasti, Brian J. Jordan and Subinoy Rana at the University of Massachusetts, USA.

Chapter Four

4 Chapter Four – "Click" Flavin Dendrons: Towards Synthetic Flavoenzymes

4.1 Introduction

4.1.1 Outline

In the early stages of research into dendron molecules and their architecture, the initial focus was on the development of their synthesis. However it became increasingly apparent that their applications were widespread not only in areas of catalysis, but also in biochemistry. In recent years there has been great interest in the investigation and development of functional dendrimer systems, in particular the discovery of functions and properties that the dendritic architecture is directly responsible for. It has been shown in the previous chapter that a dendritic architecture can be used to mimic the hydrophobic pocket usually observed in proteins and enzymes, and that the degree of branching within that architecture can affect the physical properties of an electrochemically active molecule at the foci. The aim of this study is to further investigate the effect of the dendron system on the molecule at the focal point, in particular how the architecture can be used to tune the redox capability and supramolecular binding properties of a particular species.

The relationship between complex redox processes and molecular recognition is a central theme in many different biological systems. For example, enzymes composed of redox-active core molecules, including flavins,[104] quinones,[105,106] nicotinamides[107] and pterins,[108] use specific enzyme-cofactor interactions to control the activity of a given cofactor. By using different recognition elements, including hydrogen bonding, π-stacking, and electrostatic interactions, in enzymatic processes serves to control the oxidation and protonation states of a cofactor's activity. Accordingly, understanding the cooperative recognition processes that govern complex redox enzyme activity serves as an attractive target in the development of redox-active molecular devices[109,29] and model systems.[110,111,112] The incorporation of the flavin functionality in dendron systems allows for the study of dendron environmental effects on flavin binding both in neutral and reduced redox states. This study aims to provide a better understanding of flavin-binding interactions with dendritic architectures, through the development of model systems with varying degrees of dendritic branching. An alkyne-flavin derivative was appended to three

generations of aryl-dendrons via the Huisgen 1,3-dipolar cycloaddition, more commonly referred to as a "click" cycloaddition.[113,114,115,116]

4.1.2 Aryl Dendrons

The hyper-branching in dendrimers suggests several purposes for this architecture in rational, molecular design schemes. One role of particular significance is that of encapsulation. Encapsulation in dendrimers can be studied in several contexts.[117,118,119,120] These include small molecule guest encapsulation and covalent encapsulation of a core moiety.[121] In this latter class, dendrimers are arguably ideal to act as encapsulating agents, as they can be synthesised to give mono-disperse macromolecules with well-defined primary structures, and because the interior and exterior of the dendrimer may be tailored to control both the interior nano-environment and the external functionality presented by the molecule. These features have the potential to lead to new, possibly unique physical properties in core-encapsulated dendrimers.

To probe further the relationship between dendrimer generation, structure and core encapsulation, several research groups have studied redox-active core dendrimers.[121,122] By examining the thermodynamic redox potential and/or the reversibility of the electrochemical charge transfer of these dendrimers, additional insight into the relationship between structure and physical properties for encapsulation has been obtained. A decrease in the reversibility of the electrochemical charge transfer (or, more quantitatively, the heterogeneous electron transfer rate) has often been correlated with increasing dendrimer generation. This decrease is thought to arise due to the steric shielding of the electroactive moiety from the electrode. This relationship between dendritic encapsulation and the attenuation of electron transfer rates can be illustrated by the following examples of electroactive core dendrimers.

Diederich and co-workers observed the first example of electron transfer rate attenuation with increasing dendrimer size.[73] First-, second-, and third-generation zinc porphyrin core dendrimers with four arms were synthesised and their cyclic voltammograms measured. As the generation of the dendrimer increased, the voltammetric waves shifted and broadened, which indicated slowing heterogeneous electron transfer kinetics. This decrease in the electrochemical reversibility was particularly notable going from the second to the third generation dendrimer. Frechet, Abruna and co-workers observed an even more dramatic change in electrochemical reversibility of zinc porphyrin core dendrimers.[123] Generation

three and higher dendrimers showed complete disappearance of voltammetric waves. This result indicated a substantial attenuation of the heterogeneous electron transfer rate for this dendrimer.

Gorman and co-workers have also carried out research into the effects of differing dendritic architectures on identical cores.[124] Two different dendrimers containing iron-sulphur clusters with four arms in a tetrahedral arrangement were synthesised, one with a flexible architecture based on 4,4-bis(4-hydroxyphenyl)pentanol,[125,126] and one with a more rigid structure based on phenylacetylene.[127] Heterogeneous electron transfer rates were obtained via Oysteryoung square-wave voltammetry, which revealed that the attenuation of electron transfer rates by the rigid architecture was larger than that in the flexible structures. The results from conformational searching computations on these two architectures suggested that flexible architectures permitted substantial mobility of the core throughout the architecture compared to the rigid structure. The data collected as a whole suggested that generic, flexible dendrimer architectures do not sterically shield the core as much as might be expected merely by examination of their primary structure.

These results suggest that dendrimers sterically shield redox-active cores and attenuate heterogeneous electron transfer kinetics. However recent results published by Balzani[128] and Kaifer[129] show dendrimers with bipyridinium cores that do not exhibit such large changes in voltammograms with increasing generations of dendritic branching. It seems that dendritic encapsulation of redox-active core units is not a completely general phenomenon. This study aims to examine the level of encapsulation of the core redox-active flavin unit, when covalently bound to a dendritic architecture based on benzyl units. These flexible branches should allow straightforward monitoring of the encapsulation of the flavin unit as the level of branching increases. In addition, the effect that the degree of branching has on the flavin's ability to non-covalently bind to the DAP unit will also be examined.

4.1.3 Flavin Cofactor

For this study, the flavin derivative **26** was used as the redox active functionality within the three generations of dendron molecules (Figure 4.1).

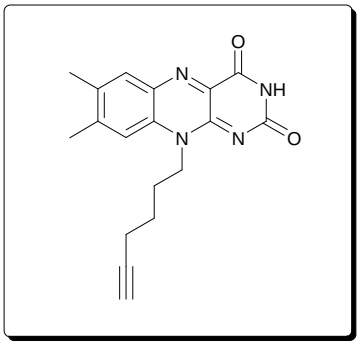

Figure 4.1 The alkyne-functionalised flavin molecule.

An alkyne functionality was appended to the flavin unit via the N(10) position. In naturally occurring flavin molecules, side groups attached to this nitrogen atom do not play a major part in tuning the redox capability of the flavin unit. Instead they are usually concerned with anchoring the molecule to the protein backbone. For this reason, the alkyne functionality is a suitable reactive group to undergo a Huisgen cycloaddition with a second, azide functionalised molecule, to enable attachment of a larger dendritic architecture to mimic the presence of the large protein backbone. Attachment of the dendron architecture through this nitrogen atom allows non-covalent binding to take place via the imide functionality. The effect of the degree of dendritic branching on the three-point hydrogen bonding that takes place at this binding site, and on the redox capability of the flavin molecule, can then be monitored.

4.1.4 "Click" Synthesis

"Click chemistry" is a chemical philosophy introduced by K. Barry Sharpless in 2001 and describes chemistry tailored to generate substances quickly and reliably by joining small units together.[116] This was inspired by the fact that nature also generates substances by joining small units together to create a larger architecture.

In biochemistry, proteins are made from repeating amino acid units while sugars are made from repeating monosaccharide units. The connecting units are based upon carbon-heteroatom bonds (C-X-C) rather than carbon-carbon (C-C) bonds. In addition, enzymes ensure that the chemical processes involved can overcome large enthalpy hurdles by division into a series of reactions, each with a small energy step. Mimicking nature in the organic synthesis of new compounds, especially in the area of drug discovery, is essential given the large number of possible structures. Click chemistry encourages the following criteria:

- Modular application with a wide scope.
- Reactions that obtain a high chemical yield.
- Generation of innocuous by-products.
- Is stereospecific in nature.
- Have simple reaction conditions.
- Have readily available starting materials.
- Simple product isolation (i.e. by crystallisation or distillation, not preparative chromatography).
- Large exothermic driving force > 84 $kJ.mol^{-1}$ to favour a reaction with a single product (a distinct exothermic reaction makes a reactant "spring-loaded").
- High atom economy.

Many of the above criteria are subjective and it is unlikely that any reaction will be perfect for every situation and application. However several applications have been identified as superior in the application of click chemistry:

- The Huisgen 1,3-dipolar cycloaddition.
- Other cycloadditions, such as the Diels-Alder reaction.
- Nucleophilic substitution especially to small strained rings like epoxy and aziridine compounds.
- Carbonyl-chemistry-like formation of ureas, but not reactions of the aldol-type due to low thermodynamic driving force.
- Addition reactions to carbon-carbon double bonds (dihydroxylation).

Of all the above processes, the azide-alkyne Huisgen 1,3-dipolar cycloaddition is one of the most reliable in terms of the "click" criteria.[130] This process of cycloaddition using a copper catalyst at room temperature was discovered concurrently and independently by the groups of K. Barry Sharpless[116] and Morten Meldal.[131] It was an improvement over the same reaction first popularised by Rolf Huisgen in the 1970s, albeit at elevated temperatures in the absence of water and without a copper catalyst.

4.1.5 The Azide-Alkyne Huisgen Cycloaddition

The azide-alkyne Huisgen cycloaddition is a 1,3-dipolar cycloaddition between an azide functional group and a terminal or internal alkyne to give a 1,2,3-triazole (Figure 4.2). Rolf

Huisgen was the first to grasp the scope of this reaction, with subsequent developments by K. Barry Sharpless, who described the reaction as the cream of the crop of click chemistry.

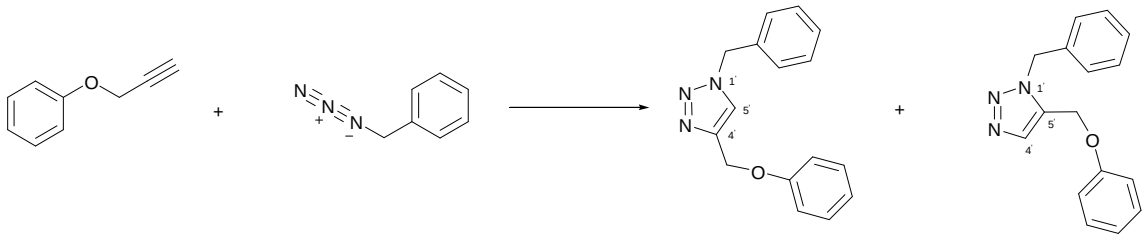

Figure 4.2 The Huisgen 1,3-dipolar cycloaddition.

In the reaction outlined in Figure 4.2, the azide reacts neatly with the alkyne to afford the triazole as a mixture of the 1,4- and 1,5-adducts at 98 °C in 18 hours. A notable variant of the Huisgen 1,3-dipolar cycloaddition is the copper(I) catalysed version in which organic azides and terminal alkynes are united to afford 1,4-regioisomers of 1,2,3-triazoles as sole products. The copper(I)-catalysed variant was first reported for solid phase synthesis of peptidotriazoles by Morten Meldal and co-workers at the Carlsberg Laboratory in Denmark. While the copper(I) catalysed variant gives rise to a triazole from a terminal alkyne and an azide, formally it is not a 1,3-dipolar cycloaddition and thus should not be termed a Huisgen cycloaddition. This reaction is better termed the Copper(I)-catalysed Azide-Alkyne Cycloaddition (CuAAC), but is certainly a click reaction. While the reaction can be performed using commercial sources of copper(I) such as cuprous bromide or iodide, the reaction is far more successful using a mixture of copper(II), such as copper sulphate, and a reducing agent, such as sodium ascorbate, to produce copper(I) in situ. As copper(I) is unstable in aqueous solvents, stabilising ligands are effective for improving the reaction outcome, especially if tris-(benzyltriazolylmethyl)amine (TBTA) is used. The reaction can be run in a variety of solvents, and mixtures of water and a variety of (partially) miscible organic solvents including alcohols, DMSO, DMF, tBuOH and acetone. Owing to the powerful coordinating ability of nitriles towards Cu(I), it is best to avoid acetonitrile as a solvent.

The utility of the Cu(I) catalysed click reaction has also been demonstrated in the polymerisation reaction of a bis-azide and a bis-alkyne with copper(I) and TBTA to a conjugated fluorine based polymer (Figure 4.3).[132] The degree of polymerisation of this reaction easily exceeds 50, and by using stopper molecules such as phenyl azide, well-defined phenyl end-groups are obtained.

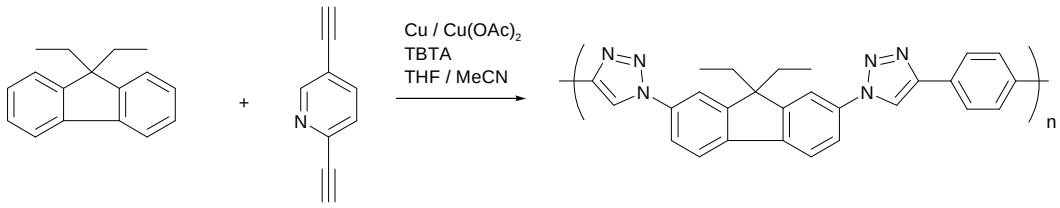

Figure 4.3 An example of a click-polymerisation reaction

The copper mediated azide-alkyne cycloaddition is receiving widespread use in material and surface sciences. Most variations in coupling polymers with other polymers or small molecules have been extensively researched, and current shortcomings are that the terminal alkyne appears to participate in free radical polymerisations. This requires protection of the terminal alkyne with a trimethyl silyl protecting group and subsequent deprotection after the radical reactions are completed. Similarly, the use of organic solvents, Cu(I), and inert atmospheres with which to carry out the reaction makes the click label inappropriate. An aqueous protocol for performing the cycloaddition with free radical polymers is highly desirable.

In this study, the copper(I) catalysed cycloaddition between a terminal alkyne and azide is used to generate flavin-functionalised dendrons with increasing levels of dendritic branching. The reaction is carried out using copper(I) iodide in DMF at room temperature, generating the 1,2,3-triazole linked flavin dendron as the 1,4-regioisomer as the sole product.

4.2 Results and Discussion

4.2.1 Synthesis

In a similar approach to that used in the previous chapter, three generations of flavin-functionalised dendrons were created using a convergent synthetic method. The core synthetic technique used was that of the “click” chemical reaction; the Huisgen 1,3-dipolar cycloaddition, or more accurately the Copper-catalysed Azide-Alkyne Cycloaddition.[133] The convergent approach involves generating the dendritic architecture, beginning with the outer-most peripheral functional groups, continuing inwards to the focal point, in this case that being the flavin unit. For each of these dendrons, the branches consisted of poly-aryl functionalities, with the flavin species attached through a 1,2,3-triazole connecting unit. The synthesis of the alkyne-functionalised flavin unit is outlined in Scheme 4.1.

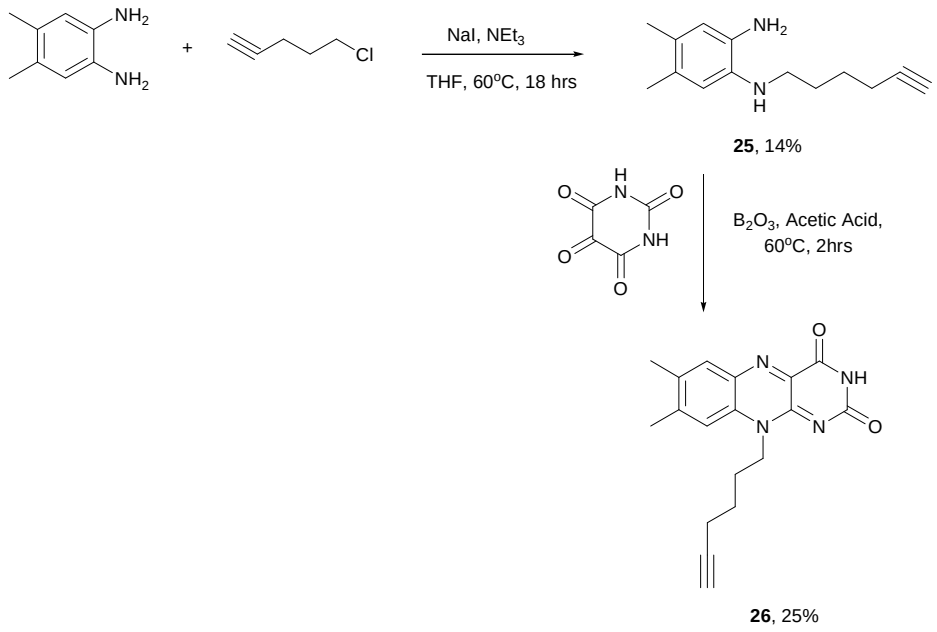

Scheme 4.1 Synthesis of the alkyne-functionalised flavin derivative.

Mono-substitution of 4,5-dimethyl-1,2-phenylenediamine with 6-chlorohexyne was carried out using sodium iodide and triethylamine as base in THF to afford the desired mono-isomer (**25**) in 14% yield. Further condensation of the mono-substituted alkyne diamine product with alloxan monohydrate yielded the alkyne functionalised flavin compound **26**. This product was then used to synthesise the three generations of flavin-functionalised dendrons. The synthesis of the 1st generation dendron is outlined in Scheme 4.2.

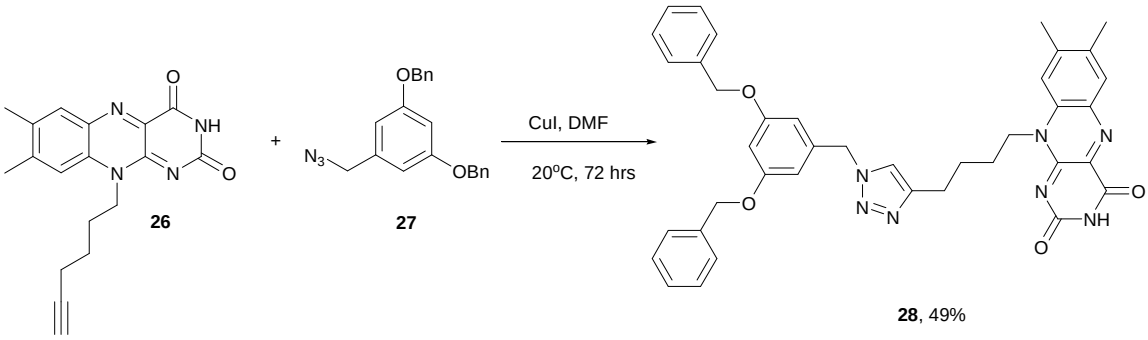

Scheme 4.2 Synthesis of the 1st generation flavin-functionalised "click" dendron.

Using the azide-functionalised dendron (**27** – please refer to acknowledgements), a cycloaddition was carried out with the alkyne-functionalised flavin species (**26**) in DMF using copper(I) iodide. The solution was stirred at room temperature for four days to afford the 1,2,3-triazole flavin-functionalised first-generation dendron species **28** in 49% yield. Further synthesis of the second- and third-generation flavin dendrons was carried out in a

similar fashion. The synthetic routes for these reactions are outlined in Schemes 4.3 and 4.4 respectively.

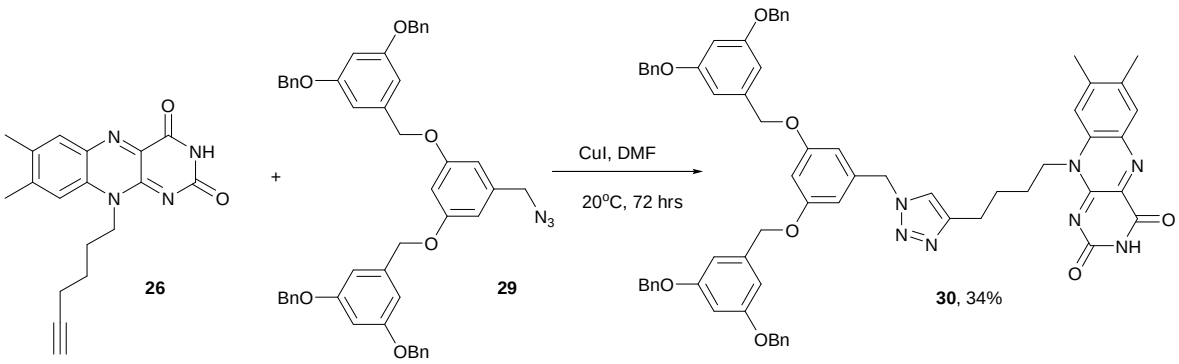

Scheme 4.3 Synthesis of the 2nd generation flavin-functionalised "click" dendron.

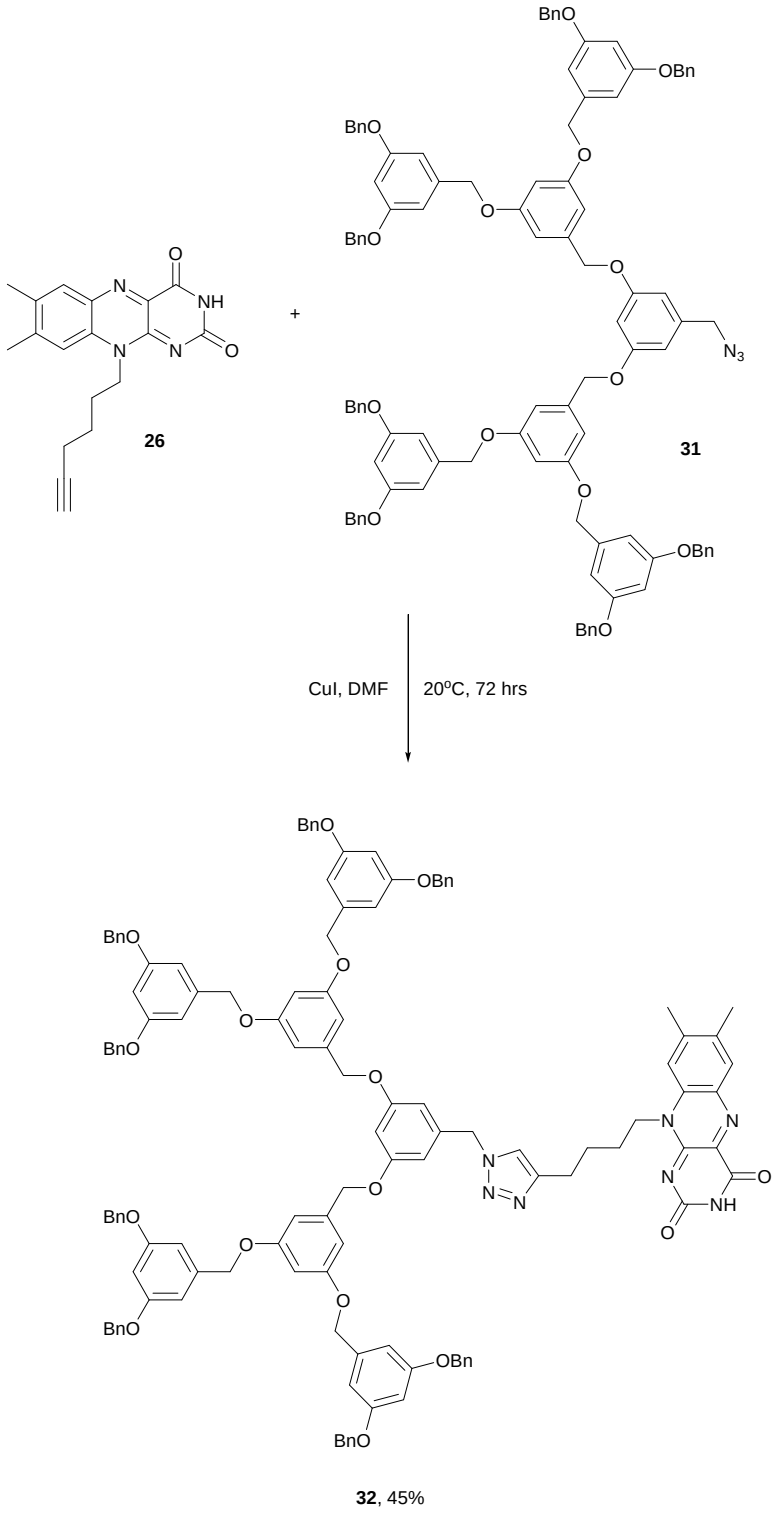

Scheme 4.4 Synthesis of the 3rd generation flavin-functionalised "click" dendron.

Cycloadditions between the azide-functionalised "parent" dendron and the flavin unit were carried out on both the second and third generations of aryl dendrons to generate the desired 1,2,3-triazole flavin-functionalised dendrons **30** and **32** in 34% and 45% yields respectively.

4.2.2 Physical Analysis

4.2.2.1 NMR Titrations

Hydrogen bonding between the flavin moiety of each of the first-, second-, and third-generation of flavin-functionalised dendron and the diaminopyridine (DAP) unit was confirmed using ^{1}H NMR spectroscopy. In the case of the first-generation dendron (**28**, Figure 4.4), aliquots of DAP were added to a solution of the flavin dendron in $CDCl_3$ which resulted in a smooth downfield shift in the resonance of H(1) of the flavin. The resulting curve was fitted to a 1:1 binding isotherm and gave a binding constant of 395 ± 40 M^{-1} for the first-generation flavin-DAP complex. Similar studies carried out on the second- and third-generation flavin-functionalised dendrons resulted in binding constants of 263 ± 26 M^{-1} and 176 ± 18 M^{-1} respectively.

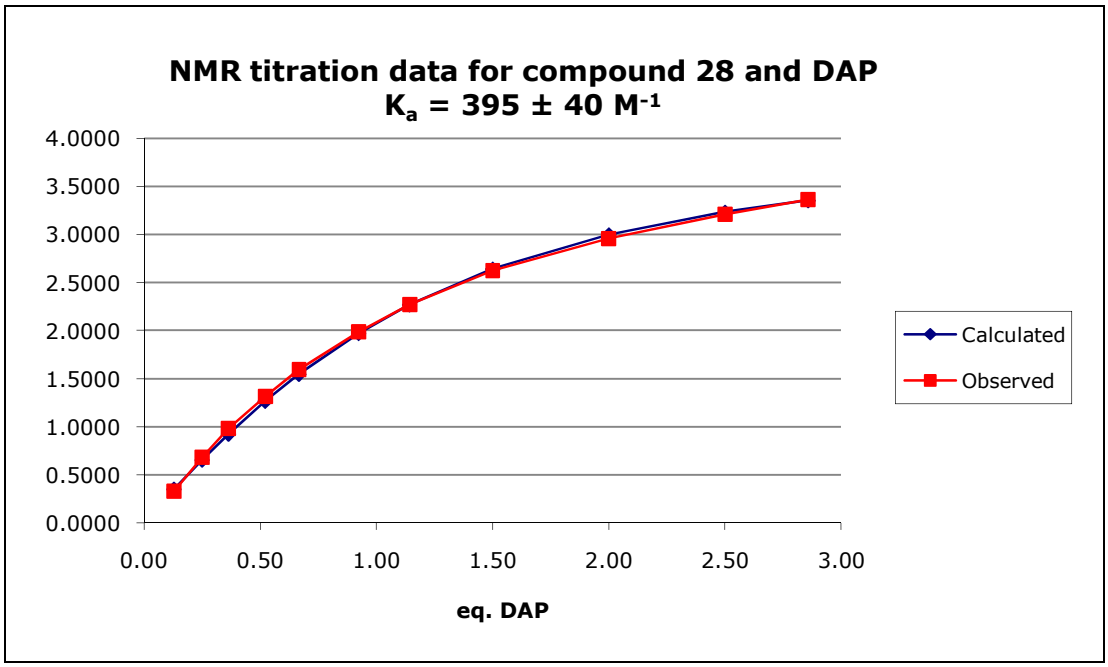

Figure 4.4 **NMR titration data for the first-generation flavin-functionalised "click" dendron in the presence of aliquots of DAP (K_a = 395 ± 40 M^{-1}) in $CDCl_3$ at 20 °C.**

It is clear from these results that as the generation of dendritic branching increases, the binding constant for the complex decreases. These results are consistent with increased levels of steric hindrance within the complex arising from the dendron's benzyl branches. This hindrance impedes the ability of the DAP unit to non-covalently bind to the flavin.

4.2.2.2 Electrochemistry

The solution electrochemistry of the first-generation flavin-functionalised dendron has been studied using cyclic voltammetry (CV). Upon reduction of **28**, a single reduction wave and two distinct oxidation waves were observed (Figure 4.5). The former process is due to the reversible formation of the flavin radical anion $\mathbf{28_{rad}^-}$ ($E_{½}$ = -0.85 V), whereas the second reoxidation wave ($E_{½}$ = -0.75 V) arises from an electrochemical-chemical-electrochemical (e-c-e) process whereby a portion of $\mathbf{28_{rad}^-}$ formed at the electrode surface rapidly deprotonates **28** in bulk medium. The protonated flavin ($\mathbf{28_{rad}H}$) radical produced in this process undergoes a further one-electron reduction at the working electrode surface to form the relatively stable fully reduced flavin anion ($\mathbf{28_{red}H^-}$), which is subsequently reoxidised at a less negative potential than $\mathbf{28_{rad}^-}$. Upon addition of an excess of the DAP unit to the electrolyte solution, the redox wave corresponding to the $\mathbf{28/28_{rad}^-}$ redox couple is immediately shifted by +80 mV, corresponding to a substantial stabilisation of the flavin radical anion of 7.7 kJ.mol^{-1}.

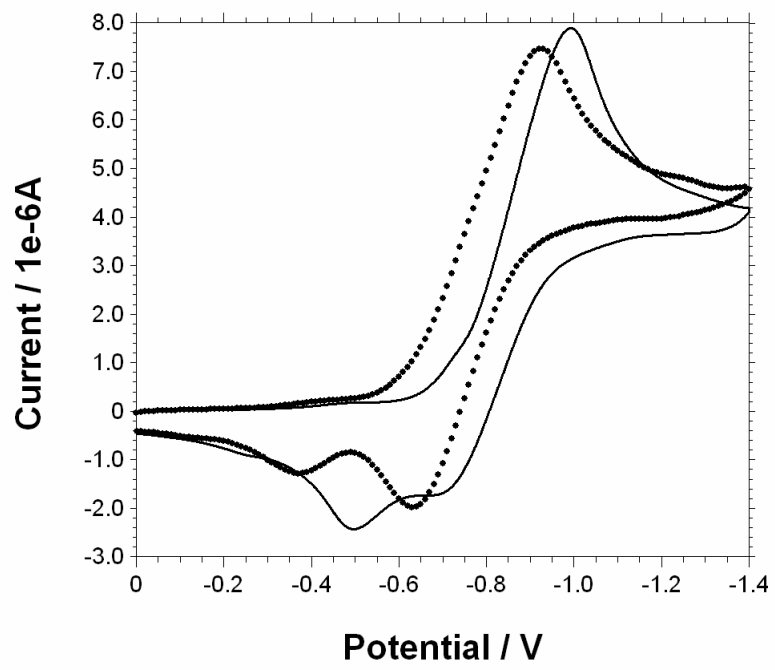

Figure 4.5 **Cyclic voltammogram of first-generation dendron (1 x 10^{-4} M) and in the presence of DAP (1 X 10^{-3} M). Scan rate = 100 mV.s^{-1}. Recorded in pH = 8.0 sodium phosphate buffer/isopropanol 95:5 (4 x 10^{-5} M).**

The solution electrochemistry of the second- and third-generations of flavin-functionalised dendrons was also studied upon the addition of DAP using the same method as employed for the first-generation dendron. In both cases, a shift of + 80 mV was observed upon addition of the DAP moiety. These results are consistent with a significant stabilisation of

the flavin radical anion and a concomitant increase in the hydrogen bonding efficiency upon the reduction of the flavin moiety within the complex.

The solution electrochemistry of the second-generation flavin-functionalised dendron **30** has been studied using cyclic voltammetry (CV) at varying scan rates at 1000, 500, 100 and 50 $mV.s^{-1}$ (Figure 4.6). Using a scan rate of 1000 $mV.s^{-1}$, the voltammogram shows a redox wave producing the largest current (1.45×10^{-5} A) for the first reduction process. Only by using a scan rate of 50 $mV.s^{-1}$ were truly reversible redox waves obtained. At higher scan rates, the reduction proved irreversible. At 50 $mV.s^{-1}$, a single reduction wave and two distinct re-oxidation waves are observed.

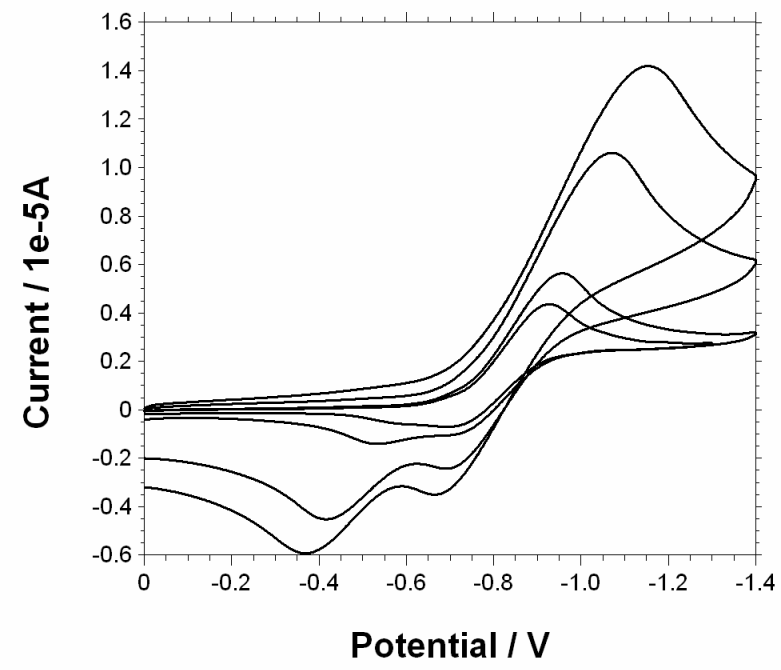

Figure 4.6 **Cyclic voltammogram of second-generation dendron (1×10^{-4} M). Scan rate = 1000 (largest current), 500, 100 and 50 (smallest current) $mV.s^{-1}$. Recorded in pH = 8.0 sodium phosphate buffer/isopropanol 95:5 (4×10^{-5} M)**

The solution electrochemistry of the third-generation flavin-functionalised dendron **32** has been studied using cyclic voltammetry (CV) at varying scan rates at 1000, 500, 100 and 50 $mV.s^{-1}$ (Figure 4.7). Using a scan rate of 1000 $mV.s^{-1}$, the voltammogram shows a redox wave producing the largest current (1.15×10^{-5} A) for the first reduction process. Only by using a scan rate of 50 $mV.s^{-1}$ were truly reversible redox waves obtained. At higher scan rates, the reduction proved irreversible. At 50 $mV.s^{-1}$, a single reduction wave and two distinct re-oxidation waves are observed.

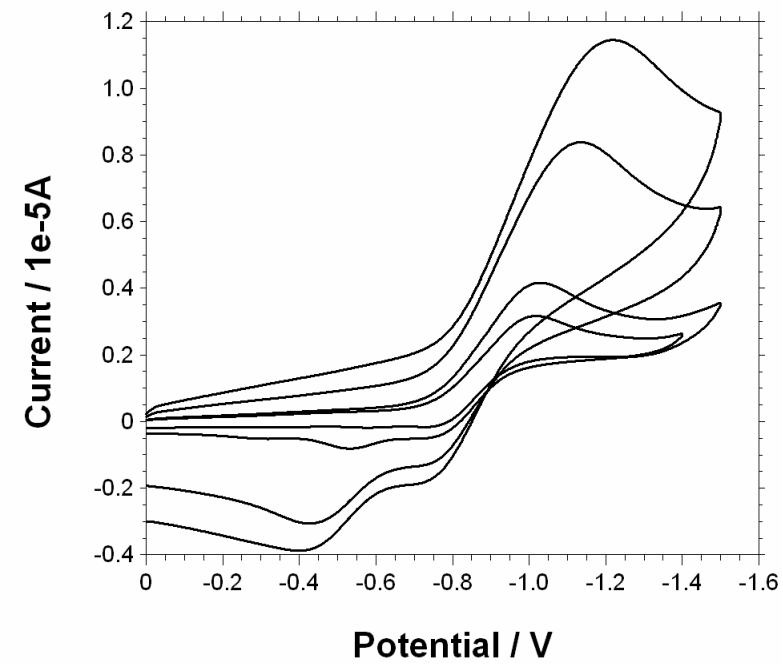

Figure 4.7 **Cyclic voltammogram of third-generation dendron (1 x 10^{-4} M). Scan rate = 1000 (largest current), 500, 100 and 50 (smallest current) mV.s^{-1}. Recorded in pH = 8.0 sodium phosphate buffer/isopropanol 95:5 (4 x 10^{-5} M)**

By comparing the electrochemical results for all three dendrons at the scan rate of 50 mV.s^{-1}, it is clear that as the level of dendritic branching (dendron generation) increases, the redox waves are shifted and broadened, indicating slowing heterogeneous electron transfer kinetics. This decrease in electrochemical reversibility is particularly noticeable going from the first to the third generation of flavin dendron. These results showing the attenuation of electron transfer rates are consistent with the theory that the flavin unit is encapsulated by the dendritic architecture, partially quenching its reversibility as a redox cofactor.

4.3 Conclusions

This study has shown the synthesis of first-, second- and third-generations of flavin-functionalised dendrons, with a benzyl-based dendritic architecture. Electrochemical analysis of these dendrons showed significant encapsulation of the flavin moiety by the dendron's benzyl branches, which becomes more pronounced as the generation level of branching increases. Analysis of the redox capability of the flavin unit in the presence of a complementary DAP species showed shift of + 80 mV, indicating a stabilisation of the flavin radical anion. This was observed in all three generations of the flavin-DAP complexes. NMR titrations performed on these complexes showed a steady decrease in the association constant of the complex as the generation level of dendron branching

increased, caused by increased levels steric hindrance. These initial studies should help pave the way for the synthesis of more elaborate flavin-based systems, with applications directed towards the creation of truly synthetic flavoenzymes.

4.4 Acknowledgements

The author gratefully acknowledges the contribution made to this work my Amitav Sanyal at at Bogazici University, Turkey, for the generous donation of the first-, second- and third-generation of azide functionalised dendrons for this study.

Chapter Five

5 Chapter Five – Pyrroloquinoline Quinone Model Systems

5.1 Introduction

5.1.1 Outline

Nicotinamides and flavins are essential cofactors in enzyme-catalysed redox reactions. However another redox cofactor, pyrroloquinoline quinone (PQQ; 4,5-dioxo-4,5-dihydro-1*H*-pyrrolo[2,3-*f*]quinoline-2,7,9-tricarboxylic acid) has received much attention as a novel coenzyme of various important oxidoreductases and dehydrogenases such as methanol dehydrogenase (MDH)[106] and soluble glucose dehydrogenase (s-GDH).[134,135] These two examples belong to a class of enzymes called the quinoproteins, all containing the PQQ redox coenzyme serving as a cofactor to perform their enzymatic function.[136,137,138]

PQQ was discovered by Hauge as the third redox cofactor after nicotinamide and flavin in bacteria.[139] It was found to stimulate growth in bacteria as well as display other antioxidant and neuro-protective effects. One of the most influential discoveries was reported by Rucker who found that mice deprived of PQQ showed various abnormalities, such as reproductive deficiencies, reduced immune response and skin problems, and it was suggested that PQQ might play an important nutritional role in mammals.[140] In 2003, it was reported that aminoadipate semi-aldehyde dehydrogenase (AASDH) might also use PQQ as a cofactor in the lysine degradation pathway (Figure 5.1),[141] suggesting the possibility that PQQ is actually a vitamin in mammals, and therefore qualifies as a new class of B vitamin, alongside more well known compounds such as riboflavin.

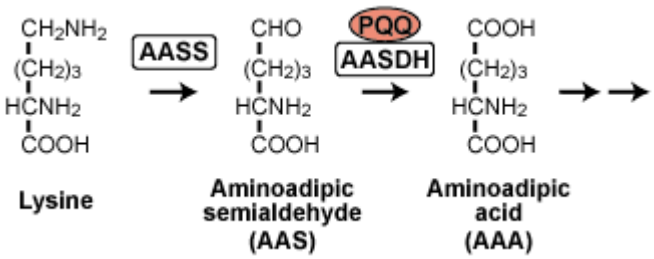

Figure 5.1 Initial steps of lysine degradation.

Recent reports also suggest that PQQ may stimulate the growth of plants in hydroponic culture and may be the causative factor in plant growth stimulation by a strain of *pseudomonas fluorescens* bacterium.[142] With such a variety of applications, it is clear why PQQ has gained much interest in current research and why further study of its reactivity is necessary.

5.1.2 PQQ Structure and Function

PQQ has a unique *o*-quinone structure (Figure 5.2).[143] The *o*-quinone ring, the active site, is condensed with an electron withdrawing pyridine nucleus and with an electron donating pyrrole. The *o*-quinone moiety of PQQ serves as the 'backbone' to the molecule, and possesses a different electronic nature than that of simple *o*-quinone compounds due to the effects of its fused substituent groups.

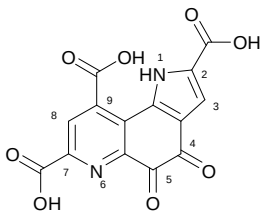

Figure 5.2 Structure of PQQ cofactor

Extensive research has been carried out by Itoh and co-workers into the structural importance of the pyrroloquinoline quinone skeleton,[144] and in particular how the fused rings and their functional groups affect the electron distribution across the *o*-quinone backbone. The studies indicate that in contrast to a standard *o*-quinone structure, the polarisation of the C-5 carbonyl function of the PQQ molecule is diminished to an extent by the electronegativity of the peri-pyridine nitrogen i.e. the electropositivity of the C-5 carbon is decreased when fused with a neighbouring pyridine ring, due to adjacent electron deficient C-5a carbon (Figure 5.3).

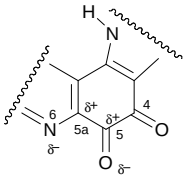

Figure 5.3 Electron distribution around the *o*-quinone backbone

Methanol dehydrogenase (MDH) is arguably the most studied quinoprotein with respect to PQQ function.[106, 145] MDH requires Ca^{2+} as well as the PQQ cofactor for activity in the oxidation of methanol to formaldehyde. Crystal structure data shows that Ca^{2+} binds to PQQ through N-6, C-5 carbonyl oxygen and C-7 carboxylate (Figure 5.4). Protein Glu and Asn side chains occupy the remaining Ca^{2+} coordination sites. The role of Ca^{2+} has been assumed to be structural, however there have been persistent speculations that it may also play a catalytic role.[146] A recent study by Itoh and co-workers has undoubtedly demonstrated a catalytic role for Ca^{2+} in a model system.[147] Their study revealed that the trimethyl ester of PQQ (PQQ-TME) is capable of oxidising methanol to formaldehyde in anhydrous acetonitrile when treated with $Ca(ClO_4)_2$ in the presence of an organic base.

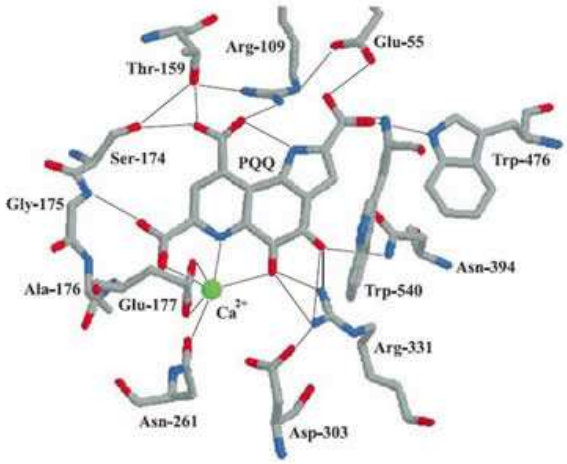

Figure 5.4 Crystal structure showing the PQQ binding pocket of MDH.[148]

Three stable redox states of PQQ are biologically relevant (Figure 5.5).[149] The oxidised, quinone state of the cofactor can be converted into the reduced, quinol form ($PQQH_2$) by the transfer of two electrons and two protons from a substrate. $PQQH_2$ can be re-oxidised to PQQ in a single two-electron transfer step. Alternatively, re-oxidation can be achieved in two separate one-electron transfer steps via the free-radical semi-quinone form (PQQH). The redox state of the cofactor is thought to be an intermediate in the stepwise re-oxidation process of reduced MDH-$PQQH_2$ by two molecules of the physiological electron acceptor cyctochrome c_L.[150]

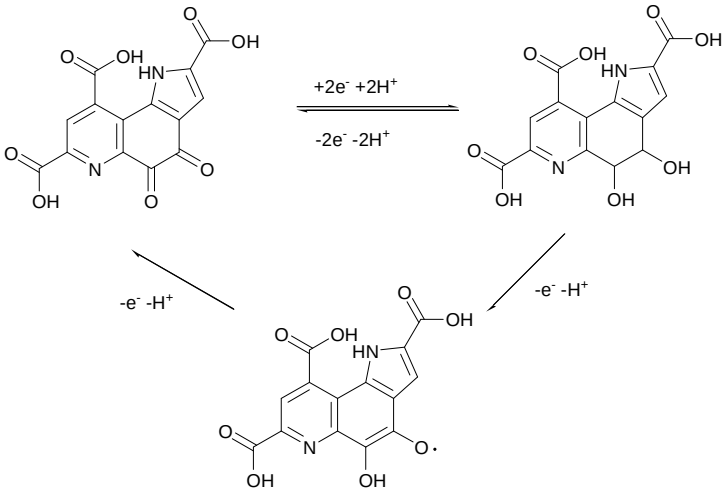

Figure 5.5 Three accessible, biologically relevant redox-states of PQQ.

5.1.3 Aim

Hydrogen bonds are one of the most important types of intermolecular interactions. Due to their strength and directionality, they are ubiquitous in biological systems, providing essential recognition, structural and control elements needed to coordinate and run the complex molecular machinery required for life.[151] Rotello and co-workers have shown how hydrogen bonds are used to modulate the redox potentials of the flavin unit in flavin-containing redox proteins.[44] This is achieved by stabilising one oxidation state relative to another.

Recent research has shown how hydrogen bonds coupled with electrochemistry can create a powerful control element in synthetic receptor-substrate systems.[152] Hydrogen bonds are known to have substantial electrostatic character. Therefore a reduction or oxidation process that leads to a change in partial charge on one of the components in a hydrogen bond will have a significant effect on the strength of that hydrogen bond. In particular if the negative charge on the hydrogen acceptor or the positive charge on the hydrogen donor is increased, the strength of the hydrogen bond will be increased. Alternatively, if the negative charge on the hydrogen acceptor or the positive charge on the hydrogen donor is decreased, the strength of the hydrogen bond will be decreased.

This study reports the synthesis of a PQQ analogue, whereby the pyrrole ring functionality has been removed and replaced by a phenyl ring. This analogue is used due to its improved electrochemical reversibility in organic solvent compared to that of naturally occurring PQQ.[153,154] Electrochemical experiments have been carried out on this species alone and

when in the presence of a suitable hydrogen bond donor, in this case a diphenyl urea analogue. Computational experiments have also been carried out to further assess the structural and electronic nature of the supramolecular complex, in order to consider what effect the structural alterations have on the nature of the hydrogen bonding and in turn what effect this has on the redox capability of the synthetic species.

5.2 Results and Discussion

5.2.1 Synthesis

The synthesis of the PQQ analogue benzoquinoline quinone (BQQ) has been successfully carried out, and is outlined in Scheme 5.1.

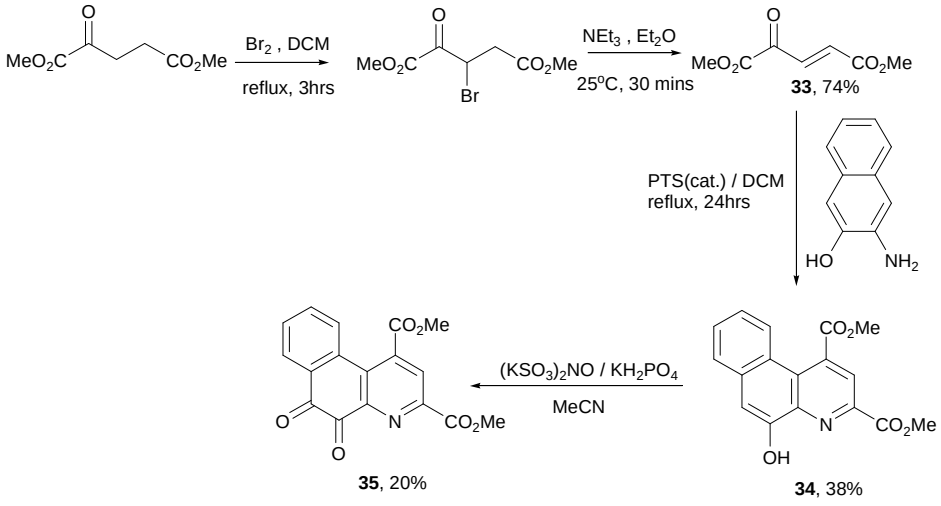

Scheme 5.1 Benzoquinoline quinone synthetic route.

Dimethyl 2-oxoglutaconate (**33**) was successfully isolated via the concomitant bromination and elimination reactions of dimethyl 2-oxoglutarate.[155] The bromination product was not isolated due to its instability, and so was immediately treated with base in diethyl ether to afford the α,β-unsaturated compound (**33**). A Doebner-von Miller type annulation was then used to construct the benzo[*f*]quinoline skeleton having carbomethoxy groups at the 2- and 4-positions.[144] This was achieved by treatment of 3-amino-2-napthol with 1.5 equivalents of dimethyl 2-oxoglutaconate and a catalytic amount of PTS in refluxing DCM overnight, resulted in the benzoquinoline derivative (**34**) in 38% yield. Subsequent oxidation of **34** with Fremy's salt gave the desired benzoquinoline quinone product (**35**) in 20% yield.

5.2.2 Molecular Modelling

Density Functional Theory (DFT) calculations have been carried out on the benzoquinoline quinone species. This computational molecular modelling focuses on both the neutral and radical anion states of the molecule in a supramolecular environment (i.e. when non-covalently bound to the dimethyl urea derivative) and when no other compound is present. The target model system is illustrated in Figure 5.7.

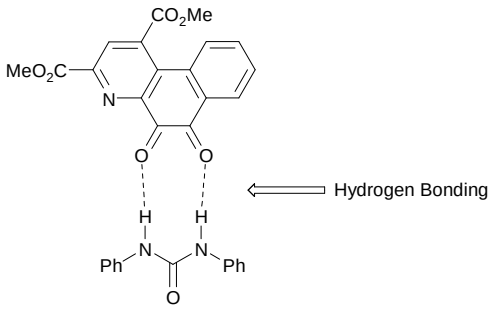

Figure 5.7 Theoretical BQQ-urea complex

Calculations were carried out using the Gaussian 03 software at the B3LYP level. Firstly, the geometry of the BQQ molecule alone was optimised using the 6-31G** basis set. This geometry was then used to run a single point energy calculation at each redox state to determine the global minimum energy level. It is at this energy level that the electrostatic potential map of the species was calculated. The same process was used to calculate the electrostatic potential maps of the BQQ molecule when non-covalently bound to a receptor. This process results in the calculation of the electrostatic potentials across the supramolecular complex on both redox states, and hence provides a picture of the electron density within the BQQ species. The dimethyl urea molecule was chosen for the theoretical calculations as opposed to its diphenyl counterpart used in the synthetic studies. This was to ensure smaller calculation times whilst still obtaining useful results with respect to the active *o*-quinone site. Previous studies have shown that replacing a larger aromatic side-group with a smaller one has no major effect on the character of the adjacent functional groups which are to be studied.

5.2.2.1 BQQ DFT Calculations

The geometry optimisation and electrostatic potential map of the BQQ species were calculated using the above procedure. The most stable geometry of the BQQ compound for

each redox state is shown in Figure 5.8, alongside the calculated Chem3D representation. Charges and spin densities for relevant atoms are listed in Table 5.1.

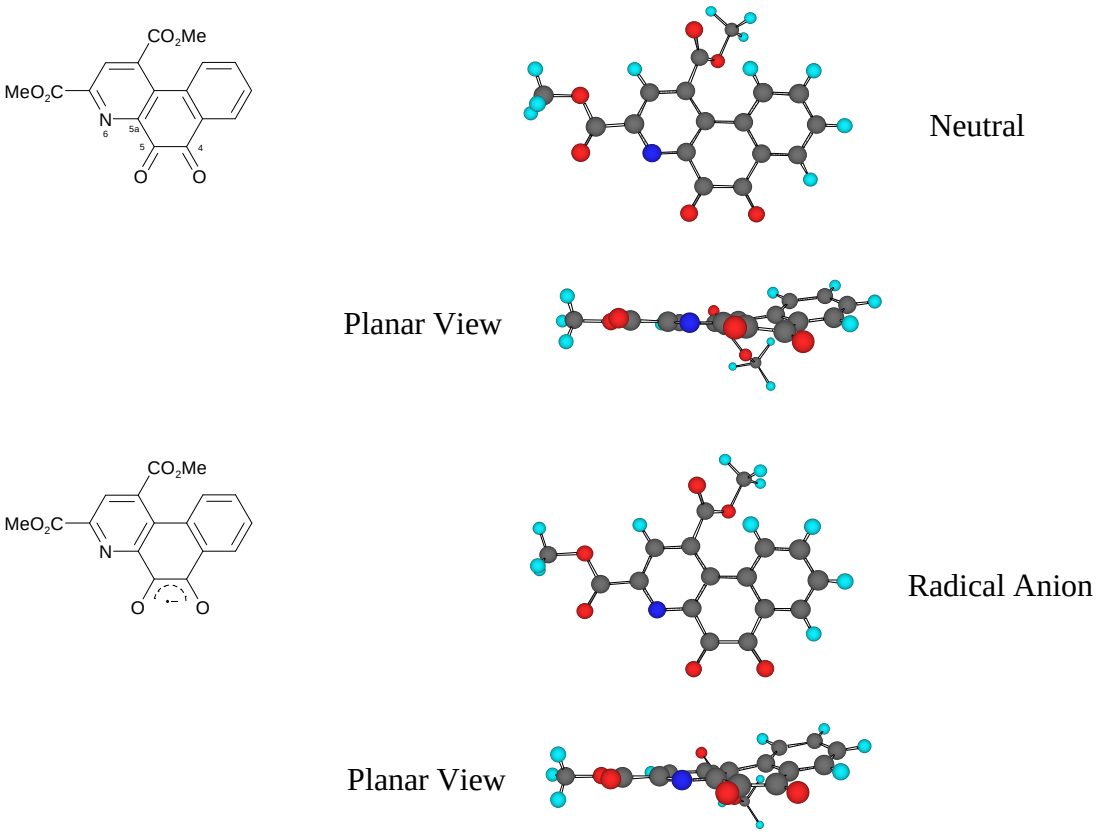

Figure 5.8 The neutral and radical anion structures of BQQ

Atom	Neutral	Radical Anion	
	Charge	Charge	Spin Density
C4	0.339370	0.292464	0.052481
(C4)O	-0.429795	-0.552649	0.221433
C5	0.377271	0.323614	0.031014
(C5)O	-0.390620	-0.515719	0.246264
C5a	0.148770	0.124545	0.078064
N6	-0.483707	-0.498293	-0.023018

Table 5.1 Charges and spin densities of relevant atoms of BQQ

From these initial calculations, the structure of BQQ in both the neutral and radical anion state can be realised. It is clear from the results that in the neutral state, the *o*-quinone backbone of the compound has an unequal distribution of electron density across the two carbonyl oxygens. This was to be expected as the effect of the nitrogen atom within one of

the conjugated fused rings results in less electron density placed upon the C5 carbonyl oxygen. In the case of the radical anion however, the electron density is more evenly distributed, due to the effect of delocalisation of the extra electron, however a slightly increased level of electron density is now seen on the C5 carbonyl oxygen. Unlike the deazaflavin redox cofactors seen in chapter two, the tri-ring system of the BQQ compound has a slightly "puckered" conformation in both redox states, with the benzyl ring pointing out of the plane of the other two rings. This is most likely due to the unfavourable steric hindrance caused by the locality of the adjacent ester group.

The next stage of the calculations involved introducing a non-covalently bonded partner species bound to the *o*-quinone active site. The resulting BQQ-dimethyl urea complex underwent geometry optimisation calculations to find its most stable conformation, when in both neutral and radical anion redox states, before calculating its single-point energy and electrostatic potential map. The results are shown in Figures 5.9 and 5.10 and charges and spin densities of relevant atoms are listed in Tables 5.2 and 5.3.

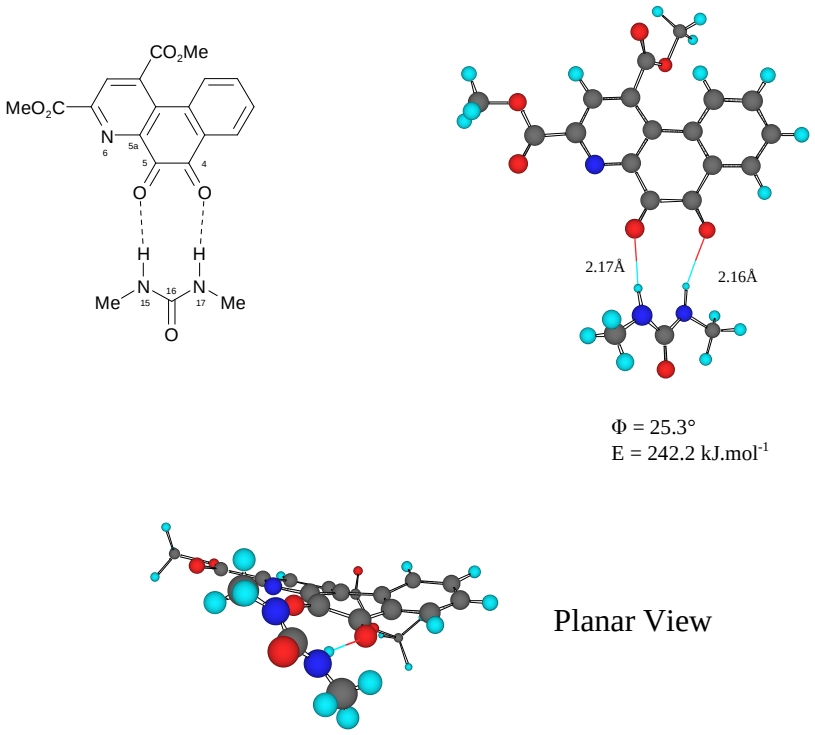

Figure 5.9 **Structure of the neutral BQQ-dimethyl urea complex. Relative free energies are shown in kJ.mol^{-1}, and the torsion angle (Φ) between the two units given in degrees.**

Atom	Neutral Charge
C4	0.350443
(C4)O	-0.437082
C5	0.391196
(C5)O	-0.412847
C5a	0.149699
N6	-0.485552
N15	-0.576655
(N15)H	0.276446
C16	0.756324
N17	-0.574751
(N17)H	0.263334

Table 5.2 Charges of relevant atoms of the neutral BQQ-dimethyl urea complex.

By examining the electron density of the *o*-quinone active site in the neutral redox state, it is clear that as with the lone BQQ calculations, the two carbonyl oxygen atoms are not identical. This is due to the effect of the differing adjacent fused ring structures, in particular the pyrimidine nitrogen atom. This results in the electronegative character of the C5 carbonyl oxygen being slightly smaller than that of the C4 carbonyl oxygen. However, in naturally occurring PQQ enzymes, the Ca^{2+} ion would normally occupy the binding site adjacent to the C5 carbonyl oxygen and N6 nitrogen, further affecting the electron distribution across the *o*-quinone backbone. A significant twist out of planarity is also seen with this complex, which is required to accommodate the appropriate hydrogen bond distance between the two molecules.

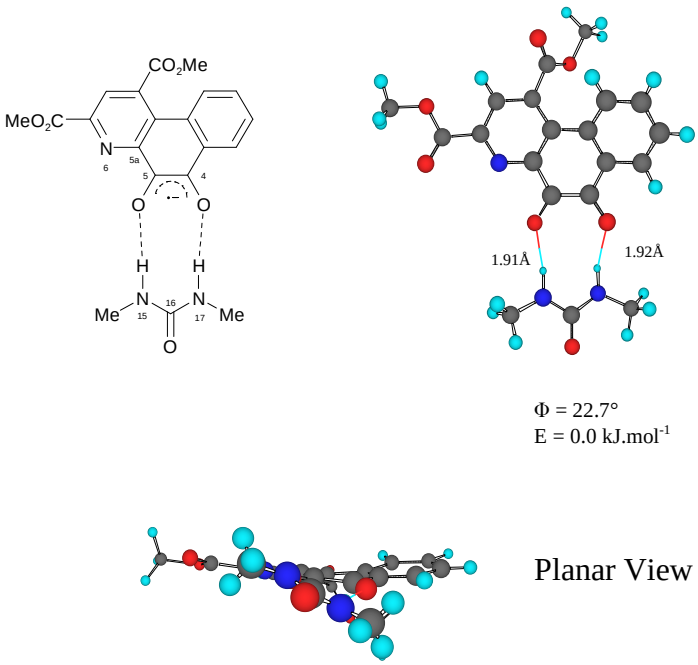

Figure 5.10 **Structure of the radical anion conformation of the BQQ-dimethyl urea complex. Relative free energies are shown in kJ.mol^{-1}, and the torsion angle (Φ) between the two units given in degrees.**

Atom	Radical Anion	
	Charge	Spin Density
C4	0.309064	0.093769
(C4)O	-0.566920	0.232282
C5	0.333069	0.074957
(C5)O	-0.533589	0.275473
C5a	0.133491	0.052753
N6	-0.501270	0.009413
N15	-0.575226	-0.000060
(N15)H	0.305009	-0.002188
C16	0.729846	0.000090
N17	-0.575043	-0.000150
(N17)H	0.300582	-0.002031

Table 5.3 **Charges and spin densities of relevant atoms of the radical anion conformation of the BQQ-dimethyl urea complex.**

In the case of the radical anion system, the anticipated delocalisation of the radical electron is shown by the similar electrostatic potentials of the carbonyl oxygens of the *o*-quinone backbone. This effect is further observed by the similar hydrogen bond distances between the hydrogen bond donors of the urea and the carbonyl acceptors on the BQQ unit, which are considerably shorter than those seen in the neutral oxidation state. The torsion angle between the two units of the complex is around 23°, illustrating that a significant twist out of planarity is require to accommodate non-covalent binding. This structural conformation appears to be similar to that seen for the neutral species.

5.2.3 Physical Analysis

5.2.3.1 NMR Titrations

Hydrogen bonding was confirmed between the BQQ compound **35** and the diphenyl urea unit using ^{1}H-NMR spectroscopy. A solution of BQQ **35** in $CDCl_3$ was treated with additional aliquots of the diphenyl urea species from 0.00 equivalents to 3.00 equivalents in 0.25 equivalent increments. Monitoring of the two NH groups of the diphenyl urea unit by NMR resulted in a smooth downfield shift of its resonance value. Plotting this shift against relative concentration of diphenyl urea resulted in a curve that was fitted to a 1:1 binding isotherm and gave an association constant of 230 ± 23 M^{-1} for the complex (Figure 5.11).

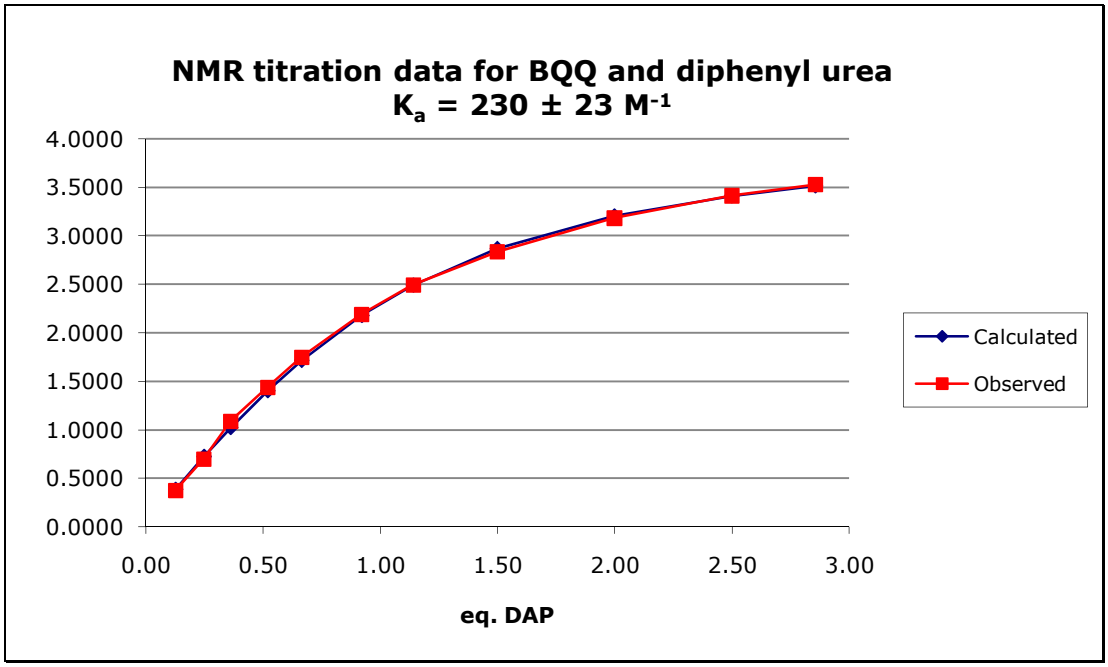

Figure 5.11 **NMR titration data for the BQQ species in the presence of aliquots of diphenyl urea (K_a = 230 ± 23 M^{-1}) in $CDCl_3$ at 20 °C.**

Comparison of the ^1H NMR spectrum of BQQ when dissolved in $CDCl_3$ in the presence of an excess of diphenyl urea, versus the spectrum of BQQ alone, clearly shows that hydrogen bonding is taking place by the relative downfield positions of the two NH groups of the urea unit.

5.2.3.2 Electrochemistry

The solution electrochemistry of BQQ has been studied using cyclic voltammetry (CV). Upon reduction of BQQ, a single reduction wave and a single re-oxidation wave is observed with $E_{½}$ = -0.46 V (Figure 5.12 – solid line).

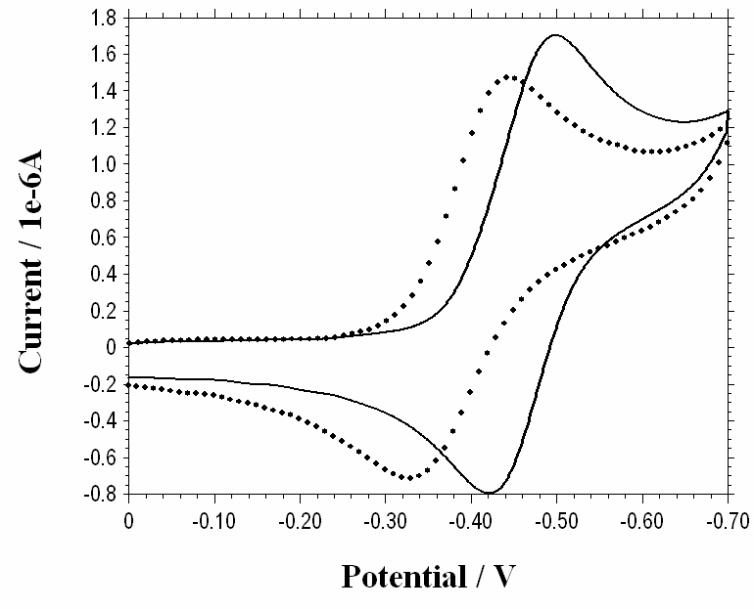

Figure 5.12 **CV data for compound BQQ ($1x10^{-4}$ M in 0.1 M Bu_4NPF_6) recorded in the absence (—) and in the presence (····) of an excess (8×10^{-2} M) of diphenylurea. Solvent is acetonitrile. Scan rate = $0.1Vs^{-1}$. Reference electrode was Ag/AgCl. $\Delta E_{½}$ = +0.06 V.**

In comparison to voltammograms seen in the literature for PQQ derivatives, the voltammogram observed for the BQQ derivative (**35**) is relatively simple, and more significantly, reversible. This simple, reversible redox wave seen for BQQ can be attributed directly to the absence of the pyrrole NH group present in naturally occurring PQQ. The semiquinone radical species, formed upon reduction of the neutral compound, has been previously reported to form complexes with the quinone and itself causing a complex voltammogram.[154] Since this is not seen in this case, this result agrees with Itoh's observations that the acid-base equilibrium of the pyrrole proton (present in naturally occurring PQQ) is most likely responsible for complicated, irreversible voltammograms.[143]

The solution electrochemistry of BQQ was also studied upon the addition of excess of diphenyl urea. In this instance, a shift of +60 mV was observed upon addition of the diphenyl urea moiety ($E_{½}$ = -0.38 V). These results are consistent with a significant stabilisation of the BQQ radical anion upon complexation with the urea compound.

5.3 Conclusions

The synthesis of the PQQ derivative benzoquinoline, quinone (BQQ) has been successfully carried out and its chemical behaviour studied via cyclic voltammetry and NMR titration experiments. A simple and reversible redox waveform was observed for the reduction and

oxidation of BQQ alone, and when in the presence of diphenyl urea as a hydrogen bonding partner. On addition of excess of diphenyl urea to a solution of BQQ, a stabilising shift of +60 mV was seen corresponding to a stabilisation of the BQQ radical anion by the presence of hydrogen bonds. NMR titration showed the association constant between the two species to be 230 ± 23 M^{-1}. DFT calculations have also been carried out on the BQQ unit in both the radical anion and neutral redox states, individually and when non-covalently bound to a urea compound. Although these calculations show the relative conformations of these two species and how they are likely to bond to one another, the next stage of calculations would require the incorporation of the Ca^{2+} ion to build a truly representative picture of the interactions taking place within the binding site. However the calculation of the electrostatic potentials of relevant atoms involved in the non-covalent binding between these two molecules can give an idea as to the electrochemical character of the active site itself.

5.4 Acknowledgements

The author gratefully acknowledges the contributions to this study from fellow members of the Cooke research group, in particular those of Stuart Caldwell and Shanika Gutanilaka.

Chapter Six

6 Chapter Six – Summary of Conclusions

A series of chemical compounds have been synthesised for use as biomimetic models of cofactors found in various naturally occurring redox-active enzymes. These model cofactors include derivatives of the 1- and 5-deazaflavins, analogues of isobutyl flavin as a model of riboflavin, and benzoquinoline quinone as a model of pyrroloquinoline quinone. These compounds have been characterised and analysed using various chemical, electrochemical and computational techniques in order to further probe the effect of non-covalent interactions and environmental influence on their behaviour and ability to act as redox cofactors.

Analogues of 1- and 5-deazaflavin have been synthesised and characterised via UV-vis spectroscopy, cyclic voltammetry and DFT modelling. The results of these experiments show that the position, of the NH group within the isoalloxazine ring (the core of the flavin's redox behaviour) has a dramatic effect on its electrochemical capabilities. IN the case of the 1-deazaflavin species, these effects include lack of electrochemical reversibility and an increase in reduction potential compared to the parent riboflavin compound. While the 5-deazaflavin retains its electrochemical reversibility, it also shows an increase in reduction potential compared to that of riboflavin. The effect of hydrogen bonding on the 5-deazaflavin species stabilises the radical anion, illustrating the importance of these interactions during electron transfer processes within the binding site of the respective enzyme.

Continuing the study of flavin-based cofactors, a family of water-soluble flavin-functionalised dendrons have been synthesised and analysed to examine the effect that a water-soluble dendritic architecture covalently attached to the flavin unit would have on its chemical behaviour. In particular to observe whether a hydrophobic pocket, similar to that found in the active site of redox enzymes, could be recreated and in addition whether the cofactor could carry out its catalytic function in this purely synthetic super-structure. Results from the UV-vis and fluorescence experiments showed encapsulation of the flavin unit by the dendron backbone certainly takes place in all three generations of models, while molecular modelling simulations indicate the formation of a hydrophobic binding pocket in the third-generation species, which is supported by the bathochromic shift seen by UV-vis spectrometry. This was confirmed through catalytic studies in aqueous media, whereby the rate of reaction compared to that of riboflavin was increased by the presence

of the dendritic architecture in all three generations, however was more prominent in the case of the third generation due to the creation of the hydrophobic pocket.

To create a more in-depth picture of the effect that dendron encapsulation may have on redox-active cofactors, a second series of flavin-functionalised dendrons have been synthesised, and in this case have been covalently attached to the *N*(10) position of the isoalloxazine ring. This allowed the study of electrochemical behaviour of the flavin unit, and also how the hydrogen bonding through ring III of the flavin is affected by the dendron backbone. Electrochemical analysis of these dendrons showed significant encapsulation of the flavin moiety by the benzyl-based dendron architecture, which became more pronounced as the level of dendritic branching increased. Analysis of three-point hydrogen bonding of the imido motif of the flavin species showed a sequential decrease in association constant when bound to a suitable hydrogen bond partner as the level of dendritic branching increased. And as usually observed in flavin systems, the presence of hydrogen bonding stabilised the flavin radical anion significantly. The combination of results from both the water-soluble and "click" flavin-functionalised dendron studies should enable the further creation of more complex systems that fully utilise the effect of non-covalent interactions, and the presence of a large, encapsulating, dendritic architecture in order to achieve truly synthetic flavoenzymes.

Finally, as flavins have been recognised as essential cofactors in enzyme-catalysed redox reactions, this study then examined another cofactor found in a large number of redox enzymes. A model compound of pyrroloquinoline quinone (PQQ) was synthesised with a number of structural differences. Benzoquinoline quinone (BQQ) was then characterised and studied to determine its capabilities as a redox cofactor, and to what effect hydrogen bonding had on its redox behaviour. Using cyclic voltammetry, a simple redox waveform was observed for BQQ compared to that of PQQ, owing to the absence of the pyrrole NH within the system. When a suitable hydrogen bonding partner was present, the BQQ compound experienced a stabilisation of the radical anion oxidation state in a similar fashion to that previously seen with the flavin analogues. This study is certainly in its early stages, however these results will hopefully form the basis of examining how other functional groups present within the system affect its redox behaviour.

This study as a whole has probed the behaviour and characteristics of select redox cofactors present in enzyme systems, through the use of biomimetic modelling and a variety of analytical tools. Present and future studies within the Cooke research group hope

to build upon these results, in particular in the area of flavin-functionalised dendrons, as a route towards synthetic flavoenzymes and in a bid to further understand the complexity of the interactions that take place within these unique enzyme-catalysed redox systems.

Chapter Seven

7 Chapter Seven – Experimental Details

7.1 General Experimental Details

^{1}H NMR spectra were performed on a Bruker AC 200 MHz or a Bruker AV 400 FT spectrometer at room temperature. Spectra were recorded using deuterated chloroform as the solvent, using residual chloroform as the internal standard (δ = 7.26 ppm), or deuterated dimethyl sulphoxide as the solvent, using residual dimethyl sulphoxide as the internal standard (δ = 2.54 ppm). Chemical shifts are reported in ppm relative to trimethylsilane (δ = 0.00 ppm). All *J* values are reported in Hertz. ^{13}C NMR spectra were performed on a Bruker AV 400 FT spectrometer at room temperature. Spectra were performed using deuterated chloroform as the solvent, using residual chloroform as the internal standard (δ = 77.0 ppm).

All low-resolution MS-spectra were performed on a JEOL JMS 700 spectrometer at the University of Glasgow. All accurate mass spectra were obtained via the EPSRC National Mass Spectrometry Service Centre, University of Wales, Swansea.

Transmission IR spectra were recorded as thin films or KBr discs using a JASCO FT/IR 410 spectrometer.

All electrochemical experiments were carried out under the supervision of Dr. Graeme Cooke using a CH instruments 620A electrochemical workstation. The electrolyte solution was prepared from recrystallised Bu_4NPF_6. The solution was purged for two minutes with nitrogen prior to recording the electrochemical data, and voltammograms were recorded under a constant flow of nitrogen.

All reactions were carried out under inert atmosphere (nitrogen) unless otherwise stated, using oven-dried or flame-dried glassware. Tetrahydrofuran and diethyl ether were either freshly distilled from sodium benzophenone, or obtained from the in-house solvent purifier (Pure Solv 400-5MD), prior to use. Dichloromethane, dimethyl formamide, toluene and pyridine were freshly distilled from calcium hydride. Petroleum ether refers to the fraction boiling at 40-60 °C. Brine refers to a saturate sodium chloride solution. Reagents were obtained from Aldrich Chemical Company (Gillingham, Dorset, UK), Alfa Aesar Lancaster (Morecambe, Lancs., UK) or Alfa Aesar Avocado (Heysham Lancs., UK) and used without further purification unless otherwise stated. Purification by column

chromatography was carried out using Fisher Silica 60A silica gel (mesh size 35-70 μm) as the stationary phase. Melting points were measured using Gallenkamp apparatus and are uncorrected. Reactions were monitored by TLC performed on Merck Kieselgel 60 F_{254} plates, using UV light or potassium permanganate.

Binding constant (K_a) determination was determined in non-competitive solvent ($CDCl_3$) due to its stability for NMR experiments. It has been previously shown that interchange of this solvent has no measurable effect on the results obtained.[44] Experiments were performed via addition of aliquots of hosts (DAP) to respective flavin solutions. The plot of chemical shifts of the imido H of the flavin unit as a function of receptor concentration provided a titration curve. Association constants were determined through non-linear least-squares fitting. All curves provided a good fit to the 1:1 binding isotherm (error is evaluated as $K_a \pm 10$ %).

Density Functional Theory calculations were carried out at the B3LYP level using the 6-31G** basis set for all molecules and supramolecular complexes. Frequency calculations at the same theory level have been performed to identify stationary points as minima (zero imaginary frequencies). All calculations were performed using the Gaussian 03 software package.[156]

All molecular dynamics simulations were performed using the MacroModel program in Maestro v8.0 from Schrodinger Inc. Amber* force field was chosen from the subsystem "Dynamics" and the calculations were performed in a continuum of water as the solvent. Electrostatic treatment was set to the constant dielectric setting of 1.0. The external cut-offs for the continuum of water were automatically set to 8.0 (van der Waals), 20.0 (electrostatics) and 4.0 (hydrogen bonding). There were no constraints placed on the molecule. The method used was TNCG (Truncated Newton linear Conjugate Gradient), with the maximum number of iterations at 500. Convergence was based on a gradient and the threshold was set to 0.0500. Stochastic dynamics were used, and all of the bonds were shaken during the calculation. The simulation temperature was performed over the range of 1000K – 100K (decreasing). The time steps (fs) were set to 1.5, the equilibrium time (ps) set to 1.0, and the simulation time (ps) set to 10.0.

7.2 Synthesis – Chapter Two

N-Isobutyryl-3,4-dimethyl-2-nitroaniline (1)[157]

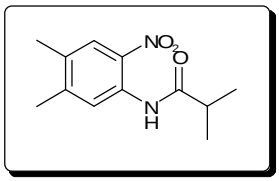

To a purged solution of 4,5-dimethyl-2-nitroaniline (5.0 g, 30.1 mmol) in DCM (250 mL) was added triethylamine (5.2 mL) and isobutyryl chloride (3.94 mL, 37.6 mmol). The mixture was then stirred at room temperature overnight. The solution was then cooled to 0 °C and quenched with HCl (1 M, 150 mL). The organic layer was separated and washed with NaOH (1 M, 200 mL) before drying with magnesium sulphate and concentration under reduced pressure to afford a light yellow solid (6.95 g, 98 %): mp 111-113 °C; IR ν_{max} (KBr)/cm^{-1}: 3254, 2978, 2947, 2874, 1669, 1590, 1550, 1355, 1218, 1100, 953, 885, 746; ^{1}H NMR (400 MHz, $CDCl_3$) δ 1.26 (6H, d, *J* 6.8 Hz, $(\underline{CH_3})_2CH$), 2.21 (3H, s, CH_3), 2.26 (3H, s, CH_3), 2.55 (1H, m, *J* 6.8 Hz, $\underline{CH}(CH_3)_2$), 7.91 (1H, s, CH), 8.52 (1H, s, CH), 10.36 (1H, br s, NH) ppm; *m/z* (CI/ISO): 236 (M^+, 100%).

_N_-(2-Amino-4,5-dimethyl-phenyl)-isobutyramide (2)[157]

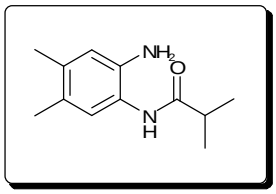

To a mixture of **1** (2.0 g, 8.5 mmol) and ammonium formate (2.14 g, 34 mmol) in degassed methanol (120 mL) was added Pd/C (600 mg) in portions. The mixture was stirred for 3 hours before the Pd/C was filtered off and the methanol removed under reduced pressure. The residue was dissolved in DCM (120 mL) and washed with water (3 × 100 mL) and the organic layer was separated, dried over magnesium sulphate and concentrated under reduced pressure to afford a white crystalline solid (1.24 g, 71 %): mp 125-127 °C; ^{1}H NMR (400 MHz, $CDCl_3$) δ 1.17 (6H, d, *J* 6.8 Hz, ($\underline{CH_3}$)$_2$CH)), 2.01 (3H, s, CH_3), 2.05 (3H, s, CH_3), 2.48 (1H, m, *J* 6.8 Hz, $\underline{CH}(CH_3)_2$), 3.10 (2H, br s, NH_2), 6.52 (1H, s, CH), 6.85 (1H, s, CH) ppm; *m/z* (CI/ISO): 206 (M^+, 100%).

_N_-Isobutyl-4,5-dimethyl-benzene-1,2-diamine (3)[157]

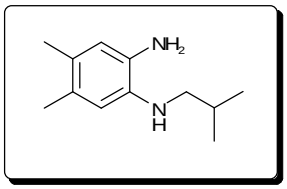

To an ice cooled solution of **2** (1.24 g, 6.0 mmol) in THF (150 mL) was added lithium aluminium hydride (911 mg, 24 mmol) in portions. The mixture was allowed to reach room temperature and stirred overnight. The solution was cooled to 0 °C before the addition of water (4 mL), NaOH (10 %, 2 mL) and water again (4 mL). The solid was then filtered off and washed with diethyl ether (20 mL). The filtrate and diethyl ether portions were combined, dried over magnesium sulphate and the solvent removed under reduced pressure. The brown residue was then purified by flash chromatography (4:1 hexane/ethyl acetate) to afford a brown oil (756 mg, 66 %): ^{1}H NMR (400 MHz, $CDCl_3$) δ 1.06 (6H, d, *J* 6.8 Hz, ($\underline{CH}_3)_2CH$)), 1.99 (1H, m, *J* 6.8 Hz, $\underline{CH}(CH_3)_2$), 2.15 (3H, s, CH_3), 2.19 (3H, s, CH_3), 2.95 (2H, d, *J* 6.8 Hz, $\underline{CH}_2CH(CH_3)_2$), 3.23 (2H, br s, NH_2), 6.51 (1H, s, CH), 6.57 (1H, s, CH) ppm; *m/z* (CI/ISO): 192 (M^+, 100%).

2-Bromo-3-oxo-pentanedioic acid diethyl ester (4)[48]

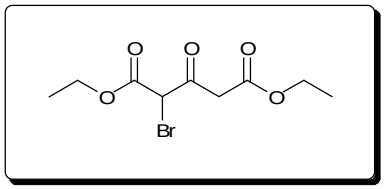

To a solution of potassium metal (1.93 g, 49.5 mmol) dissolved in absolute ethanol (100 mL) was added diethyl-1,3-acetonedicarboxylate (8.85 mL, 49.5 mmol). The solution was stirred for 15 minutes before the solvent was removed to yield a greenish/white fluffy solid. This was diluted in chloroform (140 mL) before the drop wise addition of bromine (2.35 mL, 45.6 mmol) to the mixture, which was then stirred for a further 30 minutes. The solid was then filtered off and the solvent from the filtrate removed under reduced pressure to afford an orange oil. This was then purified by flash chromatography (2:3 ethyl acetate/hexanes) to afford an orange oil (11.91 g, 86%): ^{1}H NMR (400 MHz, $CDCl_3$) δ 1.29 (3H, t, *J* 7.2 Hz, $\underline{CH_3}CH_2$), 1.31 (3H, t, *J* 5.2 Hz, $\underline{CH_3}CH_2$), 3.58 (2H, s, CH_2), 4.19 (2H, q, *J* 7.2 Hz, $CH_3\underline{CH_2}$), 4.21 (2H, q, *J* 5.2 Hz, $CH_3\underline{CH_2}$) 5.03 (1H, s, CH) ppm; *m/z* (FAB^+): 282 [M^+, (^{81}Br), 97%)], 280 [M^+, (^{79}Br), 100%].

Intermediate 1-Deazaflavin Precursor (5)

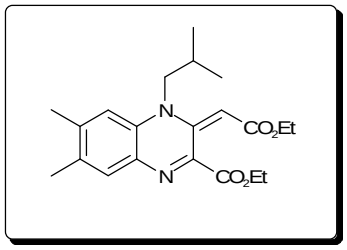

To a solution of **3** (750 mg, 4.0 mmol) and **4** (2.53 g, 9.0 mmol) in DMF (35 mL) and DCM (42 mL) was added caesium carbonate (3.91 g, 12.0 mmol). The mixture was stirred at room temperature overnight before the solid was filtered off and the solvent removed under reduced pressure. The residue was diluted in water (100 mL) and washed with ethyl acetate (3 × 100 mL). The organic washes were combined, dried over magnesium sulphate and concentrated under reduced pressure to afford a brown oil. This was then purified by flash chromatography (4:1 DCM/acetone) to give the product as an orange oil (760 mg, 51 %), however this species was found to decompose quickly at purification, causing great difficulty in obtaining characterisation results, and it was found to be more productive to use the crude product directly in the next stage: ^{1}H NMR (400 MHz, $CDCl_3$) δ 1.02 (6H, d, *J* 6.8 Hz, $(\underline{CH_3})_2CH$), 1.05 (3H, t, *J* 7.2, $\underline{CH_3}CH_2$), 1.06 (3H, t, *J* 5.2, $\underline{CH_3}CH_2$), 1.24 (2H, q, *J* 7.2 Hz, $CH_3\underline{CH_2}$), 1.28 (2H, q, *J* 5.5 Hz, $CH_3\underline{CH_2}$), 1.94 (1H, m, *J* 6.8 Hz, $\underline{CH}(CH_3)_2$), 2.14 (3H, s, CH_3), 2.17 (3H, s, CH_3), 2.90 (2H, d, *J* 6.8Hz, $\underline{CH_2}N$), 5.20 (1H, s, CH), 6.95 (1H, s, CH), 7.55 (1H, s, CH) ppm; *m/z* (CI/ISO): 372 (M^+, 100%).

_N_(10)-Isobutyl-7,8-dimethyl-1-deazaflavin (6)

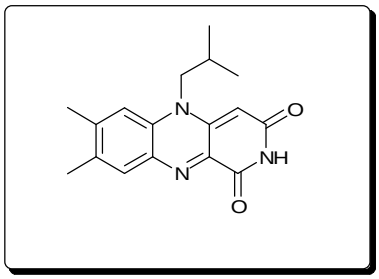

Compound **5** (340 mg, 1.0 mmol) was dissolved in methanolic ammonia (2.0 M, 25 mL) and stirred at room temperature for 48 hours. The solvent was then removed under reduced pressure and the dark red residue purified by flash chromatography (4:1 DCM/acetone) to afford the product as a purple solid (25 mg, 8%): mp > 300 °C (dec); ^{1}H NMR (400 MHz, $CDCl_3$) δ 0.99 (6H, d, *J* 6.8 Hz, $(\underline{CH_3})_2CH$), 2.27 (3H, s, CH_3), 2.33 (1H, m, *J* 6.8 Hz, $\underline{CH}(CH_3)_2$), 2.37 (3H, s, CH_3), 3.84 (2H, d, *J* 6.8 Hz, $\underline{CH_2}N$), 5.31 (1H, s, CH), 7.06 (1H, s, CH), 7.77 (1H, s, CH), 8.27 (1H, br s, NH) ppm; ^{13}C NMR (400 MHz, $CDCl_3$) δ 19.1, 20.3, 21.4, 25.8, 52.8, 86.9, 114.4, 131.8, 133.1, 133.7, 134.3, 140.7, 142.0, 145.7, 159.9, 163.9; *m/z* (ESI) calcd for $C_{17}H_{19}N_3O_2$ 298.1550, found 298.1551.

_N_-Isobutyl-3,4-dimethyl aniline (7)[48, 50]

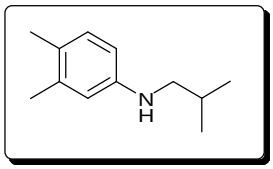

To a solution of dimethyl aniline (10.0 g, 82.6 mmol) in triethylamine (30 mL) was added 1-bromo-2-methyl pentane (22.6 g, 165.2 mmol). The solution was heated under reflux for 72 hours before cooling to room temperature. The mixture was then diluted with DCM (200 mL) before extraction with sodium carbonate solution (10%, 3 x 100 mL). The organic layer was separated and dried over magnesium sulphate before concentration under reduced pressure to afford a brown oil. This oil was then purified by flash chromatography (10% hexane in DCM) to afford the product as an orange oil (10.14 g, 69%): ^{1}H NMR (400 MHz, $CDCl_3$) δ 0.79 (6H, d, *J* 6.8 Hz, $(\underline{CH_3})_2CH$), 1.96 (1H, m, *J* 6.8 Hz, $\underline{CH}(CH_3)_2$), 2.07 (3H, s, CH_3), 2.12 (3H, s, CH_3), 3.01 (2H, d, *J* 6.8 Hz, $\underline{CH_2}N$), 6.48 (1H, d, *J* 8 Hz, CH), 6.40 (1H, s), 6.84 (1H, d, *J* 8 Hz, CH); IR (film) 3410, 3010-2880, 1620, 1580, 1505, 1465, 1385, 1320, 1315, 1260, 1215, 1170, 1150, 1120 cm^{-1}; *m/z* (FAB^+) 178 (M^+ + H, 100%).

6-Chloro-uracil (7a)[48, 50]

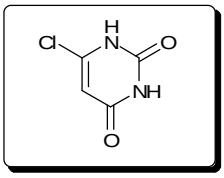

Sodium hydroxide (8.46 g, 216 mmol, 87 mL) was added to a portion of 2,4,6-trichloropyrimidine (6.3 mL, 55.0 mmol) in a round-bottomed flask. The mixture was heated under reflux for seven hours before cooling to room temperature. Concentrated hydrochloric acid (5 mL) was added to lower the pH to 3. The mixture was refrigerated at overnight to afford a white precipitate. The precipitate was filtered and recrystallised from water to afford a white solid (4.72 g, 59 %): mp 165-167 °C; ^{1}H NMR (400 MHz, DMSO) δ 5.80 (1H, s), 11.2 (1 H, br s), 12.08 (br s, 1H); *m/z* (CI/ISO) 146 (M^{+}, 100%).

6-[(3,4-Dimethyl-phenyl)-isobutyl-amino]-1H-pyrimidine-2,4-dione (8)

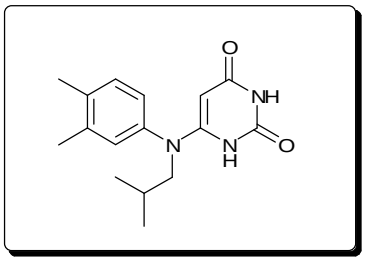

To a solution of *N*-isobutyl-3,4-dimethyl aniline (3.0 g, 17 mmol) in DMF (10 mL) was added 6-chloro-uracil (1.24 g, 8.5 mmol). The mixture was then heated at 150°C for 48 hours giving a brown-coloured solution. The solvent was then removed under reduced pressure and the residue triturated with diethyl ether to afford a yellow precipitate. The yellow solid was then recrystallised from an ethyl acetate / ethanol solution to afford the product as a yellow crystalline solid (1.014 g, 42 %): mp 186-188 °C; ^{1}H NMR (400 MHz, $CDCl_3$) δ 0.87 (6H, d, *J* 6.8 Hz, $(\underline{CH}_3)_2CH$), 1.90 (1H, m, *J* 6.8 Hz, $\underline{CH}(CH_3)_2$), 2.11 (3H, s, CH_3), 2.16 (3H, s, CH_3), 3.31 (2H, d, *J* 6.8Hz, $\underline{CH}_2N$), 4.86 (1H, s), 6.88 (2H, dd, *J* 8.0 Hz, 2.4 Hz), 7.08 (1H, br s), 7.15 (1H, d, *J* 8.0 Hz), 8.78 (1H, br s) ppm; ^{13}C NMR (400 MHz, $CDCl_3$) δ 19.5, 19.9, 20.2, 27.1, 60.0, 125.4, 129.0, 131.8, 137.5, 138.3, 139.7, 150.1, 153.4, 164.7 ppm; *m/*z (ESI) [M^+ + H] calcd for $C_{16}H_{21}N_3O_2$ 287.3884, found 287.3882.

_N_(10)-Isobutyl-7,8-dimethyl-5-deazaflavin (9)

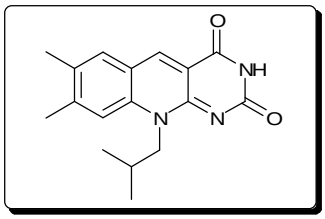

To a solution of **12** (300 mg, 1.04 mmol) in DMF (2 mL) was added phosphorus oxychloride (0.18 mL, 1.96 mmol) drop wise, slowly. The solution was stirred at room temperature for 30 minutes before heating to 100 °C for 20 minutes. The solution was allowed to cool to room temperature before ice (1.0 g) was added to afford a bright orange precipitate. The solid was filtered off and purified by flash chromatography (20 % acetone : 80% DCM) to afford a bright yellow solid (144 mg, 48 %): mp > 300 °C (dec); ^{1}H NMR (400 MHz, DMSO) δ 0.95 (6H, d, *J* 6.8 Hz, ($\underline{CH_3}$)$_2$CH), 2.35 (1H, m, *J* 6.8 Hz, $\underline{CH}(CH_3)_2$), 2.37 (3H, s, CH_3), 2.46 (3H, s, CH_3), 4.20 (2H, br d, *J* 6.8 Hz, $\underline{CH_2}$N), 7.38 (1H, s, CH), 7.57 (1H, s, CH), 8.31 (1H, s, CH), 8.78 (1H, br s, NH) ppm; ^{13}C NMR δ 14.6, 18.6, 19.5, 19.6, 20.8, 26.8, 51.1, 113.2, 114.7, 117.1, 119.5, 131.0, 133.7, 135.1, 141.0, 146.5, 156.4, 162.3 ppm; *m/z* (ESI) [M^+ + H] calcd for $C_{17}H_{19}N_3O_2$ 298.1550, found 298.1550; Elemental analysis calcd for $C_{17}H_{19}N_3O_2$: C (68.67%), H (6.44%), N(14.13%) found C (67.94%), H (6.45%), N (13.80%).

_N_-Isobutyryl-3,4-dimethyl-2-nitroaniline (10)[157]

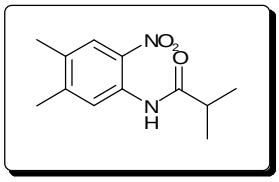

To a purged solution of 4,5-dimethyl-2-nitroaniline (5.0 g, 30.1 mmol) in DCM (250 mL) was added triethylamine (5.2 mL) and isobutyryl chloride (3.94 mL, 37.6 mmol). The mixture was then stirred at room temperature overnight. The solution was then cooled to 0 °C and quenched with HCl (1 M, 150 mL). The organic layer was separated and washed with NaOH (1 M, 200 mL) before drying with magnesium sulphate and concentration under reduced pressure to afford a light yellow solid (6.95 g, 98 %): mp 111-113 °C; IR ν_{max} (KBr)/cm^{-1}: 3254, 2978, 2947, 2874, 1669, 1590, 1550, 1355, 1218, 1100, 953, 885, 746; ^{1}H NMR (400 MHz, $CDCl_3$) δ 1.26 (6H, d, *J* 6.8 Hz, $(\underline{CH_3})_2CH$), 2.21 (3H, s, CH_3), 2.26 (3H, s, CH_3), 2.55 (1H, m, *J* 6.8 Hz, $\underline{CH}(CH_3)_2$), 7.91 (1H, s, CH), 8.52 (1H, s, CH), 10.36 (1H, br s, NH) ppm; *m/z* (CI/ISO): 236 (M^+, 100%).

_N_-(2-Amino-4,5-dimethyl-phenyl)-isobutyramide (11)[157]

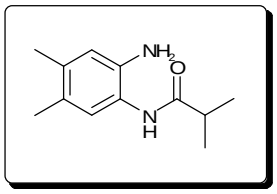

To a mixture of **1** (2.0 g, 8.5 mmol) and ammonium formate (2.14 g, 34 mmol) in degassed methanol (120 mL) was added Pd/C (600 mg) in portions. The mixture was stirred for 3 hours before the Pd/C was filtered off and the methanol removed under reduced pressure. The residue was dissolved in DCM (120 mL) and washed with water (3 × 100 mL) and the organic layer was separated, dried over magnesium sulphate and concentrated under reduced pressure to afford a white crystalline solid (1.24 g, 71 %): mp 125-127 °C; ^{1}H NMR (400 MHz, $CDCl_3$) δ 1.17 (6H, d, *J* 6.8 Hz, ($\underline{CH_3}$)$_2$CH)), 2.01 (3H, s, CH_3), 2.05 (3H, s, CH_3), 2.48 (1H, m, *J* 6.8 Hz, $\underline{CH}(CH_3)_2$), 3.10 (2H, br s, NH_2), 6.52 (1H, s, CH), 6.85 (1H, s, CH) ppm; *m/z* (CI/ISO): 206 (M^+, 100%).

_N_-Isobutyl-4,5-dimethyl-benzene-1,2-diamine (12)[157]

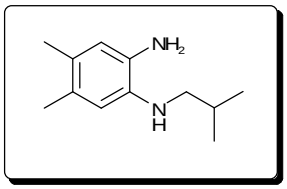

To an ice cooled solution of **2** (1.24 g, 6.0 mmol) in THF (150 mL) was added lithium aluminium hydride (911 mg, 24.0 mmol) in portions. The mixture was allowed to reach room temperature and stirred overnight. The solution was cooled to 0 °C before the addition of water (4 mL), NaOH (10 %, 2 mL) and water again (4 mL). The solid was then filtered off and washed with diethyl ether (20 mL). The filtrate and diethyl ether portions were combined, dried over magnesium sulphate and the solvent removed under reduced pressure. The brown residue was then purified by flash chromatography (4:1 hexane/ethyl acetate) to afford a brown oil (756 mg, 66 %). ^{1}H NMR (400 MHz, $CDCl_3$) δ 1.06 (6H, d, *J* 6.8 Hz, $(\underline{CH_3})_2CH$), 1.99 (1H, m, *J* 6.8 Hz, $\underline{CH}(CH_3)_2$), 2.15 (3H, s, CH_3), 2.19 (3H, s, CH_3), 2.95 (2H, d, *J* 6.8 Hz, $\underline{CH_2}CH(CH_3)_2$), 3.23 (2H, br s, NH_2), 6.51 (1H, s, CH), 6.57 (1H, s, CH) ppm; *m/z* (CI/ISO): 192 (M^+, 100%).

_N_(10)-Isobutyl-7,8-dimethylflavin (13)[157]

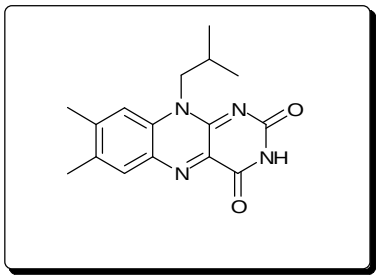

To a solution of **12** (0.72 g, 3.7 mmol) in acetic acid (30 mL) was added alloxan monohydrate (0.60 g, 3.77 mmol) and boron oxide (0.52 g, 7.5 mmol). The mixture was stirred at 60 °C for 1.5 hours, after which time a colour change from reddish brown to yellow brown with green luminescence due to flavin formation. Water (100 mL) was then added to the mixture, and then heated to dissolve any solid particulates. The mixture was then cooled by refrigeration for 72 hours. The precipitate that formed was collected by filtration and recrystallised from ethanol/water (1:1) to form a bright yellow solid (0.57 g, 1.90 mmol, 50.8 %): mp > 300 °C (dec); ^{1}H NMR (400 MHz, $CDCl_3$) δ 1.03 (6H, d, *J* = 6.8 Hz, ($\underline{CH_3}$)$_2$CH), 2.41 (1H, m, *J* 6.8 Hz, $\underline{CH}(CH_3)_2$), 2.42 (3H, s, CH_3), 2.54 (3H, s, CH_3), 4.64 (2H, br d, *J* 6.8 Hz, $\underline{CH_2}$N), 7.34 (1H, s, CH), 8.02 (1H, s, CH) ppm; *m/z* (FAB$^+$): 298 (M^+, 100%).

2,6-di(propylamido)pyridine (14)[158]

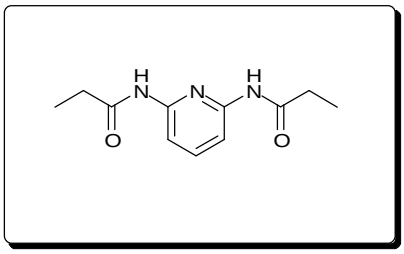

To a solution of diaminopyridine (5.00 g, 46 mmol) and triethylamine(15 mL) in THF (100 mL) was added propionyl chloride (12.0 mL, 138 mmol). The mixture was stirred at room temperature overnight. The solution was filtered and the filtrate evaporated to afford an orange oil. This was purified by flash chromatography (ethyl acetate/DCM, 1:1) to afford the product as an off-white solid (1.31 g, 13%): mp 130-131 °C; ^{1}H NMR (400 MHz, $CDCl_3$) δ 1.23 (6H, t, *J* 7.6 Hz, $\underline{CH_3}CH_2$), 2.43 (4H, q, *J* 7.6 Hz, $CH_3\underline{CH_2}$), 7.60 (2H, br s, 2 x NH), 7.73 (1H, t, *J* 8Hz, CH), 7.92 (2H, d, *J* 8Hz, 2 x CH); ^{13}C NMR (400 MHz, $CDCl_3$) δ 9.4, 30.9, 109.3, 140.9, 149.4, 172.1; *m/z* (CI/ISO): 222 (M^+ + H, 100%).

7.3 Synthesis – Chapter Three

[2-[2-(2-Methoxyethoxy)ethoxy]ethoxy]*p*-toluenesulfonate (15)[90]

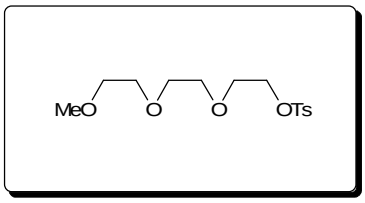

To a solution of *p*-toluene sulfonyl chloride (17.4 g, 92 mmol) and pyridine (10 mL) in DCM (200 mL) was added triethyleneglycol monomethyl ether (9.75 mL, 61 mmol). The solution was stirred at room temperature for 72 hours, before the solvent was removed under reduced pressure and the residue dissolved in DCM (100 mL). This mixture was washed with water (100 mL) and sodium carbonate solution (10%, 3 x 100 mL). The organic layer was separated and dried over magnesium sulphate, before concentration under reduced pressure to afford a colourless oil. This was then purified by flash chromatography (1:1 ethyl acetate/DCM) to afford a colourless oil (12.75 g, 66%): ^{1}H NMR (400 MHz, $CDCl_3$) δ 2.41 (3H, s, $\underline{CH_3}Ph$), 3.32 (3H, s, CH_3O), 3.49 (2H, t, *J* 6.4 Hz, CH_2), 3.55 (6H, m, 3 x CH_2), 3.64 (2H, t, *J* 4.8 Hz, CH_2), 4.14 (2H, t, *J* 4.8 Hz, CH_2), 7.30 (2H, d, *J* 8.4 Hz, 2 x CH) 7.75 (2H, d, *J* 8.4 Hz, 2 x CH) ppm; *m/z* (FAB^+): 318 (M^+, 100%).

"[G-1]-OH" (16)[90]

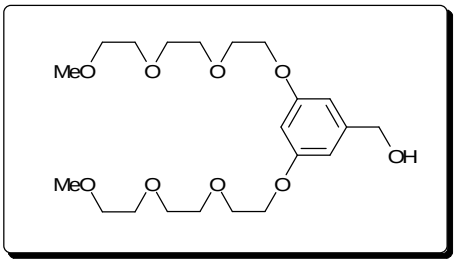

To a solution of **15** (9.77 g ,30.7 mmol) in anhydrous acetone (250 mL) was added 3,5-dihydroxybenzyl alcohol (2.05 g, 14.6 mmol), 18-crown-6 (773 mg, 2.9 mmol) and potassium carbonate (5.09 g, 36.8 mmol). The mixture was heated under reflux for 72 hours. After cooling to room temperature, the solution was filtered and the solvent removed under reduced pressure. The residue was then triturated with DCM (100 mL) before filtering off the solid (unreacted alcohol) and removing the solvent from the filtrate under reduced pressure. The orange oil was purified by flash chromatography (10 % acetone in DCM increased to 50 % acetone in DCM) to afford a viscous, yellowish oil (4.60 g, 73%): ^{1}H NMR (400 MHz, $CDCl_3$) δ 2.94 (1H, br t, *J* 5.2, OH), 3.28 (6H, s, 2 x CH_3), 3.49 (4H, t, *J* 6.4, 2 x CH_2), 3.57 – 3.64 (12H, m, 6 x CH_2), 3.78 (4H, t, *J* 4.4 Hz, 2 x CH_2), 4.02 (4H, t, *J* 4.4 Hz, 2 x CH_2), 4.52 (2H, d, *J* 5.2 Hz, $\underline{CH_2}OH$), 6.33 (1H, s), 6.44 (2H, d, *J* 12.4 Hz, 2 x CH) ppm; ^{13}C NMR (400 MHz, $CDCl_3$) δ 42.7, 53.6, 59.0, 64.8, 67.4, 69.7, 70.5, 70.7, 71.3, 71.8, 76.9, 77.2, 77.6, 100.6, 105.22, 143.8, 159.9; *m/z* (EI^+): 432 (M^+, 100%).

"[G-1]-Br" (17)[90]

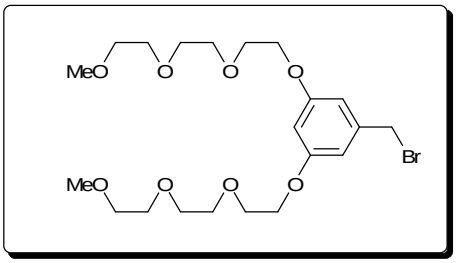

Neat PBr_3 (810 mg, 3.0 mmol) was slowly added to a solution of **16** (3.60 g, 8.3 mmol) dissolved in toluene (50 mL). The solution was then stirred at room temperature overnight. The solvent was then removed under reduced pressure, and the yellow oil purified by flash chromatography (4:1 acetone/DCM) to afford a clear, yellowish viscous oil (2.72 g, 66 %). ^{1}H NMR (400 MHz, $CDCl_3$) δ 3.32 (6H, s, 2 x CH_3), 3.51 (4H, t, *J* 3.2 Hz, 2 x CH_2), 3.61 – 3.78 (16H, m, 8 x CH_2), 4.05 (4H, t, *J* 4.8, 2 x CH_2), 4.33 (2H, s, CH_2Br), 6.35 (1H, s, CH), 6.58 (1H, s, CH), 6.59 (1H, s, CH) ppm; ^{13}C NMR (400 MHz, $CDCl_3$) δ 33.6, 33.7, 53.4, 59.0, 67.5, 69.6, 70.5, 70.6, 70.8, 71.9, 101.6, 102.4, 107.0, 108.9, 139.6, 160.0; *m/z* (FAB/NOBA): 495 (M^+ + H, 100%).

"[G-1]-Fl" (18)[103]

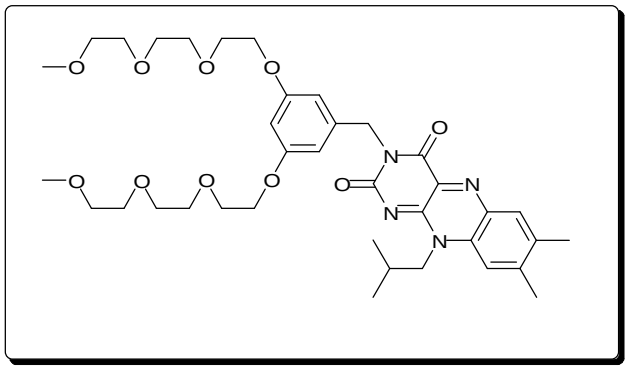

To a solution of isobutyl flavin (577 mg, 2.0 mmol) and potassium carbonate (1.16 g, 8.4 mmol) in acetonitrile (100 mL) was added **17** (1.98 g, 4.0 mmol). The mixture was stirred at room temperature for one week. The solid was then filtered off and the solvent removed under reduced pressure. The dark yellow/brown oil was then purified by flash chromatography (30 % acetone in DCM) to afford the product as a bright orange oil (1.04 g, 73 %): ^{1}H NMR (400 MHz, $CDCl_3$) δ 0.95 (6H, d, *J* 6.8 Hz, ($\underline{CH_3}$)$_2$CH), 2.35 (3H, s, CH_3), 2.38 (1H, m, *J* 6.8 Hz, $\underline{CH}(CH_3)_2$), 2.45 (3H, s, CH_3), 3.28 (6H, s, 2 x CH_3), 3.46 (4H, t, *J* 4.4 Hz, 2 x CH_2), 3.52 – 3.72 (16H, m, 8 x CH_2), 3.99 (4H, t, *J* 4.8 Hz, 2 x CH_2), 4.53 (2H, br s, CH_2N), 5.23 (2H, s, C($\underline{CH_2}$)N), 6.29 (1H, s, CH), 6.59 (2H, s, 2 x CH), 7.32 (1H, s, CH), 7.93 (1H, s, CH) ppm; ^{13}C NMR (400 MHz, $CDCl_3$) δ 19.5, 20.0, 21.6, 27.4, 30.9, 45.1, 50.9, 53.5, 59.0, 67.4, 69.6, 70.5, 70.6, 70.7, 71.9, 101.2, 108.1, 115.8, 131.5, 132.7, 134.9, 135.9, 136.5, 139.0, 147.5, 149.2, 155.4, 159.7, 159.9; *m/z* (ESI) [M^+ + H] calcd for $C_{37}H_{54}N_4O_{10}$ 713.3882 found 713.3882.

"[G-2]-OH" (19)[90]

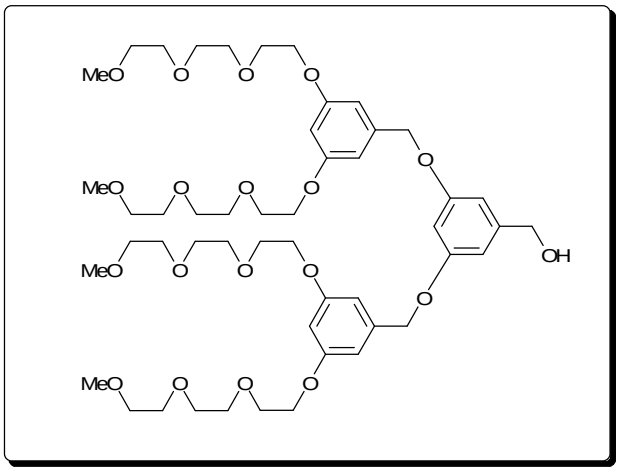

A solution of **17** (3.40 g, 6.8 mmol), 3,5-dihydroxybenzyl alcohol (467 mg, 3.3 mmol), potassium carbonate (553 mg, 4.0 mmol) and 18-crown-6 (87 mg, 0.33 mmol) in acetone (200 mL) was heated under reflux for 24 hours. The solution was then filtered and the solvent removed under reduced pressure. The residue was then triturated with DCM (100 mL) and filtered again. The filtrate's solvent was removed under reduced pressure to afford a clear, viscous oil. This was then purified by flash chromatography (acetone) to afford a clear, yellowish oil (2.16 g, 68%): ^{1}H NMR (400 MHz, $CDCl_3$) δ 3.30 (12H, s, CH_3), 3.51 (8H, t, *J* 4.8 Hz, 4 x CH_2), 3.62 – 3.64 (24H, m, 12 x CH_2), 3.69 (8H, t, *J* 4.8 Hz, 4 x CH_2), 3.78 (8H, t, *J* 5.2 Hz, 4 x CH_2), 4.05 (8H, t, *J* 5.2 Hz, 4 x CH_2), 4.55 (2H, s, CH_2OH), 4.89 (4H, s, 2 x CH_2O), 6.39 (1H, s, CH), 6.44 (2H, s, 2 x CH), 6.51 (4H, s, 4 x CH), 6.56 (2H, s, 2 x CH) ppm; ^{13}C NMR (400 MHz, $CDCl_3$) δ 31.0, 53.5, 59.0, 65.0, 67.4, 69.7, 69.9, 70.5, 70.6, 70.8, 71.9, 76.8, 77.2, 77.5, 101.0, 101.2, 105.6, 106.0, 139.2, 143.8, 160.0; *m/z* (FAB/NOBA): 992 (M^+ + Na).

"[G-2]-Br" (20)[90]

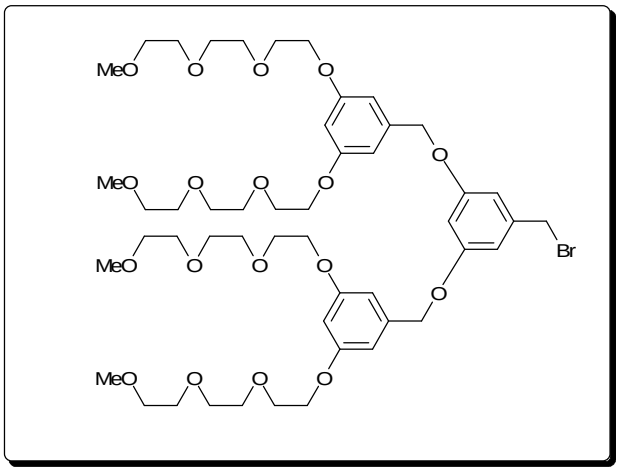

A solution of **19** (2.16 g, 2.2 mmol) in dry toluene (150 mL) was treated with neat PBr_3 (0.07 mL, 0.7 mmol) and stirred at room temperature for 5 days. The solvent was then removed under reduced pressure to afford a thick brown oil. This was then purified by flash chromatography (1:1 acetone/DCM) to afford a light yellow viscous oil (640 mg, 30 %): ^{1}H NMR (400 MHz, $CDCl_3$) δ 3.35 (12H, s, 4 x CH_3), 3.40 (8H, t, *J* 4.8 Hz, 4 x CH_2), 3.54 – 3.65 (24H, m, 12 x CH_2), 3.70 (8H, t, *J* 4.8 Hz, 4 x CH_2), 3.83 (8H, t, *J* 5.2 Hz, 4 x CH_2), 4.09 (8H, t, *J* 5.2 Hz, 4 x CH_2), 4.39 (2H, s, CH_2Br), 4.91 (4H, s, 2 x CH_2O), 6.44 (1H, s, CH), 6.49 (2H, s, 2 x CH), 6.57 (4H, s, 4 x CH), 6.59 (2H, s, 2 x CH) ppm; ^{13}C NMR (400 MHz, $CDCl_3$) δ 31.0, 31.8, 33.8, 34.2, 59.2, 67.6, 69.7, 70.1, 70.6, 70.7, 70.9, 72.0, 101.2, 101.7, 102.2, 106.1, 107.9, 108.2, 124.2, 125.3, 128.2, 129.0, 138.9, 139.8, 159.9, 160.0; *m/z* (FAB/NOBA): 1033 (M^+ + H).

"[G-2]-Fl" (21)[103]

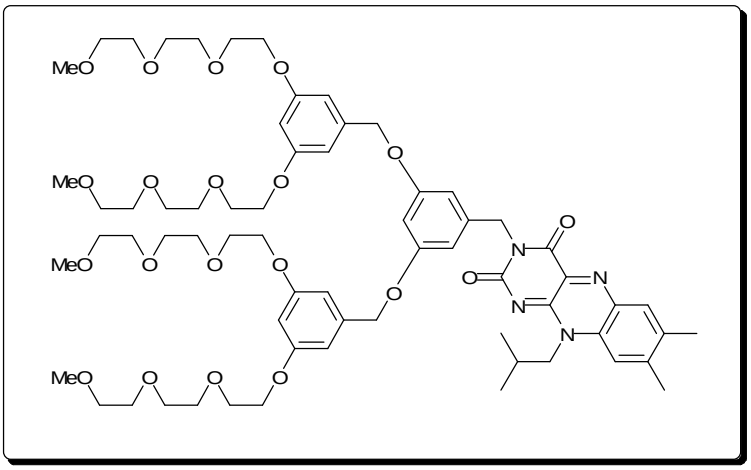

To a solution of isobutyl flavin (120 mg, 0.4 mmol) and potassium carbonate (415 mg, 3.0 mmol) in acetonitrile (20 mL) was added **20** (0.4 g, 0.4 mmol). The mixture was stirred at room temperature for eight days. The solid was then filtered off, and washed with THF (50 mL). The washings and the filtrate were combined and the solvent removed under reduced pressure. The dark yellow/brown oil was then purified by flash chromatography (25 % acetone in DCM initially and then gradually increased to 75% acetone in DCM) to afford the product as a bright orange oil (140 mg, 28 %): ^{1}H NMR (400 MHz, $CDCl_3$) δ 0.91 (6H, d, *J* 6.8 Hz, ($\underline{CH_3}$)$_2$CH), 2.36 (3H, s, CH_3), 2.40 (1H, m, *J* 6.8Hz, $\underline{CH}(CH_3)_2$), 2.56 (3H, s, CH_3), 3.30 (12H, s, 4 x OCH_3), 3.46 (8H, t, *J* 4.8 Hz, 4 x CH_2), 3.57-3.65 (24H, m, 12 x CH_2), 3.76 (8H, t, *J* 4.8 Hz, 4 x CH_2), 4.02 (8H, t, *J* 4.8 Hz, 4 x CH_2), 4.34 (2H, br d, CH_2N), 4.85 (2H, s, C(CH_2)N), 4.87 (4H, s, 2 x CH_2O), 6.35 (4H, d, *J* 2.0, CH), 6.59 (2H, d, *J* 2.0, CH), 6.51 (1H, d, *J* 2.4, CH), 6.80 (2H, d, *J* 2.4, CH), 7.32 (1H, s, CH), 7.93 (1H, s, CH) ppm; ^{13}C NMR (400 MHz, $CDCl_3$) δ 19.5, 20.1, 21.7, 27.5, 45.3, 50.7, 59.1, 67.5, 69.7, 69.9, 70.6, 70.7, 70.8, 71.9, 101.3, 101.6, 106.1, 108.4, 115.8, 132.8 ppm; Elemental analysis calcd for $C_{65}H_{92}N_4O_{20}$: C (62.48%), H (7.42%), N (4.48%) found C (62.44%), H (7.46 %), N (4.51%). *m/z* (FAB): 1250 (M^+ + H).

"[G-3]-OH" (22)[90]

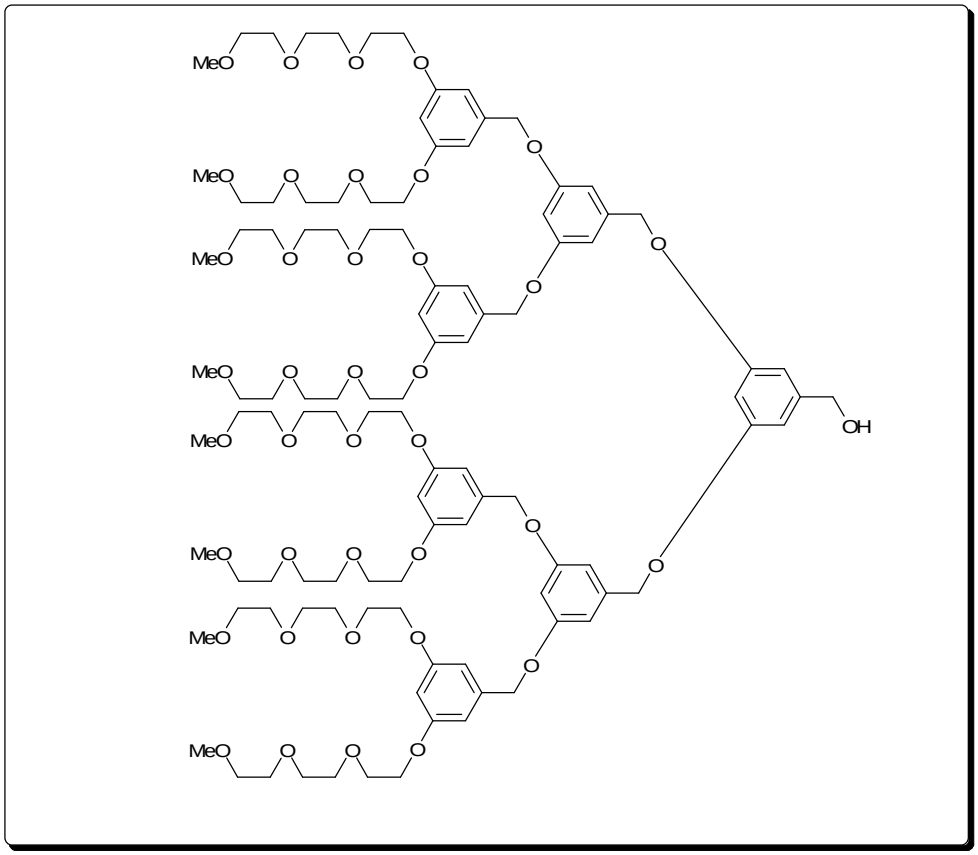

A solution of **20** (690 mg, 0.7 mmol), 3,5-dihydroxybenzyl alcohol (45 mg, 0.3 mmol), potassium carbonate (166mg, 1.2 mmol) and 18-crown-6 (21 mg, 0.08 mmol) in acetone (40 mL) was heated under reflux for four days and until TLC analysis showed no starting material present. The solid was then filtered and washed with THF (20 mL). The washings and filtrate were then combined and the solvent removed under reduced pressure. The crude residue was then purified via flash chromatography (acetone/DCM increased to pure acetone) to afford the product as a clear, viscous oil (540 mg, 88 %): ^{1}H NMR (400 MHz, $CDCl_3$) δ 3.38 (24H, s, 8 x OCH_3), 3.55 (16H, t, *J* 2.8, 8 x CH_2), 3.64 –3.69 (32H, m, 16 x CH_2), 3.70 (16H, t, *J* 4.8, 8 x CH_2), 3.81 (16H, t, *J* 2.8, 8 x CH_2) 4.16 (16H, t, *J* 4.8, 8 x CH_2), 4.61 (2H, d, *J* 5.6, CH_2OH), 4.91 (8H, s, 4 x CH_2), 4.98 (4H, s, 2 x CH_2), 6.45 (4H, t, *J* 2.4, 4 x CH), 6.48 (2H, d, *J* 2.4, 2 x CH) 6.52 (2H, t, *J* 2.0, 2 x CH), 6.54 (1H, t, *J* 2.4, CH), 6.56 (8H, d, *J* 2.4, 8 x CH) 6.65 (4H, d, *J* 2.0, 4 x CH) ppm; ^{13}C NMR (400 MHz, $CDCl_3$) δ 59.1, 64.9, 67.5, 69.7, 69.9, 70.0, 70.6, 70.7, 70.8, 71.9, 101.0, 101.1, 101.6, 105.6, 106.0, 106.3, 139.1, 139.3, 143.9, 159.9, 160.0, 160.1 ppm; *m/z* (FAB/NOBA/NaI): 2064 (M^+ + Na).

"[G-3]-Br" (23)[90]

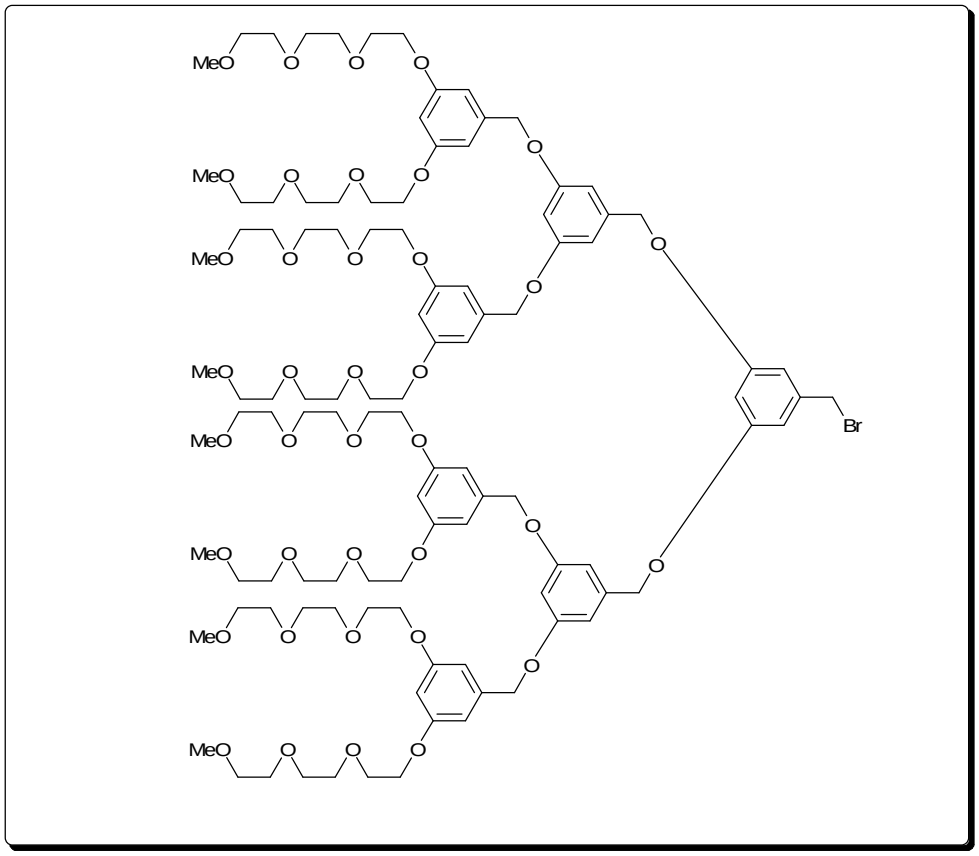

To a solution of **22** (540 mg, 0.26 mmol) in toluene (50 mL) was added neat phosphorous tribromide (0.01 mL, 0.13 mmol), The mixture was stirred at room temperature for 48 hours. The solvent was then removed under reduced pressure and the residue purified via flash chromatography (DCM / acetone) to afford the product as a clear, viscous oil (172 mg, 31 %): ^{1}H NMR (400 MHz, $CDCl_3$) δ 3.38 (24H, s, 8 x OCH_3), 3.55 (16H, t, *J* 2.8, 8 x CH_2), 3.64 –3.69 (32H, m, 16 x CH_2), 3.70 (16H, t, *J* 4.8, 8 x CH_2), 3.81 (16H, t, *J* 2.8, 8 x CH_2) 4.16 (16H, t, *J* 4.8, 8 x CH_2), 4.43 (2H, s, CH_2-Br), 4.91 (8H, s, 4 x CH_2), 4.98 (4H, s, 2 x CH_2), 6.45 (4H, t, *J* 2.4, 4 x CH), 6.48 (2H, d, *J* 2.4, 2 x CH) 6.52 (2H, t, *J* 2.0, 2 x CH), 6.54 (1H, t, *J* 2.4, CH), 6.56 (8H, d, *J* 2.4, 8 x CH) 6.65 (4H, d, *J* 2.0, 4 x CH) ppm; ^{13}C NMR (400 MHz, $CDCl_3$) δ 33.7, 59.1, 67.5, 69.7, 69.9, 70.0, 70.6, 70.7, 70.8, 71.9, 101.1, 101.6, 102.1, 106.1, 106.4, 108.2, 138.9, 139.0, 139.8, 143.9, 160.0, 160.2 ppm; *m/z* (FAB/NOBA): 2064 (M^+ + H).

"[G-3]-Fl" (24)[103]

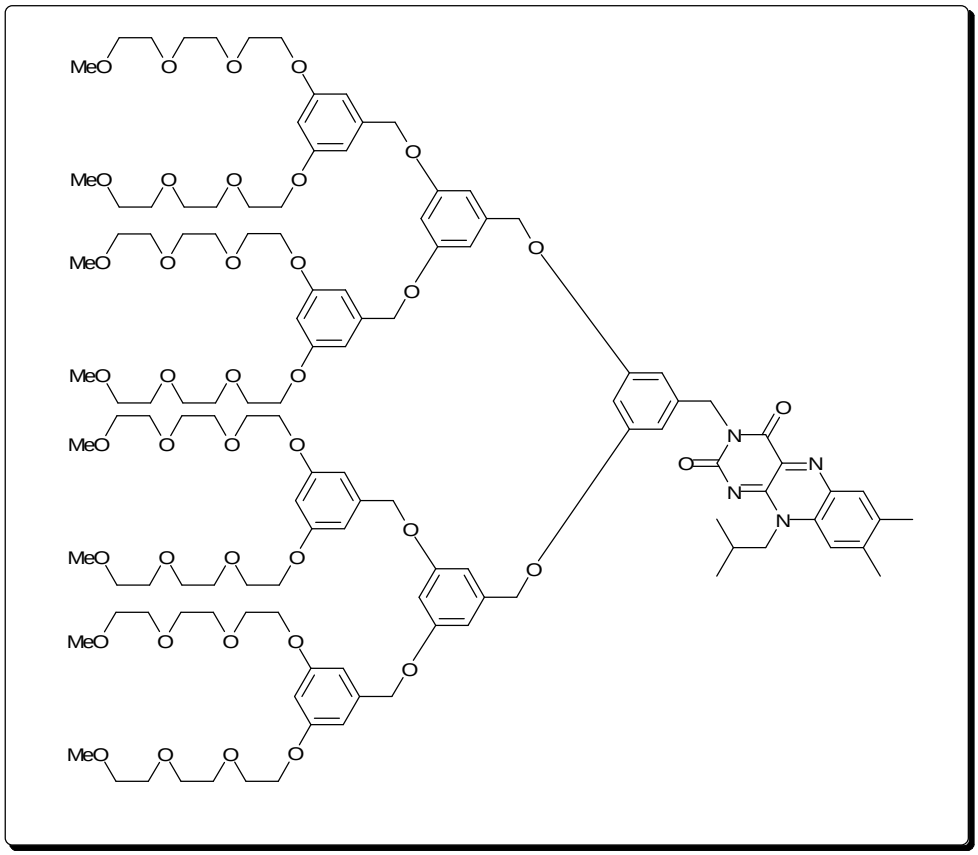

A solution of **23** (172 mg, 0.08 mmol), isobutyl flavin (52 mg, 0.17 mmol), potassium carbonate (55 mg, 0.4 mmol) and 18-crown-6 (10 mg, 0.04 mmol) in acetonitrile (10 mL) was stirred at room temperature for seven days. The solid was then filtered and washed with THF (20 mL). The washings and filtrate were then combined and the solvent removed under reduced pressure. The crude residue was then purified via flash chromatography (25% acetone/DCM increased to acetone/DCM) to afford the product as a yellow wax (23 mg, 12 %): ^{1}H NMR (400 MHz, $CDCl_3$) δ 0.94 (6H, d, *J* 6.8 Hz, ($\underline{CH_3}$)$_2$CH), 2.34 (3H, s, CH_3), 2.38 (1H, m, *J* 6.8Hz, $CH(CH_3)_2$), 2.49 (3H, s, CH_3), 3.35 (24H, s, 8 x OCH_3), 3.48 (16H, t, *J* 4.4 Hz, 8 x CH_2), 3.55 – 3.65 (48H, m, 24 x CH_2) 3.74 (16H, t, *J* 4.2 Hz, 8 x CH_2), 4.03 (16H, t, *J* 4.2 Hz, 8 x CH_2), 4.51 (2H, s, CH_2-N), 4.88 (8H, s, 4 x CH_2), 4.90 (4H, s, 2 x CH_2), 5.17 (2H, s, CH_2), 6.37 (4H, t, *J* 2.4 Hz, 4 x CH), 6.43 (2H, d, *J* 2.4 Hz, 2 x CH) 6.47 (1H, t, *J* 2.4 Hz, CH), 6.52 (8H, t, *J* 2.0 Hz, 8 x CH), 6.59 (4H, d, *J* 2.0 Hz, 4 x CH) 6.82 (2H, d, *J* 1.6 Hz, 2 x CH), 7.31 (1H, s, CH), 7.94 (1H, s, CH) ppm; ^{13}C NMR (400 MHz, $CDCl_3$) δ 21.0, 31.0, 59.1, 67.5, 69.7, 70.6, 70.7, 70.8m, 71.9, 76.7, 77.1, 77.4, 102.0, 132.3, 141.0, 106.1 ppm; Elemental analysis calcd for $C_{121}H_{172}N_4O_{40}$: C (62.57 %), H (7.46 %), N (2.41 %) found C (62.56 %), H (7.50 %), N (2.43 %).

7.4 Synthesis – Chapter Four

N-Hex-5-ynyl-4,5-dimethyl-benzene-1,2-diamine (25)[133]

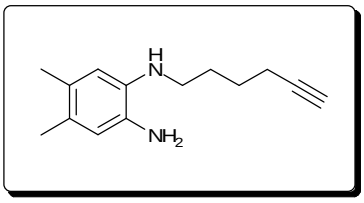

To a solution of 4,5-dimethyl-1,2-phenylenediamine (7.3 mmol, 995 mg) and triethylamine (14.6 mmol, 2.0 mL) in THF (20 mL) was added 6-chlorohexyne (7.3 mmol, 851 mg) and sodium iodide (14.6 mmol, 2.19 g). The mixture was heated at 60 °C overnight before cooling to room temperature. The solvent was then removed under reduced pressure and the remaining brown solid was diluted in DCM (100 mL) and washed with saturated brine (3×100 mL). The organic layer was separated and dried over magnesium sulphate before concentration under reduced pressure to afford a dark brown solid (910 mg, 58 %). Due to the product's unstable nature, the crude material was used directly in the next step.

10-Hex-5-ynyl-7,8-dimethyl-10H-benzo[g]pteridine-2,4-dione (26)[133]

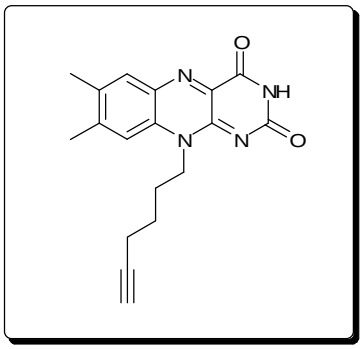

A solution of crude compound **25** (830 mg, 3.8 mmol), alloxan monohydrate (608 mg, 3.8 mmol) and boron oxide (529 mg, 7.6 mmol) in acetic acid (20 mL) was heated at 60 °C for two hours before allowing the mixture to cool to room temperature and further stirring for 24 hours. The solution was then precipitated onto water (100 mL) and extracted with DCM (3 × 100 mL). The organic layers were collected, combined and dried over magnesium sulphate before concentration under reduced pressure. The residue was then loaded onto silica before purification by flash chromatography (1:10 THF/DCM) to afford the product as a dark yellow solid (796 mg, 65 %, mp 279-282 °C): ^{1}H NMR (400 MHz, $CDCl_3$) δ 1.72 (2H, m, *J* 6.8 Hz, CH_2), 1.94 (1H, s, $\underline{HC}{\equiv}CCH_2$), 1.95 (2H, m, *J* 6.8 Hz, CH_2), 2.28 (2H, m, *J* 6.8 Hz, CH_2), 2.39 (3H, s, CH_3), 2.45 (3H, s, CH_3), 4.68 (2H, br s, CH_2N), 7.43 (1H, s, CH), 8.00 (1H, s, CH), 8.42 (1H, br s, NH); *m/z* (FAB^+): 322 (M^+).

First generation flavin-functionalised aryl dendron "[G-1]-AFl" (28)

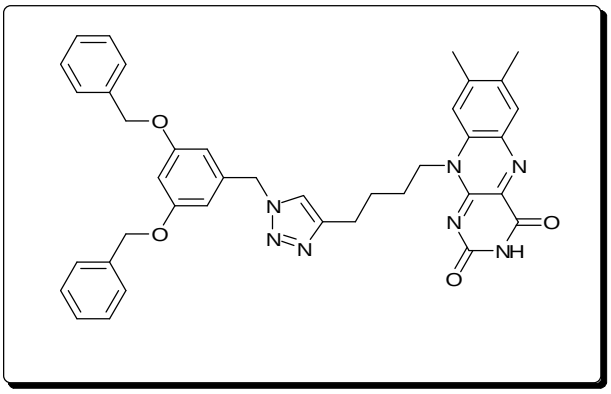

A solution of alkyne-functionalised flavin **26** (175 mg, 0.5 mmol) and [G-1]-N_3 dendron **27** (172 mg, 0.5 mmol) in DMF (5 mL) was treated with copper iodide (9 mg, 50 μmol) and stirred at room temperature for 96 hours. The solvent was removed under reduced pressure and the remaining residue diluted in DCM (150 mL) before washing with water (100 mL), saturated sodium carbonate solution (100 mL) and brine (100 mL). The organic layer was separated, dried over magnesium sulphate and concentrated under reduced pressure to afford a greenish yellow solid. This was purified by flash chromatography (3:1 DCM/THF) to afford the product as a bright yellow solid (164 mg, 49 %, mp 121-123 °C): ^{1}H NMR (400 MHz, $CDCl_3$) δ 1.82 (2H, m, *J* 6.8 Hz, CH_2), 1.88 (2H, m, *J* 6.8 Hz, CH_2), 2.26 (3H, s, CH_3), 2.50 (3H, s, CH_3), 2.80 (2H, t, *J* 6.8 Hz, CH_2), 4.61 (2H, br s, CH_2N), 4.89 (4H, s, 4 x CH), 4.95 (2H, s, 2 x CH), 6.38 (2H, d, *J* 2.0 Hz, 2 x CH), 6.49 (1H, t, *J* 2.0 Hz, CH), 7.23 (10H, m, 2 x Ph), 7.46 (1H, s, CH (imidazole)), 7.52 (1H, s, CH), 7.92 (1H, s, CH), 8.48 (1H, br s, NH); *m/z* (FAB$^+$): 668 (M^+ + H, 100%); Elemental analysis for $C_{39}H_{37}N_7O_4$ requires C (70.15 %), H (5.58 %), N (14.68 %), found C (70.35 %), H (5.60 %), N (14.79 %).

Second generation flavin-functionalised aryl dendron "[G-2]-AFl" (30)

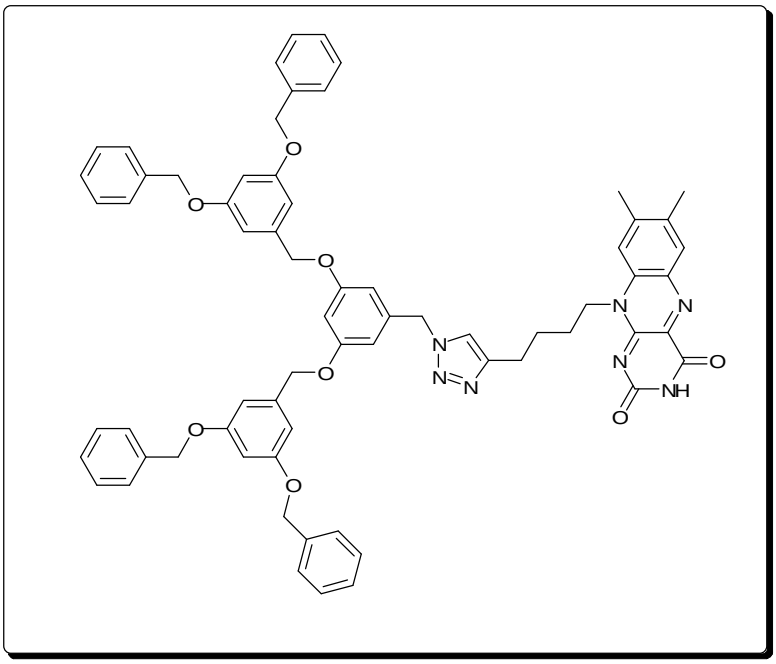

A solution of alkyne-functionalised flavin **26** (100 mg, 0.3 mmol) and [G-2]-N_3 dendron **29** (234 mg, 0.3 mmol) in DMF (5 mL) was treated with copper iodide (6 mg, 30 μmol) and stirred at room temperature for 96 hours. The solvent was removed under reduced pressure and the remaining residue diluted in DCM (150 mL) before washing with water (100 mL), saturated sodium carbonate solution (100 mL) and brine (100 mL). The organic layer was separated, dried over magnesium sulphate and concentrated under reduced pressure to afford a greenish yellow solid. This was purified by flash chromatography (1:4 acetone/DCM increasing polarity to 1:1 acetone/DCM) to afford the product as a bright yellow solid (110 mg, 34 %, mp 99-101 °C): ^{1}H NMR (400 MHz, $CDCl_3$) δ 1.78 (2H, m, *J* 6.8 Hz, CH_2), 1.87 (2H, m, *J* 6.8 Hz, CH_2), 2.32 (3H, s, CH_3), 2.47 (3H, s, CH_3), 2.79 (2H, t, *J* 6.8 Hz, CH_2), 4.57 (2H, br s, CH_2N), 4.81 (4H, s, 4 x CH), 4.94 (8H, s, 8 x CH), 5.37 (2H, s, 2 x CH), 6.35 (2H, d, *J* 1.6 Hz, 2 x CH), 6.43 (1H, t, *J* 1.6 Hz, CH), 6.47 (2H, d, *J* 2.0 Hz, 2 x CH), 6.52 (4H, d, *J* 2.0 Hz, 4 x CH), 7.22 – 7.34 (20H, m, 4 x Ph), 7.43 (1H, s, CH), 7.53 (1H, s, CH), 7.90 (1H, s, CH), 8.34 (1H, br s, NH); *m/z* (FAB^+): 1093 (M^+ + H, 100%); Elemental analysis calcd for $C_{67}H_{61}N_7O_8$ requires C (73.68 %), H (5.63 %) N (8.98 %), found C (73.36 %), H (5.51 %), N (9.10 %).

Third generation flavin-functionalised aryl dendron "[G-3]-AFl" (32)

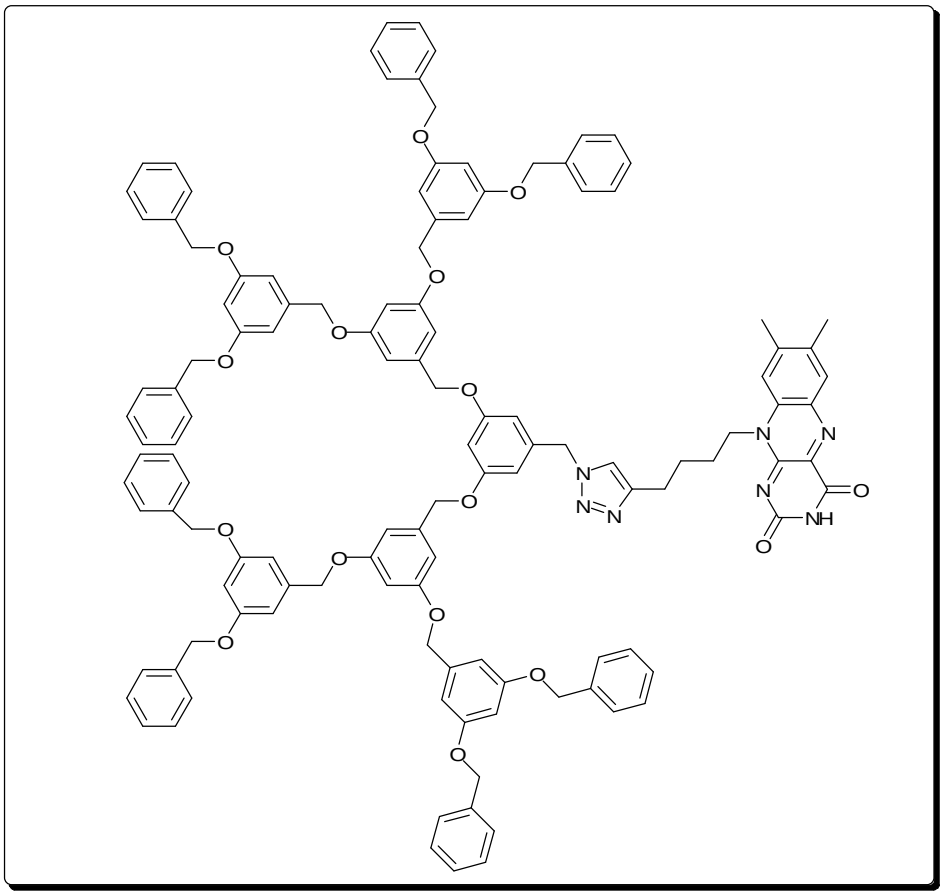

A solution of alkyne-functionalised flavin **26** (20 mg, 0.06 mmol) and [G-3]-N_3 dendron **31** (100 mg, 0.06 mmol) in DMF (5 mL) was treated with copper iodide (2 mg, 10 μmol) and stirred at room temperature for 96 hours. The solvent was removed under reduced pressure and the remaining residue diluted in DCM (150 mL) before washing with water (100 mL), saturated sodium carbonate solution (100 mL) and brine (100 mL). The organic layer was separated, dried over magnesium sulphate and concentrated under reduced pressure to afford a greenish yellow solid. This was purified by flash chromatography (DCM increasing polarity to 1:4 acetone/DCM) to afford the product as a dark green solid (52 mg, 45 %, mp 88 – 90 °C). ^{1}H NMR (400 MHz, $CDCl_3$) δ 1.75 (2H, m, *J* 7.2 Hz, CH_2), 1.81 (2H, m, *J* 7.2 Hz, CH_2), 2.32 (3H, s, CH_3), 2.40 (3H, s, CH_3), 2.75 (2H, t, *J* 7.2 Hz, CH_2), 4.50 (2H, br s, CH_2N), 4.74 (4H, s, 2 x CH_2), 4.79 (8H, s, 4 x CH_2), 4.92 (16H, s, 8 x CH_2), 5.22 (2H, s, CH_2), 6.33 (2H, s, 2 x CH), 6.43 (2H, s, 2 x CH), 6.43 (1H, s, CH), 6.46 (4H, s, 4 x CH), 6.47 (4H, s, 4 x CH), 6.58 (8H, s, 8 x CH), 7.23 (40 H, s, 8 x Ph), 7.32 (1H, s, CH (imidazole)), 7.52 (1H, s, CH), 7.86 (1H, s, CH), 8.40 (1H, br s, NH); *m/z* (FAB^+): 1942 (M^+ + H, 100%); Elemental analysis calcd for $C_{123}H_{109}N_7O_{16}$ requires C (76.10 %), H (5.66 %), N (5.05 %), found C (76.37 %), H (5.83 %), N (5.37 %).

7.5 Synthesis – Chapter Five

Dimethyl-2-oxoglutaconate (33)[155]

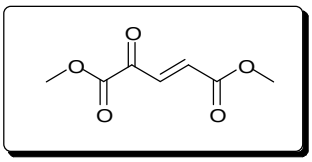

Dimethyl-2-oxoglutarate (2.50 mL, 17.2 mmol) was dissolved in anhydrous DCM (100 mL) and heated to reflux. Bromine (0.9 mL, 17.5 mmol) was added drop-wise via syringe to the refluxing mixture. The solution was then heated under reflux for a further three hours and left to cool overnight without stirring. The solvent and excess hydrogen bromide were then removed from the dark orange solution under reduced pressure, and the resulting orange residue was diluted in diethyl ether (120 mL) and treated with triethylamine (2.40 mL, 17.5 mmol). The mixture was then stirred at room temperature for 30 minutes, forming a white solid in a yellow solution. The solid was removed by filtration, before removal of the filtrate's solvent under reduced pressure. The resulting orange solid was purified by flash chromatography on SiO_2 (5% ethyl acetate in DCM) to afford a bright yellow solid (2.18 g, 74%, mp 140 – 142 °C): ^{1}H NMR (200 MHz, $CDCl_3$) δ 3.75 (3H, s, CH_3), 3.85 (3H, s, CH_3), 6.90 (1H, d, *J* 14.0 Hz, CH), 7.55 (1H, d, *J* 14.0 Hz, CH); *m/z* (EI^+) 172 (M^+, 100%).

Dimethyl 10-hydroxybenzo[*f*]quinoline-2,4-dicarboxylate (34)[144]

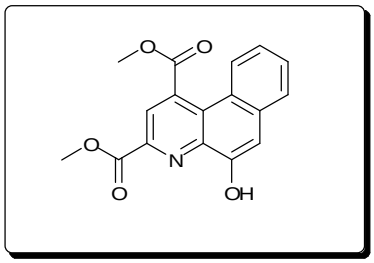

To a solution of 3-amino-2-napthol (1.18 g, 7.4 mmol) and dimethyl-2-oxoglutaconate (**33**, 2.750 g, 16.0 mmol) in anhydrous DCM (200 mL) was added a catalytic amount of PTS (0.15 g, 0.8 mmol). The mixture was heated under reflux for twenty-four hours under N_2. The solvent was removed under reduced pressure to afford a brown residue, which was then purified by flash chromatography on SiO_2 (40% acetone in hexane) to afford a yellow crystalline solid (880 mg, 38%, mp 162 - 164 °C): ^{1}H NMR (200 MHz, $CDCl_3$) δ 4.03 (3H, s, CH_3), 4.09 (3H, s, CH_3), 7.30 (1H, dt, CH, *J* 1.8, 7.9), 7.40 (1H, s), 7.55 (1H, ddd, *J* 1.8, 7.9, 8.8 Hz, CH), 7.65 (1H, dd, *J* 1.1, 7.9 Hz, CH), 7.99 (1H, br d, *J* 8.4 Hz, CH), 8.25 (1H, s, CH), 8.49 (1H, br s, OH); *m/z* (EI^+): 312 (M^+ + H, 100%)

Dimethyl 9,10-dihydro-9,10-dioxobenzo[*f*]quinoline-2,4-dicarboxylate ("BQQ", 35)[144]

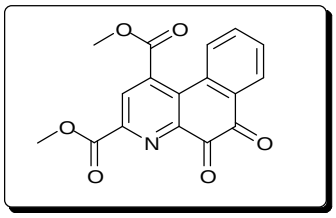

To an ice-cooled solution of **34** (400 mg, 1.3 mmol) in acetonitrile (50 mL) was added an aqueous solution of Fremy's salt ($(KSO_3)_2NO$, 1.0 g, 3.73 mmol, 50 mL) and potassium phosphate (483 mg, 3.55 mmol). The mixture was stirred at room temperature for eighteen hours then extracted with chloroform (4 × 50 mL). The organic layer was separated and dried over magnesium sulphate before the solvent was removed under reduced pressure. The resulting brown residue was washed with diethyl ether (30 mL) and recrystallised from toluene to give a yellow solid (82 mg, 20%, mp 216-218 °C): ^{1}H NMR (200 MHz, $CDCl_3$) δ 3.97 (3H, s, CH_3), 3.98 (3H, s, CH_3), 7.50 (1H, d, *J* 7.4 Hz, CH), 7.70 (1H, t, *J* 7.4 Hz, CH), 8.15 (1H, dt, *J* 1.8, 7.4 Hz, CH), 8.15 (1H, dd, *J* 1.8, 7.4 Hz, CH), 8.35 (1H, s, CH); *m/z* (EI^+): 327 (M^+ + 2, 100%); Elemental analysis for $C_{17}H_{11}NO_6$ requires C (62.77 %), H (3.41 %), N (4.31 %), found C (62.41 %), H (3.35 %), N (4.29 %).

Chapter Eight

8 Chapter Eight – List of References

1. J. W. Steed and J. L. Atwood, *Supramolecular Chemistry*, John Wiley & Sons, Chichester, 2002.
2. P. D. Beer, P. A. Gale and D. K. Smith, *Supramolecular Chemistry*, Oxford University Press, Oxford, 1999.
3. D. J. Cram, *Angew. Chem. Int. Ed*, 1986, **25**, 1039.
4. D. J. Cram, *Angew. Chem. Int. Ed*, 1988, **27**, 1009.
5. Y. Murakami, J. Kikuchi, Y. Hisaeda and O. Hayashida, *Chem. Rev.*, 1996, **96**, 721.
6. J. S. Lindsey, *New J. Chem.*, 1991, **15**, 153.
7. J. P. Behr, *The Lock and Key Principle*, John Wiley & Sons, Chichester, 1994.
8. J. Polster and H. Lachmann, *Spectrometric Titrations*, VCH, Weinhein, 1989.
9. K. A. Conners, *Binding Constants*, John Wiley and Sons, Chichester, 1987.
10. J.-M. Lehn, *Pure Appl. Chem.*, 1994, **66**, 1961.
11. C. J. Pedersen, *J. Am. Chem. Soc.*, 1967, **89**, 7017.
12. G. A. Jeffrey, *An Introduciton to Hydrogen Bonding*, Oxford University Press, Oxford, 1997.
13. L. J. Prins, D. N. Reinhoudt and P. Timmerman, *Angew. Chem. Int. Ed*, 2001, **40**, 2382.
14. J. D. Watson and F. H. Crick, *Nature*, 1953, **171**, 737.
15. C. A. Hunter and J. K. M. Sanders, *J. Am. Chem. Soc.*, 1990, **112**, 5525.
16. C. S. Wilcox, J. C. Adrian, T. H. Webb and F. J. Zawacki, *J. Am. Chem. Soc.*, 1992, **114**, 10189.
17. T. Szabo, G. Hilmersson and J. Rebek, *J. Am. Chem. Soc.*, 1998, **120**, 6193.
18. L. R. Pratt, *J. Am. Chem. Soc.*, 1981, **103**, 7700.
19. D. B. Smithrud, E. M. Sanford, I. Chao, S. B. Ferguson, D. R. Carcanague, J. D. Evanseck, K. N. Houk and F. Diederich, *Pure Appl. Chem.*, 1990, **62**, 2227.
20. A. J. Kirby, *Angew. Chem. Int. Ed*, 1994, **33**, 551.
21. Y. M. Legrand, *PhD Thesis*, 2005, Heriot-Watt University, Edinburgh EH14 14AS.
22. T. L. Brown, *Making Truth: Metaphor in Science*, University of Illinois Press, 2003.
23. V. Massey, *Biochem. Soc. Trans*, 2000, **28**, 283.
24. Y. Murthy, V. Massey and Y. Meah, *J. Am. Chem. Soc.*, 1999, **121**, 5344.
25. B. J. Jordan, G. Cooke, J. F. Garety, M. A. Pollier, N. Kryvokhyzha, A. Bayir, G. Rabani and V. M. Rotello, *Chem. Comm.*, 2007, **12**, 1248.
26. D. Walton and P. Lorrimer, *Polymers*, Oxford University Press, Oxford, 2000.
27. D. K. Smith and F. Diederich, *Chem. Eur. J.*, 1998, **4**, 1353.
28. P. J. Dandliker, F. Diederich and J.-P. Gisselbrecht, *Angew. Chem. Int. Ed. Engl.*, 1995, **34**, 2725.
29. A. E. Kaifer and G.-K. Kaifer, *Supramolecular Electrochemistry*, Wiley-VCH, Chichester, 2001.
30. A. J. Bard and L. R. Faulkner, *Electrochemical Methods: Fundamentals and Applications*, Wiley, New York, 1980.
31. F. Muller, *Chemistry and Biochemistry of Flavoenzymes*, CRC Press, Boca Raton, 1991.
32. K. Stevenson, V. Massey and C. Williams, *Flavins and Flavoproteins*, University of Calgary, Calgary, 1996.
33. O. Warburg and W. Christian, *Biochem. Z.*, 1933, **266**, 377.
34. H. Theorell, *Biochem. Z.*, 1935, **275**, 344.
35. A. Niemz and V. M. Rotello, *Acc. Chem. Res.*, 1999, **32**, 44.
36. D. Sheng, D. P. Ballou and V. Massey, *Biochemistry*, 2001, **40**, 11156.

37. C. Walsh, *Enzymatic Reaction Mechanisms*, W. H. Freeman, New York, 1979.
38. D. M. Zeigler, *Trends. Pharm. Sci.*, 1990, **11**, 321.
39. V. Massey and P. Hemmerich, *The Enzymes*, Academic Press, New York, 1976.
40. G. Swensen and K. Eren, *Flavins and Flavoproteins*, Berlin, 1987.
41. Y. Yano, K. Mitsui, Y. Ohsawa, T. Kobayashi and T. Nabeshima, *J. Chem. Soc. Chem. Commun.*, 1993, **23**, 1719.
42. R. B. Silverman and X. Lu, *J. Am. Chem. Soc.*, 1994, **116**, 4129.
43. J. Kim, M. A. Bogdan and P. S. Mariano, *J. Am. Chem. Soc.*, 1993, **115**, 10591.
44. E. Breinliger, A. Niemz and V. M. Rotello, *J. Am. Chem. Soc.*, 1995, **117**, 5379.
45. A. Niemz and V. M. Rotello, *J. Mol. Recognit.*, 1996, **9**, 158.
46. R. Deans, G. Cooke and V. M. Rotello, *J. Org. Chem.*, 1997, **62**, 836.
47. T. Bugg, *An Introduction to Enzyme and Coenzyme Chemistry*, Blackwell Science, Oxford, 1997.
48. E. E. Carlson and L. L. Kiessling, *J. Org. Chem.*, 2004, **69**, 2614.
49. E. Warkentin, B. Mamat, M. Sordel-Klippert, M. Wicke, R. K. Thauer, M. Iwata, S. Iwata, U. Ermler and S. Shima, *The EMBO Journal*, 2001, **20**, 6561.
50. F. Yoneda, Y. Sakuma, S. Mizumoto and R. Ito, *J. C. S. Perkin I*, 1976, **16**, 1805.
51. G. R. Newkome, C. N. Moorefield and F. Vogtle, *Dendritic Molecules: Concepts, Syntheses, Perspectives*, VCH, Weinheim, 1996.
52. M. Liu and J. M. J. Frechet, *Pharm. Sci. Technol. Today*, 1999, **2**, 393.
53. D. A. Tomalia, A. M. Naylor and W. A. Goddard III, *Angew. Chem.*, 1990, **102**, 119.
54. C. J. Hawker and J. M. J. Frechet, *J. Chem. Soc. Chem. Commun.*, 1990, **15**, 1010.
55. H. L. Levine and E. T. Kaiser, *J. Am. Chem. Soc.*, 1978, **100**, 7670.
56. H. E. Fried and E. T. Kaiser, *J. Am. Chem. Soc.*, 1981, **103**, 182.
57. J. P. C. Bootsma, G. Challa and F. Muller, *J. Poly. Sci.*, 1984, **22**, 705.
58. K. Tomizaki, Y. Tsunekawa, H. Akisada and N. Hishino, *J. Chem. Soc. Perkin. Trans. 2*, 2000, **4**, 813.
59. J. Kofoed and J.-L. Reymond, *Curr. Opp. Chem. Biol.*, 2005, **9**, 656.
60. A.-M. Caminade, P. Servin, R. Laurent and J.-P. Majoral, *Chem. Soc. Rev.*, 2008, **37**, 56.
61. M. J. Hannon, P. C. Mayers and P. C. Taylor, *J. Chem. Soc. Perkin Trans. 1*, 2000, **12**, 1881.
62. E. Buhleier, W. Wehner and F. Vogtle, *Synthesis-Stuttgart*, 1978, **2**, 155.
63. D. A. Tomalia, H. Baker, J. Dewald, M. Hall, G. Kallos, S. Martin, J. Roeck, J. Ryder and P. Smith, *Polymer Journal*, 1985, **17**, 117.
64. G. R. Newkome, Z. G. Yao, G. R. Baker and V. K. Gupta, *J. Org. Chem.*, 1985, **50**, 2003.
65. G. R. Newkome, C. N. Moorefield and F. Vogtle, *Dendrimers and Dendrons. Concepts, Synthesis and Perspectives*, Wiley-VCH, Chichester, 2001.
66. D. A. Tomalia and D. P. R., *Nature*, 1994, **372**, 617.
67. J. K. M. Sanders, *Chem. Eur. J.*, 1998, **4**, 1378.
68. H. Brunner, *J. Organomet. Chem.*, 1995, **500**, 39.
69. J. W. J. Knapen, A. W. van der Made, J. C. de Wilde, P. W. N. M. van Leeuwen, P. Wijkens, D. M. Grove and G. van Koten, *Nature*, 1994, **372**, 659.
70. C. O. Liang and J. M. J. Frechet, *Prog. Polym. Sci.*, 2005, **30**, 385.
71. C. J. Hawker, K. L. Wooley and J. M. J. Frechet, *J. Am. Chem. Soc.*, 1993, **115**, 4375.
72. G. R. Moore and G. W. Pettigrew, *Cytochromes c: Evolutionary, Structural and Physiochemical Aspects*, Springer, New York, 1990.
73. P. J. Dandliker, F. Diederich, M. Gross, C. B. Knobler, A. Louati and E. M. Sanford, *Angew. Chem. Int. Ed. Engl.*, 1994, **33**, 1739.
74. L. J. Twyman, A. S. H. King and I. K. Martin, *Chem. Soc. Rev.*, 2002, **31**, 69.

75. P. Bhyrappa, J. K. Young, J. S. Moore and K. S. Suslick, *J. Am. Chem. Soc.*, 1996, **118**, 5708.
76. T. Butz, P. Murer and D. Seebach, *Polym. Mater. Sci. Eng.*, 1997, **77**, 132.
77. T. Habicher and F. Diederich, *Helv. Chim. Acta*, 1997, **82**, 1066.
78. L. Crespo, G. Sanclimens, M. Pons, E. Giralt, M. Royo and F. Albericio, *Chem. Rev.*, 2005, **105**, 1663.
79. K. Sadler and J. P. Tams, *Rev. Mol. Biotechnol.*, 2002, **90**, 195.
80. J. D. Stevenson and N. R. Thomas, *Nat. Prod. Rep.*, 2000, **17**, 15642.
81. D. Qi, C. M. Tann, D. Haring and M. D. Distefano, *Chem. Rev.*, 2001, **101**, 3081.
82. S. J. Miller, *Acc. Chem. Res.*, 2004, **34**, 4897.
83. T. J. Prosa, B. J. Bauer and E. J. Amis, *Macromolecules*, 2001, **34**, 4897.
84. P. K. Maiti, T. Cagin, G. Wang and W. A. Goddard III, *Macromolecules*, 2004, **37**, 6254.
85. V. M. Rotello, *Curr. Opp. Chem. Biol.*, 1999, **3**, 747.
86. S. Shinkai, Y. Ishikawa, H. Shinkai, T. Tsuno, H. Makishima, K. Ueda and O. Manabe, *J. Am. Chem. Soc.*, 1984, **106**, 1801.
87. V. T. D'Souza, *Supramolecular Chem.*, 2003, **15**, 221.
88. S. Ghisla and V. Massey, *Eur. J. Biochem.*, 1989, **181**, 1.
89. E. G. Pai and G. E. Schulz, *J. Biol. Chem.*, 1983, **258**, 1752.
90. K. J. C. van Bommel, G. A. Metselaar, W. Verboom and D. N. Reinhoudt, *J. Org. Chem.*, 2001, **66**, 5405.
91. G. R. Newkome, B. D. Woosley, E. He, C. N. Moorefield, R. Guther, G. R. Baker, G. H. Escamilla, J. Merril and H. Luftman, *Chem. Commun.*, 1996, **24**, 2737.
92. M. Wells and R. M. Crooks, *J. Am. Chem. Soc.*, 1996, **118**, 3988.
93. J. F. G. A. Jansen, E. M. M. de Brabander-van den Berg and E. W. Meijer, *Science*, 1994, **266**, 1226.
94. C. B. Gorman and J. C. Smith, *Polymer*, 2000, **41**, 675.
95. M. D. Greaves, R. Deans, T. H. Glaow and V. M. Rotello, *Chem. Comm.*, 1999, **9**, 785.
96. J. Koziol, *Photochem. Photobiol.*, 1966, **5**, 41.
97. P. F. Heelis, *Chem. Soc. Rev.*, 1982, **11**, 15.
98. R. P. Haugland, *Handbook of Fluorescent Probes and Research Chemicals*, OR, Eugene, 1996.
99. N. Marme, J.-P. Knemeyer, M. Sauer and J. Wolfrum, *Bioconjugate Chem.*, 2003, **14**, 1133.
100. J. D. Pellett, D. F. Becker, A. K. Saenger, J. A. Fuchs and M. T. Stankovich, *Biochemistry*, 2001, **40**, 7720.
101. H. Ye, D. Rong, W. Tong and V. T. D'Souza, *Perkin Trans. 2*, 1992, **11**, 2071.
102. B. Helms and J. M. J. Frechet, *Adv. Synth. Cat.*, 2006, **348**, 1125.
103. S. S. Agasti, S. T. Caldwell, G. Cooke, B. J. Jordan, A. Kennedy, N. Kryvokhyzha, G. Rabani, S. Rana, A. Sanyal and V. M. Rotello, *Chem. Commun.*, 2008, **35**, 4123.
104. P. Chaiyen, J. Sucharitakul, J. Svasti, B. Entsch, V. Massey and D. P. Ballou, *Biochemistry*, 2004, **43**, 3933.
105. S. Y. Reddy and T. C. Bruice, *Protein Science*, 2004, **13**, 1965.
106. C. Anthony, *Biochem. J.*, 1996, **320**, 697.
107. V. Sundaresan, J. Chartron, M. Yamaguchi and C. D. Stout, *J. Mol. Biol.*, 1996, **346**, 617.
108. A. L. Pey, M. Thorolfsson, K. Teigen, M. Ugarte and A. Martinez, *J. Am. Chem. Soc.*, 2004, **126**, 13670.
109. Y. Liu, A. H. Flood and J. F. Stoddart, *J. Am. Chem. Soc.*, 2004, **126**, 9150.
110. J. J. Hasford and C. J. Rizzo, *J. Am. Chem. Soc.*, 1998, **120**, 2251.
111. R. Deans and V. M. Rotello, *J. Org. Chem.*, 1997, **62**, 4528.

112. Y. M. Legrand, M. Gray, G. Cooke and V. M. Rotello, *J. Am. Chem. Soc.*, 2003, **125**, 15789.
113. R. Huisgen, *Pure Appl. Chem.*, 1989, **61**, 613.
114. R. Huisgen, G. Szeimics and L. Mobius, *Chem. Ber.*, 1967, **100**, 2494.
115. V. V. Rostovstev, L. G. Green, V. V. Fokin and K. B. Sharpless, *Angew. Chem. Int. Ed*, 2002, **41**, 2596.
116. H. C. Kolb, M. G. Finn and K. B. Sharpless, *Angew. Chem. Int. Ed*, 2001, **40**, 2004.
117. C. B. Gorman, *Adv. Mater.*, 1998, **10**, 295.
118. A. W. Bosman, M. H. Janssen and E. W. Meijer, *Chem. Rev.*, 1999, **99**, 1665.
119. G. R. Newkome and C. N. Moorefield, *Chem. Rev.*, 1997, **99**, 1689.
120. F. Zeng and S. C. Zimmerman, *Chem. Rev.*, 1997, **97**, 1681.
121. C. B. Gorman and J. C. Smith, *Acc. Chem. Res.*, 2001, **34**, 60.
122. C. B. Gorman and J. C. Smith, *J. Am. Chem. Soc.*, 2000, **122**, 9342.
123. K. W. Pollak, J. W. Leon, J. M. J. Frechet, M. Maskus and H. D. Abruna, *Chem. Mater.*, 1998, **10**, 30.
124. C. B. Gorman, J. C. Smith, M. W. Hager, B. L. Parkhurst, H. Sierzputowska-Gracz and A. Haney, *J. Am. Chem. Soc.*, 1999, **121**, 9958.
125. K. L. Wooley, C. J. Hawker and J. M. J. Frechet, *J. Am. Chem. Soc.*, 1991, **121**, 4252.
126. K. Y. Chen and C. B. Gorman, *J. Am. Chem. Soc.*, 1996, **61**, 9229.
127. C. Devadoss, P. Bharathi and J. S. Moore, *Angew. Chem. Int. Ed. Engl.*, 1997, **36**, 1633.
128. V. Vicinelli, M. Maestri, V. Balzani, W. M. Muller, U. Muller, U. Hahn, F. Osswald and F. Vogtle, *New J. Chem.*, 2001, **25**, 989.
129. R. Toba, J. M. Quintela, C. Peinador, E. Roman and A. E. Kaifer, *Chem. Commun.*, 2001, **9**, 857.
130. R. A. Evans, *Australian Journal of Chemistry*, 2007, **60**, 384.
131. C. W. Tornoe, C. Christensen and M. Meldal, *J. Org. Chem.*, 2002, **67**, 3057.
132. D. J. V. C. van Steenis, O. R. P. David, G. P. F. van Strijdonck, J. H. van Maarseveen and J. N. H. Reek, *Chem. Comm.*, 2005, **34**, 4333.
133. J. B. Carroll, B. J. Jordan, H. Xu, B. Erdogan, L. Lee, L. Cheng, C. Tiernan, G. Cooke and V. M. Rotello, *Org. Lett.*, 2005, **7**, 2551.
134. A. Oubrie, H. J. Rozeboom and B. W. Dijkstra, *Proc. Natl. Sci. USA*, 1999, **96**, 11787.
135. A. Oubrie, H. J. Rozeboom, K. H. Kalk and J. A. Duine, *J. Mol. Biol.*, 1999, **289**, 319.
136. S. A. Salisbury, H. S. Forrest, W. B. T. Cruse and O. Kennard, *Nature*, 1979, **280**, 843.
137. A. Oubrie and B. W. Dijkstra, *Protein Science*, 2000, **9**, 1265.
138. A. Sato, K. Takagi, N. Kato, J. A. Duine and T. Ikeda, *Biochem. J.*, 2001, **357**, 893.
139. J. G. Hauge, *J. Biol. Chem.*, 1964, **239**, 3630.
140. F. M. Steinberg, M. E. Gershwin and R. B. Rucker, *J. Nutr.*, 1994, **124**, 744.
141. T. Kasahara and T. Kato, *Nature*, 2003, **422**, 832.
142. O. Choi, J. Kim, J.-G. Kim, Y. Jeong, J. S. Moon, C. S. Park and I. Hwang, *Plant Physiology*, 2008, **146**, 657.
143. S. Itoh, Y. Fukui, S. Haranou, M. Ogino, M. Komatsu and Y. Ohshiro, *J. Org. Chem.*, 1992, **57**, 4452.
144. S. Itoh, Y. Fukui, M. Ogino, S. Haranou, M. Komatsu and Y. Ohshiro, *J. Org. Chem.*, 1992, **57**, 2788.
145. Y.-J. Zheng and T. C. Bruice, *Proc. Natl. Sci. USA*, 1997, **94**, 11881.
146. C. Anthony and M. Ghosh, *Curr. Sci.*, 1997, **72**, 716.
147. S. Itoh, H. Kawakami and S. Fukuzumi, *J. Am. Chem. Soc.*, 1997, **119**, 439.

148. P. R. Afolabi, F. Mohammed, K. Amaratunga, O. Majekodunmi, S. L. Dales, R. Gill, D. Thompson, J. B. Cooper, S. O. P. Wood, P. M. Goodwin and C. Anthony, *Biochemistry*, 2001, **40**, 9799.
149. A. Oubrie, *Biochimica et Biophysica Acta*, 2002, **1647**, 143.
150. C. Anthony, *Principles and Applications of Quinoproteins*, Marcel Dekker, New York, 1993.
151. Y. Ge, L. Miller, T. Ouimet and D. K. Smith, *J. Org. Chem.*, 2000, **65**, 8831.
152. Y. Ge, R. R. Lilienthal and D. K. Smith, *J. Am. Chem. Soc.*, 1996, **118**, 3976.
153. S. Itoh, H. Kawakami and S. Fukuzumi, *J. Am. Chem. Soc.*, 1998, **120**, 7271.
154. T. S. Eckert, T. C. Bruice, J. A. Gainor and S. M. Weinreb, *Natl. Acad. Sci. USA*, 1982, **79**, 2533.
155. E. J. Corey and A. Tramontano, *J. Am. Chem. Soc.*, 1981, **103**, 5599.
156. G. W. T. M. J. Frisch, H. B. Schlegel, G. E. Scuseria, , J. R. C. M. A. Robb, J. A. Montgomery, Jr., T. Vreven, , J. C. B. K. N. Kudin, J. M. Millam, S. S. Iyengar, J. Tomasi, , B. M. V. Barone, M. Cossi, G. Scalmani, N. Rega, , H. N. G. A. Petersson, M. Hada, M. Ehara, K. Toyota, , J. H. R. Fukuda, M. Ishida, T. Nakajima, Y. Honda, O. Kitao, , M. K. H. Nakai, X. Li, J. E. Knox, H. P. Hratchian, J. B. Cross, , J. J. C. Adamo, R. Gomperts, R. E. Stratmann, O. Yazyev, , R. C. A. J. Austin, C. Pomelli, J. W. Ochterski, P. Y. Ayala, , G. A. V. K. Morokuma, P. Salvador, J. J. Dannenberg, , S. D. V. G. Zakrzewski, A. D. Daniels, M. C. Strain, , D. K. M. O. Farkas, A. D. Rabuck, K. Raghavachari, , J. V. O. J. B. Foresman, Q. Cui, A. G. Baboul, S. Clifford, , B. B. S. J. Cioslowski, G. Liu, A. Liashenko, P. Piskorz, , R. L. M. I. Komaromi, D. J. Fox, T. Keith, M. A. Al-Laham, , A. N. C. Y. Peng, M. Challacombe, P. M. W. Gill, , W. C. B. Johnson, M. W. Wong, C. Gonzalez, and J. A. Pople, and I. Gaussian, Wallingford CT, 2004.
157. A. Niemz, J. Imbriglio and V. M. Rotello, *J. Am. Chem. Soc.*, 1997, **119**, 887.
158. B. Feibush, A. Figueroa, R. Charles, K. D. Onan, P. Feibush and B. L. Karger, *J. Am. Chem. Soc.*, 1986, **108**, 3310.

Chapter Nine

9 Chapter Nine - Appendices

9.1 Appendix One: Published Papers

COMMUNICATION www.rsc.org/chemcomm | ChemComm

Dendron-based model systems for flavoenzyme activity: towards a new class of synthetic flavoenzyme†

Sarit S. Agasti,[a] Stuart T. Caldwell,[b] Graeme Cooke,*[b] Brian J. Jordan,[a] Andrew Kennedy,[b] Nadiya Kryvokhyzha,[b] Gouher Rabani,[b] Subinoy Rana,[a] Amitav Sanyal[c] and Vincent M. Rotello[a]

Received (in Cambridge, UK) 5th June 2008, Accepted 18th July 2008
First published as an Advance Article on the web 31st July 2008
DOI: 10.1039/b809568j

Three generations of water-soluble flavin dendrons have been synthesized and the role dendrimer generation has on the physical and catalytic properties of these assemblies has been investigated.

Flavoenzymes are an important class of redox enzymes that are involved in a variety of biological processes including electron transfer, redox transformations and signal transduction.[1] The redox active flavin groups (cofactors) (*e.g.* **Riboflavin**, **FMN** or **FAD**) of typical flavoenzymes are usually bound to the active-site of the apoenzyme *via* a range of non-covalent interactions.[2] The delicate cooperation of these interactions are thought to be responsible for fine-tuning the redox properties of the cofactor, and also for creating a hydrophobic binding pocket to isolate the cofactor from competing interactions with the aqueous environment.

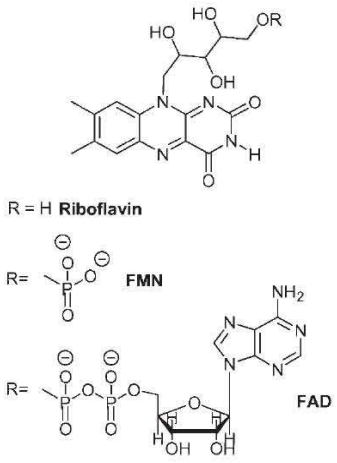

In order for an artificial enzyme to be constructed that adequately simulates the structure and reactivity of the prototype flavoenzyme, a detailed understanding of how non-covalent interactions tune the properties of the flavin cofactor is desirable. To aid this process, a range of molecular model systems have been synthesized and studied to elucidate the role various supramolecular interactions (*e.g.* hydrogen bonding, π–stacking and donor atom–π interactions) have in modulating the redox properties[3] and reactivity[4] of the flavin moiety. Although these systems have provided some insight into how these interactions modulate the redox potential of the flavin, they have failed to accurately recreate the biomimetic environment that surrounds the flavin cofactor. Polymer-based model systems have also been synthesised by attaching flavin moieties onto biomolecules,[5] synthetic polymers[6] and peptides.[7] However, the lack of active site structural homogeneity and lengthy synthetic protocols have limited their potential applications. Therefore, a highly efficient synthetic flavoenzyme model system still remains a great challenge for the synthetic community.

Recently, we have reported a fully synthetic polymeric flavoenzyme model, where we have incorporated the key attributes of flavoenzymes (cofactor isolation, redox tuning and catalytic activity) by synthesising a water-soluble polymeric system using atom transfer radical polymerisation.[8] Herein we have turned our attention to take advantage of the microenvironment provided by dendrons in order to generate a new class of synthetic flavoenzyme. Dendron architectures were selected for this study in view of their superior structural characteristics compared to conventional synthetic polymers for creating effective biomimetic environments.[9] In particular, dendron architectures can be precisely controlled at the molecular level and can confer: (i) a well-defined monodisperse structure; (ii) a large number of terminal functionalities offering effective interactions with their surrounding media, and at the same time, isolating reactive catalytic functionality at their foci.[10]

A series of water soluble dendrons featuring triethylene glycol units were designed and synthesised to mimic the flavoenzyme activity (Fig. 1). In the dendritic architecture, the catalytic centre (the flavin residue) was introduced at the focal point of the dendron in order to achieve a substrate accessible biomimetic hydrophobic pocket around the active site. The detailed synthetic protocols for preparing **G1_flavin**, **G2_flavin** and **G3_flavin** are described in the ESI.† Molecular dynamics simulations performed in water for **G1_flavin**, **G2_flavin** and **G3_flavin** indicated that as the dendron generation is increased from G1 to G3, the degree of encapsulation

[a] *Department of Chemistry, University of Massachusetts at Amherst, Amherst, MA 01003, USA*
[b] *Glasgow Centre for Physical Organic Chemistry, WestCHEM, Department of Chemistry, Joseph Black Building, University of Glasgow, Glasgow, UK G12 8QQ. E-mail: graemec@chem.gla.ac.uk*
[c] *Department of Chemistry, Bogazici University, Bebek, 34342 Istanbul, Turkey*

† Electronic supplementary information (ESI) available: Synthesis and characterisation of the flavin dendrons. See DOI: 10.1039/b809568j

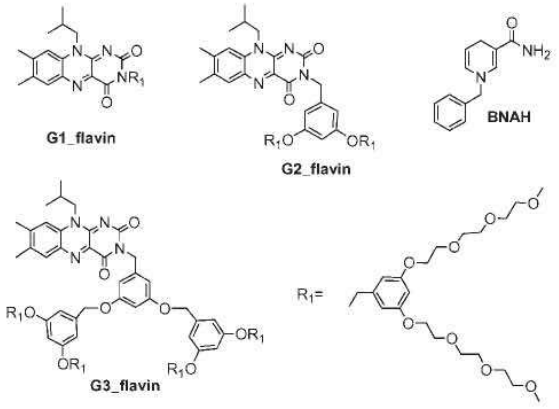

Fig. 1 Structure of the flavin dendrons (**G1_flavin**, **G2_flavin** and **G3_flavin**) and **BNAH**.

increases, with the flavin in **G3_flavin** being partly located in a hydrophobic environment that is near the surface, a feature commonly observed in flavin-based electron-transfer proteins (Fig. 2).

As the flavin unit is a very effective system for probing the polarity of its surrounding microenvironment, we have recorded the UV-vis spectra of **Riboflavin** and the flavin dendrons in pH = 8.0 phosphate buffer–isopropanol (95 : 5).[11] It has previously been shown that the S_0–S_2 transition of the flavin nucleus is solvatochromic and undergoes a bathochromic shift in going from non-polar to polar media, thereby offering a simple method of probing the microenvironment conferred by the dendron units.[12] The overlaid UV-vis spectra of **Riboflavin** and dendrons **G1_flavin–G3_flavin** are shown in Fig. 3. The S_0–S_2 transition for riboflavin and the first and second generation flavin dendrons were very similar and occurred at around 370 nm. However, for the third generation flavin dendron the S_0–S_2 transition was shifted 20 nm to a shorter wavelength (λ = 370 nm for **Riboflavin** *versus* λ = 350 nm for **G3_flavin**). This blue shift is consistent with the ethylene glycol moieties of the third generation dendron creating a biomimetic hydrophobic pocket for the flavin unit in aqueous media.[8]

Fluorescence spectra of **Riboflavin** and the dendron systems **G1_flavin–G3_flavin** were recorded and revealed that the dendron moieties significantly quenched the fluorescence of the flavin moiety (compared to **Riboflavin**), presumably due to

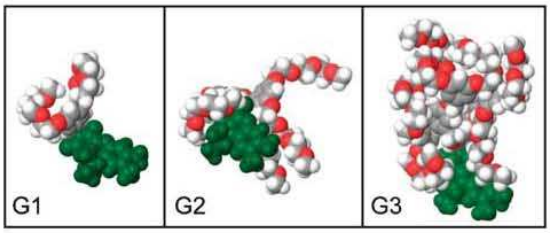

Fig. 2 Molecular dynamic simulations of dendron generations (G1-G3) demonstrating the degree of encapsulation of the flavin unit (green) within the dendron wedges. Water molecules have been omitted for clarity.

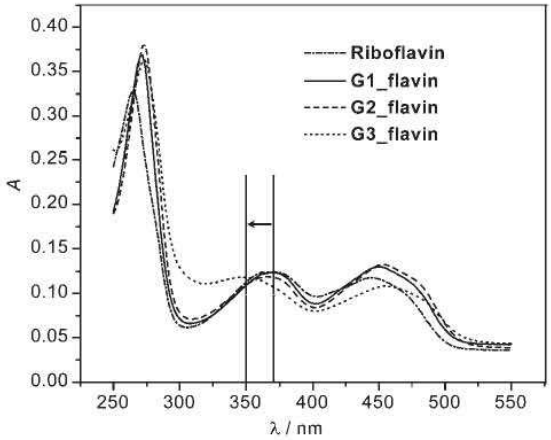

Fig. 3 Overlaid UV-vis spectra of **Riboflavin** and flavin dendrons **G1_flavin–G3_flavin** (5 mM solutions in phosphate buffer (pH = 8.0) isopropanol (95 : 5)). Spectrum of **G3_flavin** shows a hypsochromic shift.

aromatic interactions between the electron deficient flavin and the electron rich aromatic units of the dendron moiety (Fig. 4). We have compared the solution electrochemistry of **Riboflavin** and dendrons **G1_flavin–G3_flavin** in pH = 8.0 phosphate buffer–isopropanol (95 : 5) using square wave voltammetry (see ESI†). It is clear from the electrochemical data that the dendron architecture has little influence on the electrochemical properties of the flavin moiety under the conditions examined.

We next investigated the role dendron generation has in the tuning of the catalytic activity of the flavin units of **G1_flavin–G3_flavin**. In particular, we have investigated the kinetics of the aerobic oxidation of NADH analogue **BNAH** by **Riboflavin** and the flavin dendrons.[13] As BNAH rapidly oxidised in the presence of flavins, the catalysis was followed by monitoring the decrease in absorbance of **BNAH** at 358 nm. Fig. 5 depicts the plots of initial velocity (v_0) *vs.* **BNAH** concentration for **Riboflavin** and the flavin dendrons.

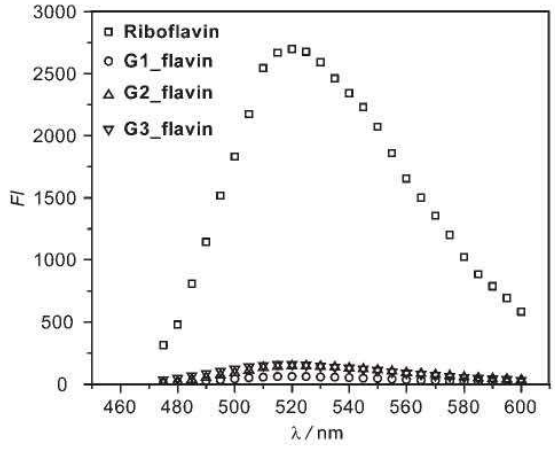

Fig. 4 Fluorescence spectra of the **Riboflavin** and the flavin dendrons in pH = 8.0 buffer isopropanol (95 : 5) solution at 30 °C (λ_{ex} = 450 nm).

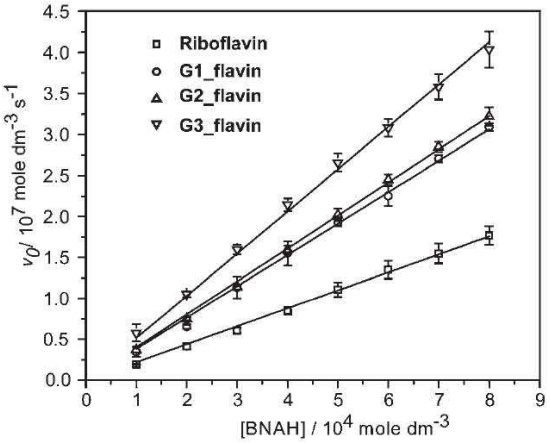

Fig. 5 Plots of initial velocities (v_0) *vs.* substrate concentration (**BNAH**) for the oxidation by **Riboflavin** and flavin dendrons. The lines represent the best fit of the data using pseudo-first order reaction kinetics.

Table 1 Effect of dendron generation on kinetic parameters for the flavin catalysed oxidation of **BNAH**. The concentration of flavin unit in all the cases maintained at 5 μmole dm^{-3}

Substrate	Flavin	k_{pseudo}/ 10^{-5} s^{-1}	k_2/ mole dm^{-3} s^{-1}
BNAH	**Riboflavin**	22	44
	G1_flavin	38	76
	G2_flavin	40	80
	G3_flavin	52	104

The observation of straight line correlation in the kinetic plots indicates the existence of pseudo-first-order kinetic behaviour for these reactions. Nonlinear least-squares curve fitting analysis was then used to evaluate the pseudo-first order (k_{pseudo}) and second order (k_2) rate constants for the reactions. The rate constants are compiled in Table 1.

The comparison of the rate constants in Table 1 reveals a significant increase of catalytic reaction rate for the flavin dendrons as compared to **Riboflavin**. Relative to **Riboflavin**, an increased second order rate constant of 1.7–2.4 fold was observed in the case of flavin dendrons. Interestingly, within the dendron family, a significant rate acceleration can also be noticed upon increase in dendron generation.[10e] We believe that the increased reaction rates for the dendron systems compared to **Riboflavin** is likely due to an enhanced association between the substrate (**BNAH**) and the catalyst. We attribute this enhanced association for the dendron systems originates from the π-stacking interactions between the aryl moieties of the dendrons and the reduced form of **BNAH**. As the dendron generation is increased, this feature becomes more prominent with the **G3_flavin** system, presumably aided by the presence of a hydrophobic pocket which helps to localise the hydrophobic **BNAH** near the flavin unit.

In summary, we have prepared a family of water soluble flavin dendrons. We have shown that the dendron moieties provide both a biomimetic binding pocket and a means of tuning the catalytic properties of the flavin unit in aqueous environments. As the dendrons behave similarly to the apoenzyme of natural flavoenzymes, this study paves the way for the synthesis of more elaborate derivatives whereby functionality can be introduced to control the redox properties and reactivity of the flavin moiety. The development of systems displaying electron transfer and improved catalytic properties will be reported in due course.

GC gratefully acknowledges the EPSRC and the Royal Society of Edinburgh for supporting this work. VMR acknowledges NSF for MRSEC instrumentation (DMR-0213695) and CHE-0518487. BJJ thanks the NSF for an IGERT fellowship (DUE-044852). AS thanks TUBITAK (105S353) for financial support.

Notes and references

1 (*a*) *Flavins and Flavoproteins*, ed. K. Stevenson, V. Massey and C. Willams, University of Calgary, Calgary, 1997; (*b*) *Chemistry and Biochemistry of Flavoenzymes*, ed. F. Muller, CRC Press, Boca Raton, 1991, vol. 1–3.
2 For representative examples see: (*a*) V. Massey and P. Hemmerich, in *The Enzymes*, ed. P. D. Boyer, Academic Press, New York, 1976, vol. 12, pp. 191–240; (*b*) R. Swenson, G. Krey and M. Eren, in *Flavins and Flavoproteins*, ed. D. Edmondson and D. McKormick de Gruyter, Berlin, 1987, pp. 98–107.
3 For recent reviews see: (*a*) A. Niemz and V. M. Rotello, *Acc. Chem. Res.*, 1999, **32**, 44; (*b*) V. M. Rotello, *Curr. Opin. Chem. Biol.*, 1999, **3**, 747; (*c*) Y. Yano, *Rev. Heteroat. Chem.*, 2000, **22**, 151; (*d*) Y. Yano, *Antioxid. Redox Signaling*, 2001, **3**, 899.
4 For representative examples see: (*a*) S. Shinkai, Y. Ishikawa, H. Shinkai, T. Tsuno, H. Makishima, K. Ueda and O. Manabe, *J. Am. Chem. Soc.*, 1984, **106**, 1801; (*b*) J. Takeda, S. Ohta and M. Hirobe, *Tetrahedron Lett.*, 1985, **26**, 4509; (*c*) Y. Yano, N. Tamura, K. Mitsui and T. Nabeshima, *Chem. Lett.*, 1989, 1655; (*d*) V. T. D'Souza, *Supramol. Chem.*, 2003, **15**, 221; (*e*) S. Watanabe, N. Kosaka, S.-I. Kondo and Y. Yano, *Bull. Chem. Soc. Jpn.*, 2004, **77**, 569.
5 For representative examples see: (*a*) H. L. Levine and E. T. Kaiser, *J. Am. Chem. Soc.*, 1978, **100**, 7670; (*b*) H. E. Fried and E. T. Kaiser, *J. Am. Chem. Soc.*, 1981, **103**, 182.
6 For a representative example see: J. P. C. Bootsma, G. Challa and F. Müller, *J. Polym. Sci., Polym. Chem. Ed.*, 1984, **22**, 705.
7 For representative examples see: (*a*) K. Tomizaki, Y. Tsunekawa, H. Akisada, H. Mihara and N. Nishino, *J. Chem. Soc., Perkin Trans. 2*, 2000, 813; (*b*) K. Tomizaki, H. Nishino, T. Arai, T. Kato and N. Nishino, *Chem. Lett.*, 2003, **32**, 813.
8 B. J. Jordan, G. Cooke, J. F. Garety, M. A. Pollier, N. Kryvokhyzha, A. Bayir, G. Rabani and V. M. Rotello, *Chem. Commun.*, 2007, 1248.
9 For a review of dendrimers as artificial enzymes see: J. Kofoed and J.-L. Reymond, *Curr. Opin. Chem. Biol.*, 2005, **9**, 656.
10 For recent reviews of dendrimer-based catalysts see: (*a*) A.-M. Caminade, P. Servin, R. Laurent and J.-P. Majoral, *Chem. Soc. Rev.*, 2008, **37**, 56; (*b*) R. Andrs, E. de Jesús and J. C. Flores, *New J. Chem.*, 2007, **31**, 1161; (*c*) B. Helms and J. M. J. Fréchet, *Adv. Synth. Catal.*, 2006, **348**, 1125; (*d*) D. Méry and D. Astruc, *Coord. Chem. Rev.*, 2006, **250**, 1965.
11 M. D. Greaves, R. Deans, T. H. Galow and V. M. Rotello, *Chem. Commun.*, 1999, 785.
12 (*a*) J. Coziol, *Photochem. Photobiol.*, 1966, **5**, 41; (*b*) P. F. Heelis, *Chem. Soc. Rev.*, 1982, **11**, 15.
13 For analogous methodology see: H. Ye, D. Rong, W. Tong and V. T. D'Souza, *J. Chem. Soc., Perkin Trans. 2*, 1992, 207.

9.2 Appendix Two: X-Ray Crystallography Data

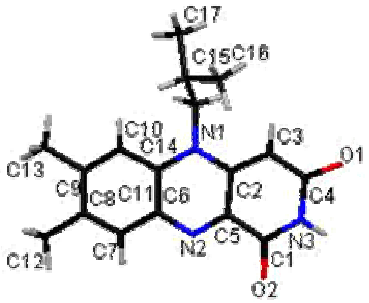

Table 1. Crystal data and structure refinement for ak1.

Identification code	ak1
Empirical formula	C17 H19 N3 O2
Formula weight	297.35
Temperature	150(2) K
Wavelength	1.54184 A
Crystal system, space group	Triclinic, P-1
Unit cell dimensions	a = 7.4795(10) A alpha = 61.936(17) deg. b = 10.392(2) A beta = 79.173(12) deg. c = 10.9302(17) A gamma = 78.984(13) deg.
Volume	731.1(2) A^3
Z, Calculated density	2, 1.351 Mg/m^3
Absorption coefficient	0.730 mm^-1
F(000)	316
Crystal size	0.085 x 0.068 x 0.023 mm
Theta range for data collection	4.61 to 61.84 deg.
Limiting indices	-8<=h<=8, -11<=k<=11, -11<=l<=12
Reflections collected / unique	4988 / 2246 [R(int) = 0.0340]
Completeness to theta = 61.84	97.7 %
Absorption correction	Analytical
Max. and min. transmission	0.983 and 0.954
Refinement method	Full-matrix least-squares on F^2
Data / restraints / parameters	2246 / 0 / 203
Goodness-of-fit on F^2	0.767
Final R indices [I>2sigma(I)]	R1 = 0.0357, wR2 = 0.0734
R indices (all data)	R1 = 0.0667, wR2 = 0.0793
Extinction coefficient	none
Largest diff. peak and hole	0.16 and -0.18 e.A^-3

Table 2. Atomic coordinates (x 10^4) and equivalent isotropic displacement parameters (A^2 x 10^3) for ak1.
U(eq) is defined as one third of the trace of the orthogonalized Uij tensor.

	x	y	z	U(eq)
O(1)	4396(2)	-1967(2)	10974(2)	44(1)
O(2)	4154(2)	-4215(2)	8352(1)	42(1)
N(1)	4187(2)	-3049(2)	9646(2)	34(1)
N(2)	2969(2)	-1650(2)	6211(2)	30(1)
N(3)	3107(2)	1024(2)	6236(2)	29(1)
C(1)	4104(3)	-1790(2)	9830(2)	34(1)
C(2)	3733(3)	-399(2)	8663(2)	32(1)
C(3)	3408(2)	-290(2)	7429(2)	29(1)
C(4)	3379(3)	-1609(2)	7290(2)	28(1)
C(5)	3933(3)	-3072(2)	8462(2)	31(1)
C(6)	2520(2)	-326(2)	5086(2)	28(1)
C(7)	2058(3)	-345(2)	3917(2)	31(1)
C(8)	1666(3)	925(2)	2732(2)	32(1)
C(9)	1711(3)	2282(2)	2718(2)	32(1)
C(10)	2198(3)	2319(2)	3861(2)	32(1)
C(11)	2611(2)	1024(2)	5069(2)	27(1)
C(12)	1281(3)	862(2)	1459(2)	40(1)
C(13)	1206(3)	3707(2)	1474(2)	43(1)
C(14)	3499(3)	2417(2)	6130(2)	33(1)
C(15)	1825(3)	3463(2)	6277(2)	35(1)
C(16)	807(3)	2859(3)	7742(2)	55(1)
C(17)	2439(3)	4929(2)	5877(3)	50(1)

Table 3. Bond lengths [A] and angles [deg] for ak1.

O(1)-C(1)	1.231(2)
O(2)-C(5)	1.227(2)
N(1)-C(5)	1.355(3)
N(1)-C(1)	1.403(3)
N(1)-H(1)	0.8800
N(2)-C(4)	1.294(2)
N(2)-C(6)	1.381(2)
N(3)-C(3)	1.391(2)
N(3)-C(11)	1.393(3)
N(3)-C(14)	1.479(3)
C(1)-C(2)	1.428(3)
C(2)-C(3)	1.364(3)
C(2)-H(2A)	0.9500
C(3)-C(4)	1.453(3)
C(4)-C(5)	1.500(3)
C(6)-C(7)	1.395(3)
C(6)-C(11)	1.408(3)
C(7)-C(8)	1.375(3)
C(7)-H(7)	0.9500
C(8)-C(9)	1.409(3)
C(8)-C(12)	1.506(3)
C(9)-C(10)	1.384(3)
C(9)-C(13)	1.506(3)
C(10)-C(11)	1.404(3)
C(10)-H(10)	0.9500
C(12)-H(12A)	0.9800
C(12)-H(12B)	0.9800
C(12)-H(12C)	0.9800
C(13)-H(13A)	0.9800
C(13)-H(13B)	0.9800
C(13)-H(13C)	0.9800
C(14)-C(15)	1.531(3)
C(14)-H(14A)	0.9900
C(14)-H(14B)	0.9900
C(15)-C(17)	1.513(3)
C(15)-C(16)	1.522(3)
C(15)-H(15)	1.0000
C(16)-H(16A)	0.9800
C(16)-H(16B)	0.9800
C(16)-H(16C)	0.9800
C(17)-H(17A)	0.9800
C(17)-H(17B)	0.9800
C(17)-H(17C)	0.9800

C(5)-N(1)-C(1)	126.02(17)
C(5)-N(1)-H(1)	117.0
C(1)-N(1)-H(1)	117.0
C(4)-N(2)-C(6)	117.44(16)
C(3)-N(3)-C(11)	120.25(16)
C(3)-N(3)-C(14)	120.55(16)
C(11)-N(3)-C(14)	118.88(15)
O(1)-C(1)-N(1)	117.57(18)
O(1)-C(1)-C(2)	125.00(19)
N(1)-C(1)-C(2)	117.41(19)
C(3)-C(2)-C(1)	121.64(19)
C(3)-C(2)-H(2A)	119.2
C(1)-C(2)-H(2A)	119.2
C(2)-C(3)-N(3)	124.76(18)
C(2)-C(3)-C(4)	120.05(18)
N(3)-C(3)-C(4)	115.19(17)
N(2)-C(4)-C(3)	125.86(17)
N(2)-C(4)-C(5)	115.47(18)
C(3)-C(4)-C(5)	118.62(18)
O(2)-C(5)-N(1)	122.11(18)
O(2)-C(5)-C(4)	122.16(19)
N(1)-C(5)-C(4)	115.73(18)
N(2)-C(6)-C(7)	118.37(18)
N(2)-C(6)-C(11)	121.66(17)
C(7)-C(6)-C(11)	119.88(18)
C(8)-C(7)-C(6)	122.05(19)
C(8)-C(7)-H(7)	119.0
C(6)-C(7)-H(7)	119.0
C(7)-C(8)-C(9)	118.45(19)
C(7)-C(8)-C(12)	120.63(19)
C(9)-C(8)-C(12)	120.87(18)
C(10)-C(9)-C(8)	120.18(18)
C(10)-C(9)-C(13)	119.07(19)
C(8)-C(9)-C(13)	120.75(19)
C(9)-C(10)-C(11)	121.50(19)

C(9)-C(10)-H(10)	119.3
C(11)-C(10)-H(10)	119.3
N(3)-C(11)-C(10)	122.90(18)
N(3)-C(11)-C(6)	119.19(16)
C(10)-C(11)-C(6)	117.91(18)
C(8)-C(12)-H(12A)	109.5
C(8)-C(12)-H(12B)	109.5
H(12A)-C(12)-H(12B)	109.5
C(8)-C(12)-H(12C)	109.5
H(12A)-C(12)-H(12C)	109.5
H(12B)-C(12)-H(12C)	109.5
C(9)-C(13)-H(13A)	109.5
C(9)-C(13)-H(13B)	109.5
H(13A)-C(13)-H(13B)	109.5
C(9)-C(13)-H(13C)	109.5
H(13A)-C(13)-H(13C)	109.5
H(13B)-C(13)-H(13C)	109.5
N(3)-C(14)-C(15)	115.90(17)
N(3)-C(14)-H(14A)	108.3
C(15)-C(14)-H(14A)	108.3
N(3)-C(14)-H(14B)	108.3
C(15)-C(14)-H(14B)	108.3
H(14A)-C(14)-H(14B)	107.4
C(17)-C(15)-C(16)	110.47(18)
C(17)-C(15)-C(14)	108.90(17)
C(16)-C(15)-C(14)	112.50(16)
C(17)-C(15)-H(15)	108.3
C(16)-C(15)-H(15)	108.3
C(14)-C(15)-H(15)	108.3
C(15)-C(16)-H(16A)	109.5
C(15)-C(16)-H(16B)	109.5
H(16A)-C(16)-H(16B)	109.5
C(15)-C(16)-H(16C)	109.5
H(16A)-C(16)-H(16C)	109.5
H(16B)-C(16)-H(16C)	109.5
C(15)-C(17)-H(17A)	109.5
C(15)-C(17)-H(17B)	109.5
H(17A)-C(17)-H(17B)	109.5
C(15)-C(17)-H(17C)	109.5
H(17A)-C(17)-H(17C)	109.5
H(17B)-C(17)-H(17C)	109.5

Symmetry transformations used to generate equivalent atoms:

Table 4. Anisotropic displacement parameters (A^2 x 10^3) for ak1.
The anisotropic displacement factor exponent takes the form:
-2 pi^2 [h^2 a*^2 U11 + ... + 2 h k a* b* U12]

	U11	U22	U33	U23	U13	U12
O(1)	61(1)	40(1)	32(1)	-15(1)	-13(1)	-8(1)
O(2)	60(1)	25(1)	38(1)	-11(1)	-12(1)	-3(1)
N(1)	45(1)	23(1)	29(1)	-7(1)	-8(1)	-4(1)
N(2)	31(1)	28(1)	29(1)	-10(1)	-4(1)	-4(1)
N(3)	34(1)	23(1)	29(1)	-9(1)	-5(1)	-4(1)
C(1)	33(1)	32(1)	34(1)	-12(1)	-3(1)	-8(1)
C(2)	36(1)	30(1)	33(1)	-15(1)	-3(1)	-6(1)
C(3)	25(1)	26(1)	31(1)	-9(1)	-2(1)	-4(1)
C(4)	24(1)	27(1)	29(1)	-10(1)	0(1)	-5(1)
C(5)	34(1)	25(1)	30(1)	-9(1)	-5(1)	-5(1)
C(6)	25(1)	29(1)	28(1)	-11(1)	-2(1)	-2(1)
C(7)	30(1)	29(1)	33(1)	-14(1)	-1(1)	-4(1)
C(8)	28(1)	35(1)	31(1)	-13(1)	-1(1)	-4(1)
C(9)	27(1)	33(1)	27(1)	-7(1)	-1(1)	-3(1)
C(10)	30(1)	29(1)	34(1)	-12(1)	-1(1)	-4(1)
C(11)	25(1)	27(1)	26(1)	-10(1)	-1(1)	-3(1)
C(12)	42(1)	42(1)	32(1)	-13(1)	-4(1)	-6(1)
C(13)	47(1)	38(1)	34(1)	-10(1)	-6(1)	-4(1)
C(14)	39(1)	25(1)	33(1)	-9(1)	-6(1)	-7(1)
C(15)	40(1)	30(1)	35(1)	-13(1)	-8(1)	-2(1)
C(16)	61(2)	42(1)	51(1)	-19(1)	7(1)	0(1)
C(17)	55(2)	35(1)	60(2)	-22(1)	-8(1)	-3(1)